A Computational Study of the Mammalian Subiculum

by

David Ian Delany

A thesis presented to the University of Dublin in fulfilment of the requirements for the degree of Doctorate of Philosophy in Psychology

Submitted April 2006; accepted in final form June 2007

Declaration

I hereby declare that I am the sole author of this thesis and that this work has not been submitted as an exercise for a degree at this or any other university. I authorize the University of Dublin to lend this thesis to other institutions or individuals for the purpose of scholarly research. I further authorize the University of Dublin to lend or reproduce this thesis, in total or in part, at the request of other institutions or individuals for the purposes of scholarly research.

Signed

_____

David Delany

Summary

The subiculum occupies a central position as the mediator of information flow between the hippocampal memory system and both cortical and subcortical brain structures. To further the goal of understanding how the subiculum fulfils this critical role, we constructed detailed biophysically realistic computational models of subicular principal neurons.

In chapter III we developed Hodgkin-Huxley and Markov models of a total of fourteen sodium, potassium, calcium, and mixed cation currents that are prominent in pyramidal cells of the hippocampal complex. In chapter IV active models of subicular principal cells were created by selectively incorporating subsets of these currents into models of passive subicular membranes. Mechanisms for an unprecedentedly wide range of electrophysiological features (EPFs) of subicular pyramidals were simulated. These included inward and outward membrane rectification, M- and H-resonance, burst and single spiking, frequency-dependent bursting, spike frequency adaptation, plateau potentials, delayed firing, afterhyperpolarizations and rebound firing. The number of electrophysiological events treated in this thesis necessarily constrains the level of detail at which many EPFs were investigated. However, given the evident importance of burst firing within the brain (Lisman, 1998), particular attention was paid to the mechanisms, ionic composition, and regulation of the subicular burst event. A novel theory of subicular burst firing, the adaptive two-component burst firing theory, was proposed.

A central theme of this thesis is that the expression of subicular EPFs are subject to adaptive regulation. Evidence for this hypothesis was marshalled and major findings within the subicular electrophysiological literature were re-interpreted from the adaptive EPF perspective. In chapter V the evidence for the adaptive regulation of subicular frequency preferences, bursting, and spike frequency adaptation was discussed in more detail along with the possibility of integrated adaptive control mechanisms. Finally, the limitations of the prevailing electrophysiological analysis paradigm were noted and a novel empirical framework for investigating adaptive EPFs, feature-based analysis, was proposed.

Acknowledgements

Wholehearted thanks are due to the man who puts the 'super' in PhD supervisor, Shane O'Mara. His implacably optimistic expectation that I would eventually complete my PhD (whilst I took several years off to pursue other projects) eventually paid off. Regards are due to the members of the O'Mara lab, especially the 'old school' crowd of Drs Richard Roche, Sean Commins, and Michael Anderson, for friendship and support. Appreciative thanks are also due to the support staff of the TCD School of Psychology; June, Lisa, Dave, Eddie, Rose, Marcella, and Pat for all their friendly help over the years.

I would also like to take this opportunity to thank my mum and dad, Patricia and Dermot O'Connor, for all the support they have given me over the many years of my seemingly perpetual education. Many thanks also to Michael and Grace Boran for their generous support and encouragement. And finally, this thesis would probably never have been completed without the deep love and support of my wonderful and gifted partner, Lorraine Boran.

Abstract

The subiculum occupies a pivotal position as the mediator of the interaction of the hippocampus with cortical and subcortical structures. To further the goal of understanding this critical structure, we developed detailed computational models of subicular principal neurons. Fourteen models of prominent subicular sodium, calcium and potassium currents were constructed and used in the development of biophysically detailed single compartment models of subicular bursting and regular firing cells. These cell models exhibit an unprecedented number of accurately simulated subicular cell electrophysiological events (EPFs) including; inward and outward membrane rectification, M- and H-resonance, burst and single spiking, frequency-dependent bursting, spike frequency adaptation, plateau potentials, delayed firing, afterhyperpolarizations and rebound firing. In particular, the ionic composition of subicular burst firing is analysed in detail, and a novel 'adaptive two-component' theory of subicular bursting is advanced.

A central supposition of this thesis is that subicular EPFs are subject to brain state-dependent adaptive regulation. Accordingly, major findings within the subicular electrophysiological literature are re-interpreted from this perspective. Evidence for the adaptive regulation of subicular frequency preferences, bursting, and spike frequency adaptation are discussed in detail, along with the possibility of integrated adaptive control mechanisms. The implications of the proposed EPF mechanisms for subicular function are also considered. Evidence of, and mechanisms by which, bursting and regular firing cells can be dynamically interconverted are investigated. Finally, the limitations of the prevailing electrophysiological analysis paradigm are addressed and feature-based analysis, a novel empirical framework for investigating adaptive EPFs, is proposed.

List of figures

List of Tables

Glossary

4-AP	4-aminopyridine
AA	Arachidonic acid
ACh	Acetylcholine
ADP	Afterdepolarization
AHP	Afterhyperpolarization
ATP	Adenosine Triphosphate
DAP	Depolarizing Afterpotential
DNMS	Delayed-Nonmatch-To-Sample
EBC	Early Burst Component
EC	Entorhinal Cortex
EPSC	Excitatory Postsynaptic Current
EPSP	Excitatory Postsynaptic Potential
I_{FIR}	Fast inward rectifier current
HH	Hodgkin-Huxley
HPA	Hypothalamic-Pituitary-Adrenocortical
HVA	High Voltage Activated
I_A	Fast transient potassium current
I_{CaL}	High threshold non-inactivating calcium current
I_{CaN}	High threshold inactivating calcium current
$I_{CaP/Q}$	High threshold, slowly inactivating calcium current
I_{CaR}	Residual calcium current
I_{CaT}	Low threshold transient calcium current
I_{CT}	Fast transient Ca^{2+}-dependent potassium current
I_D	Slowly inactivating delay potassium current

I_{DR}	Delayed rectifier current
I_H	Mixed cation anomalous rectifier
I_M	Muscarinic slow potassium current
I_{NaF}	Fast transient sodium current
I_{NaP}	Persistent sodium current
IPSP	Inhibitory Postsynaptic Potential
ISI	Interspike Interval
LBC	Late Burst Component
LVA	Low Voltage Activated
mGluR	Metabotropic Glutamate Receptor
PP	Plateau Potential
PSTH	Peristimulus Time histogram
REM	Rapid Eye Movement
SPC	Subicular Pyramidal Cell
SE	Status Epilepticus
SWS	Slow Wave Sleep
TEA	Tetraethylammonium
TPM	Topiramate

Table of contents

Chapter I
INTRODUCTION

It is not the strongest species that survive, nor the most intelligent, but
the ones most responsive to change.

Charles Darwin (1809-1882)

1.1 Thesis goals and structure

The subiculum is a single layer network occupying a strategic position between the hippocampal memory system and both cortical and subcortical brain structures. Befitting its central location in the limbic memory system, the subiculum has been implicated in a range of neurophsyiological functions including spatial (Sharp and Green 1994) and non-spatial learning and memory (Deadwyler and Hampson 2004) tasks. The subiculum is also a locus of epileptiform activity (Wellmer et al. 2002) and can act as an intrinsic generator of high frequency gamma population oscillations (Harris and Stewart 2001).

Subserving the behaviour of the subiculum are several classes of cells including pyramidal cells and a range of inhibitory interneurons. Subicular pyramidal cells, which form the focus of this thesis, are broadly differentiated, on the basis of their electrophysiological activity profiles, into bursting and nonbursting or regular firing cells. These cellular populations play different roles in the generation of physiological rhythms and epileptiform activity (Menendez de la Prida and Gal 2004) although the detailed mechanisms by which this occurs are the subject of ongoing investigation. To further the goal of understanding how the differential electrophysiology of subicular pyramidal cells contributes to subicular function we constructed, for the first time, detailed biophysically realistic computational models of subicular principal neurons.

The developmental methodology that informs this thesis is informed by what might be called a "continuum modelling" philosophy. That is, neuroscientific models should be able to account for transitions between states, for the gain and loss of electrophysiological features. In short, models should be able to explicate cellular plasticity whereby the input–output relationship of the entire neuron is modified. This thesis contends that the molecular mechanisms that subserve

electrophysiological phenomenon such as bursts, spike frequency adaptation and subthreshold oscillations, are subject to dynamic regulation on a number of spatiotemporal scales. We perform a detailed interrogation of the subicular literature in our investigation of the validity of this hypothesis.

1.1.1 Feature-based approach

Rather than exhaustively list the electrophysiological properties of the respective subicular cells types, we discuss the expression patterns and characteristics of electrophysiological features (EPFs) such as bursts, anodal break potentials, and subthreshold oscillations in their own sections. The association of a given EPF with particular cell types is then naturally treated in these sections.

This approach to structuring the thesis reflects a perspective on electrophysiological research that is somewhat at odds with convention. Namely, we contend that the use, and proliferation, of cell types, such as bursters and regular firers, as an organising framework for neuronal information serves to limit, rather than expand, our ability to comprehend the workings of the brain. A fundamental change in the way that intracellular electrophysiological data is collected and analysed is urgently required if we are to substantively extend our understanding of the brain. In the discussion chapter, we expand upon this point and propose an alternative framework called feature-based analysis.

1.2 Overview of subicular cell types

We present here a brief overview of the cell types typically encountered in the subiculum. The electrophysiological features these cells are treated in considerably more depth in the Cell chapter.

Subicular pyramidal neurons are conventionally divided into burst firers and regular firers based on their responses to intracellular and orthodromic stimulation (Mason 1993; Stewart and Wong 1993; Taube 1993). A similar classification has emerged from *in vivo* studies (Segal 1972; Finch, Tan, et al., 1988; Sharp and Green 1994; Gigg, Finch, et al., 2000).

1.2.1 Bursting cells

Burst firing cells respond to a suprathreshold depolarization with a brief train of 2 to 6, high frequency (150-300 Hz) action potentials riding on a depolarizing envelope. The burst is

terminated by a hyperpolarization tens of milliseconds in duration. More recently, the bursting phenotype has been subdivided into strong and weak bursters (Staff, Jung, et al., 2000). Strong bursters respond to sustained depolarization with two or more bursts, whereas weak bursters exhibit a single burst followed by repetitive spiking. Despite having essentially identical electrophysiological properties, strong bursters are significantly more likely to fire in response to orthodromically-induced excitatory postsynaptic potentials (EPSPs) than are weak bursters (Menendez de la Prida et al., 2003). Since few regular firers (~13%) and most burst firers (~75% of strong and 45% of weak) respond to local glutamatergic stimulation, burst firers constitute the main projection cells of the subiculum (Menendez de la Prida, Suarez, et al., 2003). Interestingly, a subset of subicular bursters is spontaneously active and appears to have the characteristics of pacemaker cells (Harris and Stewart 2001).

Based on the high reported proportion of bursting cells (from 54 to 100%) the subiculum has conventionally been viewed as a bursting structure (Behr, Empson, et al., 1996; Mattia, Hwa, et al., 1993). However, a recent analysis of the effect of electrophysiological sampling criteria on the apparent proportion of bursters by Menendez de la Prida et al. (2002) undermines this view. These workers found that the proportion of bursters recorded is critically dependent on the choice of soma size (large or small) and shape (pyramidal or ovoid). Using various criteria, from 15% to 62% of recorded cells were bursters. Significantly, when no criteria were used the proportion of total cells that are bursters is only 30%.

1.2.2 Regular firing cells

Regular firing cells respond to sustained suprathreshold stimuli with a train of spikes (Mason 1993; Stewart and Wong 1993; Taube 1993). As with subicular bursters, regular firers have recently been subdivided. Menendez de la Prida et al. (2003) divided regular firers into adapting and non-adapting forms. Adapting regular firers display a progressive increase in the interspike interval (ISI) of their spike train. In contrast, the ISI of non-adapting regular firers are constant. Adapting and non-adapting regular firers are also identical in all electrophysiological properties except for input resistance, which is higher in adapting cells.

1.2.3 Interneurons

Inhibitory interneurons (fast spiking cells, theta cells, local circuit neurons, non-pyramidal neurons) display a high rate of spike firing (60-150 Hz) in response to depolarizing stimuli that is strongly modified by the hippocampal theta EEG oscillation *in vivo* (Sharp and Green, 1994).

These cells have higher input resistances and membrane time constants than pyramidal cells (Menendez de la Prida, Suarez, et al., 2003). Both $GABA_A$ (fast) and $GABA_B$ (slow) interneurons are present in the subiculum (Harris-Warrick and Sparks 1995).

1.3 Cell type morphology

There appear to be no definitive morphological criteria by which bursting and regular firers can be differentiated. However, Greene and Totterdell (1997) reported that, whilst it was impossible to distinguish burst firing neurons from regular firers on morphological grounds (including soma size and dendritic width), the apical dendrites of burst firing neurons tend to have longer distances to the first branch point than the regular spiking neurons. However, the apical dendrites of subicular pyramidal cells tend to extend into the molecular layer prior to dividing (Taube, 1993), therefore, cells in the hippocampal formation that are farthest from the molecular layer, as bursting cells tend to be (Greene and Mason, 1996; Greene and Totterdell, 1997; Menendez de la Prida et al., 2003), will typically produce apical dendrites that branch later. In other words, the first apical branch-point distance is potentially primarily a function of location, and not necessarily an expression of electrophysiological cell type. A similar argument can be applied to the finding that the somata of bursting cells tend to be larger than those of regular firers (Menendez de la Prida, 2002; Menendez de la Prida et al., 2003) i.e. longer dendrites can reasonably be expected to necessitate larger somata. Accordingly, there is a pronounced trend towards increased soma size along the superficial-deep axis (Ishizuka 2001; Harris, Witter, et al., 2001). Furthermore, Greene and Totterdell (1997) and Harris et al. (2001) found no differences in soma size across subicular pyramidals. Significantly, there are no differences in the dendritic morphology of subicular regular firers, or strong or weak bursters as assessed using Scholl analysis (Staff et al., 2000; Menendez de la Prida et al., 2003). CA1 pyramidals, by contrast, do exhibit significantly greater levels of dendritic arborisation than subicular pyramidals (Staff et al., 2000).

Menendez de la Prida et al. (2003) found that strong bursters overwhelmingly have pyramidal somata whereas regular firers and weak bursters were equally likely to have ovoid somata. Greene and Totterdell (1997) also reported that regular firers are equally likely to have pyramidal or ovoid somata whereas roughly 60% of bursters had pyramidal somata. This study did not subclassify bursters. The majority of bursters and regular firers exhibit both locally and

projecting axon collaterals that enter the alveus (Harris, Witter, et al., 2001; Menendez de la Prida, Suarez, et al., 2002)

Morphologically, interneurons have variably shaped somata and smooth or varicose dendrites (Greene and Totterdell 1997). These neurons do not exhibit an apical dendrite and have short, locally terminating, axonal collaterals (Greene and Totterdell, 1997; Menendez de la Prida et al., 2003).

1.4 Cell type location

The somata of subicular pyramidals are located in the pyramidal cell layer of the subiculum where they are oriented with their bases towards the white matter of the alveus, and their apical dendrites towards the molecular layer (Greene and Totterdell 1997).

Along the alveus-hippocampal fissure (deep-superficial) axis, a deep cell layer distribution bias for bursting cells has been reported (Greene and Mason 1996; Greene and Totterdell 1997; Harris, Witter, et al., 2001; Menendez de la Prida, Suarez, et al., 2003). A converse distribution bias towards the superficial cell layers (towards the hippocampal fissure) is reported for regular firers. In contrast, Staff et al. (2000) noted a flat gradient for all cell types in this dimension.

Greene and Totterdell (1997) reported a complex distribution of regular firers in the CA1-presubiculum (proximodistal) axis. These workers found that the distribution of regular firers rose from 16% at the proximal end to over 50% at the median, before falling to only 10% at the distal end. An inverse, although non-significant, distribution for regular firers was observed by Harris et al. (2001) whereby the median layer had the fewest regular firing cells. A less extreme dispersion was reported by Staff et al. (2000) who found that that regular firers, weak bursters and strong bursters had overlapping proximodistal distributions, in that order. Although the absolute proportions involved (~45% for regular firer and ~65% for strong bursters) were not tremendously dissimilar, the distributions of the regular firers and strong bursters were significantly different. Sharp and Green (1994) also found higher levels of bursters in the distal region in freely moving rats.

Subicular interneurons appear to have a random distribution across the deep-superficial axis (Menendez de la Prida et al., 2003). Although, a specific subtype, chandelier cells, are preferentially located in the stratum radiatum, where they give rise to descending axons that branch in the deeper pyramidal cell layer (Soriano, Martinez, et al., 1993).

1.5 Overview of the anatomy and hodology of the subiculum

1.5.1 Local circuitry

An appreciation of the local circuitry and hodology of the subiculum is important for understanding how the subiculum operates as a relay, integrator, distributor, and also as a locus for epileptiform activity.

The subiculum is composed of three cell layers: the molecular layer, the pyramidal layer, and the polymorphic or fibre layer. The molecular layer, adjacent to the hippocampal fissure, is continuous with the stratum lacunosum-moleculare and the stratum radiatum of the contiguous CA1 region. The enlarged pyramidal layer contains the somata of the large pyramidal cells. Dispersed throughout the subiculum are smaller interneurons (Witter and Amaral 1991).

Harris et al. (2001) suggest that subicular cytoarchitectonics exhibits both columnar and laminar architecture. Columns are potentially defined by ascending collaterals from cells the deep layer that remains largely within the apical dendrite volume. Whereas layers are defined by the axonal collaterals of superficial cells that branch extensively in the cell layer. Since bursters tend to predominate in the deep layer, Harris et al. (2001) speculate that bursters form functional columns that are regulated by laminar collaterals of the superficial cells.

There is a tendency for the apical dendrites of superficial cells to tilt away from the deep-superficial axis, and more towards CA1, the more proximal their location (Harris, Witter, et al., 2001). The inverse trend is noted on the distal side towards presubiculum. Harris et al. (2001) suggest that the consequently larger aspects presented by the more proximal or distal cells to the ascending axons of deep cells, may enable these cells to receive sufficient input to allow them to act as foci for epileptiform activity.

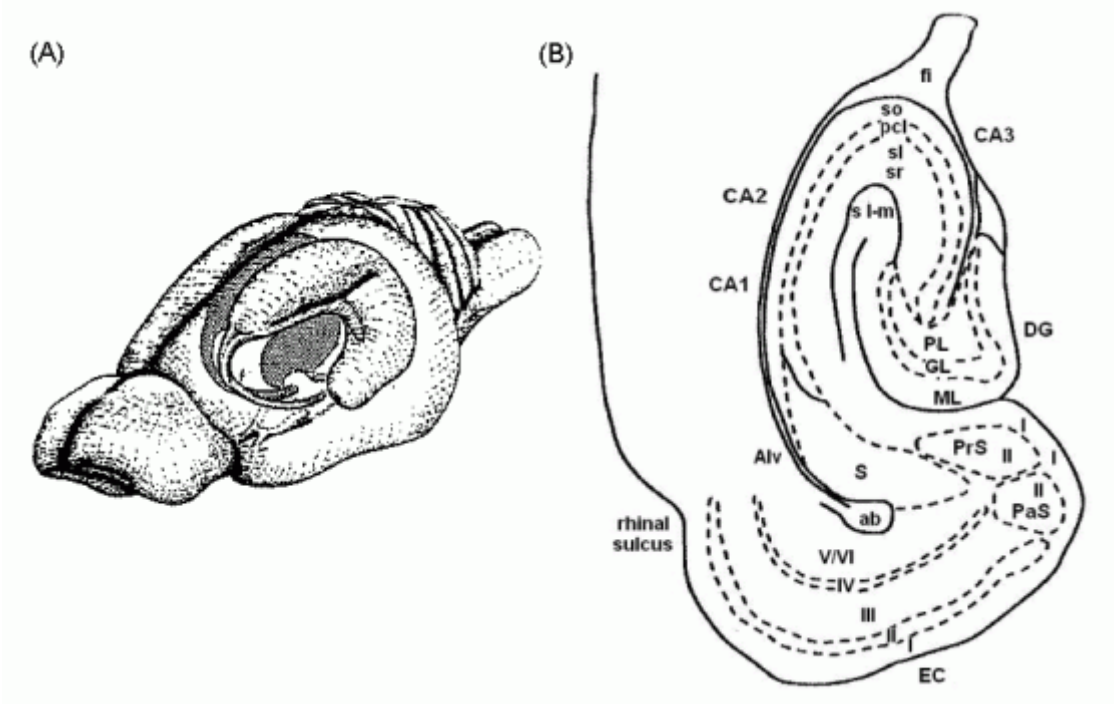

Figure I-1. Two schematic representations of the hippocampal complex. A: A line drawing depicting a pellucid view of the rat brain that reveals the bilateral hippocampal complex. B: An annotated line drawing of a transverse section of the hippocampal complex. Key: S, subiculum; PrS, presubiculum; PaS, parasubiculum; DG, dentate gyrus; EC, entorhinal cortex; PL, GL, and ML, polymorphic, granular, and molecular layers of the dentate gyrus; so, stratum oriens; pcl, pyramidal cell layer; sl, stratum lucidum; sr, stratum radiatum; sl-m, stratum lacunosum-moleculare; ab, angular bundle; alv, alveus; fi, fimbria (adapted from Amaral and Witter 1995, reproduced by permission of Academic Press).

The typical extracellular sequence of responses of subicular pyramidal cells to stimulation of afferent sites is antidromic spike-EPSP-IPSP (Taube 1993). Analysis of the respective circuit delays suggests that feed-forward inhibition, rather than feedback inhibition, accounts for this response sequence (Finch, Tan, et al., 1988). In other words, the subiculum receives excitatory inputs that activate principal cells and interneurons simultaneously. These interneurons then suppress the activity of the local subicular principal cells. In a more detailed investigation Menendez de la Prida et al. (2003) reached similar conclusion regarding the control of principal cell activity by interneurons. These workers found that subicular output and local activity is predominately carried by bursters and that the activity of these cells is strongly regulated by local interneurons.

1.5.2 Subicular hodology

The subiculum is part of the hippocampal complex, which includes the entorhinal cortex, dentate gyrus, and Ammon's horn or *Cornu Ammonis* containing areas CA1-3) (Witter and Amaral 1991). Physically, the rat hippocampus is a bilateral limbic structure resembling two 'Cs' leaning against each other. The dorsal aspect of the hippocampus rests near the medial septum, and is also known as the septal pole. The ventral hippocampus terminates in the temporal pole. A transverse section of the hippocampus reveals the familiar hippocampal architecture dominated by the trisynaptic circuit. This architectonic structure is continued along the septotemporal extent of the hippocampus.

Historically, the subiculum has been considered as part of the subicular complex (Witter, Groenewegen, et al., 1989). However, this term, which refers to the contiguous subiculum, presubiculum and parasubiculum regions, is now deprecated on architectonic and hodological grounds (O'Mara, Commins, et al., 2001). Anatomically, the subiculum shares the three cell layers characteristic of the allocortex, whereas the pre- and parasubiculum have deep layers continuous with the nominally six layered entorhinal cortex (EC). Hodologically, the subiculum is a robust component of the hippocampal circuit, unlike presubiculum and parasubiculum. Conversely, both pre- and parasubiculum receive a strong input from the neocortex, as does the entorhinal cortex. These, and other, differences suggest that the subicular complex does not constitute a useful structural or functional classification.

The subiculum receives the primary output from the hippocampal trisynaptic circuit, a cascade of three pathways: efferents from layers II and III of the entorhinal cortex extend, via the perforant pathway, to terminate on the granule cells of the dentate gyrus. These granule cells, in turn, project 'mossy fibre' axons onto the large pyramidal cells of area CA3. Finally, via the Schaffer collateral system, the CA3 pyramidals project onto the pyramidals of area CA1 (Swanson 1982). From area CA1 the subiculum receives the largest output from the hippocampus (Witter, Groenewegen, et al., 1989). The output from CA1 to subiculum emerges from along the entire proximodistal extent of the CA1 and innervates the full proximodistal extent of the subiculum in a simple inverse topographical pattern (Amaral, Dolorfo, et al., 1991). That is, proximal subiculum (bordering CA1) receives input from distal CA1 and distal subiculum (bordering the presubiculum) receives input from proximal CA1. The existence of a reciprocal path is suggested by the propagation of epileptiform activity from subiculum back into

CA1 (Harris and Stewart 2001), and has recently been confirmed in a tracing study (Knopp, Kivi, et al., 2005).

However, Naber et al. (2000) argue that the trisynaptic circuit model is an oversimplified representation that underestimates the importance of the subiculum in the hippocampal memory system. They provide evidence for multiple direct and indirect parallel pathways that form nested loops. Within these loops, the subiculum occupies a central position where 'raw' and processed information from cortical and subcortical structures converge, is processed, and redistributed (Naber, Witter, et al., 2000). The central position of the subiculum also contributes to its prominent role in seizure propagation (Dreier and Heinemann 1991). Key to this central role is the extensive range of subicular connections to and from cortical and subcortical structures (O'Mara, Commins, et al., 2001).

1.5.2.1 Cortical connections

Whereas the pre- and parasubiculum produce relatively weak projections to the subiculum, the subiculum sustains a strong projection to both of these cortical areas (Witter, Ostendorf, et al., 1990). Anatomically, this connection exhibit a broad reciprocal one-to-one pattern, whereby ventral and dorsal subiculum projects to ventral and dorsal pre- and parasubiculum and *vice versa*. The potential importance of these reciprocal connections is underlined by the ability of re-entrant activity in this circuit to support epileptiform activity (Funahashi, Harris, et al., 1999). Pre- and parasubicular cells play a role in spatial memory and navigation (McNaughton, Barnes, et al., 1996).

The subiculum receives substantial direct inputs from the entorhinal cortex, which, in the rat, terminate in the outer portion of the molecular layer (Witter and Amaral 1991). These inputs appear to be organised topographically whereby projections originating in the lateral EC terminate on the proximal subiculum while medial EC projections target the distal subiculum (Witter, Wouterlood, et al., 2000). Subicular outputs to EC reciprocate these connections, such that proximal and distal subiculum project to lateral and medial EC, respectively (Kloosterman, Witter, et al., 2003). Furthermore, along the septotemporal axis, septal subiculum projects to lateral EC and temporal subiculum projects to medial EC (Kloosterman, Witter, et al., 2003). Entorhinal cortex plays an important role in spatial learning (Schenk and Morris 1985; Taube, Kesslak, et al., 1992).

The perirhinal cortex, which contributes to visual and haptic memory (Suzuki, Zola-Morgan, et al., 1993; Suzuki, Zola-Morgan, et al., 1993), sustains a strong projection to the subiculum that terminates in the molecular layer (Kosel, Van Hoesen, et al., 1983). Projections from the dorsoventral extent of the perirhinal cortex converge primarily on the mid-dorsoventral subiculum. Subicular projections to the perirhinal cortex emerge from the septoproximal subiculum (Kloosterman, Witter, et al., 2003).

1.5.2.2 Subcortical connections

The subiculum forms connections with a variety of subcortical structures including the mammillary bodies, the hypothalamus, the amygdala, the septal complex, and the thalamus (Canteras and Swanson 1992; Witter and Groenewegen 1990). A tri-laminar organisation in the transverse plane is evident in the projections of the subiculum to a number of subcortical structures. Projections to the anteroventral thalamic nucleus, the medial mammillary body, and the nucleus accumbens emerge from the deep, medial and superficial subiculum, respectively (Ishizuka 2001). This pattern is broadly preserved along the entire septotemporal extent of the subiculum.

The projections of the subiculum to the nucleus accumbens, which is involved in instrumental learning (Fibiger and Phillips 1988), are of particular interest because they illustrate the level of control the subiculum can exert over target structures. The proximodorsal and proximoventral regions of the subiculum project to the rostrolateral and caudomedial regions of the nucleus accumbens, respectively (Witter and Groenewegen 1990; Aylward and Totterdell 1993). Ventrally originating subicular projections provide the glutamatergic drive for nitric oxide synthase interneurons in the nucleus accumbens (French, Ritson, et al., 2005), which suggests that the subiculum is in a position to exert substantial control over the activity of the nucleus accumbens. This view is further supported by the effect of subicular input on the median spiny cells of the nucleus accumbens. These neurons exhibit bistable activity states; an active depolarized and an inactive hyperpolarized state (Yim and Mogenson 1988). Subicular afferents selectively, and apparently exclusively, induce these bistable cells to switch to their depolarized active state, thereby gating the activity of the nucleus accumbens (O'Donnell and Grace 1995).

1.5.3 The subiculum and learning and memory

As a central component of the limbic memory system, the subiculum has been implicated in a range of spatial and non-spatial learning and memory tasks.

Three classes of spatially responsive cells have been described in the subiculum of freely moving animals: place cells, head-direction cells, and place and head-direction cells (Kubie JL 1991). The activity of place cells is correlated with the animal's location such that a spike density contour map of the animal's environment reveals 'location specific' firing patterns known as place fields (O'Keefe 1979). Sharp and Green (1994) found that the majority (84%) of subicular principal cells carry spatial information. Interestingly, subicular bursters and regular firers exhibit similar spatial coherence levels (a measure of the strength of the spatial signal carried by the cell), although the place field size of bursters are significantly larger than that of regular firers (Sharp and Green, 1994). The firing rate of bursters and regular firers also exhibits some degree of modulation by the EEG theta rhythm (Sharp and Green 1994; Anderson and O'Mara 2003). An activity gradient is also seen across the subiculum such that average activity levels and spatial signal strength increases across the proximodistal axis (Sharp and Green, 1994).

Although both hippocampal and subicular principal cells carry spatial signals, the nature of these representations are fundamentally different. Whilst hippocampal place fields are generally relatively small and contain a single region of high firing, subicular cells tend to fire throughout the environment and display a graded location-specific rate modulation resulting in local regions of high and low firing activity. This pattern of firing is consistent with convergent input to a single subicular cell from several hippocampal place cells (Sharp and Green 1994; O'Mara 2005). Interestingly, hippocampal cells display spatial maps that are sensitive to specific environments, whereas subicular cells show essentially the same pattern across different environments (Sharp 1999). Subicular cells evidently sustain a more abstract representation of the environment than upstream regions. However, the stable 'universal' representations formed by subicular cells are not simply convergent reflections of upstream activity. Whereas, hippocampal place fields anticipate future location by 30-40 ms, subicular place fields are best correlated with locations 50-70 ms into the future (Sharp 1999).

Sharp and Green (1994) also found that the activity of many (61%) subicular cells, including place cells, is modulated by head direction. Unusually, some head direction cells exhibit two preferred directions (Kubie JL 1991). Nonetheless, head direction is a comparatively minor correlate of subicular firing rate, since it only accounts for a maximum of 13% of the firing rate variance.

There is substantial evidence supporting a role for the subiculum in nonspatial memory and learning tasks. Subicular lesions produce a significant reduction in operant learning (Govindaiah, Rao, et al., 1997; Nutan and Meti 2000). Govindaiah et al. (1997) suggest that the subiculum is primarily involved in the acquisition phase of operant learning tasks since subicular lesions significantly increase the time taken to acquire a task but do not effect the retention of tasks learned after the lesion. A similar post-lesion acquisition deficit is seen in spatial discrimination tasks (Cho and Jaffard 1995).

Lesions of the hippocampal complex (including the subiculum) produce post-lesion deficits in performance on the delayed-nonmatch-to-sample (DNMS) test of spatial working memory tasks that were learned pre-operationally (Aggleton, Keith, et al., 1992). The specific contribution of the subiculum to this task has been elucidated by Deadwyler and Hampson (2004), who had previously identified several classes of subicular and hippocampal 'functional' neurons whose ensemble activity is tightly correlated with specific phases of the DNMS task (Hampson and Deadwyler 2003). These workers showed that the dorsal subiculum is responsible for maintaining a 'real time' representation of the task for delays less than 15 seconds. Beyond this time, the quality of subicular task information degrades as the activity of functional subicular neurons declines to baseline. For delays of over 15 seconds, task performance is passed off to the hippocampus, where the activity levels of ‘off-line’ hippocampal functional neurons start to rise. Remarkably, practically all of the behavioural variability in this task can be accounted for by the ensemble activity of these functional cells in the subiculum and CA1.

The finding that lesions of the ventral subiculum impair spatial working memory (Riegert, Galani, et al., 2004) reinforces the idea that the subiculum is involved in short-term memory. However, the level of subicular involvement in different forms of short term memory may be variable since subicular lesions appear to have limited effect on spatial working and reference memory as measured by the Morris water maze (Galani, Jarrard, et al., 1997). Lesioned rats only exhibited impairment in the probe trial of the water-maze task. Interestingly, subicular lesion-induced deficits seem to be amenable to functional recovery by enriched environments (Galani, Jarrard, et al., 1997). In humans, a functional imaging study suggests that the subiculum is involved in working memory (Gabrieli, Brewer, et al., 1997), while subicular volume is strongly correlated with the number of words recalled after a delay (Mortimer, Gosche, et al., 2004).

The ventral subiculum is centrally involved in mediating the interaction between the cognitive and behavioural aspects of the stress response. Ventral subiculum appears to regulate HPA

responses to cognitively processed stressors (e.g. restraint and open field exposure), but not to physical stressors (e.g. ether inhalation) (Herman, Dolgas, et al., 1998). Thus ventral subicular lesions cause a significant increase in the duration of the glucocorticoid response (corticosterone in the rat) to 'abstract' stressors. Baseline levels of the stress hormone corticosterone are unaffected. Similar lesions to the hippocampus proper have no effects on the stress-induced response (Herman, Cullinan, et al., 1995).

Ventral subiculum is also involved in the acquisition and retention of Pavlovian fear conditioning to both contextual and acoustic conditional stimuli in rats (Maren 1999). Another subiculum-mediated learning paradigm is the partial reinforcement extinction effect, whereby the behaviour of animals trained to perform a task for which they are inconsistently rewarded (partial reinforcement) is, paradoxically, significantly more resistant to extinction than that of animals trained on the same task, but with continuous reinforcement. Ventral, but not dorsal, subiculum appears to be critical to maintaining this behaviour (Rawlins, Feldon, et al., 1989).

Chapter II
METHODS

It is by logic we prove, it is by intuition we invent.

Henri Poincare (1854-1912)

2.1 Computational resources

All computational models were developed and run using the interactive ordinary differential equation solver XPP (Ermentrout 1998) on a Pentium desktop PC. The variable step Runge-Kutta numerical integration method was employed for all simulations. A default time step of 0.5 ms was generally used, although the robustness of integration results was frequently tested using shorter time steps. Additional analyses were performed using Matlab (The Mathworks 2002). Curve fitting was carried out using CurveExpert (Hyams 2001), and the graphing packages graphmatica (Hertzer 2005) and Sigmaplot (Systat Software 2004) were used for equation plotting. Figures were prepared using Sigmaplot and Microsoft Paint (Microsoft 2001)

2.2 The compartmental approach

The electrophysiological properties of neuronal membranes behave as simple electrical circuits with resistance, capacitance and voltage sources (Segev and Burke 1998). In this thesis, we modelled subicular pyramidals as a single compartment (corresponding to an isopotential patch of membrane). The general RC circuit electrical equivalent of this model is shown in Figure II-1. Such single compartment models form the building blocks of more complex spatially extended multi-compartmental neuronal simulations.

Since the cell membrane separates two conducting ionic solutions, the cytoplasm and extracellular fluid, it acts as a capacitor. The membrane capacitance, C_m, is charged or discharged by current flowing into or out of the compartment. The transmembrane voltage is V_m since the voltage of the extracellular space, V_{out}, is defined as zero. The battery term, E_{leak}, represents the reversal potential (the voltage at which there is no net current across the membrane) of the passive leak conductances, g_{leak}. Membrane resistance, R_m, is simply the inverse of g_{leak}. I_{inject} represents externally applied current injections.

The active properties of the membrane are represented by the variable conductance, g_{active}, in series with a reversal potential, E_{active}. In a fully specified model, each active channel is represented by such variable conductance-battery pairs. As we will see below in more detail, the value of the variable conductance is typically some time-dependent function of voltage or ligand concentration.

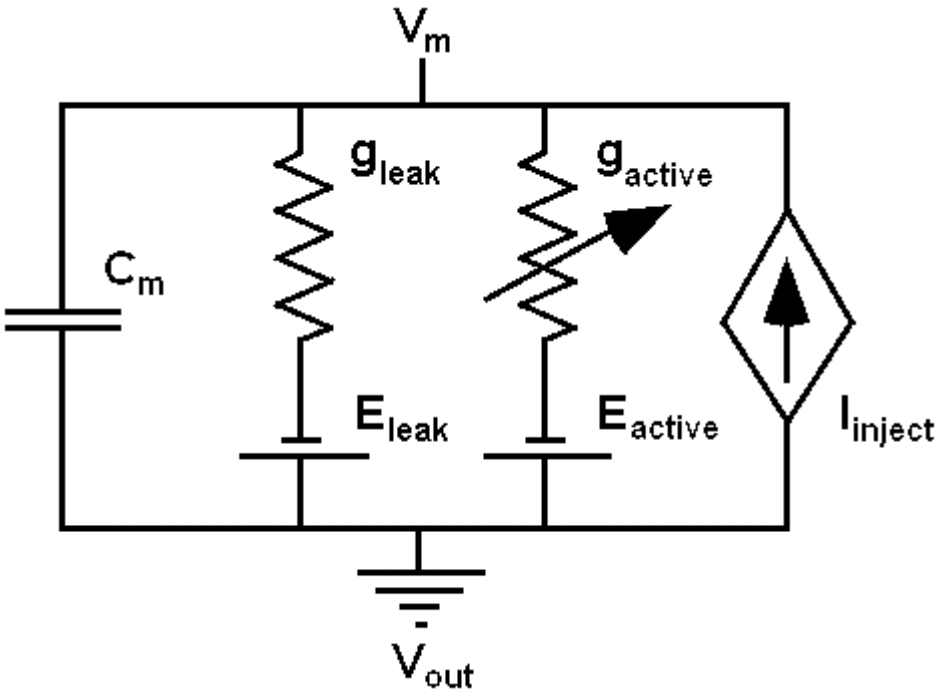

Figure II-1 An electric circuit diagram of an isopotential cell model.

The behaviour of the membrane voltage of this model over time is determined by solving the first order differential equation

$$\frac{dV}{dt} = \frac{-I_{leak} + I_{active} + I_{inject}}{C_m}$$

where

$$I_{leak} = g_{leak}(V_m - E_{leak})$$

and

$$I_{active} = g_{active}(V_m - E_{active})$$

The current I_{active} is the sum of all the active currents present in the model.

Despite the gross simplification of neuronal morphology the single compartment approach represents, such simulations have a proven record of accurate and insightful reproduction of the

salient aspects of current and voltage clamp behaviour of a broad range of neuronal cell types (McCormick and Huguenard 1992; LeMasson, Marder, et al., 1993; White, Klink, et al., 1998; Kopell, Ermentrout, et al., 2000; Schreiber, Erchova, et al., 2004; Wu, Enomoto, et al., 2005). Conceptually, single compartment simulations are broadly similar to acutely dissociated neuron studies. In both cases, dendritic and axonal processes are shorn away eliminating the contribution of gated dendritic currents and ectopic axonal spikes to the somatic electrophysiological profile.

An obvious limitation of the single compartment approach is the inability to accurately model processes that evolve spatially or that depend on the interactions of spatially separated ionic mechanisms. This limitation can manifest itself in one of two ways: a failure to model a particular process or the development of a conceptually inaccurate model of a process. These 'failure modes' are respectively illustrated in models developed to emulate the relationship between the excitatory peak of the PSTH and the underlying EPSP in cat motoneurons (Jones and Bawa 1997), and the stepwise repolarization of calcium spikes in cortical dendrites (Reuveni, Friedman, et al., 1993). In both cases the final simulations employed multi-compartment models because it was found that the target behaviour could not be accurately emulated using single compartment models.

The pitfalls associated with single compartment modelling can be largely avoided by a careful reading of the experimental literature in order to determine whether the processes of interest are spatially segregated. For example, there is good evidence that the most dramatic aspect of subicular pyramidal electrophysiology, the burst, is localised to the axosomatic region (Jung et al., 2001; Menendez de la Prida et al., 2003). Of relevance in this regard is the observation that synaptically evoked bursts are indistinguishable from those triggered by direct somatic current injection (Stewart 1997). More generally, there has been a steady accumulation of evidence for the active electrotonic compartmentalisation of dendrites and soma of central neurons (Hausser and Mel 2003).

2.3 Hodgkin-Huxley formalism

With the exception of the fast sodium current, the passive and active current models presented here conform broadly to the standard Hodgkin-Huxley (HH) formalism (Hodgkin and Huxley 1952). A HH channel consists conceptually of a transmembrane conducting pore and one or more gating particles that open and close the pore. The behaviour of a channel is determined by the voltage/ligand dependence and kinetics of its independent two-state ('open' and 'closed')

gating particles. For a channel to conduct all its gating particles must be in the open state. At the single channel level gating particles attain a value between 0 and 1 representing the probability of finding the gate in an open (1) or closed (0) position. At the channel population level the value is interpreted as the fraction of the population in the open position. There are two types of gating particles; activating and inactivating. With activating particles the probability of opening increases with increasing depolarization/ligand concentration. The converse holds for inactivating particles.

The open probability of a channel is therefore given by the product of the unitless time-dependent and voltage- and/or concentration-dependent open probabilities for the activation and inactivation gate (conventionally denoted by the letters m and h) raised to the empirically determined powers p and q, respectively. These powers represent the number of gates of each type carried by the channel. The current through a 'universal' HH channel is therefore simply described using a variant of Ohm's law.

$$I = g_{max} m^p h^q (V_m - E_{rev})$$

where g_{max} is the maximum conductance (for a single channel or a channel population), V_m is the membrane voltage, and E_{rev} is the reversal potential for the carrier ion(s). The current passing through the channel is thus the product of the maximum conductance, the open probability, and the electrochemical driving force (given by the difference between the membrane voltage and the reversal potential of the charge carrying ion).

2.3.1 Current types

By varying the available gating particles four fundamental HH current types emerge that constitute abstractions of known channel types:

2.3.1.1 Passive current

The passive channel has no gating particles and therefore the current through the passive channel is proportional to the potential difference across the membrane.

$$I = g_{max} (V_m - E_{rev})$$

2.3.1.2 Persistent (non-inactivating) current

The activation gate allows this current to turn on in response to increasing depolarization potentials. However, because this current lacks an inactivation gate it can only close when the membrane potential is hyperpolarized to a level below the activation threshold of the activation gate:

$$I = g_{max} m^p (V_m - E_{rev})$$

2.3.1.3 Transient (inactivating) current

A transient current turns on in response to depolarization. The inactivation gate ensures that this current will eventually turn off even if a highly depolarized voltage is sustained:

$$I = g_{max} m^p h^q (V_m - E_{rev})$$

2.3.1.4 Anomalous (activated by hyperpolarization) current

The anomalous current is the counterpart of the persistent current insofar as the probability of this channel being open decreases with increasing voltage. Anomalous currents do not inactivate:

$$I = g_{max} h^q (V_m - E_{rev})$$

2.3.2 Kinetics

The state dynamics of each gate are rooted in the mass action model of chemical kinetics and are described using a first-order kinetic scheme of the form

$$m\text{-}1 \underset{\beta_m}{\overset{\alpha_m}{\rightleftharpoons}} m$$

This scheme has the solution

$$m = m_{inf} + (m_0 - m_{inf}) e^{-t/\tau_m}$$

where m_{inf} is the steady state value of m at a particular voltage, m_0 is the initial open probability, and τ_m is the time constant of opening:

The rate constant functions α and β generally take an exponential, linear-exponential, or a sigmoid form, with the free parameters chosen to fit the empirical data for the steady state open probability, m_{inf}, and time constant function, τ_m, typically using a least-squares algorithm. The rate constants are related to m_{inf} and τ_m by

$$m_{inf} = \alpha_m / (\alpha_m + \alpha_m)$$

and

$$\tau_m = 1/(\alpha_m + \beta_m)$$

The empirically determined form of the steady state open probability, m_{inf}, is typically described using a sigmoidal 'Boltzmann' function of the form:

$$m_{inf} = \frac{1}{1 + e^{\frac{V_m + V_{half}}{k}}}$$

where V_{half} is the half activation voltage and k is the slope factor. The form of the empirical time constant function is more variable but typically takes some form of bell-shaped function, such as

$$\tau_m = \frac{\exp^{\frac{V+a}{b}}}{1+\exp^{\frac{V+c}{d}}}$$

where a, b, c, and d are the fitting parameters.

2.3.3 Constant field equation

The foregoing HH model assumes an ohmic (i.e. linear) relationship between channel current and membrane voltage. The ohmic assumption is well approximated where the concentration gradient of the permeant ion across the membrane is relatively low (as is the case for sodium and potassium) but is violated in the case of free calcium where the extracellular to intracellular concentration ratio is about 10^5. This results in a concentration-dependent rectification whereby calcium current flows more easily into the cell than out of it. Consequently, calcium current models are more accurately described by the Goldman-Hodgkin-Katz constant field equation (Goldman 1943; Hodgkin and Katz 1949) extension of the HH model

$$I_{Ca} = p_{max} m^p h^q z_{Ca}^2 \frac{VF^2}{RT} \frac{[Ca^{2+}]_i - [Ca^{2+}]_o \exp^{-z_{Ca}FV/RT}}{1 - \exp^{-z_{Ca}FV/RT}}$$

where p_{max} is the maximum channel permeability (cm/sec), z_{Ca} is the valency of calcium (i.e. 2), F is the Faraday constant (96487 coulombs/mole), R is the gas constant (8.3145 J/mol-K,), and T is the temperature in degrees Kelvin. $[Ca^{2+}]_o$ and $[Ca^{2+}]_i$ are the extracellular and intracellular concentrations of calcium, respectively.

2.3.4 Suitability of the HH model

A number of limitations of the canonical HH model of I_{NaF} have emerged since its original introduction during the early 50's. Perhaps the most significant is the discovery that the channel inactivation process is not independent of activation (Hille. 1992), as is assumed in the HH approach. The ability of the HH scheme to adequately model individual channels is also suspect. For example, Horn and Vandenberg (1984) performed a statistical analysis of the kinetics of single sodium channels in outside-out patches of tissue cultured GH3 cells derived from rat pituitary gland. These workers surveyed 25 different Markov models (of which the HH model is a constrained subclass) and concluded that the HH model was inadequate on the basis that it failed to adequately predict open time, closed time, first latency density functions, the probability of the channel being open after a step depolarization, the burst duration distribution, autocorrelation, and the distribution of number of openings per record (Horn and Vandenberg 1984). Clearly, the HH model is not necessarily the most appropriate scheme for simulating single channels.

2.3.5 Rationale for the HH model

Given the potential problems and limitations associated with the HH formalism why is it still so popular within computational neuroscience? Despite some theoretical shortcomings, the HH model is a robust and well-established phenomenological approach that captures many of the essential characteristics of large channel populations. Even in the realm of single channel modelling, the HH formulation can outperform certain Markov approaches (Chay 1991). Nonetheless, the superior generality of the Markov approach will always mean that it can operate successfully in situations where the HH approach fails.

2.4 Markov kinetic formalism

A Markov system is one in which the transitions between system states are stochastic and are independent of the history of the system. In a Markov channel model, the movement of a channel between different conformational states is defined by a set of first order differential equations. Markov models are described using state diagrams that define the available states and the permissible transitions between those states. Transitions between states are controlled by rate functions.

The simplest Markov model corresponds to the HH first order, two-state gate description described previously. However, whilst each state represents the position of a gate in the HH formalism, in the more general Markov approach each state represents the state of the entire channel protein. By breaking the gate independence criteria imposed by the HH approach, the Markov approach allows a far broader repertoire of channel models.

Although Markov models are the de facto approach for detailed modelling of channel biophysics, there is comparatively little use of Markov schemes in neural modelling (Destexhe, Mainen, et al., 1994). This appears to be primarily because Markov models tend to be less intuitive, and considerably more computationally expensive, than HH models (Borg-Graham, 1998). In the following chapter we develop, amongst other currents, Markov and HH models of the subicular fast sodium current in parallel.

Chapter III
SUBICULAR CURRENTS

A scientist must organize. One makes a science with facts in the same way that one makes a house with stones; but an accumulation of facts is no more a science than a pile of stones is a house.

Henri Poincare (1854-1912)

3.1 Abstract

The intrinsic firing properties of nerve cells vary widely across neuron types. Properties such as the geometry of the action potential, the trajectory of the membrane potential before and after the spike, and reaction of a neuron to sustained inputs are all subject to variation, between neurons and even within the same cell at different times. The substrate for these variegate electrophysiological behaviours is the complement of ion channels present in the cell membrane. In this chapter, we analyse the contribution of the salient currents produced by these channels to hippocampal and subicular electrophysiology. We then develop models of subicular currents carefully constrained by the available subicular empirical literature.

3.2 Overview

There is a comparative dearth of detailed information on subicular currents. This forces a reliance on core current descriptions from related brain areas. Fortunately, the known electrophysiology of subicular pyramidals provides many constraints on the possible current models and permits the development of plausible models of subicular currents based on non-subicular templates. The structure of each current section in this chapter reflects this approach. Firstly, a detailed overview of each current is provided with a particular emphasis upon hippocampal currents. This overview is typically broken down into subsections that cover topics such as channel structure, neuronal distribution, gating properties (e.g. activation dependence and kinetics), modulators and inhibitors, and function. The function subsection covers some of the conspicuous electrophysiological events, such as bursting or spike frequency adaptation, that the particular current is known to participate in. Secondly, this analysis is then repeated for the

subiculum. The final section draws together the insights regarding the properties of the subicular variant and covers the development of the current model.

3.2.1 Limitations of voltage clamp data

A certain degree of interpretational latitude is inevitable in neural modelling; artefacts in voltage-clamp recordings, intrinsic biological variability, errors in measurement and differences in experimental protocols, combined with the modeller's necessary kinetic and morphological simplifications conspire to ensure that accurate current clamp simulations are rarely achieved by the direct insertion of voltage clamp data. This situation is compounded by the fact that the complement of currents modelled in most cell simulations is rarely comprehensive and reflects only a selected subset of known channels. As a result, such data can only provide a broad empirical framework within which the kinetics of prominent conductances may be modified in the attempt to robustly reproduce salient features of neural activity.

The expediency of this assumption is justified by reference to the success of other composite cell simulations in reproducing prominent aspects of the behaviour of a wide variety of neuronal subtypes including CA1 and CA3 pyramidal neurons (Borg-Graham 1987; Jaffe, Ross, et al., 1994), Purkinje neurons (De Schutter and Bower 1994) and thalamic relay neurons (Huguenard and McCormick 1992).

3.2.2 Which channels should be modelled?

The number of channels expressed in the hippocampal complex is considerable (Brown, Gahwiler, et al., 1990; Storm 1990) and far exceeds the 14 channel types described in our model. Most channel types exist in a number of isoforms that differ in their kinetics and pharmacological and/or activity-dependent regulation sites (Froehner 1988; Schaller, Krzemien, et al., 1995; Maletic-Savatic, Lenn, et al., 1995). A brief perusal of the IUPHAR Ion Channel Compendium (2005), a comprehensive online database of currently recognised ion channels, suggests that the number of basic voltage-gated sodium and calcium channels and voltage- and calcium-gated potassium channels is well in excess of eighty.

This estimate does not account for alternative ancillary subunits, gene splice variants, differential post-translational processing (such as phosphorylation), functional modification by neuromodulators, and blithely ignores entire ion channel families such as the cyclic nucleotide-modulated channels, the fast inward rectifiers, and the transient receptor potential channels.

These possibilities constitute a combinatorial explosion in the total number of individual channel types present in a particular organism and potentially raises the number of distinct channel subtypes into the thousands.

In the face of such complexity it is necessary to make certain simplifying assumptions in order to make the problem of modelling the currents flowing through the cell membrane more tractable. A central assumption employed in this thesis is that the salient electrophysiological features of a neuron can be captured by a relatively small class of functionally distinct currents - regardless of the number of ion channel subtypes subserving that current. For example, Purkinje cells express at least three fast sodium channel isoforms with slightly different properties (Vega-Saenz De Miera, Rudy, et al., 1997). Whilst, the mouse hippocampal A-type potassium current can be resolved into at least three distinct components (Li and McArdle 1997). In other words, although each functionally distinct voltage- and/or calcium-gated current can almost certainly be empirically dissected into distinct classes of subcurrents carried by distinct channel subtypes. We will assume that the collective impact of these subcurrents can be adequately characterised as a composite current.

In essence, in attempting to develop 'biophysically realistic' neural models we will behave as if the electrical properties of subicular neurons are defined by a relatively small number of compound sodium, potassium and calcium currents, each of which is carried by a hybrid ion channel population that represents the collective operation of a number of channel subtype populations.

3.3 Functional classification of channels based on firing

Descriptions of ion channels are conventionally organised by ion species. However, for the purposes of this thesis, ion channels are organised according to their functional properties. Since the firing pattern of a neuron is determined by the complement of ion channels it carries, a functional classification provides a convenient conceptual framework within which to understand the mechanisms by which particular currents contribute to particular firing patterns. As noted previously, the HH approach allows the classification of basic current types such as transient, persistent and anomalous. Bargas and Galarraga (1995) developed a simple functional channel classification by extending this framework. They divided ion channels into broad functional families depending on the form of activation profile (transient, persistent or anomalous) and the direction of charge flow (inward or outward). Five groupings of currents arise out of this

approach: transient inward, persistent inward, transient outward, persistent outward, and anomalous (Bargas and Galarraga 1995). A complementary functional framework utilises the relative activation voltage range (i.e. resting, subthreshold, suprathreshold) of the channels (Storm 1990). These functional families of ion channels serve as a productive conceptual framework for scaffolding thinking about neural modelling. We have found that the process of developing effective cell models is appreciably furthered by the use of such functional frameworks.

3.3.1 Transient inward currents

Activation of transient, or fast inactivating, inward currents results in an explosive positive feedback that responsible for the action potential, the most dramatic aspects of neural activity. The rate in inactivation for these channels ranges from milliseconds (fast transient sodium current, I_{NaF}, and the residual calcium current, I_{CaR}) to tens of milliseconds (transient calcium current, I_{CaT}, and the neuronal calcium current, I_{CaN}). The amplitude and duration of the transient current contributes substantially to the time-course of the spike. Because these channels can be de-inactivated by hyperpolarization their contribution of the neuronal response can be shaped by the input history of the neuron (Bargas and Galarraga, 1995). Thus, I_{CaT} can drive rebound bursts from very negative potentials and effectively confer a hyperpolarized firing threshold upon the neuron (McCormick and Huguenard, 1992).

3.3.2 Persistent inward currents

Like the transient currents, activation of these currents causes a positive feedback response. Although the maximum amplitude of these persistent currents is generally too small to drive voltage spikes, the gradual regenerative depolarizations these currents engender can reach threshold. Persistent inward currents, such as I_{NaP} and I_{CaL}, can dramatically augment the behavioural repertoire of the neuron by facilitating events such as prepotentials, subthreshold oscillations, and bursting.

3.3.3 Transient outward currents

Fast inactivating outward currents, such as I_A and I_{CT}, are important in spike repolarization and repetitive firing. Due to their rapid inactivation kinetics, these currents are largely switched off between spikes, but their fast kinetics allow them to oppose initial depolarization and mediate a

delay in firing. The duration of the delay is controlled by the inactivation time constant of the current and constitutes a form of 'time threshold' (Bargas and Galarraga, 1995).

3.3.4 Persistent outward currents

Persistent, or slowly inactivating, outward currents serve as a negative feedback system for decreasing the excitability of a neuron. Currents, such as I_M and I_D, oppose the depolarization of the cell membrane by activating under depolarization, causing the membrane to hyperpolarize and thereby causing the persistent outward current to deactivate. The functional consequences of this behaviour are that the effective stimulus required to reach the firing threshold is raised, the firing threshold is stabilised and, a drop in frequency gain due to spike frequency adaptation (Bargas and Galarraga, 1995).

3.3.5 Anomalous currents

The class of anomalous rectifiers acts to stabilise the resting membrane potential by generating an inward current in opposition to hyperpolarizing stimuli and deactivating upon depolarization. There are two basic types, fast inward rectifiers, I_{FIR}, (Segal, Barker, et al., 1987) and the slow mixed cation anomalous rectifier, I_H (Halliwell and Adams 1982). Beyond their generic membrane stabilising activities, the key role of I_{FIR} is to alter the electrotonic length of the dendrites to alter as a function of network activity. Since we utilise single compartment models, for the purposes of this thesis, we neglect the I_{FIR} and focus upon the functionally salient I_H.

3.4 Molecular classification of ion channels

For completeness, in this section we provide a brief overview of the molecular properties of the sodium, potassium, and calcium ion channels.

3.4.1 Sodium channels

Voltage-gated sodium channels are large transmembrane glycoproteins that serve as Na^+-selective pores in the membranes of excitable cells (Hille. 1992). Sodium channels form the root of a superfamily of ion channels that includes voltage-gated potassium and calcium channels. Nine mammalian sodium channel isoforms of subfamily 1 (currently the only recognised subfamily) have been identified and functionally expressed (Catterall, Goldin, et al., 2003). The functional properties of these sodium channel isoforms are comparatively similar and this is

reflected in a greater than 50% similarity in amino acid sequence for the channel transmembrane and extracellular domains (Goldin 2001).

The standardised International Union of Pharmacology (IUPHAR) nomenclature for ion channels consists of the permeating ion, the principal channel regulator, the gene subfamily, the channel isoform and the splice variant. For example, the 'a' splice variant of isoform 1 of the voltage-gated sodium channel from gene subfamily 1 is designated as $Na_{V1.1}a$. Four sodium channel isoforms are expressed primarily in the central nervous system, $Na_{V1.1}$, $Na_{V1.2}$ (and a splice variant termed $Na_{V1.2}a$), $Na_{V1.3}$, and $Na_{V1.6}$.

Structurally, sodium channels consist of a pore-forming α subunit, with a molecular mass of approximately 260 kD, associated with auxiliary β subunits (Catterall 2000). Whilst the highly processed α subunit is sufficient for basic sodium-selective channel functionality, the precise kinetics and voltage dependence of the fully constituted sodium channel gating are determined by the β subunits. In the CNS, the channel exhibits one of two possible trimeric compositions: α-β_1-β_2 or α-β_3-β_2. In contrast, the skeletal muscle variant is a dimer composed of the α and β_1 subunits.

The α subunit is composed of four homologous domains (I-IV) of six transmembrane α helices each (S1-S6). Segments S5 and S6 line the inner exit from the pore (on the cytosolic side) and a pore loop, between segments S5 and S6, serves to line the outer entry to the pore. Receptor sites on the α subunit are the target for all known pharmacological agents including the important experimental tools, tetrodotoxin and saxitoxin, which have been localised to neurotoxin receptor site 1 (Fozzard and Hanck 1996).

The S4 segments in each domain subserve sodium channel activation. Each S4 segment contains positively charged amino acid residues at every third position. Channel activation occurs when these 'gating charges' are moved across the membrane in response to membrane depolarization. A short intracellular loop, lying between domains III and IV, functions as the sodium channel inactivation gate. During sustained depolarization this loop folds into the channel pore thereby blocking it from the inside (Catterall, Goldin, et al., 2003).

3.4.2 Potassium channels

As with the sodium channels, the potassium channels are composed of a pore-forming α unit with associated β subunits. The extensive set of potassium α subunits are divided into voltage-

gated (12 subfamilies covering 38 members), calcium-gated (5 subfamilies with 8 members), inward rectifiers (7 subfamilies with 15 members) and the two-pore channels (17 subfamilies of 1 member each). Although originally thought to be inward rectifiers (Lesage, Guillemare, et al., 1996), the functional role of the two-pore family of channels is currently unknown.

3.4.3 Calcium channels

Each calcium channel is composed of four or five subunits of which the largest (190–250kDa) and most significant is the α_1 subunit, which contains the voltage sensor and conductance pore. Calcium channels are organised into three α subunit subfamilies comprising 10 members each. The α_1 unit of voltage-gated calcium channels shares a similar molecular structure to that of the sodium channel family in that they are composed of four homologous domains (I-IV) of six transmembrane segments (S1-S6) each. The voltage sensor function is subserved by segment S4, whilst the pore loop linking segments S5 and S6 controls ion conductance and selectivity. Interestingly, conversion of a sodium channel into a calcium-selective channel only requires the modification of three amino acids in the pore loops of domains I, III, and IV (Catterall 2000).

3.4.4 Chloride channels

The position of chloride as the most abundant extracellular anion is reflected in the diverse range of cellular functions in which chloride channels participate. Functions include regulation of intracellular pH (Brown and Dudley 1996) and cell volume (Hoffmann and Dunham 1995), stabilisation of the membrane potential (Franciolini and Petris 1988) and signal transduction (Jentsch and Gunther 1997).

Despite the obvious importance of chloride in neuronal function, chloride currents are routinely omitted from neural simulations. This is presumably because the primary effect of chloride conductances, stabilisation of the membrane potential, can be approximated by an appropriate value for the membrane input resistance. In keeping with our implied philosophy of parsimony, the present model omits chloride currents.

3.5 Fast sodium current, I_{NaF}

3.5.1 I_{NaF} overview

The voltage-gated fast sodium current, I_{NaF}, drives the rising phase of the action potential and is, by a large margin, the largest and fastest membrane current. As a result, the kinetics of this channel plays a crucial role in shaping the repetitive and bursting properties of the cell.

3.5.2 Channel

As described in more detail previously, the sodium channel responsible for the fast sodium current consists of a pore-forming α subunit associated with auxiliary β subunits that modify the precise kinetics and voltage dependence (Catterall 2000).

3.5.3 Distribution of isoforms

In neocortical neurons, there appear to be no substantive differences between pyramidal and non-pyramidal cell types in the voltage dependence of activation, inactivation kinetics, voltage dependence of steady-state inactivation, and recovery from inactivation (Huguenard, Hamill, et al., 1988). Likewise, the ionic selectivity gradient of the voltage-dependent sodium channel of rat central nervous system neurons is similar to that in the squid axon, myelinated frog nerve fibre and rat ventricle muscle (Kaneda, Oomura, et al., 1988). Such evolutionary conservation of kinetic and ionic properties implies that the differences in action potentials between pyramidal and non-pyramidal cell types are largely due to differences in sodium channel density.

3.5.4 Sodium channels in the dendrites

Substantial evidence supports the existence of sodium channels in the dendrites. Autoradiographic analysis using radiolabeled tetrodotoxin (TTX), a selective sodium channel inhibitor, revealed the presence of putative sodium channels in the proximal and distal dendrites, as well as the soma (Mourre, Cervera, et al., 1987). Several papers report dendritic sodium spikes (Benardo, Masukawa, et al., 1982; Colling and Wheal 1994; Hausser 2000), although relatively high stimuli are required to initiate spikes in the dendrites (Coulter, Huguenard, et al., 1989). Fast spikes recorded intracellularly from isolated dendrites (Benardo, Masukawa, et al., 1982) are similar to those of somatic origin. Two forms have been described with similar rise-times but slightly different decay rates with mean durations (at 37°C) of 1.21 and 2.85 ms.

3.5.5 Gating properties

An orthodox Hodgkin-Huxley fast sodium current is expressed in the soma and dendrites of dissociated guinea pig (Sah, Gibb, et al., 1988) and rat (Kaneda et al., 1988) hippocampal neurons. In guinea pig, the somatic current has an activation threshold of -60 mV with a time-to-peak of 0.9 ms at 0 mV measured at 23˚C. Activation is described by a Boltzmann expression with a half-activation voltage (V_{half}) of -39 mV and a slope factor (k) of 6.6 mV, yielding a gating particle valency of about 4. Inactivation fits a Boltzmann expression with a V_{half} of -75 mV and k of 7.7 mV. Inactivation is complete throughout the activation range with no overlap between the activation and inactivation curves implying that the steady-state conductance or 'window current' is negligible (Sah et al., 1988).

3.5.6 Slow inactivation

Sustained tonic or phasic depolarizations can induce a form of slowly recovering inactivation in the fast sodium channels of the somata and dendrites of CA1 pyramidals (Colbert et al., 1997; Jung et al., 1997). The recovery from, and degree of, slow inactivation is both voltage- and frequency-dependent (Mickus, Jung, et al., 1999). The level of slow inactivation in the dendrites also increases linearly with distance from the cell body until it plateaus at about 200 μm from the soma. This gradient has been proposed to regulate dendritic excitability by reducing the amplitude of back-propagated action potentials (Jung et al., 1997).

3.5.7 Window currents

In the Hodgkin-Huxley formalism, a small steady state current, known as a window current, is generated at membrane potentials where the activation and inactivation curves of I_{NaF} overlap (Patlak 1991). The voltage dependence of this current is bell shaped. Activity tapers to minimal levels beyond 15 mV either side of a peak located at about -40 mV. The maximal activity is less than 2% of I_{NaF} at the same potential (French, Sah, et al., 1990).

3.5.8 Modulation

Across the central nervous system, sodium channel activity is actively regulated in neurons in response to physiological signals (Cantrell and Catterall 2001). For example, the firing and signal processing properties of medium spiny neurons of the striatum are modified by dopamine which activates the cAMP pathway via D_1-like receptors to reduce sodium currents and, consequently, the generation of action potentials (Cantrell, Scheuer, et al., 1999). In hippocampal

CA1 neurons, activation of muscarinic acetylcholine receptors inhibits intrinsic burst firing by a reduction in the peak sodium current and a slowing down of channel inactivation (Cantrell, Ma, et al., 1996). This change in sodium channel behaviour is partly mediated by protein-kinase-C-dependent phosphorylation of the inactivation gate (Colbert and Johnston 1998). Other second messenger systems implicated in sodium channel modulation includes the tyrosine kinase pathway (Hilborn, Vaillancourt, et al., 1998), G-protein subunits (Ma, Catterall, et al., 1997) and the calcium-sensing calmodulin system (Tan, Kupershmidt, et al., 2002).

3.5.9 Function

The primary function of the classical fast transient sodium channel is to generate the strong current needed to overcome membrane capacitance and resistance and drive the upstroke of the self-regenerating action potential. Several additional roles for dendritic fast sodium channels have been proposed including amplification of synaptic inputs (Crill 1999; Gonzalez-Burgos and Barrionuevo 2001), supporting back propagation of spikes into the dendrites (Stuart and Sakmann 1994), boosting of "graded" transmission in non-spiking neurons (Zenisek, Henry, et al., 2001), and providing a contribution to the bursting properties of central neurons (Magee and Carruth 1999; Turner, Maler, et al., 1994).

3.5.10 I_{NaF} in the subiculum

3.5.10.1 Spike threshold

Given the overwhelming contribution of the I_{NaF} to the rising phase of the action potential a number of characteristics of the underlying current dynamics may be inferred from the spike threshold. Chiefly, the foot of the activation curve of I_{NaF} must be within several mV of the spike threshold - assuming there is not significant steady state inactivation of I_{NaF} at the resting potential. Spike thresholds reported for action potentials in subicular pyramidal cells range from (the average V_{rest} for the study follows in brackets) -46.2 mV (-67) (Staff, Jung, et al., 2000), -50.0 mV (-64 mV) (Wellmer, Su, et al., 2002), -54.3 mV (-65 mV) (Behr, Empson, et al., 1997) (each of the preceding values is an average over cell groups with firing thresholds that were not statistically different) and -49 mV (-64 mV) (Mason 1993). The threshold-V_{rest} difference ranges from about 10 to 20 mV.

Menendez de la Prida (2003) observed statistically significant differences between the firing thresholds of strong bursters (-47.9 mV), weak bursters (-51 mV) and regular firing cells (-41.8

mV) without seeing any differences in the resting membrane potentials of the three cell types. Since the firing threshold is largely determined by the position of the I_{NaF} activation curve, this result implies that the activation characteristics of I_{NaF} in each cell group are substantially different.

Such variation in firing thresholds is potentially related to differences in I_{NaF} subunit isoform expression between and within cell types. This idea receives some support from molecular studies of the properties of the α subunits. The voltage dependence of activation and inactivation of sodium channel α subunits expressed individually in exogenous expression systems are shifted positively or negatively depending on the combination of co-expressed β subunits (Qu, Curtis, et al., 2001). The possibility of active splice variants increases the range of potential sodium channel configurations and attendant voltage dependent properties for these currents. As noted above, hippocampal I_{NaF} is also subject to modulatory control, so this variation in firing threshold could constitute evidence that subicular pyramidal subtypes are differentially regulated. Whilst we will argue in subsequent sections that this is indeed generally the case, for the purposes of developing a subicular I_{NaF} model we will assume that a similar fast sodium channel is shared by all subicular pyramidals.

3.5.10.2 Burst spike thresholds

Since a key feature of the burst is a depolarizing envelope, a characteristic corollary is that the firing threshold of successive spikes increases. In the subiculum, the difference in threshold between the first and last spikes of a burst depends on the number of burst spikes and can be substantial. For example, in a figure illustrating zero Ca^{2+} bursting in Jung et al. (2001) this difference is nearly 15 mV. For conventional bursts this difference is less pronounced but can range up to 10 mV (Stewart and Wong, 1993).

3.5.10.3 Kinetics

The most comprehensive study of sodium currents in subicular pyramidals to date was by Vreugdenhil et al. (2004) who assessed the pharmacologically isolated human sodium current in dissociated subicular neurons from patients with temporal lobe epilepsy (TLE). Their experiments were performed at 23˚C using a whole-cell voltage clamp protocol. Control cells were derived from the rat subiculum.

3.5.10.4 Activation

Vreugdenhil et al. (2004) used two protocols to determine the voltage dependence of the activation process. The first process assessed currents elicited after a 500 ms conditioning potential of -120 mV followed by a stepwise series of 10 ms depolarizations that ranged from -70 mV to 0 mV. The evoked current was fitted to a mono-exponential function on the assumption that the 10 ms interval ensures that the current decay represents only fast transient current whilst the persistent current remains constant.

The voltage dependence of the activation was fitted to a Boltzmann equation. No statistical differences were found between the half-activation voltage of the transient sodium current components in groups of cells with low (-35.9 mV) or high (-39.6 mV) percentages of persistent current or in rat cells (-34.7 mV). The respective values for the Boltzmann slope factors are 4.4, 4.6 and 4.9 mV. The fact that no significant differences were found in the steady state activation characteristics of fast sodium current of the human and rat suggests a high level of evolutionary conservation and lends credence to the assumption of kinetic uniformity.

The average transient half-activation voltage of -36.7 mV is significantly higher than the value of about -46 mV for the persistent sodium current in subiculum but 5-10 mV but more hyperpolarized than CA1 and neocortical cells from a similar patient set (Vreugdenhil, van Veelen, et al., 1998). In a subgroup of human cells expressing high levels of persistent sodium current, an alternative subtractive protocol was also used to reduce the likelihood of contamination of the analysis by sodium channels with intermediate inactivation kinetics, non-TTX sensitive components and leak. As in the first protocol, the half activation voltages of the transient (-35.4 mV) and persistent (-42.4 mV) components of the sodium current were found to be significantly different. Similar results were found for a single rat cell.

3.5.10.5 Activation kinetics

The time-to-peak of the transient component at -30 mV was 0.76 ms in rat pyramidals (Vreugdenhil, Hoogland, et al., 2004), which is comparable with the value of about 0.5 ms obtained for the transient sodium current in CA1 neurons (Sah, Gibb, et al., 1988).

3.5.10.6 Deactivation kinetics

Although not explicitly measured, rapid deactivation kinetics for subicular I_{NaF} can be inferred from the Vreugdenhil et al. (2004) paper. Cells with a low fraction of I_{NaP} exhibit a fast mono-

exponential sodium current decay time course, following termination of the command pulse that appears broadly similar to the activation kinetics. For this reason, we treat activation and deactivation kinetics as symmetrical and do not model deactivation separately.

3.5.10.7 Inactivation

The inactivation of the fast sodium current in human and rat subicular pyramidal cells is both rapid and complete. Vreugdenhil et al. (2004) investigated the voltage dependence of inactivation using a tail current analysis protocol in which a variable voltage (from -140 to -30 mV) conditioning step of 500 ms was used to attain steady state inactivation before depolarization to a fixed voltage (10 ms at -20 mV). The initial amplitude of the tail current at the fixed voltage was proportional to the percentage of channels remaining open at the conditioning voltage. The subsequent fit to a Boltzmann equation modified to account for the persistent component yielded steady state half inactivation voltages of -74.8, -71.2 and -66.7 mV for cells with a human cells with a high and low percentage of persistent sodium current and rat cells, respectively. There was a significant difference between the human cell groups and between the human and rat cell groups. The corresponding slope factors were -7.6, -6.9 and 6.3 mV. The voltage dependence of both activation and inactivation of I_{NaF} derived from TLE patients was found to be 5-10 mV more hyperpolarized than that of TLE I_{NaF} derived from CA1 (Vreugdenhil, van Veelen, et al., 1998) or neocortex (Vreugdenhil, van Veelen, et al., 1998). Vreugdenhil et al. (2004) suggested an explanation for this difference in terms of the effects of "subtle differences in incubation methods", presumably based on the assumption that the voltage dependencies of the various channels should be similar.

3.5.10.8 Inactivation kinetics

Cooper et al. (2005) report a time constant of inactivation at 32-35˚C for I_{NaF} of 0.35 ms at 0 mV. Vreugdenhil et al. (2004) did not systematically characterise I_{NaF} inactivation kinetics but did note an average time constant of inactivation for a step from -100 mV to -30 mV of 2.5 ms in human cells at 23˚C (rat kinetics were similar). Voltage clamp experiments with the isolated sodium current show that I_{NaF} inactivates within 1 ms under a voltage step from -70 to +20 mV (Jung et al., 2001).

3.5.10.9 Window current

In neurons with a small I_{NaP} component, Vreugdenhil et al. (2004) observed a small current with a bell-shaped voltage dependence that they suggested was a putative window current. However, the peak activation potential of about -30 mV for this current is well outside the overlap region, centred on -50 mV, of the steady state in-/activation curves reported in the same paper for both high and low I_{NaP} containing populations.

3.5.11 Subicular I_{NaF} model

Subicular bursts are characterised by spikes with successively higher firing thresholds. The evident ability of subicular I_{NaF} to effectively recover from inactivation at these depolarized potentials poses significant problems for models based on the Hodgkin Huxley formalism. Conventional HH models possess a single threshold determined by the voltage dependence of the activation state variable. Accordingly, we developed two sodium channel models, a conventional HH model (Figure III-1) and a more complex 5-state Markov model (Figure III-2).

3.5.11.1 HH model of I_{NaF}

A conventional m3.h format was used for the HH I_{NaF} model

$$I_{NaF} = g_{NaF} m^3 h (V_m - E_{Na})$$

3.5.11.2 Activation

The activation curve for rat I_{NaF} recorded at 23˚C by Vreugdenhil and colleagues yields a firing threshold in the -55 to -45 region. This threshold range is similar to that obtained for rat subicular neurons at 33˚C which suggests that subicular I_{NaF} activation does not require significant adjustment for temperature. This insensitivity of the I_{NaF} activation curve to temperature appears to be a general phenomenon (Reckziegel, Beck, et al., 1998).

$$m_{inf} = \frac{1}{1 + e^{\frac{V-(-38.2)}{-6.29}}}$$

3.5.11.3 Activation kinetics

Vreugdenhil and colleagues (2004) did not systematically characterise the voltage dependence of I_{NaF} activation kinetics but did report a time-to-peak at -30 mV of 0.76 ms (at 23˚C) for rat. This value is somewhat slower than the roughly 0.5 ms reported by Sah and colleagues (1988) at the

same temperature in guinea pig CA1 pyramidals. To compensate for temperature effects we scaled the activation and inactivation kinetics of I_{NaF} using a Q_{10} of 2. To model the time constant as a function of voltage we used an equation similar in form to that employed by Warman et al. (1994) in their model of CA1 I_{NaF} and fitted it to the temperature-scaled Vreugdenhil et al. (2004) data.

$$\tau_m = \frac{e^{\frac{V-99.5}{110.9}}}{1+e^{\frac{V+23.4}{14.9}}}$$

3.5.11.4 Inactivation

We shifted the inactivation curve for I_{NaF} determined by Vreugdenhil et al. (2004) to more positive potentials in order to compensate for temperature effects (Schwarz 1988; Sah, Gibb, et al., 1988).

$$h_{inf} = \frac{1}{1 + e^{\frac{V-(-62.7)}{6.3}}}$$

3.5.11.5 Fast inactivation kinetics

We modelled the inactivation kinetics using an exponential equation adjusted to match the reference points of 0.36 at 0 mV provided by Cooper et al. (2005) and 1.5 ms (scaled from 2.5 ms) at -30 mV derived from Vreugdenhil et al. (2004).

$$\tau_h = -0.58(-0.078 - e^{-0.026V})$$

3.5.11.6 Maximum conductance

Vreugdenhil et al. (2004) report a maximum conductance of 63 nS for dissociated rat subicular pyramidals. The final value for the model was 2 μS. This is an order of 2 higher than that reported empirically but was necessary in order to enable the cell model to switch firing mode when g_{NaF} was substantially reduced (Cooper, Chung, et al., 2005). Both regular and burst firer I_{NaF} conductances are assumed to be similar in magnitude (Staff et al., 2000).

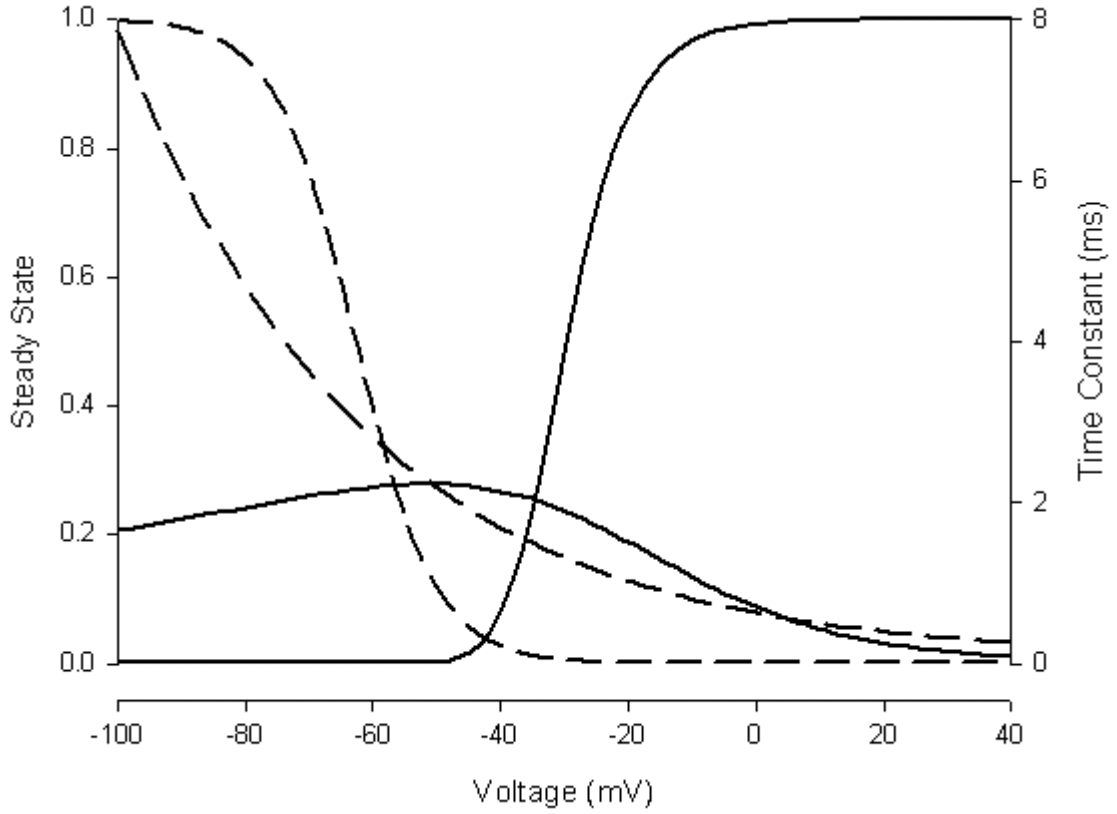

Figure III-1. Plot of the activation (solid lines) and inactivation (dashed lines) steady state and time constant curves for I_{NaF}. The steady state activation curve is raised to its exponent of 3. In order to fit the inactivation and activation curves on the same graph the activation time constant is scaled by a factor of 10.

3.5.11.7 Conclusions regarding the HH I_{NaF} model

Unfortunately, although our HH I_{NaF} model was developed based on a careful reading of the subicular literature we were unable to accurately emulate the action potential threshold for progressive burst spikes using this HH I_{NaF} channel model. Our model was unable to de-inactivate sufficiently at suprathreshold voltages to drive realistic secondary spikes. Unsurprisingly, attempts to increase the available channel at higher thresholds by adjusting the gating equations were unsuccessful.

3.5.11.8 5-state Markov model of I_{NaF}

In order to more effectively emulate subicular I_{NaF} behaviour we developed a 5-state Markov model of the channel population. This model is an adapted and extended version of a 4-state

Markov model of CA1 I_{NaF} developed by Borg-Graham (1998). The salient feature of our model is that it exhibits a range of firing thresholds that are dependent on the firing history of the cell.

Our model is composed of an open state (O), an inactive state (I), and three closed states (C1-C3). At any given time each state has an associated probability that represents the fraction of the channel population in that state. In the state diagram, arrows represent permissible state transitions. The rate constants associated with each state transition determine the distribution of channels amongst the states. All of the rate constants are voltage-dependent functions (with the exception of the open to inactive transition) such that the fractional occupancy of these states changes with the prevailing voltage.

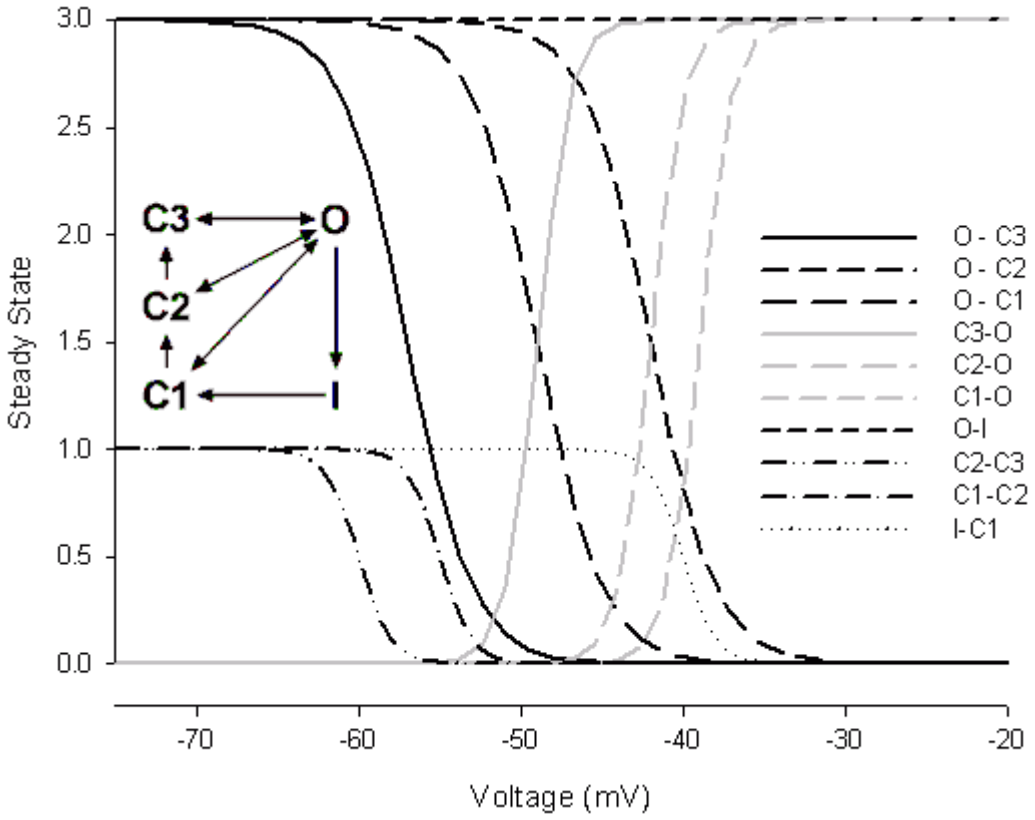

Figure III-2. The rate constant functions for state transitions in the 5-state fast sodium current Markov model. Also pictured is the state transition diagram for the channel model (inset).

The rate constant functions governing the transition to the conducting or open state from each of the three closed states (C1, C2, and C3) determine the firing thresholds associated with these states. The C1 to O firing threshold is the most depolarized (approximately -43 mV), whilst the C3 to O threshold is the most hyperpolarized at about -55 mV. Since the channel population can be variably distributed amongst the closed states the current can exhibit a range of intermediate

firing thresholds depending on the voltage history. The roughly 10 mV range for potential firing thresholds was chosen based on observed differences between the first and last burst spike thresholds (Stewart and Wong, 1993; Staff et al., 2000).

Although this model is intended as a phenomenological description of I_{NaF}, and is not necessarily empirically accurate, we were able to use it to successfully emulate a broad range of subicular behaviours including spike doublet firing and bursting.

3.6 Low threshold transient calcium current, I_{CaT}

One of the earliest reports of the presence of a low-threshold transient calcium current, I_{CaT}, in hippocampal neurons was by Halliwell (1983) in Guinea-pig CA1. This calcium current was activated by potentials positive to about -60 mV and was totally inactivated at -50 mV (Halliwell 1983).

Perez-Reyes (2002) listed the hallmark features of the T-type current

1. They are activated by small excursions of the membrane voltage from rest (LVA)
2. They are transient during sustained depolarizing pulses
3. They slowly diminish upon membrane repolarization to generate a tail current
4. They are carried by channels with 'tiny', and equivalent, single-channel conductance of Ba^{2+} and Ca^{2+}
5. They are relatively insensitive to dihydropyridines; and
6. They have similar voltage ranges for steady-state inactivation and activation.

3.6.1 Channel

Members of Cav3 α subunit family carry the T-type current. At least three subtypes have been expressed and characterised; α3.1, 3.2, and 3.3. (Cribbs, Lee, et al., 1998; Perez-Reyes, Cribbs, et al., 1998; Lee, Daud, et al., 1999). Consistent with the observation that native I_{CaT} is not dependent on auxiliary subunits (Lambert, Maulet, et al., 1997), is the finding that these genes are sufficient for the expression of I_{CaT} in the absence of other subunits (Lacinova 2004). Post-translational processing leads to a number of splice variants that differ somewhat in their kinetics and voltage sensitivity (Mittman, Guo, et al., 1999) and further extend the functional possibilities for the T-type current. Cloned T-type channels subtypes generally exhibit little difference in the

voltage ranges of activation or inactivation although there is comparatively large variation in the inactivation time constant (Klöckner, Lee, et al., 1999).

Although, the charge carrier influences the I_{CaT} amplitude in acutely dissociated CA1 pyramidals (the peak amplitude ratio for Ca^{2+}:Ba^{2+}:Sr^{2+} is 1.0:0.85), the channel kinetics of I_{CaT} are generally not dependent on the choice of permeant ion (Takahashi, Ueno, et al., 1991).

3.6.2 Distribution

T-type channels are expressed throughout the body, in tissues as diverse as nervous tissue, heart, kidney, smooth muscle, and sperm (Perez-Reyes, Cribbs, et al., 1998). Within the neuron, I_{CaT} is preferentially found in the dendrites (Pouille, Cavelier, et al., 2000; Magee and Johnston 1995; Markram and Sakmann 1994). Although, the presence of a calcium-dependent subthreshold depolarization in cultured rat embryonic neurons, prior to the development of processes, provides evidence for a significant somatic presence (Yaari, Hamon, et al., 1987). Overall, T-type current density in dendrites has been estimated to be about five times higher than that in the soma (Destexhe, Neubig, et al., 1998). CA3 neurons exhibit a higher incidence of T-type channels than CA1 or dentate granule cells which may account for the characteristic endogenous bursting behaviour of CA3 neurons (Fisher, Gray, et al., 1990).

3.6.3 Activation

The half-activation voltage is roughly -45 mV for all subtypes (Klöckner, Lee, et al., 1999). In dissociated rat CA1 neurons, for example, the current threshold is around -60 mV with a current peak at -30 mV (Takahashi, Wakamori, et al., 1989).

3.6.4 Activation kinetics

The activation time constant for I_{CaT} varies, depending on the subtype, from 1 to less than 10 ms at -10 mV (Klöckner, Lee, et al., 1999). Of functional interest, Randall and Tsien (1997) found that in response to a simulated action potential, the kinetics of T-type channels caused the peak current to be delayed compared to R-type and other HVA channels. Further, the effects of broadening the spike on current influx was significantly more pronounced for I_{CaT} than I_{CaR}. Overall, I_{CaT} both reached its peak and declined more slowly than HVA calcium currents.

3.6.5 Inactivation

In CA1 pyramidals, at 22˚C the steady-state inactivation of T-type Ca^{2+} current conforms to the Boltzmann equation with a half-inactivation voltage of -79 mV and a slope factor of 6.0 mV (Takahashi, Ueno, et al., 1991). The corresponding values for CA3 dendritic T-type currents are -80 mV and -6.4 mV (Avery and Johnston 1996). The half-inactivation voltage of the cloned T-type α subunits centres around -72 mV (Perez-Reyes, Cribbs, et al., 1998).

3.6.6 Inactivation kinetics

Broadly speaking, T-type inactivation is slow at -60 mV, accelerates from -50 to -30 mV and is relatively constant beyond this (Perez-Reyes 2003). Above around -30 mV, I_{CaT} inactivates rapidly with a time constant of inactivation of between 15 and 30 ms (Fishman and Spector 1981). Inactivation rates differ between T channel subtypes. The $Ca_{V3.1}$ and $Ca_{V3.2}$ display fast inactivation, while $Ca_{V3.3}$ is responsible for a more slowly inactivating current with an inactivation time constant of about 70 ms at -10 mV (Huguenard, Gutnick, et al., 1993; Lee, Daud, et al., 1999; Talley, Cribbs, et al., 1999). If these anomalous forms are excluded, the average inactivation rate across twenty-two studies at -10 mV is 20 ms (Perez-Reyes 2003).

LVA T-type currents exhibit a kinetic signature that distinguishes them from HVA calcium channels - a stereotypical pattern of current traces whereby successive traces cross each other (Randall and Tsien 1997) in a manner reminiscent of the canonical voltage-gated fast sodium channels (Hodgkin and Huxley 1952). This phenomenon is due to the voltage dependent increase in the rates of both activation and inactivation. HVA currents, such as I_{CaR}, typically lack this signature because their inactivation rates are much slower than their activation rates (Randall and Tsien 1997). In CA1 pyramidals, between 60 and 90% of the recovery from inactivation is voltage dependent with a time constant at -100 mV of 215 ms (Takahashi, Wakamori, et al., 1989).

3.6.7 Temperature dependence

Activation, inactivation, and I_{CaT} amplitude are temperature sensitive with Q_{10} (temperature coefficient) values of between 1.7 and 2.5 (Takahashi, Wakamori, et al., 1989).

3.6.8 Modulation

The current is blocked by 100 μM Cd^{2+} and 100 μM verapamil (Halliwell 1983; Yaari, Hamon, et al., 1987). I_{CaT} is blocked by Ni^{2+} with an IC50 of 0.2-0.4 mM (Fox, Nowycky, et al., 1987). Calcium antagonists dose-dependently block I_{CaT} in the order of flunarizine > nicardipine > D600 > diltiazem and La^{2+} > Zn^{2+} > Cd^{2+} > Ni^{2+} > Co^{2+}, respectively (Takahashi and Akaike 1991). I_{CaT} is also strongly inhibited by nimodipine, the classical L-type channel blocker (Randall and Tsien, 1997).

A wide range of neuromodulators including serotonin (Berger and Takahashi 1990), cholinergic agonists such as carbachol and muscarine (Fisher and Johnston 1990), erythropoietin (Assandri, Egger, et al., 1999), and noradrenaline (Tseng and Boyden 1989) stimulate T-type currents. Neuromodulators reported to inhibit I_{CaT} include dopamine (Marchetti, Carbone, et al., 1986), somatostatin (Chen, Zhang, et al., 1990) and enkephalin (Kasai, Takagi, et al., 1996).

3.6.9 Function

The role of the low threshold calcium current is partly determined by the resting membrane potential of the cell (Perez-Reyes, Cribbs, et al., 1998). For cells with relatively depolarized Vm (> -70 mV) I_{CaT} is largely inactivated. However, the ability of I_{CaT} to rapidly de-inactivate enables the current to drive rebound bursts in response to inhibitory postsynaptic potentials (IPSPs). In cells with a hyperpolarized Vm (-90 to -70 mV), excitatory postsynaptic potentials (EPSPs) can directly trigger a LVA calcium spike that can support bursting (Huguenard and Prince 1992).

3.6.10 Subthreshold oscillations

The considerable overlap of the activation and inactivation curves of T-type channels creates a non-inactivating 'window' current in response to modest depolarizations (Randall and Tsien 1997). One functional consequence of this window current is subthreshold oscillations. Whilst separate currents usually provide the resonance and amplification functions required to drive STOs, I_{CaT} is unusual in that it can generate STOs unaided (Hutcheon and Yarom, 2000). For example, in guinea pig magnocellular neurosecretory cells of the supraoptic nucleus, the T-type current is uniquely associated with damped membrane oscillations following the break of a hyperpolarizing stimulus (Erickson, Ronnekleiv, et al., 1993). In this case, I_H drives the rebound

potential above the firing threshold for the de-inactivated I_{CaT}, which then interacts with potassium currents to produce damped oscillations.

3.6.11 Epileptogenesis

The T-type current appears to play a role in epileptogenesis since blockade of I_{CaT} in acutely dissociated and cultured hippocampal neurons reduces the spike count in ictal-like afterdischarges following tetanic stimulation (Higashima, Kinoshita, et al., 1998).

3.6.12 LTP

The density of T-type channels in CA1, but not dentate gyrus, is sufficient to allow I_{CaT} to significantly contribute to the magnitude of LTP (long term potentiation) and the late depolarizing potential in CA1 (Song, Wang, et al., 2002). Both of these parameters are decreased under I_{CaT} blockers.

3.6.13 I_{CaT} in the subiculum

No direct analysis of the role of I_{CaT} in subicular neurons has been carried out to date. Nonetheless, some tentative conclusions may be drawn regarding I_{CaT} in the subiculum. Surprisingly, despite the obvious importance of I_{CaT} in other neurons there is little evidence for a substantive functional role for the low threshold calcium current in subicular pyramidals.

3.6.13.1 Subthreshold oscillations

Prima facie evidence for such a role was presented by Mattia et al. (1997b) who noted a 25% drop in the frequency of subthreshold oscillations under Co^{2+} and Cd^{2+} suggestive of the existence of a subthreshold calcium channel. However, there was no effect on STO amplitude, as would be expected, if a low threshold calcium current were present to act as a resonant amplifier. It seems more likely that the frequency drop reflects collateral effects on the frequency-setting M-type 'resonator' current since the kinetics of this current are known to be altered by extracellular divalent cations, such as cobalt and cadmium (Tokimasa and Akasu 1990).

3.6.13.2 Anodal break potential

The aforementioned inability of calcium channel inhibitors to reduce STO amplitude also hints that the slow afterdepolarization, or anodal break potential (ABP), that follows sustained hyperpolarizing command steps (Behr et al., 1996) is not mediated by I_{CaT} to any significant

extent. This notion is supported by the fact that Mattia et al. (1997a) found that TTX markedly reduced the ABP in bursting cells.

A role for I_{CaT} was suggested by Menendez de la Prida et al. (2003) who noted that the residual ABP, following Cs^{2+} elimination of I_H, was abolished by 50 μM Ni^{2+}, a nominal inhibitor of I_{CaT}. However, the robust finding, in the same study, that the afterdepolarization elicited by subthreshold depolarizing current pulses are completely eliminated by low levels (10 nM) of TTX, undermines the conclusion that I_{CaT} amplifies the ABP. The reduction of the ABP by Ni^{2+} is probably due to the ability of this divalent metal cation to suppress the sodium current (Jung et al., 2001).

3.6.13.3 Bursting

Almost half of the calcium-tail current that drives subicular bursting is carried by an LVA current (Jung et al., 2001). However, a significant fraction is likely to be due to a variant of the R-type channel since over 75% of the voltage-dependent deactivation time course is accounted for by a rapid component (Jung, Staff, et al., 2001). In conjunction with the aforementioned comments, a number of other observations hint at a low upper limit on the contribution of I_{CaT} to subicular bursting. For example, T-type, but not R-type, channels of cerebellar granule cells are over 60% inhibited by 10 μM nimodipine, a canonical L-type channel blocker, (Randall and Tsien 1997) but nimodipine inhibits only 12% of the Ca^{2+} tail current (Jung, Staff, et al., 2001). An I_{CaT}/I_{CaL} density ratio of 1:10 observed in dentate granule cells (Fisher, Gray, et al., 1990) further suggests that I_{CaT} may account for only a small proportion of the 12% nimodipine tail current contribution in the subiculum.

3.6.14 Subicular I_{CaT} model

Due to the lack of explicit data on subicular I_{CaT}, the model is based primarily on the characteristics of I_{CaT} as described in hippocampal area CA1 (Figure III-3). The basic model is

$$I_{CaT} = p_{CaT} m h z^2 \frac{VF^2}{RT} \frac{[Ca^{2+}]_i - [Ca^{2+}]_o \exp^{-z_{Ca}FV/RT}}{1 - \exp^{-z_{Ca}FV/RT}}$$

3.6.14.1 Activation

Pyramidal CA1 I_{CaT} is induced by step depolarization beyond about -60 mV from a holding potential of -100 mV, and peaks around -30 mV. The I_{CaT} steady state activation curve has a half

activation voltage of -45.1 and a slope factor of -4.0 mV. This half activation voltage incorporates a depolarizing bias in order to account for the effect of the reduced calcium electrochemical driving force at more depolarized potentials. Failure to do so can lead to anomalously hyperpolarized estimates of the V_{half} (Perez-Reyes 2003).

$$m_{inf} = \frac{1}{1 + e^{\frac{V-(-45.1)}{-4}}}$$

3.6.14.2 Activation kinetics

The activation time constant for I_{CaT} varies, depending on the subtype, from 1 to 7 ms at -10 mV (Klöckner, Lee, et al., 1999). The activation kinetics are a temperature scaled fit of Randall and Tsien's (1997) I_{CaT} activation data to an exponential association equation.

$$\tau_m = -0.3(-1.1-e^{-0.03V})$$

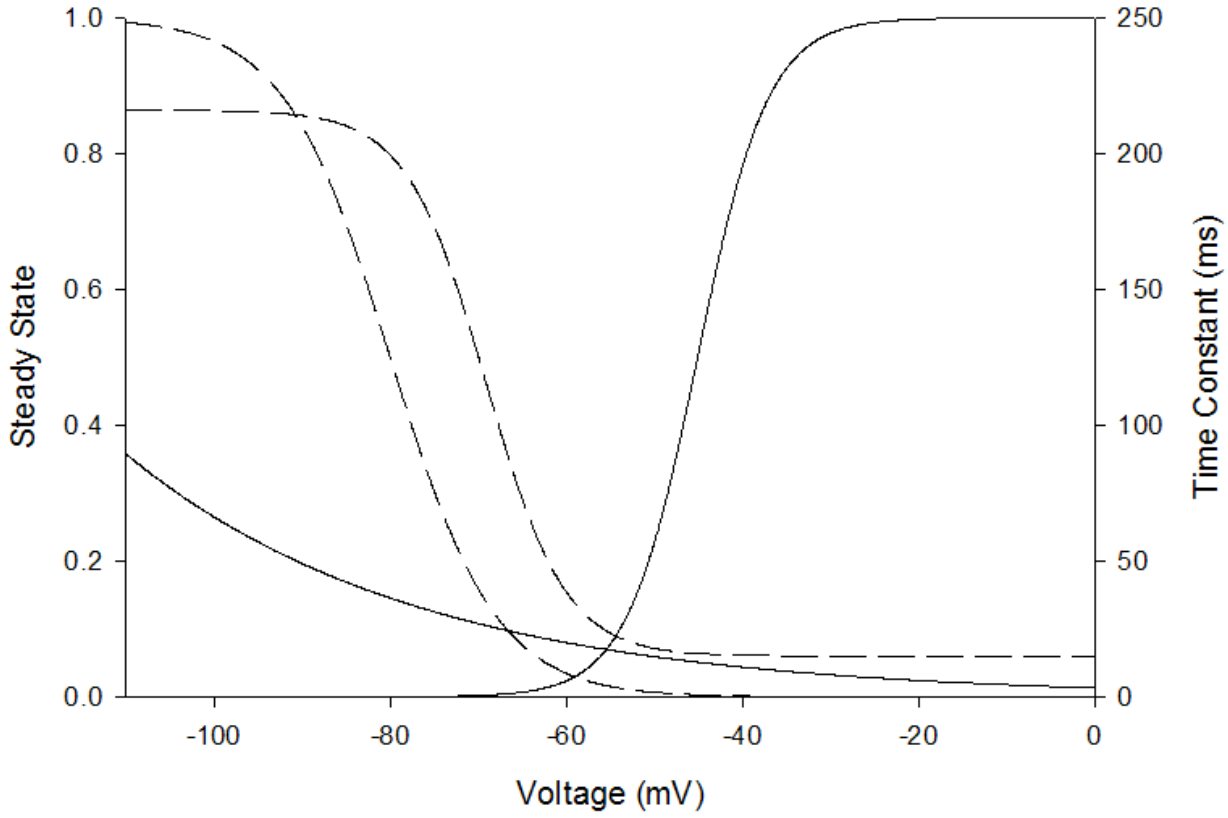

Figure III-3. Plot of the activation (solid lines) and inactivation (dashed lines) steady state and time constant curves for I_{CaT}. The activation time constant is multiplied by 10 in order to fit the inactivation and activation curves on the same graph.

3.6.14.3 Inactivation

A consensus steady-state inactivation curve, with a half-inactivated voltage of -80 mV and a slope factor of 6 mV, based on average activation characteristics is used.

$$h_{inf} = \frac{1}{1 + e^{\frac{V-(-80)}{6}}}$$

3.6.14.4 Inactivation kinetics

Our sigmoidal model of T-type inactivation follows the canonical phases of I_{CaT} kinetics whereby the time constant is slow (> 40 ms) before about -60 mV but asymptotes at about 10 ms beyond this value.

$$\tau_h = \frac{201.0}{1+e^{\frac{V-(-69.1)}{4.5}}} + 15.0$$

3.7 Residual calcium current, I_{CaR}

R-type currents, I_{CaR}, were originally described as the residual calcium current observed in rat cerebellar granule neurons following pharmacological inhibition of L-, N-, and P/Q-type calcium channels (Zhang, Valiante, et al., 1993; Randall and Tsien 1995). R-type currents have composite gating and modulation characteristics. In rat cerebellar granule cells, for example, I_{CaR} has some biophysical properties similar to those of LVA (voltage range for steady-state inactivation) and HVA (high sensitivity to Cd^{2+} inhibition) Ca^{2+} channels. Other properties are intermediate between those of LVA and HVA channels (Tottene, Moretti, et al., 1996). In whole cell mode, this current is difficult to distinguish from N and Q-type currents (Randall and Tsien, 1995).

3.7.1 Channel

Whilst, the molecular basis for I_{CaR} is still uncertain, the channel that most closely mirrors the I_{CaR} characteristics is the $Ca_{V2.3}$ (α_{1E}). Cloned $Ca_{V2.3}$ channels are sensitive to Ni^{2+} (Williams, Marubio, et al., 1994) and omega-Aga-IIIA (Randall and Tsien 1998), and have a single channel conductance of 12-14 pS in 100 mM Ca^{2+} (Tottene, Moretti, et al., 1996).

$Ca_{V2.3}$ subunits underlie a significant fraction of I_{CaR} in different types of central neurones (Sochivko, Pereverzev, et al., 2002). Thus, in $Ca_{V2.3}$-deficient mice, native I_{CaR} expression is reduced by 79% in CA1 neurons (Sochivko, Pereverzev, et al., 2002), whilst peak R-type current

density is reduced by 52.5% using antisense $Ca_{V2.3}$ oligonucleotides in cerebellar granule cells (Piedras-Renteria and Tsien 1998).

As with most other channels, there is evidence of a degree of variation in the specific properties of the R-type channels. Hence, the synthetic peptide neurotoxin, SNX-482, can block I_{CaR} in some cell types but not in others (Valentino, Newcomb, et al., 1993). Even within the same cell type, variation in the I_{CaR} activation threshold has been reported (Tottene, Moretti, et al., 1996). The source of this variation can be traced to the presence of, at least, three R-type isoforms with different pore properties; two differentially SNX-sensitive components and an SNX-resistant component with divergent pharmacological and biophysical properties (Tottene, Moretti, et al., 1996). The relative resistance of CA1 I_{CaR} to SNX-482 (Sochivko, Chen, et al., 2003) suggests that the SNX-resistant subtype is predominately expressed in this region.

Although, human $Ca_{V2.3}$ is more permeable to barium (Bourinet, Zamponi, et al., 1996), the calcium permeability of cloned rat $Ca_{V2.3}$ is similar to that for barium (Williams, Marubio, et al., 1994). However, characterisation of channels using barium, rather than calcium, as a charge carrier is potentially problematic as Ba^{2+} can alter some ion channel gating properties (McDonald, Trautwein, et al., 1994).

3.7.2 Distribution

Hippocampal R-type channels appear to be distributed more abundantly at the distal apical dendrite than at the proximal dendritic area or soma (Isomura, Fujiwara-Tsukamoto, et al., 2002). However, the ability of I_{CaR} to drive the somatic burst ADP in CA1 pyramidals (Metz, Jarsky, et al., 2005) suggests a substantial somatic presence. Indeed, Sochivko et al. (2003) observed messenger RNA for N-, P/Q-, R-, and L-type channels in the ratio 1:0.88:0.56:0.084 in acutely isolated CA1 pyramidals.

3.7.3 Activation

There is wide variation in the reported activation parameters for I_{CaR}. Rat $Ca_{V2.3}$, cloned and expressed in xenopus oocytes, exhibits a V_{half} of -29.1 mV with Ba^{2+} as the charge carrier (Soong, Stea, et al., 1993). In contrast, cloned human I_{CaR} expressed in the HEK293 cell line exhibit a considerably more depolarized activation curve with a V_{half} of +3.5mV (Williams, Marubio, et al., 1994). In CA1, an R-like current was characterised with a V_{half} of +2.5 mV and a k factor of 11 mV (Metz, Jarsky, et al., 2005). This value is more hyperpolarized than the V_{half} of

-17 mV reported for acutely dissociated CA1 cells (Sochivko, Chen, et al., 2003) but is very similar to the V_{half} of -1.7 mV and k of 8.6 mV for R-type channels expressed in primary culture rat cerebellar granule cells (Randall and Tsien 1997). Tottene et al. (1996) observed a range of R-type channels with a mixture of LVA and HVA properties in rat cerebellar neurons.

The markedly depolarized half-activation potential of native, as compared to cloned, rat R-type channels suggests the possibility of post-translational modification and/or the presence of modulating subunits. The non-$Ca_{V2.3}$ blocker-resistant component (19% in CA1 pyramidals), at least partly attributable to the low threshold T-type transient calcium current, is also likely to contribute to these differences (Sochivko, Chen, et al., 2003).

3.7.4 Activation kinetics

Randall and Tsien (1997) reported rapid voltage-dependent activation kinetics for I_{CaR} with the time taken to rise from 10% to 90% of the peak current at 22˚C falling from 13 to about 1 ms between -10 mV and +40 mV. Cloned human and rat I_{CaR} exhibit similarly rapid activation kinetics with respective time constant of 1.3 ms at 0 mV and 2.1 ms at -10 mV (Williams, Marubio, et al., 1994; Soong, Stea, et al., 1993).

3.7.5 Deactivation kinetics

Metz et al. (2005) observed bi-exponential deactivation kinetics of the Ni^{2+}-sensitive, R-like component of the CA1 calcium tail current that underlies the ADP. The fast component, with a τ_{fast} on the order of 0.35 ms, constituted over 90% of the total, whilst the slow component (τ_{slow} = 5.8 ms) comprised the rest (Metz, Jarsky, et al., 2005). Randall and Tsien (1997) also reported very rapid (<<1 ms) I_{CaR} deactivation kinetics using Ba^{2+} as the charge carrier in cultured rat cerebellar granule cells. The R-type current deactivated approximately eight-fold faster than the T-type current with a deactivation rate that increased with increasing hyperpolarization (Randall and Tsien 1997).

3.7.6 Inactivation

Rat $Ca_{V2.3}$, cloned and expressed in xenopus oocytes, exhibits a V_{half} of -71 mV with Ba^{2+} as the charge carrier (Soong, Stea, et al., 1993). CA1 I_{CaR} has an inactivation V_{half} of -60.9 mV with a k factor of 7.9 mV (Metz, Jarsky, et al., 2005). Again, cerebellar granule cells in primary culture exhibit very similar values: a V_{half} of -68.4 and a slope factor of 11.1 mV (Randall and Tsien,

1997). Sochivko et al. (2003) found that over 80% of R-type current in acutely dissociated CA1 cells can be inactivated by a holding potential of -60 mV and reported a blocker-resistant current with R-type current-like properties in CA1 with a half-maximal inactivation voltage of -76 mV. This current constituted approximately 21% of the total Ba^{2+} current (Sochivko, Chen, et al., 2003).

3.7.7 Inactivation kinetics

The magnitude of the inactivation time constant of I_{CaR} in granule cells falls from about 60 to 25 ms between -10 and 50 mV at 22˚C (Randall and Tsien 1997). The inactivation time constant for cloned human and rat I_{CaR} are 74 ms at 0 mV and 100 ms at -10 mV (Williams, Marubio, et al., 1994; Soong, Stea, et al., 1993). Tottene et al. (1996) reported blocker-resistant currents with very slow inactivation kinetics. One subtype was only 46% inactivated at the end of a 720 ms depolarizing pulse whilst another exhibited no decrement over the same duration (Tottene, Moretti, et al., 1996).

3.7.8 Modulation

The R-type current is classically resistant to inhibitors of L-, N-, and P/Q-type calcium channels such as nimodipine, omega-CTx-MVIIC, and omega-CTx-MVIIA (Zhang, Valiante, et al., 1993; Randall and Tsien 1995). When expressed in Xenopus oocytes or HEK293 cells $Ca_{V2.3}$ generates currents that are highly susceptible to block by Ni^{2+} ions (Williams, Marubio, et al., 1994). In acutely dissociated rat CA1 neurons, R-type currents are very sensitive to Ni^{2+} (half-maximal block at 28 μM) but relatively resistant to SNX-482 (8% and 52% block at 0.1 and 1 μM, respectively) (Sochivko, Chen, et al., 2003). Interestingly, Ni^{2+}-sensitivity is not diagnostic for R-type currents in either neocortical or neostriatal neurons (Foehring, Mermelstein, et al., 2000).

Cholinergic upregulation of I_{CaR} in hippocampal neurons allows the current to participate in plateau potentials (Kuzmiski, Barr, et al., 2005). In cultured spinal cord motoneurons from day 15 rat embryos, R-type current density is selectively upregulated, with a half-time of 12 h, to a maximum of approximately 80% by BDNF (Baldelli, Magnelli, et al., 1999). Conversely, cannabinoid activation reduced I_{CaR} by 55% in cerebellar granule cells (Brown, Safo, et al., 2004).

3.7.9 Function

Unlike the LVA T-type current, there is little overlap of the activation and inactivation curves of R-type channels. This lack of an appreciable 'window current' renders the fast inactivating R-type channel ill suited for supplying sustained currents but well adapted to producing surge currents in response to brief depolarizations (Randall and Tsien 1997). The large amplitude of the current is significant in this regard; in hippocampal CA1 pyramidals and cerebellar granule neurons, the R-type current contributes over 20% of the total calcium current (Sochivko, Pereverzev, et al., 2002; Mintz, Adams, et al., 1992; Randall and Tsien 1995).

In CA1 pyramidal neurons, R-type calcium current has been shown to be an important source of calcium entry during distal dendritic signalling (Christie, Eliot, et al., 1995). R-type currents are also involved in synaptic plasticity (Isomura, Fujiwara-Tsukamoto, et al., 2002) where the ability of LTP-inducing stimuli to upregulate R-type calcium channels suggests a role for these channels in the mechanism of LTP (Yasuda, Sabatini, et al., 2003; Dietrich, Kirschstein, et al., 2003). Presynaptic R-type current has been reported to be involved in fast glutamatergic transmission at hippocampal synapses (Gasparini, Kasyanov, et al., 2001), as well as transmitter release at other rat central synapses (Wu, Borst, et al., 1998). A more recent report dissected the contribution of $Ca_{V2.3}$ subunits to synaptic plasticity of mossy fibres and concluded that, whilst I_{CaR} contributes to the induction of mossy fibre LTP and post-tetanic potentiation, these channels are not involved in mossy fibre fast synaptic transmission, paired-pulse facilitation, or frequency facilitation (Dietrich, Kirschstein, et al., 2003).

In CA1 pyramidals, a Ni^{2+}-sensitive (200 μM) current with an I_{CaR}-like pharmacological and biophysical profile appears to contribute appreciably to the single spike afterdepolarization (APD) (Metz, Jarsky, et al., 2005). Since there is a strong correlation between ADP size and propensity to burst (Jung, Staff, et al., 2001), this finding implicates I_{CaR} in burst behaviour. Although the CaV2.3 blocker SNX-482 does not block the ADP, CA1 $Ca_{V2.3}$ is reported to be relatively insensitive (27% block at 300 nM SNX-482) to this inhibitor (Sochivko, Pereverzev, et al., 2002). Conversely, another study of I_{CaR}-like currents in CA1 pyramidals found that a lower concentration of Ni^{2+} (100 μM) had no effect on somatic bursting but did inhibit distal LTP (Isomura, Fujiwara-Tsukamoto, et al., 2002).

Investigation of the mechanism of the anticonvulsant topiramate has revealed an important role for I_{CaR} in mediating the excitatory effects of acetylcholine. Topiramate (TPM) suppresses cholinergically mediated plateau potentials (PP) in hippocampal neurons (Coulter, Sombati, et

al., 1993; DeLorenzo, Sombati, et al., 2000). These plateau potentials are driven by a cholinergic induction of a dormant calcium-dependent cyclic nucleotide-gated (CNG) current (Kuzmiski and MacVicar 2001). Acetylcholine also augments I_{CaR}, which then provides the calcium trigger required to induce CNG-mediated plateau potentials (Kuzmiski, Barr, et al., 2005). TPM evidently exerts its effect on plateau potentials, not by inhibiting the CNG current, but by suppressing the cholinergic upregulation of I_{CaR} by inducing a hyperpolarizing shift in its steady-state inactivation curve (Kuzmiski et al., 2005).

3.7.10 I_{CaR} in the subiculum

3.7.10.1 Activation

The apparent lack of an appreciable T-type current in subicular neurons suggests that the R-type calcium current mediates a sizable proportion of the LVA component of the subicular calcium tail current. The implied hyperpolarized activation threshold for subicular I_{CaR} is not implausible since cloned $Ca_{V2.3}$ subunits express R-type currents exhibiting a wide range of activation and inactivation characteristics (Parent, Schneider, et al., 1997). In addition, Tottene et al. (1996) characterised blocker-resistant calcium current in cerebellar neurons with a V_{half} of -22 mV and an activation threshold of -40 mV.

Further, the LVA component constitutes nearly half of the tail current (Jung, Staff, et al., 2001) whereas the T-type component constitutes less than 20% of the blocker resistant calcium current in CA1 pyramidal cells (Sochivko, Pereverzev, et al., 2002).

In response to brief depolarizing stimuli, I_{CaR} typically reaches its peak approximately twice as fast as I_{CaT} (Randall and Tsien 1997). Consequently, the contribution of I_{CaT} to the subicular tail current seen under voltage clamp is likely to be even smaller, since the brief (1 ms) depolarizing stimulus used to evoke the tail current is likely to bias the tail current composition disproportionately towards the faster activating I_{CaR}. On the other hand, the activation characteristics (V_{half} of 2 mV, k of 5 mV) of the HVA component of the subicular calcium tail current are very similar to those of the I_{CaR} reported in CA1 and cerebellar granule cells (Metz, Jarsky, et al., 2005; Randall and Tsien 1997). This suggests a more conventional I_{CaR} activation threshold. Moreover, the LVA calcium tail component V_{half} of -31 mV is over 20 mV more hyperpolarized than the intermediate I_{CaR} V_{half} reported by Magistretti et al. (2000). In addition, the rapid R-like kinetics cannot be reliably assigned to either the LVA or HVA fraction in the Jung et al. experiment.

3.7.10.2 Activation kinetics

The activation kinetics of the subicular I_{CaR} has not been directly measured. However, Jung et al. (2001) reported deactivation kinetics that are substantially faster than the activation kinetics for the calcium tail current, which suggests that complex kinetics are required for subicular I_{CaR}.

3.7.10.3 Deactivation kinetics

The subicular calcium tail current exhibits bi-exponential deactivation (Jung et al., 2001). The fast component, which comprises about 70% of the total tail, is comparable to the Ni^{2+}-sensitive, R-like current in CA1 pyramidals (Metz, Jarsky, et al., 2005). Slow deactivation has been described as a defining characteristic of I_{CaT} (Nakashima, Todorovic, et al., 1998).

3.7.10.4 Inactivation

Like the steady state activation curve, inactivation of the subicular tail current can be resolved into at least two depolarized and hyperpolarized components (Jung, Staff, et al., 2001). Unlike the activation curves, identification of an I_{CaR} signature is less certain. The V_{half} of the hyperpolarized component is only -33 mV. This value is considerably more depolarized than the -60.9 mV reported for the CA1 I_{CaR} by Metz et al. (2005) using 5 mM Ba^{2+} as a charge carrier.

3.7.10.5 Function

Investigation of subicular I_{CaR} has been largely restricted to its apparent role in bursting. Jung et al. (2001) suggested that a Ni^{2+}-sensitive R-like current activated by the initial action potential contributes significantly to the ADP underpinning subicular bursting. The lack of an appreciable 'window current' renders the fast inactivating R-type channel well adapted to producing the required 'surge currents' in response to brief depolarizations (Randall and Tsien 1997). Further, the inability of L-, P/Q or N-type calcium channel blockers to abolish bursting in subicular pyramidals and the lack of an I_{CaT}-like LVA subthreshold response hints at the relative importance of the R-type current for subicular bursting (Jung et al., 2001).

This conclusion is somewhat undermined by the finding that subicular, like CA1, bursting is not blocked by Ni^{2+} at concentrations of 100 μM (Jung, Staff, et al., 2001). Further, only 20% of the calcium tail current responsible for the ADP is blocked at this concentration (Jung, Staff, et al., 2001). In contrast, blockade of P/Q and N currents reduces the tail current by over 30%. If we assume that CA1 and subiculum share pharmacologically similar R-type channels, then the

half-maximal block of CA1 I_{CaR} of just 28 μM Ni^{2+} (Sochivko, Chen, et al., 2003) dictates that subicular I_{CaR} should be nearly completely abolished by 100 μM Ni^{2+}. If this is true, the inability of 100 μM Ni^{2+} to block subicular bursting would seem to suggest that I_{CaR} has a weaker role in this phenomenon than has been proposed. In mitigation, charge transfer through the R-type channel is highly sensitive to action potential shape and changes in resting membrane voltage (Sochivko et al., 2003). It is therefore possible that the I_{CaR} makes an important contribution to subicular bursting predicated on its unique kinetics. While subicular bursting and the calcium tail current are not blocked by low concentrations of Ni^{2+} they are completely abolished by 1 mM Ni^{2+} (Jung et al., 2001). High concentrations of Ni^{2+} strongly suppress (79%) the calcium tail current (Jung et al., 2001), probably via broad-spectrum inhibitory effects on calcium (Zamponi, Bourinet, et al., 1996) and sodium channels (Jung et al., 2001).

The perisomatic origin of bursting in subicular bursters and the contribution of I_{CaR} to the calcium tail current (Jung et al., 2001) places I_{CaR} in or near the soma of subicular pyramidals. A dendritic presence for I_{CaR} is obviously not excluded by this conclusion.

3.7.10.6 Plateau potentials

As in CA1 pyramidals, topiramate suppresses cholinergically induced plateau potentials in subicular bursting cells (Palmieri, Kawasaki, et al., 2000). Therefore, whilst the existence of specific cholinergic interactions with subicular I_{CaR} have not been described to date, they would appear likely based on observations in CA1 (Kuzmiski et al., 2005).

3.7.11 Model of subicular I_{CaR}

The ICaR model employed here uses unusual double activation kinetics in order to accommodate experimental reports of asymmetry between activation and deactivation. The methodology and kinetics are explained below (Figure III-4):

3.7.11.1 Activation

We develop an IVA I_{CaR} model to partially account for the LVA activation component of the tail current. Compared to the LVA activation curve, our I_{CaR} model has a somewhat more depolarized V_{half} and a steeper slope factor. Our channel activates about -50 mV and saturates near +30 mV. We justify this shift by observing that whilst an action potential is required to trigger the calcium tail, the LVA activation curve, reported as constituting over half of the total

tail current, activates at about -65 mV, well below the spike threshold. Yet, Jung et al. (2001) saw no depolarizing subthreshold response. This apparent contradiction may reflect an artificial amplification of the LVA component in the nucleated patch configuration used.

$$m_{inf} = \frac{1}{1 + e^{\frac{V-(-14.5)}{-6.4}}}$$

3.7.11.2 Activation kinetics

See the deactivation kinetics section.

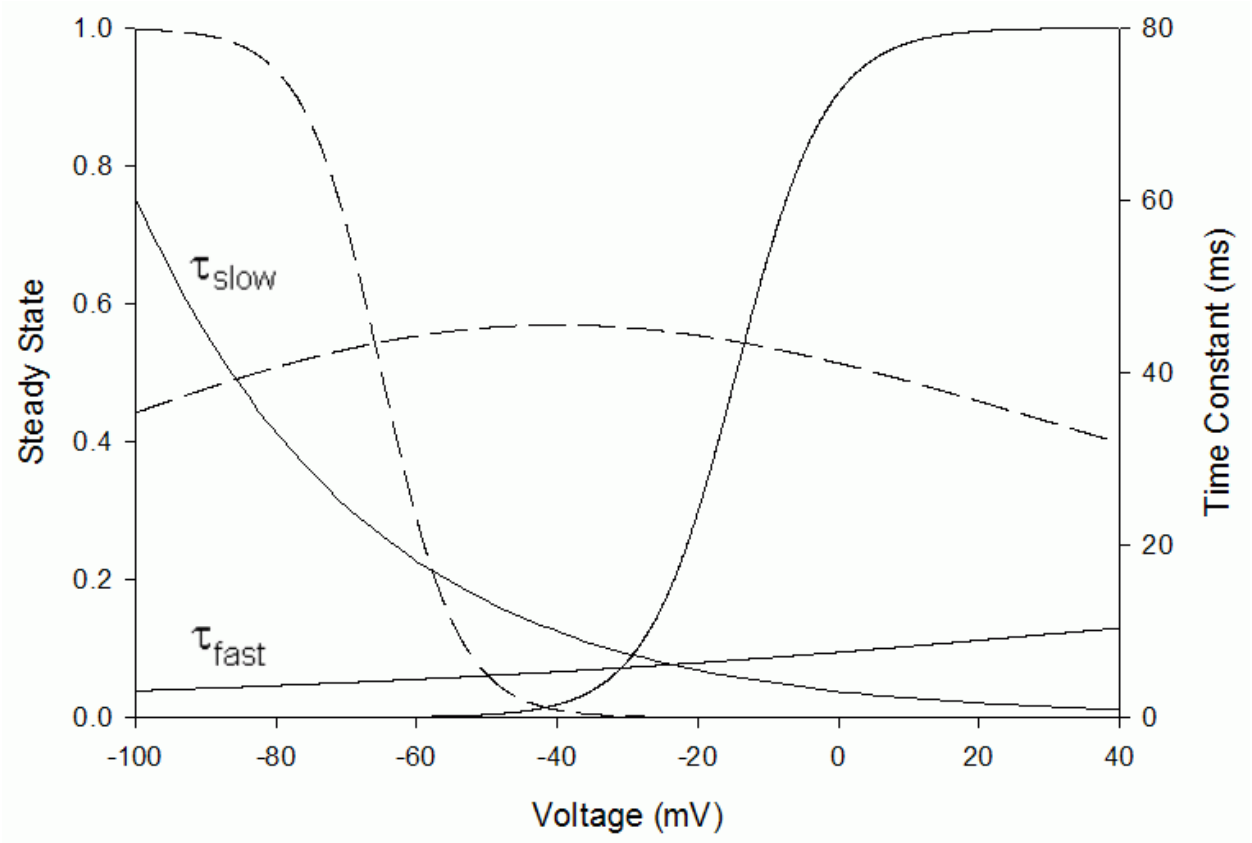

Figure III-4. Plot of the activation (solid lines) and inactivation (dashed lines) steady state and time constant curves for I_{CaR}. The fast and slow time activation/deactivation time constants are shown. The fast activation time constant is multiplied by 100 in order to fit all the activation and inactivation curves on the same graph.

3.7.11.3 Inactivation

The hybrid steady state inactivation curve begins to inactivate about -100 mV. Inactivation is complete by about -20 mV. There is minimal overlap between the activation and inactivation curves in this model of subicular I_{CaR}.

$$h_{inf} = \frac{1}{1 + e^{\frac{V-(-65)}{5.5}}}$$

3.7.11.4 Inactivation kinetics

The inactivation time constant is a temperature-adjusted version of that presented by Randall and Tsien (1997) and falls from nearly 7 ms at -30 mV to 1 ms at +50 mV.

$$\tau_h = \frac{e^{\frac{V+370.6}{70.1}}}{1+e^{\frac{V+55.5}{41.5}}}$$

3.7.11.5 Deactivation kinetics

The deactivation kinetics of the calcium tail current determines the duration of the tail. In subicular bursters, the rate of deactivation is bi-exponential with a fast and slow component (Jung et al., 2001). For both components, the rate of deactivation decreases with increasing depolarization. The very rapid (<1ms) fast component is similar to that reported for I_{CaR} in hippocampal CA1 and cultured rat cerebellar granule cells (Metz, Jarsky, et al., 2005; Randall and Tsien 1997) and hence we assume that it reflects subicular I_{CaR} deactivation.

CA1, and presumably subicular, I_{CaR} exhibits relatively slow activation but faster (~10x) deactivation over the same voltage range. In other words, there is an asymmetry between the time constants of activation and deactivation of I_{CaR} in CA1 and subicular pyramidals. Since customary HH models assume symmetrical activation and deactivation kinetics this dissociation poses a problem. Conventionally, deactivation is simply assumed to be activation in reverse, such that the steady state activation and deactivation curves and the voltage-dependent activation and deactivation time constant curves are equivalent. However, in the case where this symmetry is broken more complex kinetics are required.

One HH-based approach to this problem is to assume double activation kinetics (Destexhe and Babloyantz 1993) for I_{CaR}. In this scheme I_{CaR} is proportional to the product of two activation variables m_{fast} (fast activation) and m_{slow} (slow activation). These activation variables share the

same steady state activation function but have different voltage-dependent time constants of activation. The double activation scheme allows asymmetrical activation and deactivation kinetics in the following manner. During activation, m_{fast} and m_{slow} begin close to zero. Clamping the voltage to a value where m_{fast} and m_{slow} are both activated causes m_{fast} to rapidly attain its steady state value. As the two variables share the same steady state activation curve m_{slow} will approach the same value as m_{fast} but at a significantly slower rate. Since I_{CaR} is proportional to the product $m_{fast}m_{slow}$ the time course of the measured current will largely follow the activation kinetics of m_{slow}. During deactivation, m_{fast} and m_{slow} begin close to 1. A hyperpolarizing command step that moves the voltage to a value where m_{fast} and m_{slow} deactivate causes m_{fast} to quickly move to its steady state level. This time, the dependence of I_{CaR} on the product $m_{fast}m_{slow}$ now causes the current kinetics to largely follow the decrease in m_{fast}.

Applying double activation kinetics the appropriate model for I_{CaR} is:

$$I_{CaR} = p_{max} m_{fast} m_{slow} h z^2 \frac{VF^2}{RT} \frac{[Ca^{2+}]_i - [Ca^{2+}]_o \exp^{-z_{Ca}FV/RT}}{1 - \exp^{-z_{Ca}FV/RT}}$$

where

$$\frac{dm_{fast}}{dt} = (m_{inf} - m_{fast}) / \tau_{m_{fast}}$$

and

$$\frac{dm_{slow}}{dt} = (m_{inf} - m_{slow}) / \tau_{m_{slow}}$$

The parameters of the double activation model were adapted from the fast subicular calcium tail current deactivation time constants and the relatively slow CA1 I_{CaR} activation data from Randall and Tsien (1997).

3.7.11.6 Slow activation time constant

The voltage-dependent 10 to 90% activation time reported by Randall and Tsien (1997) was linearly interpolated to the 67% activation time point. This was used as a rough estimate of the time constant. The data was temperature adjusted from 22°C using an assumed Q_{10} of 2. The resultant data was well fitted by an exponential decay equation that drops from about 25 ms at -70 mV to around 3 ms at 0 mV.

$$\tau_{slow} = 3.0e^{-0.03V}$$

3.7.11.7 Fast activation time constant

The fast component represents 60-80% of the tail current deactivation kinetics. The fast activation time constant is a smoothed version of the fast deactivation component reported for the subicular calcium tail current reported by Jung et al. (2001). It increases with increasing depolarization but averages about 0.06 ms. The resultant curve is within the reported standard error. The slow and fast curves converge at about +110 mV.

$$\tau_{fast} = \frac{e^{\frac{V-284.0}{110.2}}}{1+e^{\frac{V-94.6}{19.1}}}$$

3.8 High threshold inactivating calcium current, I_{CaN}

The high-threshold, slowly inactivating N-type ("Neuronal" or "Neither L nor T") current, I_{CaN}, was first reported in hippocampal neurons as an early component of an envelope current that appears on depolarizing steps from -90 to +10 mV, but is absent from holding potentials of -30 mV (Madison, Lancaster, et al., 1987). The current appears to be heterogeneous, and can be mistaken for an L-type current (Yamakage and Namiki 2002).

3.8.1 Channel

I_{CaN} is carried by the $Ca_{V2.2}$ channel which, when purified from the rat brain, is a complex of four subunits with molecular weights of 230 (α1), 140 (α2), 95 (gamma), and 57 (β) kD. N-type channels have a unitary conductance, in 110 mM barium, of approximately 10 pS (Shen and Surprenant 1991). In CA1/3 and dentate gyrus a 14 pS channel with N-type characteristics has been reported with a relative abundance 10-fold higher than T- and L-type channels (Fisher, Gray, et al., 1990).

3.8.2 Distribution

N-type channels are found on somata and throughout the dendritic arbour in all hippocampal subfields (Mills, Niesen, et al., 1994). In CA3 pyramidals, levels of N-type channel expression are higher in the dendrites and associated presynaptic terminals than in the cell body (Elliott, Malouf, et al., 1995).

Generally speaking, the expression of particular channels in specific neuronal compartments alters during development (Obermair, Szabo, et al., 2004). Thus, I_{CaN} is found in the axons of

immature hippocampal neurons, where it is involved in controlling synaptic vesicle recycling prior to synaptogenesis, but is gradually excluded from the axon as the neuron differentiates (Pravettoni, Bacci, et al., 2000). The time of axonal I_{CaN} exclusion differs between brain regions and has consequently been proposed as a useful marker of the developmental onset of synaptic transmission in discrete hippocampal subfields (Jones, Bernstein, et al., 1997).

3.8.3 Modulation

In sympathetic neurons, N-type channels are inhibited by a range of D_2 dopamine receptor antagonists including phenothiazines, diphenylbutylpiperidines, and butyrophenones (Sah and Bean 1994). The neurotransmitters GABA, norepinephrine and serotonin also exert inhibitory effects on the N-type channel (Cox and Dunlap 1992; Normann, Peckys, et al., 2000). Metabotropic glutamate receptor activation suppresses I_{CaR} in CA3 pyramidals via a G-protein mediated mechanism (Swartz and Bean 1992). Activators of protein kinase C in hippocampal cells (Doerner, Pitler, et al., 1988) substantially reduce the N-type current. Neuromodulators such as noradrenaline, somatostatin and opioids can suppress I_{CaN} by reducing the frequency of single channel opening per depolarizing pulse (Shen and Surprenant 1991). These agonists are only effective in the presence of GTP, which suggests that a single convergent G-protein mechanism mediates the effects of multiple receptors on I_{CaN} (Shen and Surprenant, 1991). Activation of receptors for adenosine, a marker of metabolic status, differentially regulates calcium currents. In CA3 pyramidals, activation of A1 receptors primarily suppresses I_{CaN} whilst A2b receptor activation potentiates P-type currents (Mogul, Adams, et al., 1993). I_{CaN} is also implicated in the action of certain psychotropics. For instance, the ability of cannabinoid receptor activation to interfere with neurotransmitter release is due to the inhibition of presynaptic Q- and N-type calcium channels (Sullivan 1999).

Pharmacologically, its resistance to dihydropyridines and sensitivity to omega-conotoxin GVIA (Stanley and Atrakchi 1990) distinguish I_{CaN}. I_{CaN} is also affected, with less specificity, by omega-conotoxin MVIIC and omega-agatoxin IIIA (Yamakage and Namiki 2002).

3.8.4 Function

Despite a predominantly dendritic distribution, I_{CaN} appears to contribute to the somatic slow afterhyperpolarization (sAHP) since the N-type selective inhibitor omega-conotoxin GVIA can reduce the amplitude of the sAHP in hippocampal neurons by nearly 40% (Shah and Haylett 2000). This value increases to over 50% in layer II/III neocortical pyramidal neurons (Pineda,

Waters, et al., 1998). In the same study I_{CaN} was found to contribute to the late phase of spike repolarization, as evidenced by a pronounced broadening of the spike base under I_{CaN} blockade. These results suggest that, in neocortical neurons, calcium influx through I_{CaN} selectively activates the calcium-dependent potassium currents responsible for the sAHP and late phase spike repolarization. The overall effect of I_{CaN} inhibition in these neurons is to increase cell excitability through a reduction in spike frequency adaptation and an increase in firing rate (Pineda, Waters, et al., 1998).

N-type channels play a prominent role in some forms of neurotransmitter release (Wheeler, Randall, et al., 1994) and synaptic plasticity (Norman et al., 2000). At central synapses, N-type channels can functionally compensate for the absence of P/Q subunits in knockout mice and evoke synaptic currents that are approximately two-thirds of the magnitude of wild-type responses (Inchauspe, Martini, et al., 2004). The induction of associative long-term depression (LTD) is dependent on the activation of I_{CaN} (Normann, Peckys, et al., 2000). Further, the gain of LTD can be modulated by serotonin via an inhibitory effect on the N-type channel (Normann, Peckys, et al., 2000). Significantly, in CA1 dendrites, the pathological synaptic reinforcement induced by kindling is characterised by a persistent, local redistribution of N-type channels (Bernstein, Mendonc, et al., 1999).

Voltage-dependent relief of the presynaptic inhibition of voltage-gated calcium channels by G-protein subunit binding (facilitation) is a common mechanism for regulating neurotransmitter release. The extent of facilitation is determined by the presynaptic spike train frequency. N-type channels are about twice as resistant to facilitation than P/Q-type channels (Currie and Fox 2002). However, unlike P/Q-type channels their level of facilitation is dramatically dependent upon the spike train duration and amplitude. Coupled with wide variation in the ratio of N- to P/Q-type channels at synapses, Currie and Fox noted that such differential facilitation is likely to broaden the neuron's repertoire of synaptic transfer functions. Differential recruitment by different firing patterns of calcium channel subtypes involved in the control of dopamine release has also been observed in the neostriatum (Phillips and Stamford 2000). In this study, N-type channels were more strongly activated by regular than by burst firing. Unlike neocortical neurons, the role of hippocampal I_{CaN} appears to be largely confined to the synapses since in CA1 neurons omega-CgTx, a selective inhibitor of I_{CaN}, blocked synaptic events but had no effect on non-synaptic events (Rascol, Potier, et al., 1991).

The calcium current through N-type currents appears to be important in initiating neuronal cell death, since inhibition of I_{CaN} protects CA1 pyramidal neurons from the effects of transient forebrain ischemia (Valentino, Newcomb, et al., 1993). The systemic importance of I_{CaN} is indicated by the fact that only about one third of mice lacking a functional $Ca_{V2.2}$ gene survive to weaning (Ino, Yoshinaga, et al., 2001). Those that do survive exhibit a normal life span and few detectable behavioural deficits compared to wild type mice (Ino et al., 2001). Evidently, other currents under certain circumstances can adequately perform the roles subserved by N-type currents.

3.8.5 Activation

In CA1/3 and dentate gyrus, I_{CaN} activates around -30 mV and is half-activated at 0 mV, using Ba^{2+} as a charge carrier (Fisher, Gray, et al., 1990). This value is close to the 1.5 mV observed in chick sensory neurons (Fox, Nowycky, et al., 1987). The V_{half} of cloned N-type channels is somewhat higher. Human $Ca_{V2.2}$ expressed in the HEK 293 cell line has a V_{half} of +7.8 mV, with Ba^{2+} as the charge carrier (Williams, Marubio, et al., 1994), whilst cloned rat N-type channel expressed in Xenopus oocytes has a V_{half} of +9.7 mV (Stea, Dubel, et al., 1999).

3.8.6 Activation kinetics

At 37˚C (23˚C) the activation time constant of I_{CaN}, under a step depolarization from -80 to 0 mV, is approximately 0.3 (1.8) ms in chick sensory neurons (King Jr. and Meriney 2005). Cloned human and rat N-type channels have respective activation time constants of 3 ms at +10 mV and 2.8 ms at +20 mV (Williams, Marubio, et al., 1994; Stea, Dubel, et al., 1999).

3.8.7 Inactivation

Fisher et al. (1990) noted a wide variation in the inactivation properties of hippocampal N-type currents under patch clamp across preparations. The responses of different patches to voltage steps from -80 mV to 0 mV of 160-ms duration ranged from less than 10% to complete inactivation. Several potential explanations were proposed, including the existence of multiple channels subpopulations and differential channel regulation due to differences in the metabolic state of the cells (Fisher, Gray, et al., 1990). In dorsal root ganglion neurons, the range of inactivation of I_{CaN} is between -120 and -30 mV (Fox, Nowycky, et al., 1987). The V_{half} values for steady state inactivation curves for cloned human and rat N-type channels are -67 and -67.5 mV, respectively (Williams, Marubio, et al., 1994; Stea, Dubel, et al., 1999).

The nature of N-type inactivation is incompletely determined. The utility of V_{half} values is rendered suspect by anomalous aspects of N-type inactivation that violate several key hallmarks of conventional voltage-dependent inactivation (Jones, DeMaria, et al., 1999). Most notably, N-type calcium channel inactivation is fastest in response to moderate but not strong depolarization. This tendency is reflected in a U-shaped dependence of inactivation rate - in contrast to the conventional monotonic acceleration of inactivation rate with increasing depolarization. A U-shaped inactivation curve is generally diagnostic of current-dependent (e.g. calcium) inactivation. However, this interpretation is confounded by the observation that N-type channel inactivation is also insensitive to the species of charge carrier (Cox and Dunlap 1994; Patil, Brody, et al., 1998) and is generally insensitive to internal divalent cation buffering (Patil, Brody, et al., 1998). Jones et al. (1999) examined recombinant N-type channels and concluded that N-type inactivation is entirely voltage-dependent. These workers proposed a 'preferential closed state' inactivation mechanism whereby inactivation is most rapid from intermediate closed states along the activation pathway (Jones, DeMaria, et al., 1999). Conversely, Cox and Dunlap (1990) provided evidence that I_{CaN} inactivation is, at least in part, calcium dependent. They found that the ratio of rapid to slow inactivation increased when the extracellular Ca^{2+} concentration was raised from 0.5 to 5 mM and total inactivation increased 50% when the concentration of the calcium chelator EGTA in the patch pipette was reduced from 10 to 0.1 mM. Apropos to this debate, analysis of single channel kinetics in sympathetic neurons suggests that N-type currents can reversibly switch between rapidly inactivating and non-inactivating modes over several seconds (Plummer and Hess 1991).

3.8.8 Inactivation kinetics

The original descriptions of I_{CaN} noted that the current decays over about 100 ms in hippocampal pyramidals (MadisonD. V., Lancaster, et al., 1987). Conversely, Shen and Surprenant (1991) reported no inactivation of an N-like current over 100 ms during depolarizing pulses in acutely dissociated guinea-pig sub-mucosal neurones. Cloned human and rat N-type channels exhibit inactivation time constants in excess of 200 ms at +10 mV and 112 ms at +20 mV, respectively (Williams, Marubio, et al., 1994; Stea, Dubel, et al., 1999). In embryonic chick dorsal root ganglion (DRG) neurons, inactivation is biphasic for voltage steps from -80 or -40 mV to 0 mV and is well fitted using the sum of two exponentials, with approximate time constants of 100 ms and over 2000 ms (Cox and Dunlap 1994). Inactivation of I_{CaN} in these cells is strictly voltage-dependent between -80 and -40 mV.

3.8.9 I_{CaN} in the subiculum

3.8.9.1 Bursting

Little is known about the role of I_{CaN} subicular neurons. However, a somatic presence for subicular I_{CaN} is insinuated by the finding that application of the P-/Q-, N-type inhibitor omega-conotoxin MVIIC caused a 31% reduction in the somatic calcium tail current, implicated in subicular bursting (Jung et al., 2001). Notably, inhibition of these currents did not abolish subicular bursting. We suspect that the relative contribution of I_{CaN} to subicular I_{CaTail} is likely to be small given the lack of evidence for a role for this current in hippocampal somatic events (Rascol, Potier, et al., 1991).

3.8.10 A model of subicular I_{CaN}

We follow Jaffe et al. (1993) in giving I_{CaN} an m^2h format (Figure III-5):

$$I_{CaN} = p_{CaN} m^2 h z^2 \frac{VF^2}{RT} \frac{[Ca^{2+}]_i - [Ca^{2+}]_o \exp^{-z_{Ca}FV/RT}}{1 - \exp^{-z_{Ca}FV/RT}}$$

3.8.10.1 Activation

The activation characteristics are based on Fisher et al. (1990), but follow Jaffe et al. (1992) in shifting the half activation voltage by about -10 mV to compensate for their use of barium, rather than calcium, as charge carrier.

$$m_{inf} = \frac{1}{1 + e^{\frac{V-(-24.8)}{-9.5}}}$$

3.8.10.2 Activation kinetics

The voltage-dependent activation gate incorporated into the I_{CaN} model opens in less than 1 ms.

$$\tau_m = \frac{e^{\frac{V-0.5}{120}}}{1+e^{\frac{V+50.6}{80.1}}}$$

3.8.10.3 Inactivation

Hippocampal I_{CaN} has inactivation properties intermediate between the LVA T-type channel and the HVA L-type channel (Fisher, Gray, et al., 1990).

$$h_{inf} = \frac{1}{1 + e^{\frac{V-(-48.6)}{8.2}}}$$

3.8.10.4 Inactivation kinetics

The inactivation time constant function of subicular I_{CaN} model plateaus at 150 ms.

$$\tau_h = \frac{150}{1+e^{\frac{V-(-20)}{30}}}$$

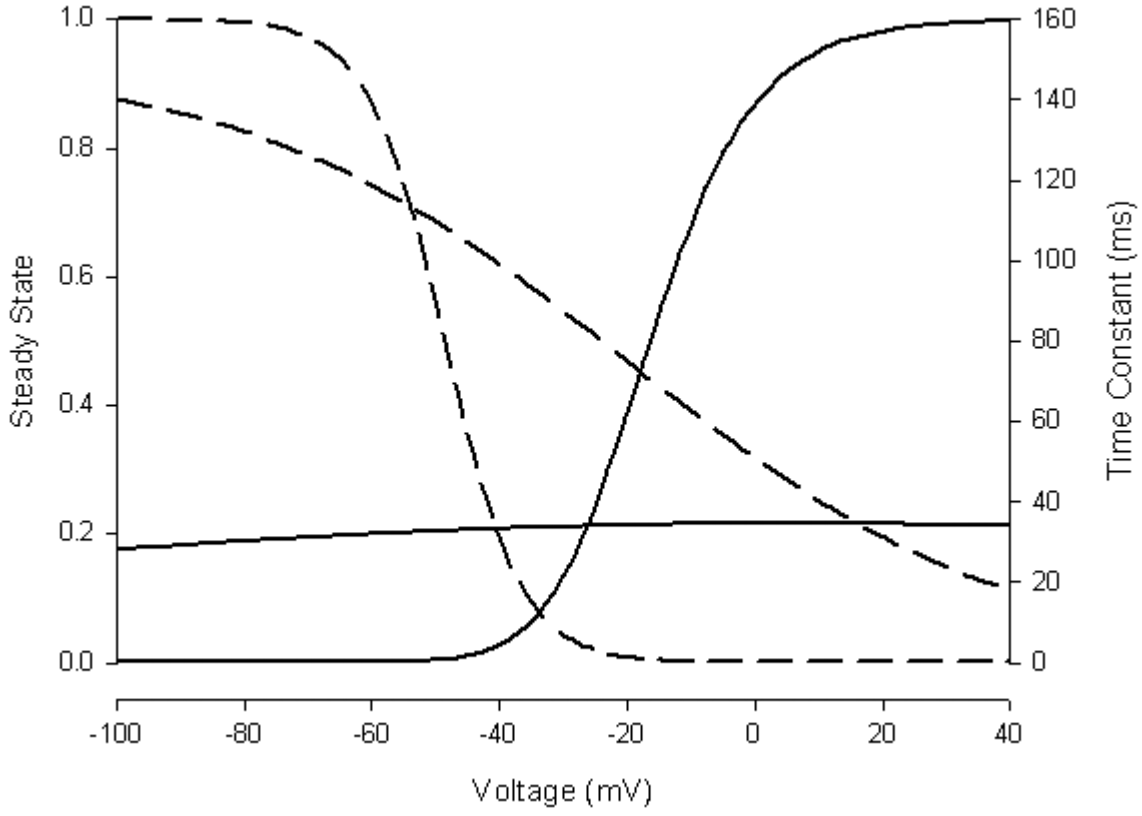

Figure III-5. Plot of the activation (solid lines) and inactivation (dashed line) steady state and time constant curves for I_{CaN}. The steady state activation variable is plotted raised to its exponent of 2. The activation time constant is multiplied by 100 in order to fit the inactivation and activation curves on the same graph.

3.9 Persistent sodium current, I_{NaP}

A non-inactivating component of the sodium current is present in most neuronal types. Although I_{NaP} usually only constitutes a small fraction of the sodium current, its strategic activation

threshold, approximately 10 mV below the fast transient sodium current, amplifies its functional significance.

3.9.1 Developmental profile

Developmentally, I_{NaP} seems to appear after I_{NaF}. Huguenard et al. (1988) tracked developmental changes in the kinetics of Na^+ conductances in rat neocortical neurons from embryonic day 16 to postnatal day 59. They found that the time course of sodium current in immature neurons complied with classical fast I_{NaF} HH kinetics but as the neurons matured a slowly decaying component became evident that necessitated the use of two decay components to obtain a good fit (Huguenard, Hamill, et al., 1988).

3.9.2 Location

A non-inactivating component of the tetrodotoxin-sensitive sodium current has been described in a wide variety of brain regions including neocortex (Fleidervish, Friedman, et al., 1996), cerebellum (Kay, Sugimori, et al., 1998), hippocampus (French and Gage 1985) and subiculum (Vreugdenhil, Hoogland, et al., 2004). However, I_{NaP} appears not to be universally distributed. For example, the Na^+ current in acutely dissociated hippocampal dentate granule cells from patients with therapy refractory temporal lobe epilepsy does not appear to contain a persistent sodium component (Reckziegel, Beck, et al., 1998). Similarly, nearly 20% of Purkinje cells lack the I_{NaP} component (Kay, Sugimori, et al., 1998).

3.9.3 Activation

The half-activation characteristics of the steady state activation curve for the persistent sodium current are quite consistent across both brain regions and cell preparations. The current activates at subthreshold membrane potentials (-70 mV) and is half-activated at around -50 mV in both hippocampal CA1 neurons and neocortical pyramidals (Brown, Schwindt, et al., 1994; French, Sah, et al., 1990). In neocortical neurons, there is no difference in half-activation voltage between acutely dissociated neurons and cells in brain slice (Brown, Schwindt, et al., 1994). This suggests that the activation characteristics of the dendritic and somatic isoforms are probably similar.

3.9.4 Activation kinetics

Activation I_{NaP} is rapid and occurs in less than 3-4 ms (within the settling time of the single-electrode voltage clamp) (Stafstrom, Schwindt, et al., 1985). In cerebellar Purkinje neurons, the activation time constant for I_{NaP} for a voltage step from -80 to -52 mV is 0.8 ms (Kay, Sugimori, et al., 1998).

3.9.5 Deactivation kinetics

Deactivation of I_{NaP} is generally rapid and exhibits a mono-exponential time course with a time constant, in cerebellar Purkinje cells, of about 0.2 ms (Kay, Sugimori, et al., 1998).

3.9.6 Inactivation

In hippocampal neurons the steady state inactivation of I_{NaP} is minimally effected by conditioning potentials between -90 and -70 mV but prepotentials from -30 to -20 mV reduce I_{NaP} to about 60% of control levels (Brown et al., 1994).

3.9.7 Function

The persistent sodium current is typically between 0.5 and 5% of the magnitude of the transient sodium current. Despite its small magnitude I_{NaP} has considerable functional significance because it is activated about 10 mV negative to the transient sodium current in a membrane voltage window where few voltage-gated channels are activated and neuron input resistance is high. Four broad functional consequences of the properties of I_{NaP} can be demonstrated: non-linear synaptic gain, plateau potentials, subthreshold oscillation (Kay, Sugimori, et al., 1998) and bursting.

3.9.8 Non-linear gain

French et al. (1990) found that the average maximum conductance for I_{NaP} of acutely dissociated neurons was 56% of intact neurons in slices suggesting that the I_{NaP} is most densely located on or close to the soma. The I_{NaP} found in the dendrites serves to increase the effectiveness of distal depolarizing synaptic activity by amplifying postsynaptic potentials. For example, in layer V cortical pyramidal cells, the current flowing through glutamate activated dendritic channels is amplified by threshold activation of persistent sodium channels (Schwindt and Crill 1995; Stuart and Sakmann 1995; Crill 1999). In CA1 pyramidals, Metz et al. (2005) found that at depolarized

(-55 mV), but not rest (-65 mV) potentials, somatic I_{NaP} provided a 29% amplification of the subthreshold response (measured as the integral of the decaying phase).

3.9.9 Plateau potential

Due to its lack of significant inactivation I_{NaP} can support a sustained suprathreshold depolarization, known as a plateau potential, which outlasts an initial depolarizing stimulus (Llinas and Sugimori 1980). Paradoxically, the nominally excitatory I_{NaP} can serve to suppress neural activity through the agency of the plateau potential since the sustained depolarization inactivates the fast transient sodium current and thus silences the neuron. Excitability can only be restored by a hyperpolarizing input that de-inactivates I_{NaF}. Chronic activation of the persistent sodium current can therefore simultaneously trigger an increase in neuronal burst discharges and a depression of both axonal (reduced afferent volleys) and network excitability (reduced fast EPSPs) (Brand, Seeger, et al., 2000).

Hippocampal persistent sodium current undergoes inactivation but to a much lesser extent than the transient current. Under long depolarizations, that completely inactivated the transient current, the persistent current was still greater than 50% of control values (French, Sah, et al., 1990). One functional implication of this situation is that the role of the persistent current grows with increasing durations of synaptic barrage. In neocortical pyramidals, the persistent Na^+ current has also been shown to undergo a very slow cumulative inactivation that is exhibited during slow voltage ramps (35 mV/s) preceded by a prolonged depolarizing pulse (Fleidervish, Friedman, et al., 1996).

3.9.10 Subthreshold oscillations

I_{NaP} possesses the two theoretical properties required for the role of a 'resonance amplifier' current (Hutcheon and Yarom 2000), a voltage-dependent time constant faster than the membrane time constant and the ability to amplify depolarizing voltage excursions. I_{NaP} has been shown to underpin a 10 Hz oscillation in layer II stellate neurons of the entorhinal cortex (Alonso and Llinas 1989) and a 40 Hz oscillation in cortical interneurons (Gutfreund, Yarom, et al., 1995). Hu and colleagues (2002) also propose that I_{NaP} plays a central role in ‘M-resonance’ - theta frequency resonance generated at membrane potentials around -60 mV by the M current and persistent Na^+ current in depolarized cells CA1 pyramidal cells.

3.9.11 Bursting

In adult CA1 pyramidal cells, a substantial I_{NaP} current is still active at the end of spike repolarization (-55 to -60 mV) and drives the afterdepolarization (ADP) that sustains burst firing (Azouz, Jensen, et al., 1996; Su, Alroy, et al., 2001). Consequently, application of I_{NaP}-specific agonists such as veratridin or anemone toxin II can convert regular firing cells into bursters (Alkadhi and Tian 1996; Mantegazza, Franceschetti, et al., 1998). Inhibition of I_{NaP} suppresses the spike ADP and associated burst activity (Alroy, Su, et al., 1999).

In contrast, Warman et al. (1994), in a modelling study of hippocampal CA1 pyramidals, found that the size of the slow afterdepolarization (ADP) was determined by the extent of overlap between the activation and inactivation curves of their I_{NaF} model i.e. the I_{NaF} window current. However, the physiological relevance of this observation is questionable. Their model lacked I_{NaP} and since the activation characteristics of the window current have been shown to be distinct from that of I_{NaP} (Kay, Sugimori, et al., 1998). It appears more probable that the Warman study unrealistically emulated the effects of I_{NaP} on the slow ADP.

3.9.12 Mechanism

The exact nature of the relationship between I_{NaP} and I_{NaF} is still a matter of considerable debate. Three general explanatory hypotheses have been advanced:

1. The window current hypothesis, which claims that the persistent current arises as a consequence of the overlapping of the steady state HH activation variable (m) and inactivation (h) curves of the transient sodium channel (Gahwiler and Llano 1989).
2. The separate channel hypothesis, which claims that the transient and persistent components are carried by separate channels.
3. The modal gating hypothesis, which argues that the two components are a consequence of the complicated gating dynamics of a single sodium channel (Alzheimer, Schwindt, et al., 1993; Nilius 1998).

The window current arises as an artefact of the Hodgkin Huxley model whereby the activation and inactivation curves overlap to produce a voltage 'window' where a steady state current is sustained. This rectification component of the transient channel is kinetically indistinguishable from an independent persistent current. The notion of a window current rests on one of the

assumptions of the HH model i.e. that the processes of activation and inactivation are independent.

In standard models of the transient current the overlap of the activation and inactivation curves is quite small. This implies that the persistent current is active only over a small voltage range. Hence, one approach to testing the window current hypothesis is to compare the predicted voltage range of the window current with the observed activation range of the persistent current. French et al (1990) calculated the steady-state window current for CA1 pyramidal cells and compared it with the measured steady state conductance for the same cell class. The predicted window current peaks at about -50 mV and fell rapidly to zero with further depolarization. In contrast, the activation curve for I_{NaP} increases monotonically. Similarly, I_{NaP}-driven plateau potentials in neocortical neurons were evident where the window current was predicted to be negligible. Corroborating evidence undermining the window current hypothesis was also found in guinea pig cerebellar Purkinje cells where the range of I_{NaP} activation exceeds the small overlap between the steady-state activation and inactivation curves of the transient current (Kay, Sugimori, et al., 1998). Kay and colleagues (1998) concluded that I_{NaP} is unlikely to be a window current.

The aforementioned difference in activation range between the window current and I_{NaP} would, prima facie, appear to provide evidence for the hypothesis that the fast transient and the slow persistent sodium currents are mediated by separate channels. Certainly, the non-inactivating sodium current has consistently been found to activate roughly 10 mV negative to the transient sodium current (French et al., 1990; Kay et al., 1998; Vreugdenhil et al., 2004).

However, this activation range anomaly may be explained as a consequence of voltage dependence of the time constant of the activation process. At small depolarizations sodium channel activation is slow and largely masked by the rapid (and largely voltage independent) inactivation process. Unmasking slow early activation by pharmacological blockade of the inactivation process shifts the macroscopic activation curve of I_{NaF} to the more negative voltage range characteristic of I_{NaP}. In neocortical neurons, for example, the activation curve for I_{NaP} is approximately 7 mV more negative than that of I_{NaF}. Nonetheless, pharmacological blockade of the inactivation process using papain unmasks I_{NaF} activation occurring at I_{NaP}-like potentials (Brown et al., 1994).

An alternative approach to resolving the nature of the relationship between I_{NaP} and I_{NaF} is illustrated by a recent study which showed how the extent and rate of channel block and unblock

by low and high concentrations of TTX (and the levels of inactivation caused by conditioning pulses) varied in tandem for the transient and persistent forms (Taddese and Bean 2002).

Taddese and Bean (2002) also proposed a simple allosteric model, in support of the modal gating hypothesis, that explained the persistent and transient currents on the basis of the modal activity of a single sodium channel type. They suggest that under depolarization the sodium channel progresses through a series of activated states. Each successive activation state has a higher affinity for the inactivation particle. Binding of the inactivation particle stabilises the channel in an activated, but non-conducting, state. However, in highly activated states the channels are stabilised in equilibrium with a small, non-zero proportion of unbound inactivation particles. In their model, it is this small conducting subpopulation of channels that is responsible for the I_{NaP} current. Taddese and Bean estimate the equilibrium ratio, I_{NaP}:I_{NaT}, to be about 1:200 or 0.5% I_{NaP}. Their model reproduces most sodium voltage clamp behaviour, including a positive-shifted I_{NaP} activation curve relative to the steady state inactivation curve and the slow and variable inactivation during voltage steps.

Perhaps the most compelling evidence for the thesis that the transient and persistent TTX-sensitive components are aspects of single modal channel is obtained from studies in which electrophysiological recordings from tissues are correlated with identification of the sodium channel isoforms present in those tissues. When expressed in exogenous expression systems, such as xenopus oocytes, isoforms of the sodium channels spontaneously exhibit a persistent current component (Goldin 2001). The three most significant sodium channel isoforms, $Na_{V1.1}$, $Na_{V1.2}$ and $Na_{V1.6}$, exhibit notable differences in both the level and voltage dependence of the intrinsic persistent current component (Smith, Smith, et al., 1998). At negative potentials the persistent component of $Na_{V1.1}$ is relatively large (over 5%) but decreases with increasing depolarization. Isoform $Na_{V1.2}$ exhibits a uniformly low persistent component of below 1% at all voltage levels. Significantly, the persistent component of $Na_{V1.6}$ increases linearly to a maximum of over 5% with increasing depolarization (Smith and Goldin 1998). This behaviour is in line with the conventional TTX-sensitive persistent sodium current reported in the literature. For example, in cerebellar Purkinje cells, in which isoforms, $Na_{V1.1}$, $Na_{V1.2}$ and $Na_{V1.6}$ have been isolated, the persistent current is mediated by isoform $Na_{V1.6}$ (Vega-Saenz De Miera, Rudy, et al., 1997). Further, mouse Purkinje cells carrying null mutations for $Na_{V1.6}$ exhibit significantly reduced persistent sodium current (Raman, Sprunger, et al., 1997).

3.9.13 Modulation

In central neurons, the persistent sodium channel is regulated by a range of neurotransmitters (Mittman and Alzheimer 1998; Pierson, Tribollet, et al., 2001). For example, in prefrontal cortex pyramidals, dopamine receptor D_1/D_5 activation can differentially modulate the persistent sodium current in a voltage-dependent manner: at potentials more negative than -40 mV I_{NaP} was augmented but decreased at more positive voltages (Gorelova and Yang 2000). The same group also showed that dopamine slows the inactivation process. Nitric oxide has a similar effect (Ahern, Hsu, et al., 2000).

I_{NaP} is activated by pro-epileptic conditions such as low extracellular calcium (Su, Alroy, et al., 2001) and high intracellular calcium (Schwindt, Spain, et al., 1992). In CA1 pyramidals cells, low extracellular Ca^{2+} induced intrinsic bursts and the underlying afterdepolarization that carries the burst was suppressed by drugs that reduce the persistent Na^+ current indicating that I_{NaP} mediates the slow burst depolarization (Azouz, Jensen, et al., 1996). Conditions such as hypoxic stress can also trigger an increase in persistent sodium channel activity (Hammarstrom and Gage 1998).

The levels of I_{NaP} expression appear to be linked to levels of network excitability. In animal models of epilepsy (Wellmer, Su, et al., 2002; Agrawal, Alonso, et al., 2003) and resections from epilepsy patients I_{NaP} (Vreugdenhil, Hoogland, et al., 2004) is substantially upregulated in pyramidal neurons. The mechanism underpinning either adaptive or maladaptive regulation is currently unknown.

Pharmacologically, I_{NaP} is targeted by a range of anti-epileptic drugs that spare I_{NaF} at therapeutically significant doses: phenyotin in hippocampal neurons (Segal and Douglas 1997), ethosuximide in thalamic neurons (Leresche, Parri, et al., 1998), and in neocortical neurons, topimarate (Taverna, Sancini, et al., 1999), valproic acid (Taverna, Sancini, et al., 1999), lamotrigine and riluzole (Spadoni, Hainsworth, et al., 2002).

3.9.14 Fast, slow, and persistent components

Kay et al. (1988) resolved the sodium current of acutely isolated guinea pig cerebellar Purkinje cells into fast inactivating, slowly inactivating and persistent components. These clearly distinguishable components exhibited identical TTX sensitivities. Of potentially functional significance, the activation threshold sequence for these three components was persistent, slow

and then fast. There was a tenfold increase in current amplitude at each stage (Kay, Sugimori, et al., 1998).

3.9.15 I_{NaP} in the subiculum

3.9.15.1 Characteristics

In a study that examined TTX-sensitive currents in subiculum resected from human TLE patients and rat controls, Vreugdenhil et al. (2004) provide the only detailed description to date of I_{NaP} in subicular neurons. Notably, voltage-dependence and kinetic characteristics of human and rat currents are statistically identical.

After eliminating K^+ and Ca^{2+} channels Vreugdenhil et al. (2004) isolated three components of the sodium current: a fast inactivating, slowly inactivating and a non-inactivating component. The amplitude of the persistent current was defined as the sum of the slowly inactivating and the non-inactivating components. The Vreugdenhil et al. (2004) study suggests the existence of at least four classes of subicular sodium current: a conventional fast transient current (with a 2 ms inactivation time constant at -30 mV), a fast transient current with intermediate inactivation kinetics (10 ms at -30 mV), a slowly inactivating persistent current (average inactivation time constant of 152 ms) and a very slowly inactivating persistent current (time constant < 10 seconds).

In human subicular cells derived from temporal lobe epilepsy (TLE) patients, the persistent current as a fraction of the total sodium current varied widely from below 1% to 53% (Vreugdenhil, Hoogland, et al., 2004). The distribution of the persistent fraction across cells was well fitted by two normal curves with averages of about 3% (the 'low' I_{NaP} group with less than 5% I_{NaP}) and 17% (the 'high' I_{NaP} group with more than 5%). Vreugdenhil et al., found I_{NaP} in only one third of rat subicular cells. The persistent sodium current fraction in rat subicular cells was normally distributed with a 5% average, which is close to that of human low I_{NaP} cells. This close correspondence between the low I_{NaP} populations in rats and humans strongly indicates that the high I_{NaP} fraction developed as sequelae to TLE.

Of potential significance for the hypothesis that I_{NaF} and I_{NaP} are aspects of the same channel, is the observation that the subicular sodium current appears to be conserved insofar as the average total sodium peak current magnitudes for both the low and high I_{NaP} populations are identical (about 6.2 nA).

3.9.15.2 Activation

The average activation half-activation voltage at 23˚C is reported as -44.9 mV for rat I_{NaP} with a slope potential of 4.3 mV (Vreugdenhil et al., 2004). This implies an activation threshold of about -65 mV. The Vreugdenhil data roughly is somewhat more depolarized than the implied I_{NaP} threshold of about -70 mV for a representative bursting neuron presented by Mattia et al. (1997a) but could account for the initiation of TTX-sensitive subthreshold membrane oscillations in subicular bursters beyond around -60 mV (Mattia, Kawasaki, et al., 1997).

3.9.15.3 Activation kinetics

The activation kinetics of subicular I_{NaP} have not been systematically characterised. Vreugdenhil et al. (2004) reported a time-to-peak at 23˚C for sodium currents of 0.71 and 0.75 ms at 30 mV in cells with a high and low contribution of I_{NaP}, respectively. The time-to-peak for rat cells with large persistent sodium contributions is not significantly different at 0.76 ms. The near-instantaneous activation kinetics of I_{NaP} are very similar to those of I_{NaF} (Vreugdenhil, Hoogland, et al., 2004; Wu, Enomoto, et al., 2005). For this reason, the activation characteristics of I_{NaF} are used to compensate for the lack of subicular I_{NaP} data.

Vreugdenhil et al. (2004) modelled slow I_{NaP} inactivation using a Boltzmann equation augmented with a constant term that represented the persistent component of the I_{NaP}. In the high (low) I_{NaP} population this constant term constituted 49% (19%) of the maximum current. Although the 'high' and 'low' populations have different V_{half} values (-66.3 and -60.1 mV, respectively) we assume that the inactivation curves for both populations are the same. We base this assumption on two observations. Firstly, the presence of the constant term in the modified Boltzmann forces the high I_{NaP} inactivation curve to level out prematurely and thus causes an artificial hyperpolarizing shift in the curve. Secondly, Vreugdenhil et al. (2004) also provide a figure showing superimposed inactivation curves from high and low cells that are identical until the high cell curve diverges to accommodate the constant term.

3.9.15.4 Inactivation kinetics

The variable potential 500 ms conditioning voltage used by Vreugdenhil et al. (2004) to determine the steady state inactivation of I_{NaP} isolated a slowly inactivating and a persistent sodium component. The average time constant of inactivation for the slowly inactivating component at -30 mV was 152 ms. The 'persistent' component disappeared in a second set of

experiments that used a 10 second conditioning potential (Vreugdenhil, Hoogland, et al., 2004). No time constants were reported for this component.

3.9.15.5 Function

In the subiculum, recent analysis has isolated two forms of bursting in subicular neurons: weak and strong bursting (Jung, Staff, et al., 2001; Menendez de la Prida, Suarez, et al., 2003). I_{NaP} appears to play a crucial role in the depolarizing afterpotential that drives high threshold (equivalent to weak) bursting in subicular cells (Wellmer, Su, et al., 2002).

Interestingly, the effects of the anticonvulsant topiramate were investigated in subicular bursting cells (Kawasaki, Tancredi, et al., 1998) before it became known that topiramate (TPM) is an I_{NaP} inhibitor (Taverna, Sancini, et al., 1999). The Kawasaki et al. (1998) study provides some insights into the function of I_{NaP} in subicular pyramidal cell electrophysiology, although the effects are somewhat confounded by the ability of TPM to potentiate $GABA_A$ receptors and high-threshold L-type calcium channels (Zhang, Velumian, et al., 2000). For example, topiramate causes a steady state hyperpolarization of V_{rest} that ranged from -2 to -16 mV (with a concomitant drop in the apparent membrane resistance of 24-62%) but this effect is abolished by the application of a $GABA_A$ antagonist (Kawasaki et al., 1998).

Topiramate increases, in a dose-dependent manner, the amount of depolarizing current required to trigger a burst response. This dose-dependency is reduced when the steady-state hyperpolarization induced by TPM is compensated with injected depolarizing current. The number of regular spikes evoked by a depolarizing current is also reduced. Both of these effects persist in the presence of $GABA_A$ receptor antagonists (Kawasaki et al., 1998). In conjunction with the finding of a pathologically increased I_{NaP} component in the hyper-excitable subicular pyramidal cells of temporal lobe epilepsy patients (Vreugdenhil et al., 2004), the implied I_{NaP}-dependent firing sensitivity suggests a prominent role for I_{NaP} in determining the excitability of subicular pyramidal cells.

Only 62% of bursting cells tested by Kawasaki and colleagues (1998) were sensitive to TPM prompting the authors to suggest that the 'variable efficacy' of TPM was due to different degrees of phosphorylation of native neurons. Perhaps a less convoluted explanation is that the variable efficacy of TPM largely reflects the variation in the distribution of the target persistent sodium channel in subicular pyramidals (Vreugdenhil et al., 2004).

3.9.15.6 Subthreshold oscillations

Subicular bursting and regular firing pyramidal cells display subthreshold oscillations at membrane potentials between rest and firing threshold (Mattia, Kawasaki, et al., 1997; Cooper, Moore, et al., 2003). The subthreshold activation range, and the ability of the sodium channel inhibitor TTX to abolish the oscillations, strongly implicates the persistent sodium channel in the generation of STOs in subicular bursters.

3.9.15.7 Anodal break potential

Stewart and Wong (1993) reported that the depolarizing rebound potential (anodal break potential or post inhibitory response), that occurs upon the release of a hyperpolarizing conditioning potential, is strongly attenuated by caesium or TTX. The TTX-sensitive component is almost certainly due to I_{NaP} and serves to amplify the I_H contribution. The magnitude of the anodal break potential (ABP) can be large enough to trigger spikes or bursts (Stewart and Wong, 1993), which implies that the component of I_{NaP} inactivated near rest and unleashed by de-inactivation is significant. For example, Figure 1A of the Stewart and Wong (1993) paper illustrates a rebound burst triggered by an ABP with amplitude of over 15 mV for a neuron with a resting potential of -75 mV.

A potentially significant function of I_{NaP} arises out of the aforementioned mobilisation of a de-inactivated pool of persistent sodium channels in response to the break of a hyperpolarizing stimulus. The ability of this reserve I_{NaP} capacity to amplify the anodal break potential to threshold provides subicular pyramidals with a firing threshold in the hyperpolarized direction. Subicular pyramidals can therefore initiate firing in response to both excitatory and inhibitory input.

3.9.16 Model of subicular I_{NaP}

For the purposes of this study we will assume that the transient and persistent sodium currents are the product of two distinct channel populations with similar activation kinetics but different activation thresholds and inactivation properties. We only model the slowly inactivating, 'persistent' sodium channel (Figure III-6).

$$I_{NaP} = g_{NaP} m^2 h (V_m - E_{Na})$$

3.9.16.1 Activation

Vreugdenhil et al. (2004) assayed subicular sodium currents at 23˚C. However, activation kinetics are temperature sensitive, so in order to convert their findings to the 33˚C used in this thesis data from CA1 is used. In CA1 neurons, Sah et al. (1988) reported time-to-peak, t_{peak}, values for I_{NaF} against voltage at 17.5, 20, 22.5, and 26.5˚C. To derive an estimate of the temperature dependence of I_{NaP} we plotted these time-to-peak values at 30 mV against temperature, T, and fitted them to a reciprocal log equation:

$$t_{peak} = \frac{1}{16.3+5.9\ln(T)}$$

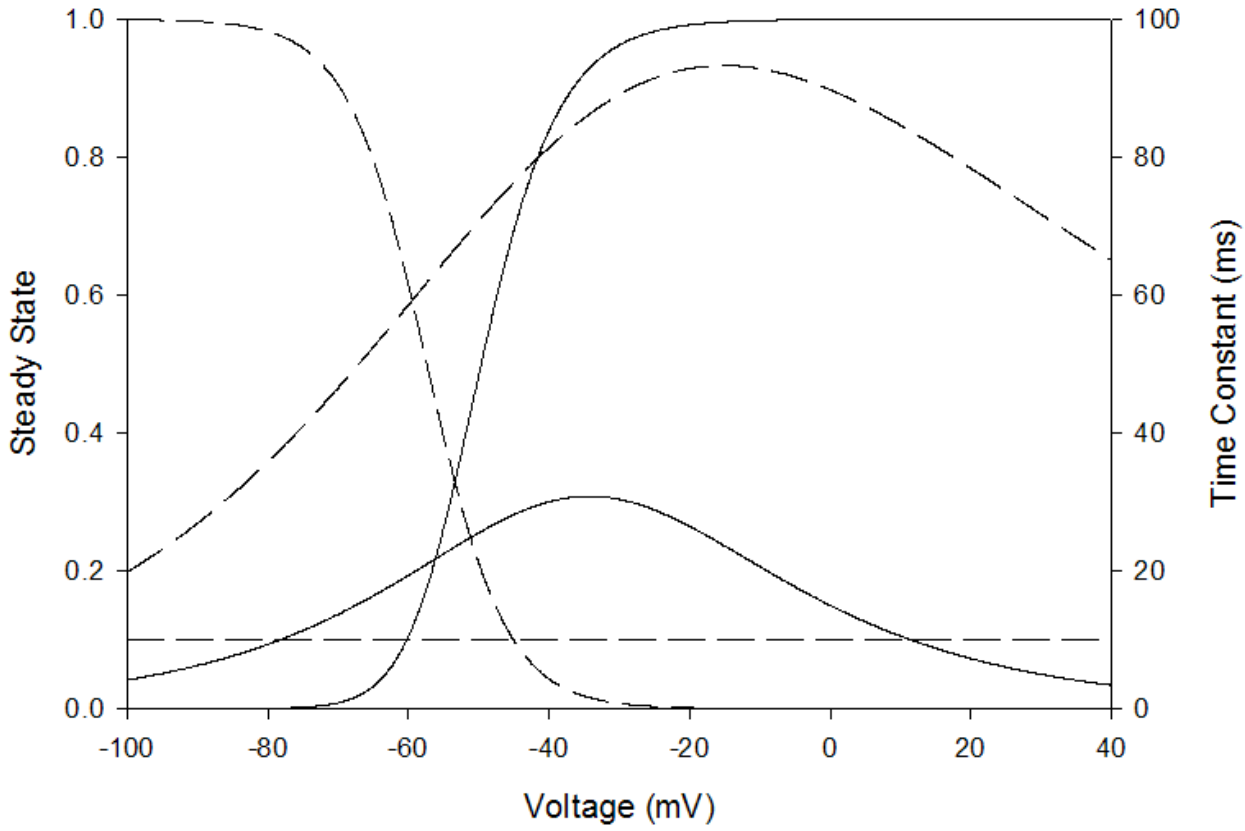

Figure III-6. Plot of the activation (solid lines) and inactivation (dashed lines) steady state and time constant curves for I_{NaP}. The steady state activation curve is raised to its exponent of 2. The activation time constants have been multiplied by 100 and the deactivation time constant has been multiplied by 10 in order to fit the inactivation and activation curves on the same graph.

This equation predicts a time-to-peak of 0.3 ms at the standardised temperature range of 32-34˚C used in this thesis. The Sah data provides a reference-scaling ratio for the Vreugdenhil data of 1.7 (0.5 ms/0.3 ms) and yields a t_{peak} at 30 mV for subicular pyramidals at 33˚C of about 0.45 ms (0.76/1.7). A rough estimate of the activation time constant at -30 mV and 33˚C of 0.28 ms was obtained by applying an approximate conversion factor of 0.67 to the time-to-peak value of 0.45 ms.

The I_{NaP} inactivation components given by Vreugdenhil et al. (2004) share the same inactivation curve steady state activation curve. In order to allow I_{NaP} to participate in STO and rebound burst events we shifted the rat cell activation curve reported by Vreugdenhil et al. (2004) leftward by several millivolts to obtain a stronger activation close to -70 mV. The resulting steady state activation curve has an apparent half activation voltage and slope factor of about -49.3 and -4.9 mV, respectively.

$$m_{inf} = \frac{1}{1 + e^{\frac{V-(-55.3)}{-6.4}}}$$

3.9.16.2 Activation kinetics

The activation kinetics of I_{NaP} are still poorly characterised in subiculum so we adjusted the voltage-dependent activation time constants of I_{NaP} around a single scaled time-to-peak value provided by Vreugdenhil et al. (2004) of 0.76 ms. We temperature-scaled this value and performed an approximate time constant conversion to obtain 0.3 ms at -30 mV.

$$\tau_m = \frac{e^{\frac{V+23.5}{24.1}}}{1+e^{\frac{V+35.2}{12.5}}}$$

3.9.16.3 Deactivation

In order to facilitate investigation of the ability of I_{NaP} to support depolarizing afterpotentials, we added a separate stationary deactivation time constant. During a simulation, I_{NaP} switches between the activation and deactivation time constant functions depending on the instantaneous slope of the membrane voltage trace. The conventional activation time constant function is used when the voltage is rising, whilst the deactivation time constant is employed on negative voltage slopes.

3.9.16.4 Deactivation kinetics

A requirement for relatively slow I_{NaP} deactivation kinetics in subicular neurons is suggested by their response to brief stimuli. Subicular bursting neurons can respond to brief (10 ms) just-threshold depolarizing stimuli with a delayed spike or burst that rides upon an ADP 'plateau potential' that persists beyond the end of the stimulus pulse for upwards of 30 ms (Mason, 1993; Wellmer et al., 2002; Menendez de la Prida et al., 2003). Under zero-Ca^{2+} conditions this ADP persists but in a greatly attenuated form (Wellmer, Su, et al., 2002), indicating that I_{NaP} plays a minor role in the burst ADP. By contrast, Menendez de la Prida et al. (2003) reported that the ADP evoked by subthreshold stimuli was completely eliminated by TTX. However, the 30-50 ms deactivation time constant required to enable this I_{NaP} contribution to persist beyond the termination of the depolarizing stimulus is considerably slower than that conventionally ascribed to I_{NaP}.

Since the absence of extracellular calcium can suppress the rate of I_{NaF} deactivation (Armstrong and Cota 1999) it is possible that the apparent I_{NaP} signature is actually due to an anomalous slowly deactivating I_{NaF} fraction. Accordingly, the aforementioned zero-Ca^{2+} experiments need to be interpreted with caution. Nevertheless, the similar spike time courses seen in both control and zero-Ca^{2+} conditions in Figure 4 of the Wellmer paper hints that this effect is unlikely to be significant in this case. A stationary deactivation constant of 1 ms was used:

$$\tau_{deact} = 1 \text{ ms}$$

3.9.16.5 Inactivation

Since the inactivation curve of sodium channels shifts towards more positive potentials with increasing temperature (Sah, Gibb, et al., 1988; Schwarz 1986) the I_{NaP} inactivation curve described by Vreugdenhil et al. (2004) for the rat I_{NaP} cell population was shifted several millivolts in the depolarizing direction.

$$h_{inf} = \frac{1}{1 + e^{\frac{V-(-57.4)}{5.6}}}$$

3.9.16.6 Slow inactivation kinetics

Preliminary simulations suggested that I_{NaP}, rather than I_{NaF}, is involved in subicular frequency-dependent firing mode switching (Cooper et al., 2005). The roughly 100 ms (10 Hz) refractory period for subicular bursting (Cooper et al., 2005) is complemented by the slow inactivation time constant for a I_{NaP} component reported by Vreugdenhil at -30 mV of 152 ms. A temperature-adjusted slow inactivation time constant function was constructed that reproduced the observed subicular burst refractory period.

$$\tau_h = \frac{1}{0.003e^{\frac{V+103.1}{89.1}} + e^{\frac{V+190}{-29.5}}}$$

3.9.16.7 Maximum conductance

Vreugdenhil et al. (2004) reported a maximum conductance for I_{NaP} of 3.4 nS in dissociated rat pyramidals. This is somewhat higher than the 1.2 nS conductance seen in hippocampal slice preparations (French et al., 1990). This reference value was adjusted to 7 nS to allow I_{NaP} to amplify 'M-resonance' and drive the early component of the burst ADP.

3.10 High threshold, non-inactivating calcium current, I_{CaL}

The 'long-lasting' dihydropyridine-sensitive, high voltage activating (HVA) L-type current is characterised by sensitivity to dihydropyridines (DHPs) and slow inactivation. The biophysical properties of L-type currents were first reported for chick dorsal root ganglion neurons (Nowycky, Fox, et al., 1985), although L-type channels have been found in all types of cells except platelets.

3.10.1 Channel

On the basis of sequence homology, L-type currents are classified under the Ca_{V1} subfamily. Four subtypes are recognised, based largely on the fact that the channels encoded by these cDNAs are all DHP sensitive: the $\alpha_{11.1}$ subunits (also known as α_{1S}), first isolated from skeletal muscle (Nowycky, Fox, et al., 1985); the $\alpha_{11.2}$ (α_{1C}) subunits derived from heart muscle (Mikami, Imoto, et al., 1989); the $\alpha_{11.3}$ (α_{1D}) of neuroendocrine tissue (Williams, Feldman, et al., 1992); and the $\alpha_{11.4}$ (α_{1F}) whose expression is evidently restricted to retina (Fisher, Noegel, et al., 1997). The activation and inactivation characteristics of cloned L-type α subtypes vary quite widely and, as with most channels, are strongly determined by the presence of auxiliary subunits.

The broad reliance on DHP sensitivity as the defining characteristic of I_{CaL} currents has lead to considerable diversity within the group. In cerebellar granule cells, for example, three subtypes coexist; two resemble the cardiac derived form whilst the other exhibits voltage-dependent potentiation (Forti and Pietrobon 1993).

The reported properties for I_{CaL} are dependent on the nature of the permeant ion. The inhibitory effects of agonists on the single-channel open time, single-channel conductance, and deactivation tail kinetics of I_{CaL} are differentially dependent on whether the charge carrier is barium or calcium (Tavalin, Shepherd, et al., 2004). In hippocampal neurons, there is a five-fold variation in the single channel amplitude of I_{CaL} using between calcium ions (~191 fA) and barium ions (~950 fA) (Marrion and Tavalin 1998).

3.10.2 Distribution

On the subcellular level, the L-type channel is generally concentrated in the perisomatic region. In hippocampal and neocortical neurons, the $\alpha_{11.2}$ and $\alpha_{1.3}$ subunits are primarily localized in neuronal cell bodies and proximal dendrites with relatively dense labelling frequently observed at the base of major dendrites (Hell, Westenbroek, et al., 1993). Similarly, in cultured GABAergic mouse cortical neurons the $\alpha_{11.2}$ and $\alpha_{1.3}$ subunits of L-type channels are found across cell bodies and dendrites (Timmermann, Westenbroek, et al., 2002). A more circumscribed distribution is found in AII amacrine cells, which express L-type channels principally at their synapses with some low-level proximal dendrite expression (Habermann, O'Brien, et al., 2003). In thalamocortical relay cells, local interneurons and reticular thalamic neurones channel density is highest in the soma and decreases significantly towards the dendritic region (Budde, Munsch, et al., 1998).

3.10.3 Activation

The L current is typically rapidly activated by potentials above between -40 and -30 mV in CA1 pyramidals (Brown and Griffith 1983; Kay and Wong 1987). In acutely isolated guinea pig CA1 pyramidals, the steady-state activation of the Ca^{2+} current was well described by a squared Boltzmann equation (i.e. cooperativity factor of two) (Kay and Wong 1987). Whilst most L-type currents are activated 15-20 mV above threshold, the variability within the broadly defined L-type class is illustrated by the lower activation potentials of $Ca_{V1.3}$ subunit class as compared to

$Ca_{V1.2}$ (Koschak, Reimer, et al., 2001). The hyperpolarized near-threshold activation threshold seen in spinal motoneurons provides a further illustration (Li and Bennett 2003).

3.10.4 Activation kinetics

Anomalously slow activation kinetics peaking 100-300 ms after the onset of a depolarizing command are reported for I_{CaL} in an early paper by Brown and Griffith (1983). Later papers report activation kinetics in the low millisecond range (Kay and Wong 1987; Tavalin, Shepherd, et al., 2004).

3.10.5 Inactivation

In sensory neurons, L-type Ca^{2+} currents display a slight inactivation during application of 200-msec depolarization pulses with an associated activation time constant greater than 500 ms (Fox, Nowycky, et al., 1987). The current begins to inactivate at holding potentials more positive than about -60 mV and, when elicited from a holding potential of -60 mV, reaches its maximum amplitude around +10 mV. Brown and Griffith (1983) found no evidence for time-dependent inactivation of I_{CaL} in CA1 using depolarizing steps of up to 700 ms. Fisher et al. (1990) noted a similar lack of inactivation of I_{CaL} in CA1 and CA3.

3.10.6 Modulation

L-type channels are targeted of a large number of clinically significant drugs. As noted previously, I_{CaL} currents are inhibited by DHPs such as niferidine (Bean 1989). Other major classes of drugs include the phenylalkylamines, and benzothiazepines (Yamakage and Namiki 2002). BAY K8644 is a well-established I_{CaL} agonist. The L-type current is blocked by Co^{2+} and Cd^{2+} and enhanced by increases in Ca^{2+} (Kay and Wong 1987). L-type (and T-type) channels are also blocked by Ni^{2+} (Ertel and Ertel 1997). Unlike other HVA currents, I_{CaL} appears to be insensitive to somatostatin (Viana and Hille 1996). The anticonvulsant topiramate (TPM) inhibits L-type currents in rat dentate gyrus granule cells (Zhang, Velumian, et al., 2000).

3.10.7 Function

I_{CaL} has been implicated in a remarkably broad range of functions. Presynaptically, L-Type channels underlie a slow excitatory synaptic transmission in rat midbrain dopaminergic neurons (Bonci, Grillner, et al., 1998). In retinal amacrine cells, I_{CaL} acts postsynaptically, in conjunction with other HVA currents, to boost excitatory synaptic input (Koizumi, Watanabe, et al., 2001).

L-Type channels have also been reported to mediate NMDA-independent long-term potentiation (LTP) at thalamic input synapses in the amygdala (Weisskopf, Bauer, et al., 1999).

Apropos to these findings is the observation that although the total contribution of I_{CaL} to intracellular calcium concentrations is relatively small, elimination of the I_{CaL} contribution exerts a disproportionate effect on gene transcription (Deisseroth, Heist, et al., 1998). Remarkably, I_{CaL} appears to underpin the ability of the neuron to selectively initiate activity-dependent gene expression in response to rises in intracellular calcium due to EPSPs but not spikes (Mermelstein, Bito, et al., 2000). The negative activation threshold and relatively slow activation kinetics of the L-type channels act as a 'kinetic filter' that distinguishes between EPSP and spike activity (Mermelstein et al., 2000).

I_{CaL} has also been implicated in electrophysiological pathologies. For example, following chronic spinal injury, motoneurons spontaneously develop persistent sodium and calcium currents. These currents contribute to a plateau potential that drives the neuronal excitability associated with post-injury spasticity (Li and Bennett 2003). In these neurons, I_{CaL} contributes equally with the persistent sodium current to the initial total persistent current. Under sustained depolarization partial inactivation of I_{CaL} reduces this contribution by about two-thirds (Li and Bennett 2003).

I_{CaL} is upregulated in reactive astrocytes following brain injury. This augmentation is selective for the $\alpha_{11.2}$ subunit and does not appear to affect the P/Q or N currents (Westenbroek, Bausch, et al., 1998). Westenbroek et al. (1998) suggest that this selective upregulation is an attempt to maintain ionic homeostasis and promote the release of neurotrophic agents in injured brain regions. A prominent role for I_{CaL} in the neuronal cell death associated with spongiform encephalopathies, such as Alzheimer's disease, is also apparent. For example, the Alzheimer's markers, amyloid β protein and human group IIA secretory phospholipase, induce neuronal apoptosis by increasing the calcium influx through L-type channels (Ueda, Shinohara, et al., 1997). Inhibition of I_{CaL}, but not I_{CaN} or $I_{CaP/Q}$, protects cortical neurons from the neurotoxic effects of these proteins (Yagami, Ueda, et al., 2004).

The upregulation of I_{CaL} in response to injury is commensurate with an observed increase in the density of L-type channels during aging (Thibault and Landfield 1996). In primary culture, hippocampal neuronal survival over 28 days is inversely related to an increased calcium current density that was largely attributable to I_{CaL} (Porter, Thibault, et al., 1997). Significantly, learning

in aged animals is inversely correlated with L-type channel density (Thibault and Landfield 1996).

The L-type current provides the dominant calcium contribution responsible for the calcium-dependent potassium current-driven slow AHP (sAHP) in CA3 pyramidals (Tanabe, Gahwiler, et al., 1998). While, N-type and P/Q-type blockers has no effect on the sAHP (although see Shah and Haylett, 2000), selective inhibition of I_{CaL} current reduces the sAHP by over 80% (Tanabe, Gahwiler, et al., 1998). I_{CaL} appears to exert its influence over I_{AHP} indirectly, via a coupling with intracellular calcium-dependent calcium stores (Tanabe, Gahwiler, et al., 1998)

The involvement of I_{CaL} in some forms of burst behaviour is indicated by the ability of the L-type channel blocker, nifedipine, to abolish apamin-induced bursting activity in nigral dopamine-containing neurons (Shepard and Stump 1999). Nifedipine also blocks serotonin-induced plateau potentials following depolarization of guinea pig trigeminal motoneurons, thus implicating I_{CaL} in the phenomenon of membrane potential bistability (Hsiao, Del Negro, et al., 1998).

3.10.8 I_{CaL} in the subiculum

Although, little is known about subicular I_{CaL}, the perisomal location of L-type channels hints at a role in controlling the somatic excitability of subicular pyramidals.

3.10.8.1 Bursting

The requirement for an action potential to trigger the burst ADP implicates HVA calcium channels in subicular neuron bursting (Jung et al., 2001). The rapid activation time constant of I_{CaL} hints at a prominent role for the L-type HVA current in this process. However, inhibition of subicular I_{CaL} by nimodipine fails to abolish the burst response and only reduces by 12% the calcium tail current involved in bursting in subicular cells (Jung et al., 2001). Although, nimodipine also inhibits the fast transient calcium current, I_{CaT}, (Randall and Tsien 1997), the aforementioned dearth of evidence for substantive levels of I_{CaT} in subicular pyramidals suggests that I_{CaL} is likely to constitute to the bulk of the nimodipine-sensitive fraction.

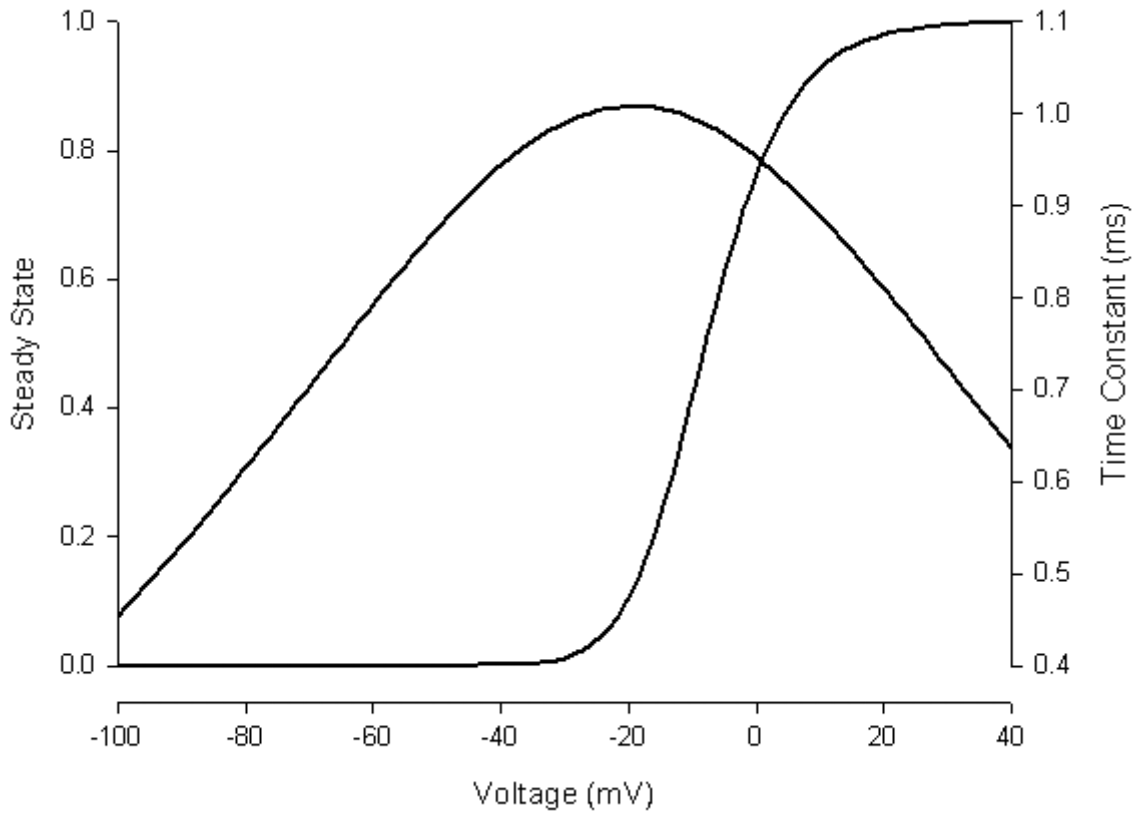

Figure III-7. Plot of the steady state and time constant activation curve for $I_{Cal.,}$ The steady state activation curve is raised to its exponent of 2.

3.10.8.2 Slow afterhyperpolarizations

Subicular regular firers, although generally not bursters, display a slow AHP following the termination of suprathreshold depolarizing stimulation (Behr, Empson, et al., 1996). The sustained activation of I_{CaL} is ideally placed to trigger activation of the Ca^{2+}-dependent I_{AHP} current responsible for the sAHP, as occurs in CA3 pyramidals (Tanabe, Gahwiler, et al., 1998).

The anticonvulsant topiramate (TPM) inhibits L-type currents in rat dentate gyrus granule cells (Zhang, Velumian, et al., 2000). In the subiculum, Kawasaki et al. (1998) noted a dampening effect of TPM on subicular bursters that may, in part, be due to the effect of TPM on subicular $I_{Cal.,}$ Unfortunately, since TPM also suppresses sodium currents (Taverna, Sancini, et al., 1999), GABA receptors (Brown, Wolf, et al., 1993), and transiently activates other HVA calcium currents (Zhang, Velumian, et al., 2000), it is impossible to isolate the contribution of I_{CaL} inhibition to the effects of TPM on subicular bursters.

3.10.9 Model of subicular I_{CaL}

We use an adapted version of the non-inactivating HH model of guinea pig CA1 I_{CaL} described by Kay and Wong (1987) (Figure III-7).

$$I_{CaL} = p_{CaL} m^2 h z^2 \frac{VF^2}{RT} \frac{[Ca^{2+}]_i - [Ca^{2+}]_o \exp^{-z_{Ca} FV/RT}}{1 - \exp^{-z_{Ca} FV/RT}}$$

3.10.9.1 Activation

The steady state activation curve has a V_{half} of 1 mV and a slope factor of 3.2 mV. The cooperativity factor of 2 gives an effective activation threshold of about -30 mV.

$$m_{inf} = \frac{1}{1 + e^{\frac{V-(-14.5)}{-7.5}}}$$

3.10.9.2 Activation kinetics

The original rate constant equations were temperature scaled from 23 ° C to 33 ° C using a Q_{10} of 2. The temperature-scaled kinetics reach a peak of about 1 ms at -20 mV.

$$\tau_m = \frac{e^{\frac{V+59.5}{55.5}}}{1+e^{\frac{V+20.6}{28.4}}}$$

3.11 High threshold P/Q-type calcium channel, $I_{CaP/Q}$

The P-type calcium current, I_{CaP}, is a high-threshold, very slowly inactivating channel. First described in the Purkinje cell (Llinas, Sugimori, et al., 1989), I_{CaP} constitutes the major calcium current in these cells (Regan 1991). The I_{CaP} current is blocked by the omega-AGA-VIA and omega-AGA-VIB components of funnel web spider venom (Mintz, Adams, et al., 1992). The associated inactivating Q-type current, I_Q, first recorded in cerebellar granule neurons, has relatively similar kinetic properties but is distinguished by a lower affinity for omega-AGA-GVIA (K_d >10 nM for Q-type, <10 nM for P-type) (Dunlap K. 1995; Randall and Tsien 1995).

3.11.1 Channel

Native I_{CaP} correlates with $Ca_{V12.1}$ subunit expression in Purkinje cells (Llinás, Sugimori, et al., 1992). However, when these subunits are expressed in Xenopus oocytes they exhibit Q-like

behaviour; such as a more depolarized activation threshold and inactivation within 100 ms (Sather, Tanabe, et al., 1993). Thus, these subunits are thought to support both P- and Q-type channel currents. Several channels of intermediate type have been found in a variety of preparations (Tottene, Moretti, et al., 1996; Forsythe, Tsujimoto, et al., 1998; Mermelstein, Foehring, et al., 1999), which suggests that P-type and Q-type represent points on a spectrum of channel properties. This conclusion is bolstered by the finding that differences in I_{CaP} and I_Q inactivation and toxin affinity can be largely explained in terms of splice variants or β subunit association (Bourinet, Soong, et al., 1999; Mermelstein, Foehring, et al., 1999).

3.11.2 Modulation

P-type currents are suppressed by noradrenaline in neocortical pyramidals (Timmons, Geisert, et al., 2004). In cerebellar Purkinje neurons, P-type channels are weakly inhibited by compounds from a range of D_2 dopamine receptor antagonist classes including phenothiazines, diphenylbutylpiperidines, butyrophenones, and a piperazine (fluphenazine) (Sah and Bean 1994). P/Q-type channels are also strongly inhibited by serotonin via the 5-HT_{1A} receptor (Bayliss, Li, et al., 1997). Cannabinoid receptor activation interferes with neurotransmitter release by inhibiting presynaptic Q- and N-type calcium channels (Sullivan 1999).

The effects of modulation can be quite dramatic. For example, P-type and Q-type currents are differentially regulated during the period of target innervation of embryonic development in mouse large diameter dorsal root ganglion neurons (Hilaire, Diochot, et al., 1996): the P-type current disappears at day 15 whereas the Q-type current increased up to three-fold during the same embryonic period. The effectors responsible for this differential regulation are currently unknown.

3.11.3 Distribution

As probed by immunolabelling, the P-type channel is distributed widely throughout the mammalian central nervous system, with particularly high concentrations in the cerebellum, brainstem, habenula, nucleus of the trapezoid body and inferior olive (Hillman 1991). Intermediate levels are seen in layer II pyramidal cells of the frontal cortex, CA1 cells of the hippocampus, the lateral nucleus of the substantia nigra, lateral reticular nucleus, and spinal fifth nucleus (Hillman 1991).

Hippocampal P/Q-type channels are concentrated in the dendrites and associated presynaptic terminals with relatively low levels in the soma (Elliott, Malouf, et al., 1995). In Purkinje cells, intense concentrations of P-type channels are found in the dendrites, especially at bifurcations whereas the soma and proximal regions are much less strongly labelled (Hillman 1991), although P/Q currents contribute substantially to somatic currents in many other central neurons (Mintz, Adams, et al., 1992).

Expression of these channels is altered by development and pathological conditions. For example, a putative non-inactivating P-type current that constituted 24% of the total Ca^{2+} current was identified in dissociated hippocampal granule cells isolated from a 10 month old therapy-resistant refractory temporal lobe epilepsy patient that was absent in adult patients (Beck, Steffens, et al., 1999).

3.11.4 Function

P/Q channels mediate neurotransmitter release at the neuromuscular junction and at many central synapses. Transgenic mice in which P/Q-type α_{1A} channels have been knocked out exhibit smaller synaptic currents and greatly reduced paired pulse facilitation (Inchauspe, Martini, et al., 2004). N- and R-type channels can partially compensate for the ablation of P/Q subunits in knockout mice, by supplying synaptic current (Inchauspe, Martini, et al., 2004). In hippocampal slices from α_{1A} null mutants, synaptic transmission is predominantly carried by N-type (Jun, Piedras-Renteria, et al., 1999). This compensation appears to imply some degree of functional overlap between these channels (Inchauspe, Martini, et al., 2004). However, the loss of calcium-dependent facilitation in P/Q-type knockout mice points to at least one P/Q specific function (Inchauspe, Martini, et al., 2004).

Mutations in P/Q-type calcium channels are also involved in a range of movement disorders characterised by ataxia, paroxysmal dyskinesia, and absence seizures (Nahm, Jung, et al., 2005). Mice in which the α_{1A} subunit is knocked out developed rapidly progressing ataxia and dystonia before dying at 3-4 weeks (Jun, Piedras-Renteria, et al., 1999). In these mice the P-type currents in Purkinje neurons and P/Q-type currents in cerebellar granule cells are eliminated completely. The involvement of P/Q-type currents in specific neurological deficits appears to be indirect, such that, in the leaner mouse model these symptoms are functionally related to subsequent changes in the expression of T-type channel subtypes in the thalamus and cerebellum (Nahm, Jung, et al., 2005).

Calcium currents generally exert a secondary level of control over neuronal firing patterns through selective coupling to the calcium-dependent potassium currents underlying the AHPs. One example of this functional coupling in striatal interneurons is the activation of BK channels involved in spike repolarization by calcium supplied by Q-type channels (Goldberg and Wilson 2005). Hippocampal pyramidals, however, provide an exception to this rule, since P/Q-type calcium channels do not appear to couple to either SK or BK channels (Marrion and Tavalin 1998).

In cerebellar Purkinje cells, where P/Q-type channels are required for normal spontaneous firing, blockade of these channels mimics the effects of blocking calcium-activated potassium channels (Womack, Chevez, et al., 2004). Evidently, activation of calcium-activated potassium channels in these cells occurs via calcium entering through P/Q-type channels (Womack, Chevez, et al., 2004). It is therefore probably not surprising to see I_{CaP}/I_Q implicated in controlling spike frequency adaptation (SFA). Thus, in caudal raphe neurons, inhibition of P/Q-type channel by serotonin causes a decrease in the fast afterhyperpolarization (fAHP) and an enhancement of the repetitive firing response to current injection (Bayliss, Li, et al., 1997).

P-type channels are involved in synaptic transmission and afterhyperpolarization activation in rat sensorimotor cortex pyramidal neurons (Vilchis, Bargas, et al., 2000). Similarly, P/Q-type channel blockers preferentially reduce the afterhyperpolarization in neostriatal projection neurons (Vilchis, Bargas, et al., 2000). In the mouse, calcium entering through L- and P-type Ca^{2+} channels activates a chloride current responsible for the ADP in isolated mouse superior cervical ganglion neurons (Martinez-Pinna, McLachlan, et al., 2000).

In cerebellar Purkinje cells, immunoglobulin G antibodies (IgG), isolated from amyotrophic lateral sclerosis (ALS) patients, cause an increase in the current through P-type calcium channels (Llinas, Sugimori, et al., 1993). The resultant enhanced calcium current is thought to contribute to the neuronal degeneration that characterises ALS (Llinas, Sugimori, et al., 1993).

3.11.5 Activation

With 5 mM Ba^{2+} as the charge carrier, native I_{CaP} has a half activation voltage, in neostriatal and cortical pyramidal neurons, of -5 mV whilst I_Q has a value of -11 mV (Mermelstein, Foehring, et al., 1999). Cloned rat P/Q-type channel α subunit variants exhibit V_{half} values between -4.1 and +2.1 mV with Ba^{2+} (Bourinet, Soong, et al., 1999). Human cloned P/Q expressed in HEK 293

cells has a V_{half} of +9.5 mV and activates with a time constant of 2.2 ms in 15 mM Ba^{2+} (Hans, Urrutia, et al., 1999).

3.11.6 Inactivation

The V_{half} of inactivation for P/Q expressed in HEK cells is -17.2 mV (Hans, Urrutia, et al., 1999) similar to the -17 mV seen for cloned rat P/Q-type currents (Bourinet, Soong, et al., 1999).

3.11.7 Inactivation kinetics

In the Mermelstein et al. (1999) study, native I_{CaP} displayed an inactivation time constant of over 1 second at 0 mV in Ba^{2+}. Q-type currents were found to vary widely in inactivation kinetics with neostriatal I_Q similar to I_{CaP} in inactivation rate. In 15 mM Ba^{2+}, at +10 mV human cloned P/Q has an activation time constant of 690 ms (Hans, Urrutia, et al., 1999).

3.11.8 $I_{CaP/Q}$ in the subiculum

3.11.8.1 Bursting

A potentially important role for these channels in subicular bursting is suggested by the finding that application of the funnel web spider toxin, omega-conotoxin MVIIC, which blocks the P/Q and N subtypes, significantly reduces (31%) the calcium tail current. Interestingly, the relative contribution of calcium channel types to bursting may differ between CA1 and subiculum. Magee and Carruth (1999) found that CA1 pyramidal cell bursting was reduced to a greater extent by the inhibition of T- and R-type channels than by blockade of N- and P/Q-type channels. The reverse situation appears to hold in the subiculum where T- and R-type channel inhibition only reduces the burst calcium tail current by 20% (Jung et al., 2001).

3.11.9 A hybrid model of subicular $I_{CaP/Q}$

Due to a paucity of data on subicular channels, the model of subicular P/Q-type current is a hybrid of several reported forms. This hybrid model draws most heavily on P-type channel characteristics (Figure III-8).

$$I_{CaP} = p_{CaP} m h z^2 \frac{VF^2}{RT} \frac{[Ca^{2+}]_i - [Ca^{2+}]_o \exp^{-z_{Ca}FV/RT}}{1 - \exp^{-z_{Ca}FV/RT}}$$

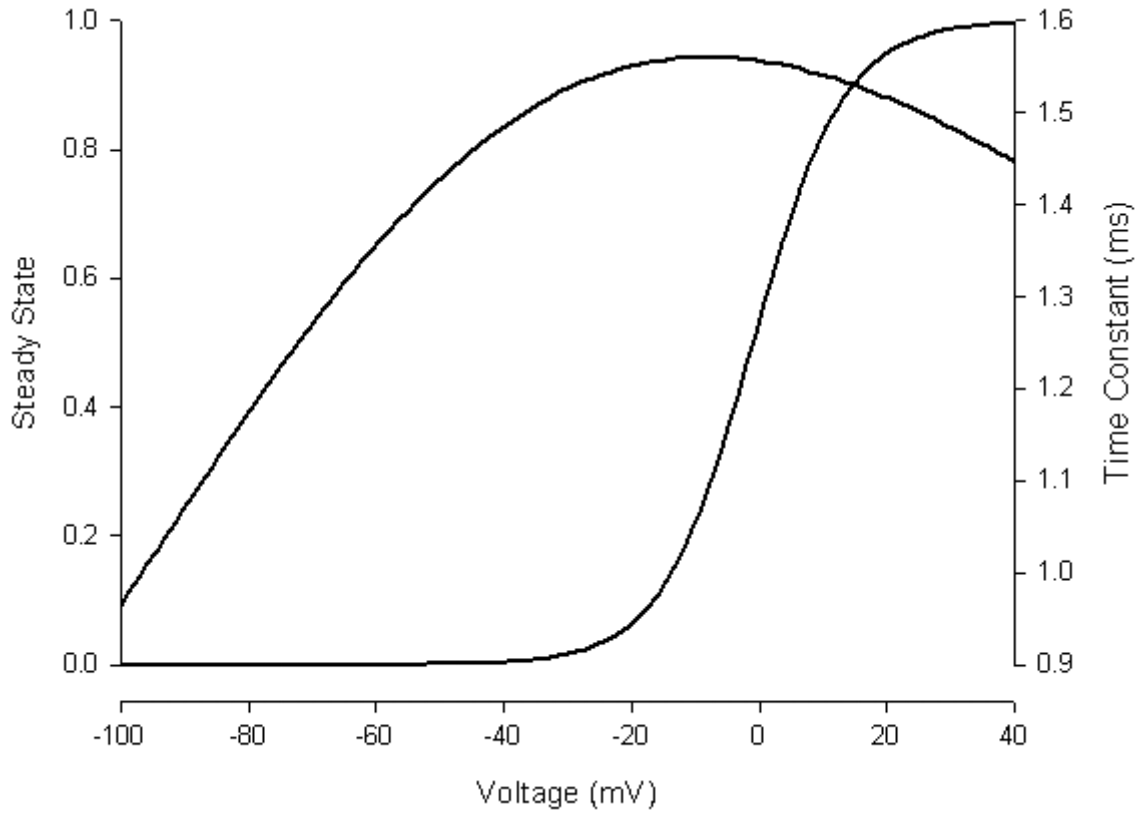

Figure III-8. Plots of the steady state and time constant activation curves for I_{CaP}.

3.11.9.1 Activation

The V_{half} of the model is -1.0 mV with a k factor of -7.1 mV. This current activates around -40 mV and saturates near +50 mV.

$$m_{inf} = \frac{1}{1 + e^{\frac{V-(-1)}{-7.1}}}$$

3.11.9.2 Activation kinetics

Rapid activation kinetics (~1.5 ms) allows P/Q-type channels to participate in fast electrophysiological events.

$$\tau_m = \frac{e^{\frac{V+119.5}{53}}}{1+e^{\frac{V+70.1}{42.9}}}$$

3.11.9.3 Inactivation

Since P/Q channels hardly inactivate over several seconds no inactivation variable was included in the model of subicular P/Q.

3.12 Fast transient K^+ current, I_A

The fast transient K^+ current, I_A, is a comparatively large current expressed in a range of neuron cell types from gastropod neural stomata (Connor and Stevens 1971) to rat hippocampal neurons (Rudy, Chow, et al., 1999). The earliest reports of this current in the hippocampal complex were in CA3 slice preparations from adult guinea pigs (Gustafsson, Galvan, et al., 1982).

Early descriptions of I_A usually included all hippocampal 4-AP sensitive Ca^{2+}-independent potassium currents (Gustafsson, Galvan, et al., 1982). However, the possibility of at least two transient K^+ currents was suggested by the unmasking, in guinea pig CA3 cells, of a slowly inactivating component of the I_A current that was very sensitive to 4-AP (Zbicz and Weight 1985). This slow component was absent from acutely dissociated guinea pig pyramidal cells or in cultured hippocampal neurons from neonatal rats (Segal and Barker 1984). The situation was eventually clarified by Storm (1988) who exploited the greater sensitivity to 4-AP of the slow component to dissect out the contribution of the slow delay current, I_D, to the transient K^+ current response.

3.12.1 Channel

Physiologically, the A-type current has been identified with a wide variety of cloned channels including $K_{V1.4}$ (Sheng, Liao, et al., 1993), $K_{V3.3\text{-}4}$ (Vega-Saenz de Miera, Moreno, et al., 1992; Schroter, Ruppersberg, et al., 1991), $K_{V4.1\text{-}3}$ (Isbrandt, Leicher, et al., 2000). The specific kinetic properties of these cloned genes depend on the expression system, recording configuration, the presence of auxiliary subunits, and the ability of A-type channels to exhibit multiple subconductances (Kang, Huguenard, et al., 2000).

3.12.2 Distribution

In CA1 pyramidal cells, I_A has an unusual distribution in that channel density increases dramatically along the apical dendrite such that the density in distal dendrites is five-fold greater than at the soma (Hoffman, Magee, et al., 1997). The distally located channels also exhibit a negative shift in voltage dependence that increases responsiveness to subthreshold fluctuations.

This high distal density of I_A acts to offset the impact of the high density of Na^+ and Ca^{2+} channels and excitatory inputs in the dendrites and explains why spikes are not usually initiated in the dendrites, why dendritic spikes are smaller than somatic spikes, and why dendritic spikes are augmented when paired with synaptic activation due to I_A inactivation (Hoffman, Magee, et al., 1997).

3.12.3 Activation

The I_A current is activated by depolarization beyond -60 mV and saturates about +20 mV in CA1 pyramidals (Numann, Wadman, et al., 1987). In neocortical pyramidals, I_A activation is more depolarized and starts about -45 mV (Kang, Huguenard, et al., 2000).

3.12.4 Activation kinetics

I_A exhibits fast activation with time constants of 5-10 ms that enable the current to participate in spike repolarization (Storm 1988).

3.12.5 Inactivation kinetics

Inactivation is relatively rapid with time constants of between 20 and 30 ms. Above -50 mV the time constant of inactivation for I_A in CA1 neurons is about 20 ms (Storm 1988). I_A also recovers rapidly from inactivation with time constants of between 10 and 50 ms.

3.12.6 Function

The classical role of I_A, elucidated from studies of invertebrate preparations, is to delay the onset of firing and to slow down repetitive firing by prolonging the fast AHP (Connor and Stevens 1971). The ability of I_A to recover from inactivation during the fast AHP allows it to activate during the depolarization towards the firing threshold. Early reports suggested that I_A could delay the onset of firing by hundreds of milliseconds (Gustafsson, Galvan, et al., 1982; Segal and Barker 1984). However, these reports probably confounded the effects of the slowly inactivating D-type current because once the I_D component had been eliminated I_A only contributed to a relatively short delay in firing of approximately 50 ms (Storm 1988). There is also evidence that I_A may play a role in the maintenance of repetitive spike firing in mammalian neurons and modulation of the spike threshold (Segal and Barker 1984).

Storm (1990) suggests that the I_A and I_D play a particularly important role in early-phase spike repolarization prior to the full activation of the calcium-dependent fast activating K^+ channel,

I_{CT}. The fact that blockade of I_A by 4-AP leads to pronounced broadening of the action potential supports this idea (Storm 1987). The 4-AP-induced spike broadening reveals a role for both I_A and I_D in this process since the broadening that occurs at 4-AP concentrations of 40 μM (where I_D is selectively blocked) is increased when the 4-AP levels are increased to eliminate I_A (Storm 1988).

A more recent examination of the role of I_A involved deletion of the A-type channel auxiliary $K_{V\beta1.1}$ subunit gene. These β subunits are thought to confer A-type behaviour on non-inactivating K^+ channels in heterologous expression systems (Pongs, Leicher, et al., 1999). $K_{V\beta1.1}$ knockout caused a general reduction in K^+ current inactivation in hippocampal CA1 pyramidal neurons that was expressed as a frequency-dependent spike broadening and a reduction in the sAHP (Giese, Storm, et al., 1998). The reduction in the slow AHP suggests a role for I_A in regulating calcium influx during action potentials. Despite exhibiting normal synaptic plasticity, the $K_{V\beta1.1}$-deficient mice were impaired in the water maze task and in the social transmission of food preference task (Giese, Storm, et al., 1998).

The very high density of A-type channels in the dendrites of hippocampal CA1 pyramidal neurons acts to regulate orthograde and retrograde propagation of dendritic potentials by suppressing large, rapid depolarization of the dendrites. Specific damping effects include prevention of dendritic spike initiation, reduction of back-propagation of spikes into the dendrites, and the diminution of excitatory synaptic events (Hoffman, Magee, et al., 1997). I_A activation during synaptic depolarization can regulate the somatodendritic integration of high frequency input trains (Ramakers and Storm 2002).

3.12.7 Modulation

The aforementioned sensitivity to 4-AP is both voltage- and time-dependent in that it is slowly relieved by depolarization (Numann, Wadman, et al., 1987). I_A is insensitive to 3-30 mM tetraethylammonium (TEA) (Gustafsson, Galvan, et al., 1982) but is sensitive to 50-300 nM dendrotoxin (DTX) (Halliwell, Othman, et al., 1986). I_A is calcium-insensitive since it persists in Ca^{2+}-free medium and resists calcium channel blockers such as cadmium, cobalt and manganese (Gustafsson, Galvan, et al., 1982; Numann, Wadman, et al., 1987). I_A is inhibited by norepinephrine (Sah, French, et al., 1985) and antagonised by acetylcholine (Nakajima, Nakajima, et al., 1986). Significant changes in the electrophysiology of neural circuits can be triggered by neurotransmitter-mediated reductions in I_A (Harris-Warrick and Sparks 1995).

Whilst the activation and inactivation kinetics of I_A are unaltered by changes in pH, the steady-state inactivation curve of I_A is reversibly depolarized by about 10 mV by low, but not by high, pH levels (Tombaugh and Somjen 1996).

3.12.8 I_A in the subiculum

The lack of I_A-specific studies in subicular neurons make the task of dissecting out the contribution of this current to the waveform difficult.

3.12.8.1 Spike broadening

The cholinergic sensitivity of I_A allows clues to its role in subicular neurons to be inferred from the effects of cholinergic agonists. Kawasaki et al. (1999), for example, reported that the muscarinic receptor agonist, carbachol, abolished the single spike fast AHP and caused a pronounced broadening of the single spikes. These effects are certainly commensurate with disruption of the classical role of I_A. Unfortunately, the broad-spectrum effects of acetylcholine on neuronal electrophysiology confound precise interpretation.

3.12.8.2 Early spike repolarization

In a voltage clamp study of the currents involved in subicular bursting, Jung et al. (2002) found that a 1 ms depolarization from -70 to 0 mV elicited two distinct inward current spikes separated by a fast (~0.5 ms latency) outward spike. This spike persisted in zero Ca^{2+}, which would appear to rule out the participation of Ca^{2+}-dependent K^+ currents in the initial potassium current response, and possibly at a role for the fast transient K^+ channel in the early phase of spike repolarization in subicular neurons.

3.12.8.3 Delay of firing

Literature voltage traces suggest that subicular regular firing and bursting pyramidal cells typically respond to long just-threshold stimuli with a firing delay of the order of 50 ms in duration (Mason 1993). This delay increases with pre-hyperpolarization and decreases with increasing stimulus strength (Stewart and Wong 1993; Mason 1993; Wellmer, Su, et al., 2002). As in CA1 pyramidals, I_A may be largely responsible for the brief delay of up to 50 ms in the onset of spiking seen in subicular pyramidals. Some of this delay is, however, likely to be attributable to the fast activating, slowly inactivating D-type current.

3.12.9 Model of subicular I_A

Our I_A model is largely based on that reported by Storm (1988) for CA1 pyramidals (Figure III-9).

$$I_A = g_A mh(V_m - E_K)$$

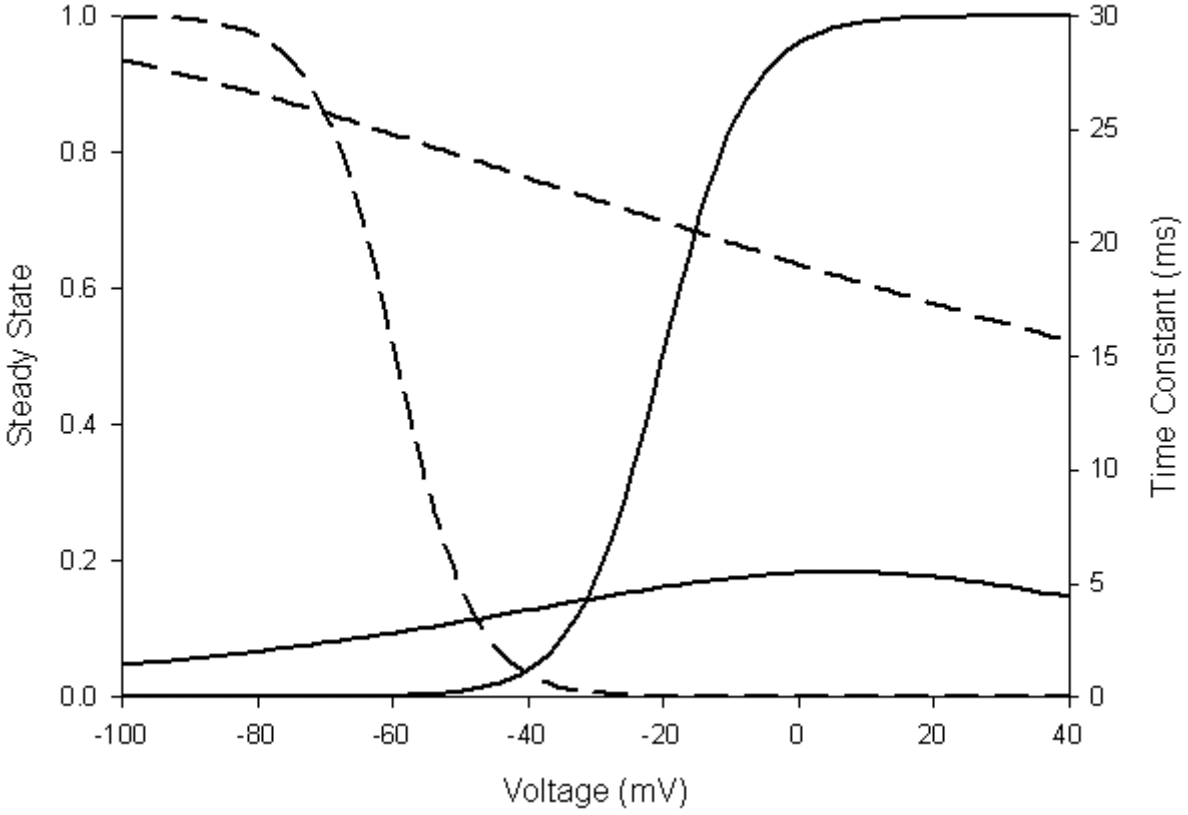

Figure III-9. Plot of the activation (solid lines) and inactivation (dashed line) steady state and time constant curves for I_A. The activation time constant has been multiplied by 10 in order to fit the inactivation and activation curves on the same graph.

3.12.9.1 Activation

Our I_A current model is activated by depolarization beyond -60 mV and saturates approaching +20 mV as in CA1 pyramidals (Numann, Wadman, et al., 1987). This yields a V_{half} of about -20.1 and a slope factor of -6.3 mV

$$m_{inf} = \frac{1}{1 + e^{\frac{V-(-20.1)}{-6.3}}}$$

3.12.9.2 Activation kinetics

The activation kinetics of this model are faster than those reported by Storm (1988) in order to allow subicular I_A to participate in early spike repolarization. The response time at -30 mV is about 0.4 ms.

$$\tau_m = \frac{e^{\frac{V-5}{55}}}{1+e^{\frac{V-10}{24.9}}}$$

3.12.9.3 Inactivation

Inactivation of the CA1 form of I_A occurs between -80 and -40 mV. The half-inactivation voltage of I_A is about -60 mV (Storm 1988). The corresponding Boltzmann curve is

$$h_{inf} = \frac{1}{1 + e^{\frac{V-(-59.5)}{5.8}}}$$

3.12.9.4 Inactivation kinetics

The subicular I_A time constant curve was adjusted to give inactivation time constants of between 20 and 40 ms over the activation range in agreement with Storm (1988).

$$\tau_h = \frac{e^{\frac{V+420}{60}}}{1+e^{\frac{V+185.1}{45.9}}}$$

3.12.9.5 Conductance

We adjusted the g_{max} of I_A to replicate the outward current spike under voltage clamp and the ~50 ms firing delay. The baseline magnitude of I_A was about 150 nS.

3.13 Fast calcium-dependent potassium current, I_{CT}

The large conductance calcium- and voltage-dependent K^+ current, I_C, represents a family of currents with a wide range of activation and inactivation characteristics (Brown and Griffith 1983; Zbicz and Weight 1985; Storm 1987; Lancaster and Nicoll 1987; Ikemoto, Ono, et al., 1989; Shao, Halvorsrud, et al., 1999; Lingle, Zeng, et al., 2001). For the purposes of this review, we focus on the transient form, I_{CT} which has been shown to be prominent in hippocampal pyramidals (Zbicz and Weight 1985; Storm 1990; Hicks and Marrion 1998).

3.13.1 Channel

I_{CT} is carried by the $K_{Ca1.1}$ (also known as BK, maxi-K, or mslo) family of calcium-sensitive potassium channels (Butler, Tsunoda, et al., 1993). In membrane patches from cultured rat hippocampal neurones, the BK channel has a conductance of between 150 and 300 pS (Brett and Lancaster 1985; Ikemoto, Ono, et al., 1989; Dworetzky, Trojnacki, et al., 1994). The specific properties of the α pore-forming subunit are determined by associated ancillary β subunits (Lingle, Zeng, et al., 2001). Prominent pharmacological inhibitors of BK include tetraethylammonium, charybdotoxin, and iberiotoxin (Golding, Jung, et al., 1999).

3.13.2 Distribution

In CA1 pyramidal neurons, I_{CT} activity is limited to the first 100-150 μm from the soma (Poolos and Johnston 1999). In hippocampal neurons, BK channels are co-localised with, and selectively activated by, N-type but not L- or P/Q-type channels in the same patch (Marrion and Tavalin 1998). Both L- and N-type channels are involved in the activation of I_{CT} in mouse neocortical pyramidal neurons (Sun, Gu, et al., 2003).

3.13.3 Function

I_{CT} is strongly activated by a single action potential, and contributes to the last two thirds of spike repolarization and the fast AHP (Storm 1987; Lancaster and Nicoll 1987). Thus, selective suppression of I_{CT} causes spike broadening of approximately 60% (Shao, Halvorsrud, et al., 1999). In addition, the ability of some forms of BK to rapidly inactivate can drive frequency-dependent spike broadening (Shao, Halvorsrud, et al., 1999; Golding, Jung, et al., 1999; Faber and Sah 2003). Concurrent with the I_{CT}-related reduction in the rate of repolarization is a decrease in the amplitude of the fast afterhyperpolarization (fAHP) (Lancaster and Nicoll 1987).

The ability of BK channels to reduce cell excitability suggests that these channels confer neuroprotective effects. Thus, endogenous upregulation of BK activity following ischemia contributes to a post-ischemic decrease in neuronal excitability and increases in fAHP amplitude (Gong, Gao, et al., 2000). Unsurprisingly, inhibition of BK channels induces increased hippocampal cell death in an animal model of ischemia-induced nerve cell degeneration (Runden-Pran, Haug, et al., 2002). Similarly, the excitotoxic effects of the spongiform encephalopathy-associated amyloid β protein are found to be due, in part, to the suppression of BK channels (Qi and Qiao 2001).

3.13.4 Modulation

BK is up- and downregulated by a variety of modulators. For example, activation of metabotropic glutamate receptors inhibits BK (Gebremedhin, Yamaura, et al., 2003) whilst acetylcholine receptor activation augments the channel (Hayashi, Poronnik, et al., 1996; Chavis, Ango, et al., 1998). Activation of specific PKC isozymes increases BK channel activity via cyclic GMP-dependent protein kinase (Barman, Zhu, et al., 2004). In CA1, I_{CT} is upregulated by adenosine triphosphate (ATP) by way of a functionally associated protein kinase A-like protein (Gong, Gao, et al., 2002).

3.13.5 Activation

Despite requiring a relatively high concentration of calcium to activate, I_{CT} is strongly potentiated by a single pyramidal cell action potential (Storm 1987). The lowest $[Ca^{2+}]_i$ in which CA1 pyramidal BK channels activate is around 0.01 μM at +20 mV, but micromolar concentrations of internal Ca^{2+} are required for complete activation (Gong, Gao, et al., 2001; Smart 1987; Franciolini 1988; Lancaster, Nicoll, et al., 1991). Under intracellular Ca^{2+} of 2 μM, the open probability of single BK channels increases e-fold with a +17.0 mV increase in the membrane potential (Gong, Gao, et al., 2001). The dependence on BK activation on Ca^{2+} concentration appears to be non-linear (Moczydlowski and Latorre 1983; Franciolini 1988). Gong et al. (2001) report a sigmoidal dependence of activation on the log of $[Ca^{2+}]_i$ such that half-activation log $[Ca^{2+}]_i$ corresponded to about 1.6 μM at +20 mV.

3.13.6 Activation kinetics

The ability of I_{CT} to participate in spike repolarization suggests rapid calcium-dependent activation kinetics. Accordingly, in CA1 pyramidals, Gong et al. (2001) reported that single channel opening could be described with two exponentials, with respective time constants of 2.8 ms and 19.2 ms at +120 mV with 2 μM calcium. Conversely, Ikemoto (1989) reported a slowly activating hippocampal variant. This variant responded to a calcium concentration jump with delayed activation kinetics of up to about 280 ms. Deactivation of this channel starts immediately and is complete within 50-150 ms, depending on voltage (Ikemoto, Ono, et al., 1989).

3.13.7 Inactivation

The ability of BK channels to inactivate is dependent on the steady state and kinetic properties of associated regulatory subunits (Lingle, Zeng, et al., 2001). For instance, inactivation levels of BK channels reconstituted with different isoforms of the β_3 subunit ranges zero to 90% (Hu, Labuda, et al., 2003). Hippocampal BK channels exhibit a Ca^{2+}-dependent inactivation process that requires at least 1 μM of intracellular Ca^{2+} (Hicks and Marrion 1998). Inactivation is characterized by an abrupt transition from a sustained high open probability, long open time behaviour to a very low open probability, short open time activity. Inactivation can be relieved by reducing $[Ca^{2+}]_i$ or by hyperpolarization of the cell membrane (Hicks and Marrion 1998). The steady-state inactivation of I_{CT} is also shifted to more negative potentials by increases in $[Ca^{2+}]_i$ from 1 to 60 μM (Ding and Lingle 2002).

3.13.8 Inactivation kinetics

The dynamics of hippocampal spike broadening constrain BK inactivation time constants to between about 10 and 30 ms (Warman EN 1994). The reported kinetics of single BK channel inactivation are highly variable with time constants ranging from near immediate to nearly two minutes (Hicks and Marrion 1998).

3.13.9 I_{CT} in the subiculum

3.13.9.1 Function

I_{CT} appears to play an important role in controlling excitability and spike repolarization in subicular pyramidal neurons since blockade of the current using the selective inhibitor charybdotoxin (100 nM) increases the number of spikes in a burst (Jung et al., 2001).

Within the burst, there is a progressive broadening of spike width (Staff et al., 2000) that, in hippocampal neurons, is associated with I_{CT} inactivation. The effect is more pronounced for strong, rather than weak bursters. This suggests that the larger calcium influx associated with strong bursters (Jung et al., 2001) increases I_{CT} activation leading to an enhancement of both the contribution of I_{CT} to spike repolarization and the effects of frequency-dependent I_{CT} inactivation.

Calcium channel blockers substantially reduce both the burst AHP and the fAHP of single spikes that follow the burst (Mattia et al., 1997b). Frequency-dependent spike broadening has not

been explicitly reported for subicular regular firers. These cells do however exhibit a fast AHP that is conventionally associated with I_{CT}.

3.13.10 Model of subicular I_{CT}

A novel model of subicular I_{CT} that uses a calcium-sensing function to determine the amplitude of the stationary voltage-dependent activation curve was developed (Figure III-10):

$$I_{CT} = g_{CT} m (V_m - E_K)$$

3.13.10.1 Activation

Our activation gate adapts the sigmoidal calcium dependence of I_{CT} reported by Gong et al. (2001) to determine the amplitude of the voltage-dependent Boltzmann-type activation gate. The I_{CT} calcium sensor is linked to the fast, submembrane calcium pool. This sensor function saturates around 1 μM. Beyond this point the current activation is primarily controlled by the voltage-dependent function.

$$m_{inf} = \frac{1+e^{\frac{\log[Ca]_{fast} - (-6.5)}{-0.1}}}{1+e^{\frac{V-(-30)}{-3.3}}}$$

3.13.10.2 Activation kinetics

We use purely voltage dependent activation kinetics with an activation time constant that is close to 1 ms for all voltages.

$$\tau_m = \frac{e^{\frac{V-10}{995.1}}}{1+e^{\frac{V-450}{134.9}}}$$

3.13.10.3 Inactivation

Although I_{CT} inactivation has been reported to depend on both voltage and calcium (Hicks and Marrion 1998) our simplified inactivation gate model, adapted from that of Warman et al. (1994), is purely voltage-dependent. Steady-state inactivation is complete about -20 mV.

$$h_{inf} = \frac{1}{1 + e^{\frac{V-(-50)}{7.3}}}$$

3.13.10.4 Inactivation kinetics

Our inactivation gate peaks at about 16 ms at -35 mV and is designed to mediate the frequency-dependent spike broadening seen in subicular pyramidals.

$$\tau_h = \frac{e^{\frac{V-78.1}{9.5}}}{1+e^{\frac{V-47}{7.8}}}$$

3.13.10.5 Conductance

A gmax for I_{CT} of 0.12 μS was used to drive spike repolarization and stabilise the cell after the addition of calcium currents.

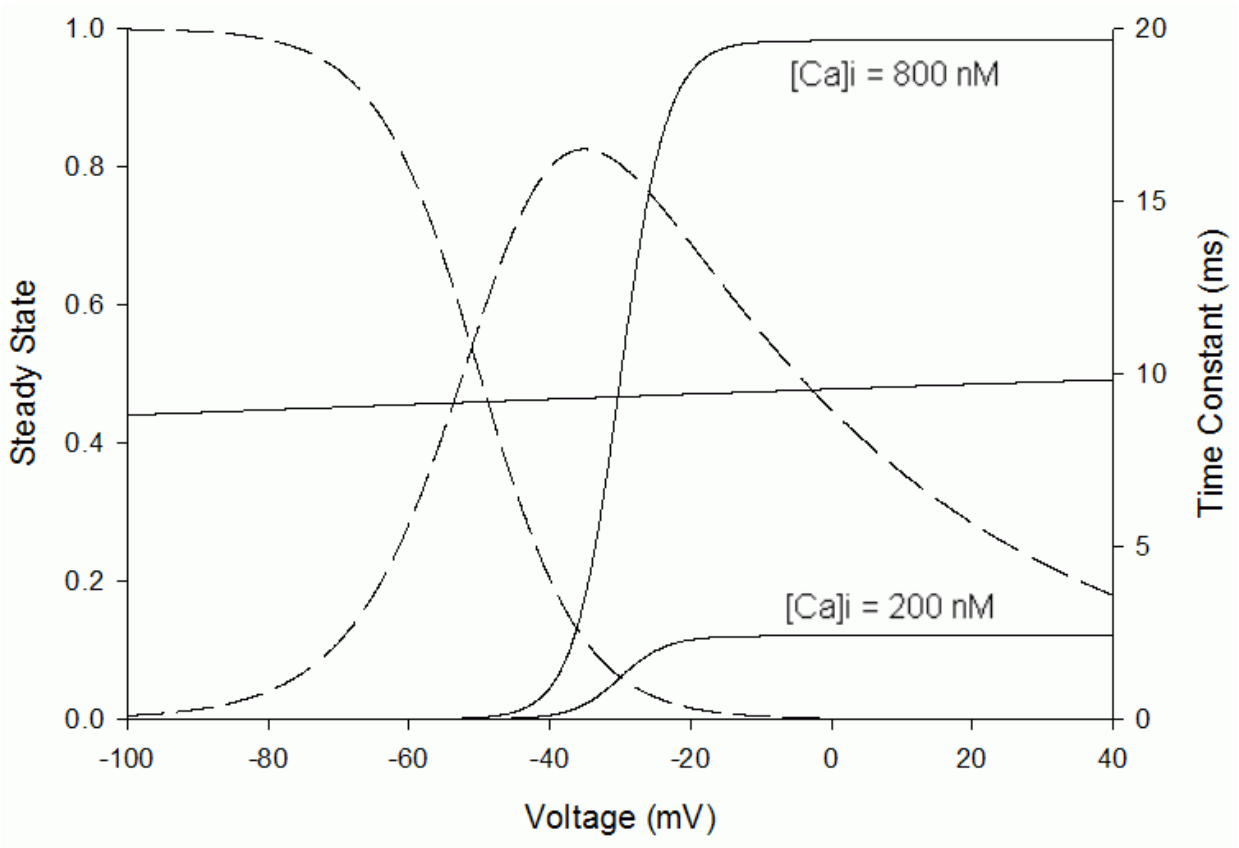

Figure III-10. Plot of the activation (solid lines) and inactivation (dashed lines) steady state and time constant curves for I_{CT}. The values of the activation curve have been plotted for two concentrations of intracellular calcium, 200 and 800 nM. The activation time constants have been multiplied by 10 in order to fit the inactivation and activation curves on the same graph.

3.14 Delayed rectifier, I_{DR}

First described by Hodgkin and Huxley in 1952, the classical delayed rectifier is responsible for spike repolarization in squid giant axons. More recently, the 'delayed rectifier' nomenclature has been applied to a range of potassium currents (Hille. 1992), but in hippocampal neurons the term generally refers to high threshold, TEA-sensitive currents with either fast or slow activation kinetics (Sah, French, et al., 1985; Storm 1988).

3.14.1 Channel

A surprisingly large number of known $K_{V\alpha}$ subunits behave as delayed rectifiers; including members of the K_V 1, 2, 3, and 7 families (Gutman 2003). However, most of the delayed rectifier current in the hippocampus appears to be carried by $K_{V2.1}$ (Murakoshi and Trimmer 1999). The $K_{V2.1}$ channel subunit is omnipresent in the mammalian brain (Du, Aloyo, et al., 1997), but is particularly strongly expressed in the somata and proximal dendrites of pyramidal cells of the hippocampus (Maletic-Savatic, Lenn, et al., 1995).

3.14.2 Modulators

I_{DR} is blocked by relatively high concentrations of TEA (25 mM), is comparatively insensitive to 4-AP (1 mM) and Cs^{2+} (1 mM), and is unaffected by zero calcium medium (Sah et al., 1988b). The current is, however, directly blocked by high (millimolar) concentrations of the calcium channel inhibitors Co^{2+} and Cd^{2+} (ibid.). I_{DR} is also inhibited by melatonin (Hou, Zheng, et al., 2004), zinc, copper (Horning and Trombley 2001), lead, and lanthanum (Talukder and Harrison 1995). The current is stimulated by somatostatin (Raynor and Reisine 1992).

3.14.3 Activation

Although a range of activation characteristics have been reported for I_{DR} we focus on the variant described by Sah et al. (1988b). This form activates around -40 mV and can be described by a Boltzmann equation with V_{half} of -4.8 and k of -13.6 (Sah et al., 1988b). The high activation threshold prevents I_{DR} from contributing to subthreshold processes.

3.14.4 Activation kinetics

A range of activation kinetics have been described for I_{DR}. Sah et al., 1988b reported a rapidly activating I_{DR} variant in CA1 neurons. The rate of I_{DR} activation is rapid and monotonically increasing beyond about -70 mV; the rate at 0 mV is about 2.5 ms at 22˚C. Doerner et al. (1988)

described a similar form. Rapid activation kinetics are also displayed by a number of the cloned delayed rectifiers from the K_{V1} and K_{V3} families (Grissmer, Nguyen, et al., 1994; Shapiro and DeCoursey 1991). Slower I_{DR} variants, with activation time constants on the order of 20-80 ms (Storm 1990), and higher (Segal and Barker 1984), have also been reported in hippocampal pyramidals and in expression systems (Lang, Lee, et al., 2000).

3.14.5 Inactivation

Inactivation of I_{DR} is generally very slow CA1 such that I_{DR} inactivates with a mono-exponential time course over several seconds (Segal and Barker 1984; Numann, Wadman, et al., 1987). Storm (1990) suggested that a portion of this inactivation could be attributed to extracellular potassium accumulation.

More than one I_{DR} variants with distinct inactivation kinetics can coexist in the same cell. For example, a pair of delayed rectifiers with ‘temporally overlapping’ inactivation kinetics (slowly inactivating and persistent components) has been observed in cultured hippocampal interneurons (Chikwendu and McBain 1996).

Interestingly, slowly inactivating I_{DR} and rapidly inactivating A-type currents can be interconverted by second messenger fatty acids. For instance, arachidonic acid (AA) confers rapid A-type inactivation upon I_{DR}, whilst phosphoinositides inhibit I_A inactivation (Oliver, Lien, et al., 2004). The spike broadening caused by AA in hippocampal cells (Keros and McBain 1997) suggests that such interconversion can profoundly affect neuronal signalling properties.

3.14.6 Function

The delayed rectifier classically acts to accelerate spike repolarization; thereby reducing spike width and facilitating high frequency spiking (Lien and Jonas 2003). However, mammalian neuronal action potentials are notably faster than those of squid, which raises doubts about the role of I_{DR} in these cells since many I_{DR} variants exhibit relatively slow activation. However, the large currents typically associated with I_{DR} means that a slow activation rate does not necessarily preclude a role for the current in spike repolarization since even partial activation could produce significant currents (Storm 1990; Zhou and Hablitz 1996).

Du et al. (1999) probed the role of the $K_{V2.1}$ channel by using antisense oligonucleotides to 'knock-down' the subunit in CA1 pyramidal neurons. Intriguingly, they found that action potential durations were identical under low frequency (0.2 Hz) stimulation but broadened in

cells subjected to higher frequencies (1 Hz). This suggests that $K_{V2.1}$ has a role in regulating spike duration but only during repetitive firing. Pertinently, Kang et al. (2003) reported that I_{DR} was not activated by single action potentials in neocortical pyramidals.

The rapidly deactivating $K_{V3.1}$-$K_{V3.2}$ delayed rectifiers appear to support high frequency firing in interneurons whereby the fast deactivation generates a deep and rapid AHP that enhances the rate of recovery of I_{NaF} (Rudy, Chow, et al., 1999).

The ability of I_{DR} to enhance excitability also has pathological implications. For example, following transient cerebral ischemia, there is a significant increase in the amplitude of I_{DR} and a hyperpolarizing shift in its steady-state activation curve that is associated with post-ischemic cell death (Chi and Xu 2000). Furthermore, scopolamine induces a significant upregulation of hippocampal pyramidal I_{DR} in rats that might be responsible for the associated cognitive impairments (Zhong, Pan, et al., 2005).

An interesting information processing extension of the putative role of I_{DR} in spike repolarization comes from modelling studies. By enhancing spike repolarization, I_{DR} can facilitate somatic coincidence detection of dendritic spikes over temporal summation (spike integration) (Softky 1994).

3.14.7 I_{DR} in the subiculum

Until specific voltage and current studies are carried out, the properties of subicular I_{DR} must be inferred indirectly. However, there has been an interesting investigation of the dependence of the micro-spatial distribution of $K_{V2.1}$ in subicular neurons on neuronal activity in parallel with an extended analysis of the same process in hippocampal neurons.

3.14.7.1 Adaptive conductances

Whilst $K_{V2.1}$ in subicular pyramidals is distributed in high-density clusters (Misonou, Mohapatra, et al., 2004) this pattern can be altered by high levels of neuronal activity. Episodes of status epilepticus induce lateral translocation of the channel to a more diffuse distribution via a mechanism that appears to be triggered by channel phosphorylation (Misonou, Mohapatra, et al., 2004). The effects of this redistribution on the electrophysiological phenotype of the cell were not investigated. In the same study, stimulation of hippocampal neurons with glutamate induced similar distribution shifts that involve a calcium-dependent process. This process was both rapid and reversible, with a half-life of several hours following the removal of glutamate.

Significantly, in hippocampal neurons, these activity-dependent changes in the phosphorylation and localisation state of Kv2.1 were coupled with a large (>-20 mV) hyperpolarizing shift in the half activation voltage of the channel (Misonou, Mohapatra, et al., 2004). The net result appears to be a significant upregulation of the delayed rectifier current following pathological neuronal activity. It seems highly likely that similar activity-dependent shifts occur in the gating of subicular I_{DR}.

3.14.7.2 Spike repolarization

A defining characteristic of I_{DR} is its sensitivity to TEA. TEA-sensitive currents play a crucial role in spike repolarization since application of TEA to subicular bursters unmasks a dramatic, large amplitude ADP (Kawasaki et al., 1999). Aside from I_{DR}, two other prominent potassium currents are blocked by TEA; I_{CT} and I_M. Unfortunately, the Ca^{2+}-dependent potassium current, I_{CT}, which is also implicated in spike repolarization, is similarly very sensitive to TEA. Since no subicular studies to date have differentially applied TEA and calcium channel inhibitors in the absence of TTX, it is difficult to adequately dissect the relative contributions of both currents to spike repolarization. However, the modest burst spike broadening, and absence of a significant ADP, observed under zero calcium (Staff et al., 2000) insinuates that I_{CT} plays an important, but not central, role in spike repolarization. Of further potential relevance for the role of I_{DR} in subicular bursting is the finding that intrinsically bursting CA3 pyramidals have larger delayed rectifier currents than regular firing CA1 pyramidal cells (Klee, Ficker, et al., 1995). Since the slowly activating I_M almost certainly contributes little to spike repolarization, we therefore infer that I_{DR} is the primary current responsible for the spike repolarization in subicular pyramidals.

3.14.8 Model of subicular I_{DR}

A conventional m^4 I_{DR} format is assumed for subicular I_{DR} (Figure III-11):

$$I_{DR} = g_{DR} m^4 (V_m - E_K)$$

3.14.8.1 Activation

The I_{DR} model activates in the suprathreshold range from about -45 mV (V_{half} of -35.6, k of -10.2).

$$m_{inf} = \frac{1}{1 + e^{\frac{V-(-35.6)}{-10.2}}}$$

3.14.8.2 Activation kinetics

The I_{DR} model utilises relatively fast activation kinetics are a temperature-scaled adaptation of those observed by Sah et al. (1988b) in CA1. The voltage-dependent time constant is about 2 ms at 0 mV.

$$\tau_m = \frac{e^{\frac{V+256.1}{162.2}}}{1+e^{\frac{V+12.4}{38.9}}}$$

3.14.8.3 Inactivation

Cooper et al. (2005) found no evidence for activity dependent alterations in the potassium currents involved in bursting. We therefore assume that subicular I_{DR} is not subject to slow inactivation and thus omit an inactivation gate.

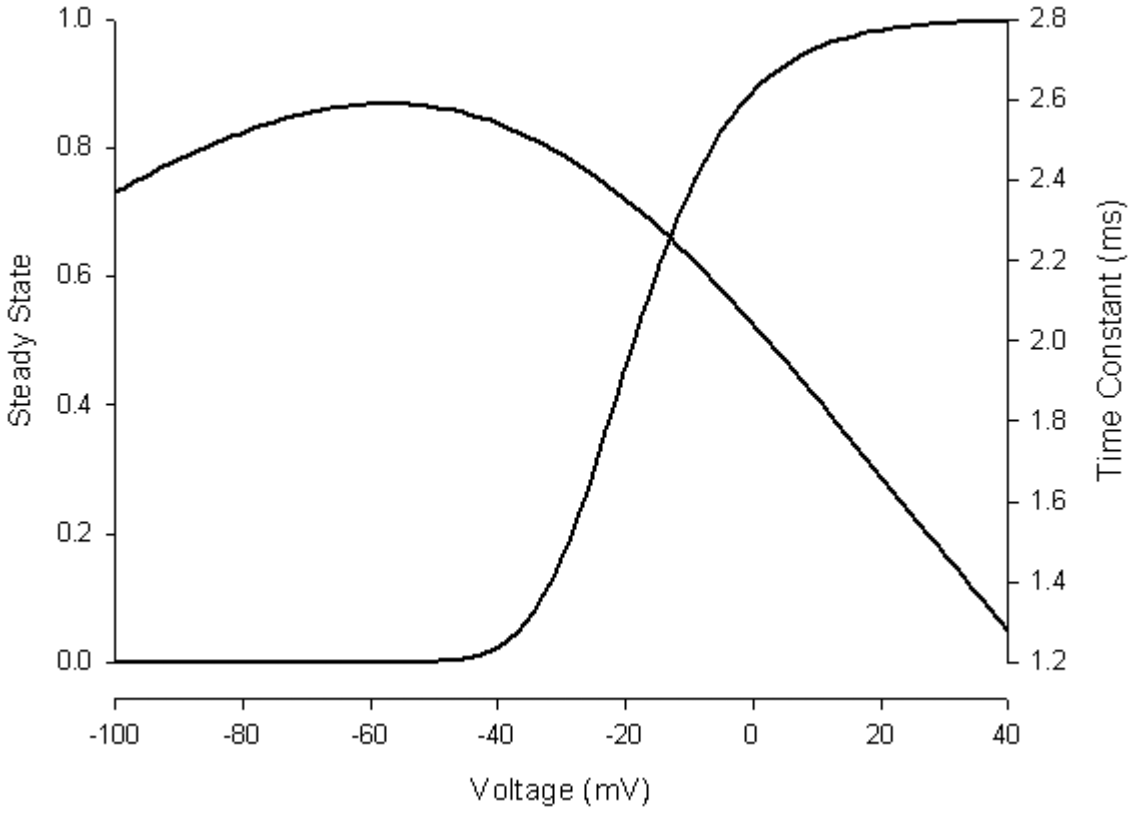

Figure III-11. Plot of the steady state activation and time constant curves for I_{DR}. The steady state activation curve has been raised to its exponent of 4.

3.14.8.4 Conductance

I_{DR} may constitute a significant fraction of the total potassium current in subiculum. Du et al. (1999) found that the $K_{V2.1}$-mediated I_{DR} represented over 70% of the measured potassium current in hippocampal neurons. In order to effectively drive spike repolarization a comparatively large maximum conductance of 0.3 μS was used for I_{DR}.

3.15 Muscarinic slow potassium current, I_M

This slow, non-inactivating, voltage-gated potassium current M current, I_M, was first identified in sympathetic neurons (Brown and Adams 1980). I_M has a strong presence in the hippocampal formation and has been found in guinea pig CA1 (Halliwell and Adams 1982) and CA3 neurons (Brown and Griffith 1983). As the name implies, muscarinic agonists suppress the M-current (Brown and Constanti 1980). By virtue of being the only sustained potassium current in the range of spike initiation, I_M exerts a powerful effect on membrane excitability.

3.15.1 Channel

The M-type channel is encoded by the KCNQ gene family (Wang, Pan, et al., 1998) (this nomenclature was developed by the Human Genome Project parallel to that of the International Union of Pharmacology). The KCNQ2 and KCNQ3 channel subunits can co-assemble to form a channel with biophysical properties and pharmacological sensitivities that are identical to those of the native M-type channel (Wang, Pan, et al., 1998). Of the five mammalian KCNQ genes the KCNQ2, KCNQ3 and KCNQ5 are heavily expressed in the nervous system (Jentsch 2000). The KCNQ2, KCNQ3, and KCNQ5 (corresponding to IUPHAR classifications K_V 7.2, 7.3 and 7.5, respectively) potassium channel subunits appear to comprise the M-type channel in areas CA1 and CA3 of the rat (Shah, Mistry, et al., 2002).

3.15.2 Activation

The threshold for M-type current activation in the depolarizing direction is about -70 mV and extends to -40 mV (Halliwell and Adams 1982). Hu et al. (2002) reported a V_{half} of -57.5 mV for CA1 neurons at 31˚C implying that the M-type current is unlikely to contribute significantly to the resting membrane potential. However, selective inhibition of I_M by linopirdine and XE991 depolarizes the resting potential by several millivolts (Yue and Yaari 2004).

3.15.3 Kinetics

Activation and deactivation occur slowly and with a single exponential time course that yields a time constant of around 50 ms. The mono-exponential activation suggests that the channel is controlled by a single activation particle (Hu, Vervaeke, et al., 2002). Higher activation values have been reported elsewhere. Sample time constants of activation at 25°C are 210 ms at -45 mV and 95 ms at -55 mV (Halliwell and Adams 1982). Interestingly, the M-type current has a relatively high reversal potential of about -75 mV (Halliwell and Adams 1982; Williamson and Alger 1990) hinting that I_M may not be a pure potassium current (Borg-Graham 1998).

3.15.4 Modulators

Apart from a greater sensitivity to the K^+ channel inhibitor TEA, the hippocampal M current shares many similarities with the archetypal M-type current of sympathetic ganglia (Brown and Adams 1980). I_M is not calcium dependent since it persists in Ca^{2+}-free medium (Storm 1989). The current is blocked by Ba^{2+} (1 mM), TEA (10 mM) but is largely unaffected by Cs^{2+} (0.1 mM) or 4-AP (1 mM) (Halliwell and Adams 1982). The M-type current exhibits a negative response to eponymous acetylcholine muscarinic (M) receptor activation (Halliwell and Adams 1982). I_M is suppressed by serotonin (Colino and Halliwell 1987), but is augmented by somatostatin (SST) (Moore, Madamba, et al., 1988; Watson and Pittman 1988). In CA1 neurons, SST also activates a voltage-insensitive potassium leak conductance that contributes more to the SST-induced hyperpolarization of the resting potential than I_M. I_M dominates the response at slightly depolarized potentials (Schweitzer, Madamba, et al., 1998).

Intracellular calcium levels appear to play a bivalent role in controlling I_M amplitude whereby the small increases (50 to 150 nM) associated with an action potential enhance I_M (Marrion, Zucker, et al., 1991) whilst the larger increases (>200 nM) caused by a calcium spike inhibit the current (Tokimasa 1985).

3.15.5 Function

The major roles classically assigned to the M-type current are the formation of the medium afterhyperpolarization (mAHP) (Storm 1989), the regulation of repetitive firing by spike frequency adaptation (Madison and Nicoll 1984; Brown, Gahwiler, et al., 1990; Storm 1990) and the mediation of muscarinic and peptidergic regulation (Jones 1985). The slow activation of I_M seems to preclude a significant role in spike repolarization. Storm (1990) estimates that only

about 10% of the relatively small I_M current in CA1 pyramidal cells is activated during a single spike. The ability of I_M to activate in the subthreshold region enables it to perform a membrane excitability damping function. This feature operates in both the depolarizing and the hyperpolarizing directions since the current switches off when the potential repolarizes towards the resting potential. Acetylcholine and certain peptides deactivate I_M leading to an overall rise in the excitability of the cell as the damping function is lifted and the membrane resistance is raised (Storm 1990).

The fact that mutations in the KCNQ genes that express M channel subunits are associated with an inherited form of neonatal epilepsy (Jentsch 2000) underlines the role of I_M in maintaining membrane stability. In a conditional-expression transgenic mouse model, switching off the I_M in adulthood lead to a CA1 pyramidal neuron phenotype characterised by increased excitability, reduced spiked frequency adaptation, reduced mAHP and reduced subthreshold resonance (Peters, Hu, et al., 2005).

The latter effect of reduced subthreshold resonance points to the role of the M-type current in slow oscillations and resonance. Evidence has been accumulating supporting a prominent role for I_M in theta oscillations and resonance in areas such as the cortex (Gutfreund, Yarom, et al., 1995), cerebellum (D'Angelo, Nieus, et al., 2001) and hippocampus (Hu, Vervaeke, et al., 2002). Hu and colleagues (2002), go so far as to suggest that generating oscillations is the key functional role of I_M, given the central importance in the brain of oscillations for neuronal coding, synaptic plasticity, learning and memory.

I_M has recently been ascribed the novel capacity of controlling the firing mode of hippocampal neurons thorough modulation of the spike afterdepolarization (Yue and Yaari 2004). By utilising the I_M-specific channel modulators linopirdine and XE991 to tease apart the contribution of I_M to the electrophysiological profile of CA1 cells, Yue and Yaari (2004) found that 75-90% inhibition of I_M released a large I_{NaP}-driven spike afterdepolarization (ADP). The increase in the magnitude of the ADP is dependent on the level of I_M inhibition: 75-90% inhibition cause a 70% increase in the ADP whilst 50% inhibition triggers a 47% increase. Significantly, blockade of I_M allowed the ADP to escalate into a burst, thereby converting regular firing cells into burst firing cells. This suggests that ostensibly regular firing cells possess the ionic machinery for burst firing in a latent, regulated state.

Interestingly, inhibition of the I_C, I_{AHP}, and I_D currents had no significant effect on the magnitude of the ADP. The size of the ADP in CA1 pyramidals therefore appears to be determined by the

I_{NaP}/I_M ratio (Yue and Yaari 2004). They also found that inhibition of I_M caused significant changes in the resting membrane potential (5 mV tonic depolarization on average), input resistance, spike width, and the duration of the fast AHP. Together these results suggest that I_M is functionally considerably more ubiquitous than was previously thought.

This view is reinforced by a recent study that examined the effects of conditional suppression of neural KCNQ2 subunits expression in a transgenic mouse model (Peters, Hu, et al., 2005). Suppression of M-type channels increased excitability, spike-frequency adaptation, mAHP amplitude, and intrinsic subthreshold theta resonance in hippocampal pyramidal neurons. On the macroscopic level, suppression of neuronal I_M was also associated with seizures, hyperactive behaviour and structural changes to the hippocampus formation (Peters, Hu, et al., 2005).

3.15.6 I_M in the subiculum

I_M has not been explicitly characterised in subicular neurons to date, however, subicular pyramidal cells exhibit several electrophysiological features classically associated with I_M: the medium AHP, spike ADPs, frequency adaptation, subthreshold oscillations, muscarinic enhancement of excitability and somatostatin-induced suppression of excitability.

3.15.6.1 Medium afterhyperpolarizations

A component of the hippocampal medium afterhyperpolarization (mAHP) is mediated by I_M (Williamson and Alger 1990). Both regular and burst firing subicular pyramidals exhibit a noticeable mAHP following the termination of a sustained suprathreshold stimulus (Behr et al., 1996; Wozny et al., 2005). Inhibition of calcium-dependent potassium currents leaves a residual 55% of the control mAHP (Mattia et al., 1997b) that can plausibly be attributed to I_M.

3.15.6.2 Spike afterdepolarization

Jung et al. (2001) and Wellmer et al. (2002) and concluded that the burst propensity of subicular cells is largely determined by the size of the Ca^{2+}-driven spike ADP. In CA1 neurons, the spike ADP is regulated by I_M (Yue and Yaari 2004). There is indirect evidence in the literature for the importance of I_M in controlling subicular bursting. Mattia et al. (1997a) found that application of TEA abolished an outward rectification in the depolarizing direction seen under TTX. Since I_M is likely to be the only significant TEA-sensitive potassium conductance operating in the subthreshold region it is plausible to conclude that the current contributes to the suppression of the burst ADP in regular pyramidals. Nonetheless, the ability of an inhibitor of the potassium

delay current, I_D, to elicit bursting in rat regular firers (Staff et al., 2000) suggests that I_M is neither a necessary nor sufficient mechanism for burst control in the subiculum.

3.15.6.3 Spike frequency adaptation

Subicular regular firing cells generally exhibit spike-firing adaptation in response to sustained suprathreshold stimulation (Behr, Empson, et al., 1996) (although see Staff et al., 2000). In contrast, the single spiking phase of bursting cells is typically non-adapting. However, although not mentioned in the respective papers, in some studies the interval between the first and second spikes following a burst is consistently smaller than subsequent interspike intervals (Mason 1993; Wellmer, Su, et al., 2002). This may well constitute the isolated early phase of accommodation, which is conventionally assigned to I_M in hippocampal neurons (Madison and Nicoll 1984).

3.15.6.4 Subthreshold oscillations

The Cs^{2+}-resistant subthreshold oscillations observed in subicular bursting cells (Mattia, Kawasaki, et al., 1997) are probably due to I_{NaP}-amplified M-resonance. The constraints this participation imposes on any possible models of subicular I_M are discussed in more detail below.

3.15.6.5 Mediation of muscarinic activation

One of the effects of cholinergic activation is I_M suppression. In subicular bursters, carbachol, a non-hydrolysable cholinergic agonist, increases the excitability of subicular bursting neurons by inducing a steady depolarization, increasing the input resistance, blocking the burst AHP and evoking a plateau potential that outlasts depolarizing stimuli (Kawasaki and Avoli 1996). Unfortunately, since cholinergic activation modulates a number of currents in addition to I_M (Caulfield, Robbins, et al., 1993) it is difficult to isolate the precise role of I_M. For example, a significant proportion of these effects are probably due to the induction of a non-selective calcium sensitive cationic conductance (Kawasaki and Avoli, 1996). Nonetheless, the observation that selective I_M suppression triggers the transition from regular to burst firing in CA1 neurons (Yue and Yaari 2004) - which are similar to subicular neurons in their response to acetylcholine receptor activation - strongly hints that I_M cholinergic regulation of I_M could play a role in regulating the burster-regular firing ratio in the subiculum.

This role is unlikely to be straightforward since the subiculum shows a considerably more pronounced increase in bursting activity during slow wave sleep than either the hippocampus or

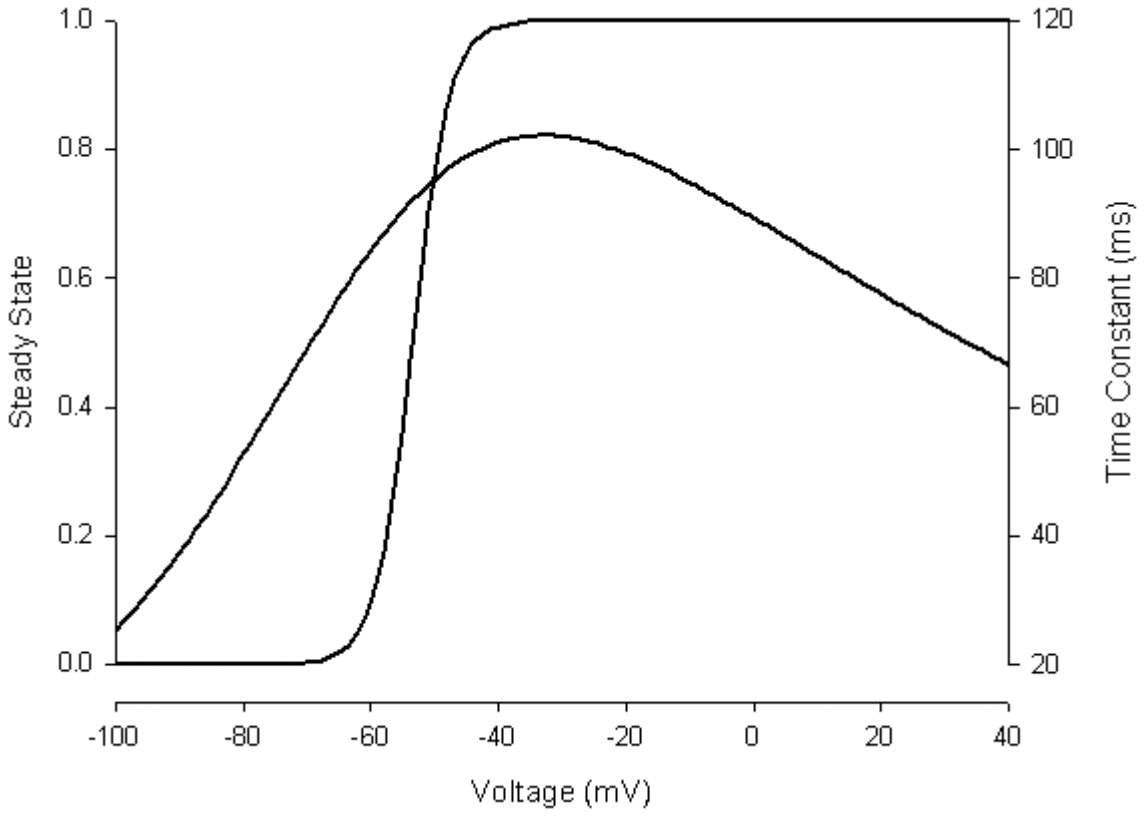

Figure III-12. Plot of the steady state activation and time constant curves for I_M.

entorhinal cortex (Staba, Wilson, et al., 2002). Cholinergic drive from the medial septum is low during slow wave sleep and hippocampal levels of acetylcholine (ACh) are considerably lower than during waking and REM sleep (Kametani and Kawamura 1990) so subicular bursting might be expected to decrease rather than increase during slow wave sleep.

3.15.6.6 Somatostatin suppression

Greene and Mason (1996) found that somatostatin (SST) hyperpolarized the resting potential of regular and bursting cells by an average of 1% and 4% respectively. These changes were associated with reductions of input resistance of 5% in regular firers and over 25% in bursters. At least part of this effect can be attributed to the somatostatin-sensitive I_M. Unfortunately, accurate attribution of the extent of this contribution is complicated by the ability of somatostatin binding to activate a range of potassium channels, including large conductance calcium-activated potassium channels (White, Tan, et al., 1991), inward and delayed rectifiers (Sims, Kelly, et al.,

1991; Akopian, Johnson, et al., 2000), and ATP-sensitive potassium channels (de, Fosset, et al., 1989).

3.15.7 Model of subicular I_M

Effective results were found with a model of the form (Figure III-12):

$$I_M = g_M m(V_m - E_K)$$

3.15.7.1 Activation

In subicular bursting cells, subthreshold oscillations appear at potentials positive to about -60 mV (Mattia, Kawasaki, et al., 1997). The amplitude of these oscillations increases from about 2 to 6 mV with further depolarizations beyond which spiking is triggered. Hu and colleagues propose that I_M and I_{NaP} mediate similar depolarized STOs seen in CA1 neurons. It is likely that this so-called 'M-resonance' (Hu et al., 2002) underlies the subthreshold oscillations reported in subicular bursting cells. If this is true then the STO threshold voltage of -60 mV constitutes an upper limit on the activation threshold of subicular I_M. To allow sufficient activation at -60 mV we set the activation threshold to around -70 mV, which is similar to CA1 (Halliwell and Adams 1982). An activation range of -70 to -40 mV (Halliwell and Adams, 1982) is approximated by the following Boltzmann activation curve:

$$m_{inf} = \frac{1}{1 + e^{\frac{V-(-53.5)}{-2.9}}}$$

3.15.7.2 Activation kinetics

The role of I_M in subthreshold oscillations imposes a constraint on the possible range of activation kinetics, since the theoretical resonance peak lies between the membrane and resonator current activation time constants expressed as frequencies (Hutcheon and Yarom, 2000). The membrane time constant of about 19 ms translates into a frequency of around 8 Hz. Hence, the presumed ability of subicular I_M to participate in resonance and subthreshold oscillations in the 5 Hz range implies a relatively low activation time constant of between about 65-85 ms (2.5-1.9 Hz) at -60 mV.

$$\tau_m = \frac{1}{0.004e^{\frac{V+126.5}{126.1}} + e^{\frac{V+170.4}{-20.9}}}$$

3.15.7.3 Conductance

Yue and Yaari (2004) report that selective I_M inhibition by linopirdine, at concentrations designed to block 75-90%, depolarizes the resting potential by an average of 5 mV and increases the membrane input resistance from 35 to 40 MOhm. This corresponds to a conductance change of about 3 nS or a total conductance of up to roughly 60 nS assuming 5% of I_M is active at rest, as determined from the foregoing Boltzmann curve. The final value for the model was 5 nS. A larger value of 110 nS was used to amplify the effect of I_M on outward rectification.

3.16 Slowly activation, calcium-dependent potassium current, I_{AHP}

The slowly activating Ca^{2+}-dependent potassium current, I_{AHP}, underlies the slow Ca^{2+}-dependent afterhyperpolarization (AHP) observed in hippocampal pyramidal cells after a train of action potentials (Hotson and Prince 1980; Lancaster and Adams 1986; Vergara, Latorre, et al., 1998). Between 80 and 90% of the sAHP in neocortical neurons is Ca^{2+}-dependent (Pineda, Waters, et al., 1998). The I_{AHP} of hippocampal pyramidals is slow, TEA-resistant and is functionally independent of voltage (Lancaster and Adams 1986).

3.16.1 Channel

Unfortunately, efforts to identify the molecular correlate of I_{AHP} are currently at an impasse (Vogalis, Storm, et al., 2003; Stocker 2004). Initial identification of I_{AHP} with the small conductance, calcium-activated SK ($Ca_{V2.1-3}$) class of potassium channels (Storm 1990) has been undermined by a number of recent contradictory findings. One of more emphatic of these results is the expression of normal I_{AHP} in the neocortical pyramidal neurons of a transgenic mouse that overexpressed SK3-1B, a universal SK channel suppressor (Wolfart and Roeper 2002). Furthermore, selective knockout of each of the SK variants fails to affect I_{AHP} in hippocampal CA1 pyramidal neurons (Bond, Herson, et al., 2004).

Current fluctuation analysis has been used to derive estimates for the single channel conductance of I_{AHP} of 2-5 pS for hippocampal CA1 neurons (Sah and Isaacson 1995) and about 7 pS for vagal motoneurons and dentate granule neurons (Sah 1995; Valiante, bdul-Ghani, et al., 1997).

3.16.2 Activation

I_{AHP} is slowly activated by Ca^{2+} influx driven by depolarizations. The magnitude of I_{AHP} activation is strongly dependent upon the number of action potentials. Sodium spikes drive increases in intracellular calcium that are mediated by voltage-sensitive calcium channels. Estimates of the increase in $[Ca^{2+}]_i$ caused by a single spike range from about 3 nM (Jaffe, Johnston, et al., 1992) to 60 nM (Spruston, Schiller, et al., 1995). I_{AHP} is activated by a rise of 30 to 60 nM Ca^{2+} (Knopfel, Rietschin, et al., 1989) and appears to be saturated by the intracellular calcium increase induced by six action potentials (Hotson and Prince 1980; Lancaster and Adams 1986). In neocortical neurons, there is a linear relationship between the plateau values of cytoplasmic calcium concentration and firing frequency in both soma and proximal apical dendrites (Abel, Lee, et al., 2004).

Once activated, the amplitude of the AHP current is resistant to membrane hyperpolarization. The calcium transient that induces I_{AHP} peaks slightly earlier and last slightly longer than I_{AHP}. I_{AHP} activation is also dependent upon the resting potential and is increased by several millivolts by depolarization of the V_m by 5-10 mV (Borg-Graham 1998).

Unlike the medium AHP, slow AHP requires a rise in calcium in the cytoplasm rather than close to the cell membrane, consistent with the existence of a cytoplasmic mediator between Ca^{2+} and the K^+ channels mediating the sAHP (Abel, Lee, et al., 2004). There is evidence that intracellular calcium stores mediate this role (Tanabe, Gahwiler, et al., 1998).

The L-type calcium channel appears to be the source of the I_{AHP} activating calcium since the slow AHP is suppressed by L-type calcium channels inhibitors, but not by blockers of other calcium currents (Marrion and Tavalin 1998). In rat CA1 pyramidals, somatic L-type calcium channels are selectively co-localized with SK1 channel (Bowden, Fletcher, et al., 2001).

3.16.3 Activation kinetics

The I_{AHP} tail current in response to short depolarizing step follows the time course of the sAHP and peaks after about 400-700 ms (Lancaster and Adams 1986). The time course of the sAHP peak is temperature sensitive implying that the long delay in the appearance of the slow AHP peak is more likely to be due to intrinsic channel kinetics rather than calcium dynamics (Thompson, Masukawa, et al., 1985; Lancaster and Adams 1986). The reported fast rise time of intracellular calcium to single action potentials reinforce this view (Jaffe, Johnston, et al., 1992). The time constant of deactivation at 30°C is a very slow 1.5 s and is independent of both the

magnitude of the current and membrane potential. There is also evidence that the rate of deactivation is determined by rate of decline of intracellular calcium (Knopfel, Rietschin, et al., 1989). I_{AHP} is non-inactivating.

3.16.4 Function

The slow Ca^{2+}-dependent current functions as a negative feedback mechanism insofar as it suppresses neuronal excitation by strongly hyperpolarizing the cell and acting as a shunt for depolarizing currents (Madison and Nicoll 1984). As mentioned previously, I_{AHP} is responsible for the slow AHP that follows bursts and single action potentials. I_{AHP} activation follows a similar time course to the AHP following an action potential train (Knopfel, Vranesic, et al., 1990). I_{AHP} also mediates late spike frequency adaptation. The early component of SFA, which persists when I_{AHP} is blocked, is largely due to I_M and I_C and (Madison and Nicoll 1984; Jones and Heinemann 1988). I_{AHP} may also contribute to the formation of the mAHP (Stocker, Krause, et al., 1999).

3.16.5 Location

Although I_{AHP} is located at the soma, there is some evidence that the proximal dendrites constitute the primary functional location of I_{AHP} (Sah and Bekkers 1996).

3.16.6 Modulation

I_{AHP} is extinguished by Ca^{2+}-free medium and calcium channel blockers and is resistant to 4-AHP (1 mM) and TEA (1-5 mM) (Pennefather, Lancaster, et al., 1985). The slow AHP, which is driven by I_{AHP}, is reduced by both kainic acid (Ashwood, Lancaster, et al., 1986) and neuroleptics (Dinan, Crunelli, et al., 1987) implying a sensitivity of the current to these agents. The current is downregulated by a range of monoamines such as dopamine, serotonin and histamine, the effects of which appear to be mediated by protein kinase C (Pedarzani and Storm 1993). Cholinergic and noradrenergic agonists also block I_{AHP} although muscarinic afferent suppression only occurs if afferent activation precedes a rise in intracellular calcium (Zhang, Fan, et al., 1996). Paradoxically, I_{AHP} is nearly 10 times more sensitive to muscarinic agonists than the eponymic I_M current (MadisonD. V., Lancaster, et al., 1987), which leads to its suppression during slow cholinergic EPSPs. Calcium currents are also suppressed by muscarinic activation but since the Ca^{2+} spikes that drive I_{AHP} are not affected during I_{AHP} activation it appears that muscarinic suppression of I_{AHP} is not due to a reduction in Ca^{2+} influx (Cole and

Nicoll 1984). The suppressing effect of noradrenaline (2-10 μM) is similarly independent of an effect on calcium influx (Madison and Nicoll 1986; Storm 1989). Madison and Nicoll (1986) suggest that I_{AHP} regulation is the principal mechanism through which the activity of the hippocampus is modulated by noradrenergic afferents. In CA1 pyramidal cells, I_{AHP} is also inhibited by apamin and some methyl derivatives of bicuculline (Khawaled, Bruening-Wright, et al., 1999; Stocker, Krause, et al., 1999).

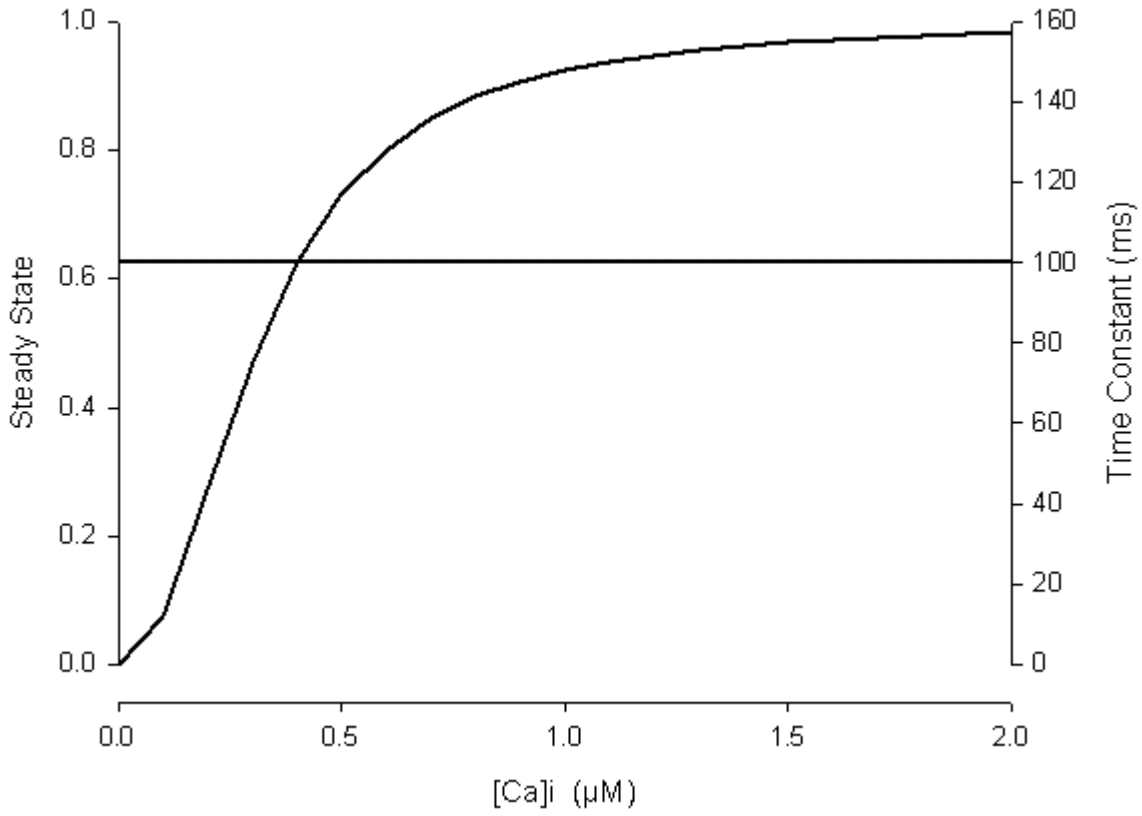

Figure III-13. Plot of the steady state calcium-dependent activation curve and the stationary time constant for I_{AHP}.

3.16.7 Subicular I_{AHP}

3.16.7.1 Slow AHP

The slow AHP is generally confined to regular firers following a spike train and is not usually seen in bursters (Behr et al., 1996). A slow Ca^{2+}-activated K^+ current, I_{AHP}, generates the sAHP in hippocampal pyramidals (Madison and Nicoll, 1984). Blockade of the sAHP in subicular

pyramidals by zero calcium (Wellmer et al., 2004) suggests a similar mechanism operates in the subiculum.

3.16.7.2 Spike frequency adaptation

Regular firing cells also exhibit spike-firing adaptation in response to sustained stimulation (Behr, Empson, et al., 1996; Wozny, Knopp, et al., 2005) the late phase of which is probably due to I_{AHP}. Unsurprisingly, given their lack of a slow afterhyperpolarization, subicular bursting cells do not generally exhibit spike frequency adaptation. The evident lack of I_{AHP} in bursting cells suggests that the current may play a role in regulating the firing mode of subicular pyramidals.

3.16.8 Model of subicular I_{AHP}

Our simple non-inactivating model of I_{AHP} has a Boltzmann-type calcium-sensitive activation function (Figure III-13).

$$I_{AHP} = g_{AHP} m(V_m - E_K)$$

3.16.8.1 Activation

We model the Ca^{2+}-dependent activation of I_{AHP} using a Boltzmann equation with a half-activation $[Ca^{2+}]$ of about 0.3 μM. This function saturates at around 1 μM.

$$m_{inf} = \frac{1}{1 + e^{\frac{\log[Ca]_{slow} - (-6.5)}{-0.2}}}$$

As in the Warman et al. (1994) model of I_{AHP} we use a stationary time constant, which we assume to be 100 ms (Lancaster and Zucker 1994).

$$\tau_{AHP} = 100 \text{ ms}$$

To allow I_{AHP} to mediate SFA and the sAHP we couple the I_{AHP} calcium sensor to the slow calcium pool, $[Ca^{2+}]_{slow}$, in which calcium slowly accumulates and decays during repetitive activity.

3.16.8.2 Conductance

A g_{max} for IAHP of 2.3 nS was found to be effective in emulating spike frequency adaptation and the slow afterhyperpolarization in regular firers.

3.17 Low voltage activating, slowly inactivating potassium, I_D

The slowly inactivating, 4-aminopyridine (4-AP)-sensitive, "delay" potassium current, I_D, of hippocampal pyramidal neurons and other CNS neurons was first adequately characterised by Storm (1988). I_D activates rapidly over a similar voltage range to I_A and, because they are both sensitive to 4-AP, early kinetic studies (Segal and Barker 1984) appear to have initially confounded the two currents. Conveniently, I_D is very sensitive to 4-AP and is blocked by (depending on the preparation) about 10 μM levels whilst I_A requires at least concentrations of 1-5 mM to abolish the current (Storm 1988). I_A is slightly reduced by 40 μM 4-AP and its inactivation is speeded up by approximately 20%. Later studies exploited this differential sensitivity to dissect out the two contributions and permit characterisation of I_D (Storm, 1988).

The primary differences between I_D and I_A can be summarised as:

1. I_D has slower kinetics,
2. I_D has a more negative threshold for activation and inactivation and
3. I_D is considerably more sensitive to 4-AP

3.17.1 Activation

Storm (1988) showed that the transient K^+ current elicited by a voltage step from -80 to -26 mV had a fast component (I_A) and a slow component (I_D). A voltage step from -60 to -26 mV involved only the I_A component. The activation threshold for I_D is about -75 mV whilst it saturates between -30 and -20 mV (Storm, 1988). This threshold is about 15-20 mV negative to that for I_A.

3.17.2 Activation kinetics

The activation kinetics of the CA1 delay current (<5 ms) are rapid enough to enable it to participate in spike repolarization (Storm, 1988).

3.17.3 Inactivation

Inactivation of I_D starts around -120 mV and is complete at -60 mV - the half inactivation of voltage is -89 mV. One consequence of the hyperpolarized inactivation curve is that over 90% of I_D is inactivated at the resting membrane potential.

3.17.4 Inactivation kinetics

The slow voltage-dependent inactivation of I_D occurs over several seconds (Storm, 1988). Recovery from voltage-dependent inactivation is very slow and ranges from 4.7 seconds at -110 mV to under a second at -26 mV.

3.17.5 Function

The combination of rapid activation and slow inactivation allows I_D to delay firing in response to a sustained suprathreshold depolarizing current (Storm 1988). Conversely, inhibition of I_D reduces the time to spike firing onset and generally increases levels of excitability. This facility of I_D for dampening neuronal excitability by shunting excessive depolarization appears to underpin the selective resistance to NMDA-induced excitotoxicity of certain cells, such as the magnocellular neurons of the paraventricular nucleus (Bains, Follwell, et al., 2001).

The subthreshold activation range of I_D in association with the long inactivation recovery time enables I_D to mediate neuronal integration of separate depolarizing inputs over several seconds (Storm, 1988). Since I_D is strongly inactivated at resting potentials, the capacity of hyperpolarizing stimuli to de-inactivate I_D make the encoding properties of the cell highly sensitive to the prevailing membrane potential.

In some hippocampal neurons low concentrations of 4-AP can slightly depolarize the resting membrane potential and increase the input resistance, which indicates that I_D may contribute to maintaining the resting membrane potential (Brown, Gahwiler, et al., 1990).

Additionally, I_D plays a role in action potential repolarization since micromolar concentrations of 4-AP act to broaden the spike (Storm 1988; Locke and Nerbonne 1997). The ability of I_D to control spike duration hints that the delay current may have a role in regulating calcium entry to the cell (Wu and Barish 1999).

More recently, this view has been challenged. Yue and Yaari, (2004), for example, found that micromolar concentrations of 4-AP had no significant effect on spike width, fAHP or the spike ADP. The lack of a 4-AP effect on spike repolarization and ADP is, perhaps, not unexpected, given that over 90% of I_D conductance is inactivated at a normal resting potential (Storm, 1988).

The high level of resting inactivation means that the ability of I_D to impose a delay in initial firing is strongly determined by the conditioning potential (prepotential). Thus, depolarizing prepotentials further inactivate I_D and markedly reduce the initial firing delay; hyperpolarizing

prepotentials have the opposite effect whilst resting prepotentials have an intermediate effect (Storm 1988). I_D has been shown to underlie a slow afterdepolarization following a sustained hyperpolarizing current step (Bains, Follwell, et al., 2001)

The ability of I_D to modulate the firing rate is determined by the dynamics of recovery from inactivation that, in turn, are strongly influenced by the degree and time course of hyperpolarization. Storm (1988) investigated the effect of the prepotential on secondary spikes as manifested in the 1st, 2nd, 3rd, and final steady state interspike intervals (ISIs) and found that I_D could modulate the firing rate by up to 100 Hz. Whilst I_D had little effect on the steady state ISI of about 20 Hz, increasing the strength of the delay current by pre-hyperpolarization forced the first few ISIs to lengthen and converge toward the steady state value (Storm, 1988). This effect was more pronounced for the second and third ISIs than for the first. The delay current effectively served to reduce the expression of spike frequency adaptation in CA1 pyramidals. By de-inactivating I_D, hyperpolarizing prepotentials facilitate an anti-SFA effect whereby the ISIs become progressively shorter as the strong D-type current slowly inactivates.

3.17.6 Modulation

I_D is suppressed by G protein–coupled metabotropic glutamate receptor (mGluR) activation by a mechanism that involves acceleration of inactivation (Wu and Barish 1999). Suppression is mediated by mGluR group I- and II-preferring agonists but not by a group III-preferring agonist. The vasoconstrictor angiotensin II tonically inhibits I_D, possibly via another G protein-coupled receptor, the angiotensin type 1 receptor (Bains, Follwell, et al., 2001). The delay current is insensitive to Ba^{2+} (1 mM), to Cs^{2+} (2 mM), and to 9-anthracene carboxylate (1 mM) (Storm, 1988). In addition to 4-AP, the delay current is sensitive to α-dendrotoxin (Bains et al., 2001).

3.17.7 I_D in the subiculum

3.17.7.1 Firing mode transition

Within the subiculum, I_D appears to play a role in suppressing bursting and perhaps regulating firing mode. Blockade of I_D by low concentrations (50 μM) of 4-AP reliably converts regular firers to weak bursters and weak bursters to strong bursters (Staff et al., 2000). Moreover, under picrotoxin inhibition of interneurons, a tetanic barrage from CA1 can induce bursting in some subicular regular firers (Stewart and Wong 1993). Since CA1 projections to the subiculum are predominantly glutamatergic (Taube 1993) and mGluR activation is known to suppress I_D (Wu

and Barish, 1999) this observation provides support for a potential role for I_D in regulating the subicular bursting/regular firing (B/R) ratio.

Indirect support for a role for I_D in suppressing bursting is supplied by the finding in area CA1 that I_D plays a negligible role in shaping the burst ADP (Yue and Yaari 2004) (the size of which appears to be the primary determinant of burst propensity). Staff et al. (2000) showed that, along with subicular regular firers, CA1 regular firers are also readily converted into bursters by 4-AP. These reports suggest that hippocampal regular firers also express stronger levels of I_D compared to bursters and support the idea that subicular regular firers are suppressed bursters.

However, the requirement that the inhibitory network must be switched off in order to induce bursts in regular firers suggests that such transitions are, at the very least, tightly regulated and may turn out to be unimportant under more realistic conditions.

3.17.7.2 Firing delay

Due to the action of I_D, CA1 cells can respond to sustained just-threshold depolarizing current injections with firing delays of over 500 ms in duration (Storm 1988). Subicular regular firers have been reported to exhibit firing delays of the order of 200 ms in duration (Staff, Jung, et al., 2000). However, literature reports imply that all types of subicular pyramidals tend to respond with much shorter delays of 50 ms and below (Stewart and Wong 1993; Wellmer, Su, et al., 2002). In CA1 pyramidals, delays of this magnitude are more typically associated with the fast transient potassium A-type current (Storm 1988). However, this conclusion may simply reflect a reporting bias since the spike latency of subicular regular firers in response to just-threshold stimuli is significantly longer than that of bursters when systematically examined (Cooper, Moore, et al., 2003). In conjunction with the observation that I_D inhibition converts regular into burst firers, this finding appears to support the theory that I_D plays an important role in regulating the firing mode of subicular pyramidals.

The high level of inactivation of I_D at rest (>90%) means that I_D exerts its greatest effects following pre-hyperpolarization (Storm, 1988). This behaviour appears to be contradicted in published figures in which pre-hyperpolarization of either regular or burst firing subicular pyramidals does not appear to significantly increase the initial firing delay (Mason 1993; Mattia, Kawasaki, et al., 1997). However, drawing conclusions about typical cell behaviour from potentially unrepresentative published voltage traces is inherently problematic.

3.17.7.3 Slow afterdepolarization and depolarizing sag

Behr et al. (1996) observed a slow 'post-stimulus' AHP that lasts over several hundred milliseconds in over 90% of regular firers. Although the slow AHP is typically attributed to the Ca^{2+}-dependent I_{AHP} current, given the hyperpolarized activation threshold for I_D, it is possible that de-inactivated I_D could also be contributing to the early component of this effect.

3.17.7.4 Spike frequency adaptation

Due to its slow inactivation, I_D classically has an anti-accommodation effect on the spike train (Storm, 1990) i.e. the interspike interval (ISI) decreases as I_D inactivates. However, in subicular pyramidals there is a paradoxical correlation of I_D with adaptation. Subicular bursters have low levels of I_D and low spike frequency adaptation (SFA), whereas regular firers have high I_D and high SFA. This paradox suggests that I_{AHP}, the current responsible for late SFA, is strong enough to mask the effects of I_D.

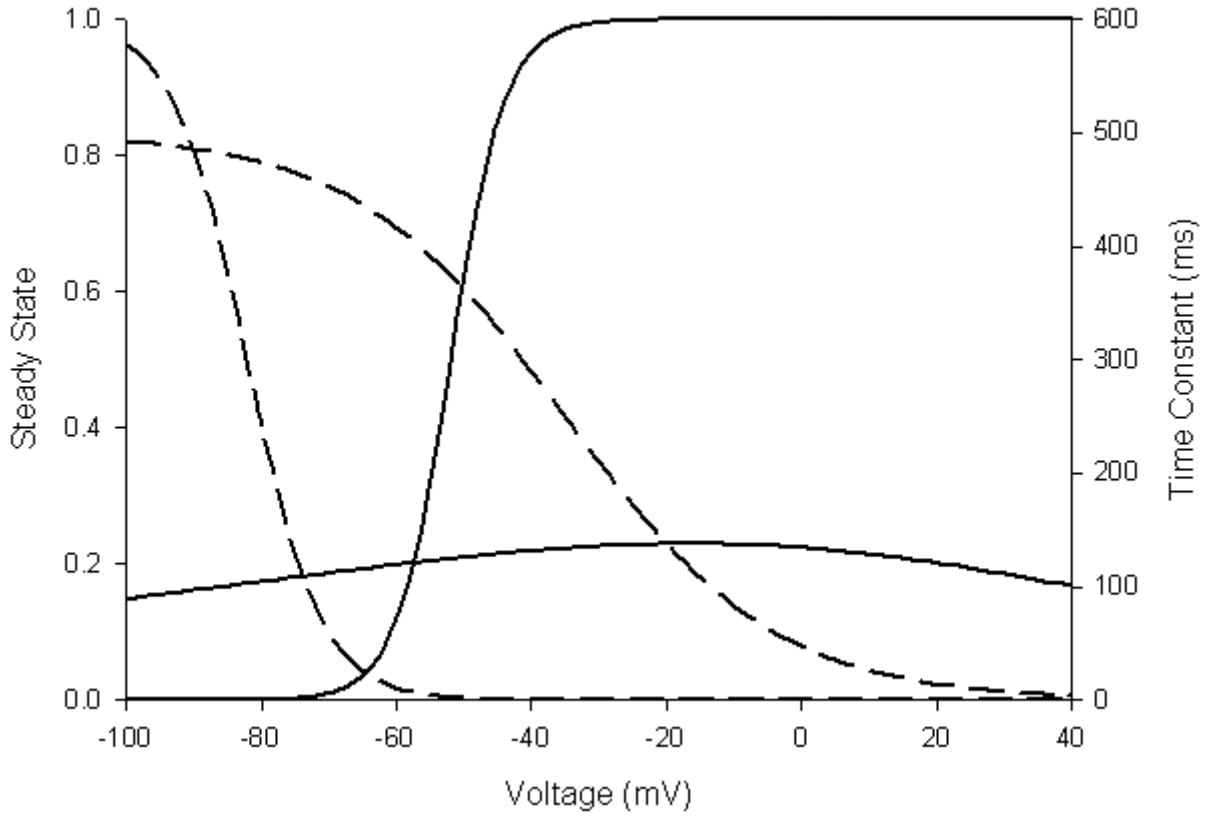

Figure III-14. Plot of the activation (solid lines) and inactivation (dashed lines) steady state and time constant curves for I_D. The activation time constant has been scaled by 100 in order to fit the activation and inactivation time constants on the same graph.

3.17.7.5 Rebound firing

Subicular regular firers generally exhibit a smaller anodal break potential than bursters following hyperpolarizing stimuli (Tbe et al., 1993; Green and Totterdell, 1993; Stanford et al., 1998; Menendez de la Prida et al., 2003). The combination of fast activation and de-inactivation by hyperpolarization of I_D suggests that I_D may contribute to the suppression of ABPs in subicular regular firers.

3.17.8 Model of subicular I_D

The structure of the subicular I_D model is (Figure III-14):

$$I_D = g_D m(V_m - E_K)$$

3.17.8.1 Activation

In CA1 pyramidals I_D has an activation range of about -75 to -20 mV with a half activation voltage of about -52 mV (Storm 1988)

$$m_{inf} = \frac{1}{1 + e^{\frac{V-(-52)}{-4}}}$$

3.17.8.2 Activation kinetics

The activation kinetics of this I_D model are slightly slower (about 1.3 ms at 0 mV) than those of I_A.

$$\tau_m = \frac{e^{\frac{V+93.2}{105.2}}}{1+e^{\frac{V-7.5}{35.1}}}$$

3.17.8.3 Inactivation

The inactivation range of I_D in CA1 is about -120 to -60 mV with a half-inactivation voltage of around -82.1 mV (Storm, 1988). The hyperpolarized inactivation curve means that only a small fraction (~10%) of I_D is not inactivated at rest.

$$h_{inf} = \frac{1}{1 + e^{\frac{V-(-82.1)}{5.5}}}$$

3.17.8.4 Inactivation kinetics

The inactivation time constant function was scaled to agree with the few data points provided by Storm (1988) and modified to match the time course of the slow AHP in subicular regular firers.

$$\tau_h = \frac{500}{1+e^{\frac{V-(-35)}{15.5}}}$$

3.17.8.5 Conductance

In CA1 pyramidals, the magnitude of I_A is over twice that of I_D (Storm 1988). Borg-Graham (1998) inferred a maximum conductance of about 50 nS from the Storm 1988 paper. The maximum conductance of I_D used in this study was adjusted to roughly one half to one third of that of I_A. The usual value was 40 nS.

3.18 Mixed cation anomalous rectifier, I_H

The hyperpolarization-activated, cyclic nucleotide-gated (HCN) current, I_H, was first identified in sinoatrial node cardiac cells (Noma and Irisawa 1976). The anomalous hyperpolarization activation properties of I_H have also earned it the name I_f for 'funny' (Brown, DiFrancesco, et al., 1979) and I_Q for 'queer' (Halliwell and Adams 1982). Phylogenetically, I_H is widely dispersed in neuronal and non-neuronal tissues in both invertebrate and vertebrate lineages. In the mammalian nervous system, I_H is found in a wide range of peripheral and central neurons (Moosmang, Stieber, et al., 2001; Robinson and Siegelbaum 2003) where its significant conductance in the subthreshold region allows the current to play an important role in shaping neural input-output functions.

3.18.1 Channel

The I_H current is carried by ion channels encoded by the HCN gene family which, in mammals, is composed of four genes, HCN1–4 (Santoro, Liu, et al., 1998; Ludwig, Zong, et al., 1998). This class of channels is selectively permeable to both K^+ and Na^+ with a 4-fold preference for K^+. This mixed cation current (Na^+/K^+) confers a reversal potential of between -20 mV (Hu et al., 2002) and -30 mV (Pape 1996). Permeability to anions is negligible.

3.18.2 Activation

The voltage-dependence and activation characteristics of I_H vary considerably across cell types. Generally, I_H inward currents are slowly activating, are non-inactivating. I_H is activated by hyperpolarizations beyond -50 to -70 mV (Brown and Adams 1980; Halliwell and Adams 1982; Brown, Gahwiler, et al., 1990; Storm 1990; Maccaferri, Mangoni, et al., 1993; Magee 1998). Deactivation tends to be faster than activation at more depolarized potentials.

Magee (1998) characterised I_H in rat CA1 pyramidals and reported a half-activation voltage of -83 mV for somatic and -89 mV for dendritic I_H with respective slope factors of 7 mV and 6 mV. Using a tail current protocol to measure the steady state activation characteristics of I_H, Magee (1998) found that (under 0 mV external Na^+) the half-activation voltage of somatic I_H to be -82 mV with a slope factor of 8.8 mV. The equivalent half-activation voltage of dendritic I_H is 8 mV more hyperpolarized. Addition of extracellular Na^+ (10-60 mM) shifted the activation curve of the dendritic I_H nearly 10 mV in the depolarized direction (V_{half} = -80.5 with a slope factor of 6.7). Extrapolating from this result, Magee estimated that under physiological conditions approximately 25% of somatic I_H channels are open at V_{rest} (-65 mV). This implies a CA1 somatic V_{half} of about -75 mV.

The voltage-dependent activation time constants are slow at relatively depolarized voltages (50 ms at -75 mV at 33 °C) but accelerate at more hyperpolarized levels (16 ms at -125 mV) (Magee 1998). The temperature dependence of activation is characterised by a Q_{10} of 4.5. Overall there is very little difference between the activation kinetics of the somatic and the dendritic forms of I_H. Current deactivation time constants are also found to be voltage-dependent (30 ms at -70 mV to 7 ms at -30 mV). The deactivation time constants at -45 mV are 18 ms and 16 ms.

Maccaferri and colleagues (1993) also describe a Cs^{2+}-sensitive anomalous rectifier in rat CA1 that contributes significantly to the resting membrane potential and is involved in the depolarizing phase of the mAHP. This current exhibits a reversal potential of about -17 mV and an activation range that extends from -50 to -140 mV with a half-maximal activation at about -98 mV. The reported time constant of 180 ms at -70 mV decreases with increasing hyperpolarization.

Another study on rat CA1 pyramidals used the intracellular inhibitor QX-314 and described an I_H with a narrower activation range and steeper activation curve that saturated around -120 mV

(Perkins and Wong 1995). A maximum conductance of around 10 nS can be inferred from the paper.

The biophysical descriptions of I_H in the literature have been inconsistent and have likely been confounded by a differential distribution of kinetically distinct HCN isoforms (Santoro, Chen, et al., 2000). Despite close amino acid sequence homology, the electrophysiological properties and activation characteristics of the HCN channel isoforms are distinct. The steady state activation time constants follow the sequence $HCN_1 < HCN_2 < HCN_3 < HCN_4$ (Tu, Deng, et al., 2004). It is also possible that the I_H isoforms exhibit different cation selectivity, which would partially account for some of the differences in reversal potentials reported for I_H. A further potential source of confusion is the presence of other Cs^{2+}-sensitive inwardly rectifying currents such as the fast inactivating K^+ inward rectifier, I_{FIR} (Constanti and Galvan 1983).

In CA1 pyramidals the voltage range of the steady-state activation curve of I_H in the distal dendrites is shifted about 10 mV negative to that of I_H found in the soma region, possibly as a result of differential modulation of cAMP along the somatodendritic axis (Magee 1998). The kinetics of activation do not appear to appear to differ substantially in both regions which would appear to rule out the possibility that the shift is due to a differential distribution of I_H isoforms along the somatodendritic axis, since the kinetics of the four primary isoforms of HCM are significantly different (Santoro, Chen, et al., 2000).

3.18.3 Distribution

Studies of mRNA expression indicate that all four isoforms are expressed in the brain but with different distributions and levels (Moosmang, Biel, et al., 1999). HCN_1 is strongly expressed in cortical regions, HCN_2 and HCN_3 are broadly expressed across the brain but at high and low levels, respectively, whilst HCN_4 is expressed strongly in subcortical regions (Santoro, Chen, et al., 2000).

3.18.4 Modulation

The activation curve of I_H is modulated by the levels of the cyclic nucleotide cAMP and, by implication, any neurotransmitters that alter cAMP levels (Robinson and Siegelbaum 2003). Increases in cAMP shift the curve in the positive direction whereas decreases in cAMP levels shift the activation curve in the negative direction (Ingram and Williams 1996; Pape 1996). Additionally, some I_H channel subunits are modulated by phosphorylation (Santoro, Liu, et al.,

1998). I_H is also modulated by acetylcholine. Carbachol, a cholinergic agonist, accelerates the kinetics of I_H at -100 mV by reducing its activation time constant (Colino and Halliwell 1993).

The channel is completely blocked by extracellular caesium (1 mM) (Halliwell and Adams 1982). Extracellular barium is ineffective against I_H although it does inhibit the functionally related class of rapidly activating (< 10 ms) inwardly rectifying K^+ currents (I_{FIR}). Intracellular blockers include the lidocaine derivative QX314 and ZD7288, a bradycardiac agent (Seutin, Massotte, et al., 2001).

3.18.5 Function

The activation and kinetic properties of I_H permit it to contribute substantially to the resting and active membrane properties of neurons. At resting membrane potentials 10-15% of HCN channels are activated and constitute about 30% of membrane conductance (Tu, Deng, et al., 2004). A primary function of I_H is thus stabilisation of the resting membrane potential, particularly against hyperpolarizing voltage excursions (Pape 1996). The role of I_H in influencing the resting membrane properties of CA1 pyramidals was investigated by Magee (1998) who estimated that approximately 25% of somatic I_H channels are open at V_m. Consequently, I_H strongly affects a number of key passive membrane parameters such as input resistance, membrane time constant, and the resting potential. Further activation of I_H by spike or burst afterhyperpolarizations enables the current to participate in active membrane phenomena such as oscillations and pace-making spike firing rates in a number of cell types. In cells from cardiac pacemaker cells to thalamic neurons (Pape 1996; Luthi and McCormick 1998; Neuhoff, Neu, et al., 2002), I_H promotes rhythmic activity by contributing a 'pacemaker' depolarization (McCormick and Bal 1997). The strength of the pacemaker depolarization is determined by the maximum conductance of I_H and determines the rhythmic burst firing rate in both cells, such as inferior olivary neurons (Bal and McCormick 1997), and inhibitory networks, such as the leech ganglionic interneuron net (Olsen, Nadim, et al., 1995). A role for I_H in the oscillations of entorhinal stellate cells was also proposed (Alonso and Llinas 1989) but later rejected (Alonso and Klink 1993). In layer V cortical pyramidals, blockade of I_H suppresses resonance (Ulrich 2002). Recently, it was suggested that I_H, and not I_M, underlies low-frequency theta-resonance in hippocampal neurons (Pike, Goddard, et al., 2000). Hu and colleagues (2002) proposed a role for I_H in a novel form of theta-band resonance that is most prominent at hyperpolarized membrane

potentials (-75 to -95 mV) called H-resonance. I_H also helps regulate the phase relation between dendritic sinusoidal excitatory inputs and somatic spike firing (Magee 2001).

The characteristic electrophysiological signatures of I_H activation are a depolarizing sag in response to sustained hyperpolarizing stimuli, such as IPSP currents, and a rebound depolarizing potentials that can trigger spiking. The magnitude of the rebound potential is proportional to the degree of hyperpolarization. Activation of I_H thus constitutes a mechanism for implementing a spike-firing threshold in the hyperpolarizing direction. An example of this mechanism in action is in developmental seizures in the immature hippocampus where a persistent upregulation of I_H is responsible for a paradoxical lowering of the seizure threshold despite enhanced inhibition within the network (Chen, Kamiryo, et al., 2001).

In rat CA1 pyramidal neurons, the current density of I_H increases linearly from the soma to the distal dendrite (Magee 1998). This spatial distribution of I_H along the somatodendritic axis leads to regional differences in input resistance and membrane polarization rates. One effect of this is to impose a directional specificity on the propagation of subthreshold membrane transients (Magee 1998). Other functional consequences include a drop in the amplitude of EPSPs, a contraction of the time window within which temporal summation can occur, a decrease in the duration of dendritic action potentials and an increase in the strength of afterhyperpolarizations. Interestingly, the more hyperpolarized half-activation voltage of dendritic I_H mentioned above acts to partially offset the higher current density of I_H found in the dendrites.

In rat cortical layer V pyramidal neurons, the level of I_H is inversely related to the spike frequency required by a train of somatic action potentials to invoke calcium spikes in the distal dendrites (Berger, Senn, et al., 2003). The effectiveness of I_H is increased by depolarizing the dendrite and decreased by hyperpolarization of the dendrite. In this way, I_H electrotonically disconnects the somatic and distal dendritic spike initiation zones by suppressing the ability of back-propagating sodium spikes to trigger dendritic calcium spikes in the absence of robust coincident dendritic activation (Berger, Senn, et al., 2003).

Whilst I_M drives the mAHP at depolarized potentials, I_H is also primarily responsible for the somatic mAHP that follows an action potential or burst at hyperpolarized potentials (Gu, Vervaeke, et al., 2005).

3.18.6 I_H in the subiculum

A Cs^{2+}-sensitive, hyperpolarization activated mixed cationic current is prominent in subicular regular firing and bursting cells. When stimulated with a sustained (>50 ms) hyperpolarizing pulse subicular regular firing and bursting cells exhibit a delayed inward rectification or depolarizing sag (Taube 1993; Stewart and Wong 1993; Mattia, Kawasaki, et al., 1997).

The peak current was attained after about 40 ms before decaying towards a more depolarized steady state level (Mattia, Kawasaki, et al., 1997). The ratio of the sag peak to the steady state potential is known as the sag ratio. This ratio has variously been reported as differing between regular and burst firers (Greene and Totterdell 1997; Greene and Mason 1996) and as being identical (Staff, Jung, et al., 2000).

The subicular 'sag' potential is inhibited by extracellular caesium (3 mM) but not by barium, which strongly suggests that the underlying conductance is the classical mixed-cation (Na^+/K^+) channel and not a member of the large barium-sensitive fast inward rectifier potassium channel family (Mattia, Kawasaki, et al., 1997). Similarly, calcium (Co^{2+} and Cd^{2+}) or Na^+ (TTX) channel blockers do not influence the sag. The sag is typically followed by an afterdepolarization (anodal break potential) that is sometimes strong enough to trigger rebound spiking or bursting (Stewart and Wong 1993; Behr, Empson, et al., 1996). The magnitude of the rebound potential is related to the duration (Mattia et al., 1997a) and strength (Stewart and Wong, 1993) of the hyperpolarizing command potential. Stewart and Wong (1993) reported that the anodal break potential was strongly attenuated by caesium or TTX, which suggests that both I_H and the low threshold persistent sodium current, I_{NaP}, contribute to the phenomenon.

A number of studies have reported that subicular bursting is voltage dependent (Mason, 1993, Stewart and Wong, 1993; Mattia et al., 1997; Stewart and Harris, 2001; Menendez de la Prida et al., 2003) (although see Staff et al., 2000). The reported ability of I_H to strongly influence the resting membrane potential suggests that modulation of I_H is a potential mechanism through which bursting propensity can be controlled. The observation that carbachol, an acetylcholine receptor agonist, potentiates the Cs^{2+}-sensitive, hyperpolarization-activated cationic conductance that contributes to the hyperpolarizing sag recorded in subicular bursting cells (Mattia, Kawasaki, et al., 1997) and CA1 pyramidal cells (Colino and Halliwell 1993) is of interest in this regard.

Subicular bursting cells exhibit subthreshold oscillations at holding potentials above -60 mV (Mattia, Kawasaki, et al., 1997). Similar oscillations have been attributed to I_H in thalamic relay neurons (McCormick and Pape 1990). However, the insensitivity of subicular oscillations to caesium (Mattia, Kawasaki, et al., 1997) and the depolarized activation range mean that they are unlikely to be mediated to any significant degree by I_H.

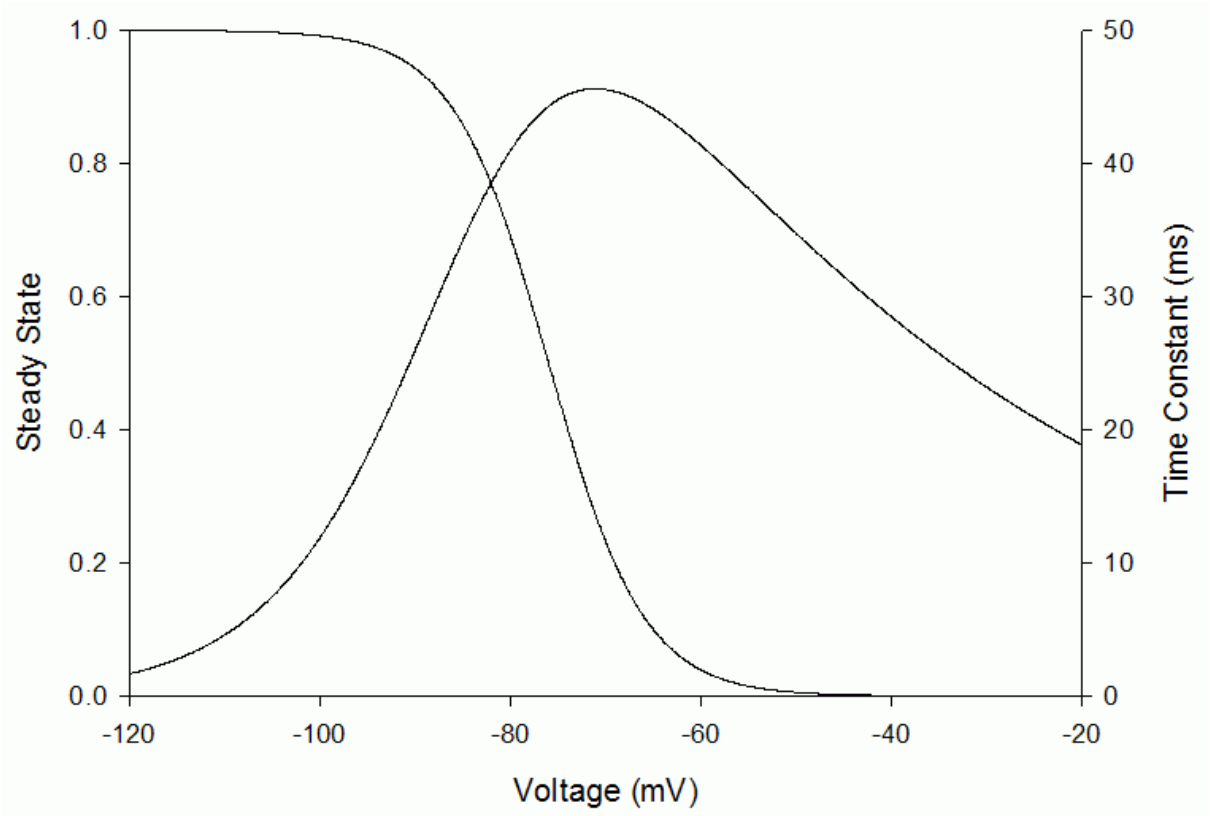

Figure III-15. Plot of the activation steady state and the time constant curves for I_H.

Mechanistically, subthreshold oscillations are amplified resonant responses of a neuron (Hutcheon and Yarom 2000). Hippocampal CA1 pyramidal cells have been shown to exhibit at least two forms of resonance: 'M-resonance', a subthreshold depolarized resonance centred at about -60 mV, often associated with STOs, and a hyperpolarized form, 'H-resonance', strongest at around -80 mV that relies on I_H (Hu et al., 2002). H-resonance has not been empirically demonstrated in subicular pyramidals but can be plausibly predicted given that I_H fulfils the theoretical criteria for a 'resonator current' (Hutcheon and Yarom 2000) i.e. a time constant of activation significantly slower than the membrane time constant and a membrane potential stabilising effect via negative feedback.

3.18.7 Model of subicular I_H

The I_H current has not been explicitly studied in subicular neurons, so for the purposes of this study we relied on the I_H characteristics as determined in pyramidal neurons of the phylogentically similar CA1 region (Maccaferri, Mangoni, et al., 1993; Magee, Hoffman, et al., 1998) and adjusted these parameters to accommodate constraints on possible I_H models inferred from the subicular electrophysiological literature (Figure III-15).

$$I_H = g_H m(V_m - E_H)$$

3.18.7.1 Lower activation range

Behr and colleagues (1996) reported that the characteristic depolarizing sag of subicular pyramidals disappears when the membrane is clamped at holding potentials 15-20 mV negative to the resting membrane potential prior to imposition of hyperpolarizing current injections. This observation conflicts with the expectation that the I_H current should increase in strength at lower potentials due to a combination of greater activation and a higher electrochemical 'driving force' as Vm moves further from the reversal potential for I_H of about -30 mV. A parsimonious explanation for this paradoxical result is that I_H activation plateaus 15-20 mV below rest thus preventing the current from responding to further hyperpolarization. This hypothesis imposes a lower limit of about -90 mV on the activation range of subicular I_H. This value is somewhat higher than the -140 to -120 mV reported in CA1 (Maccaferri, Mangoni, et al., 1993; Magee, Hoffman, et al., 1998).

3.18.7.2 Upper activation range

The upper activation limit of subicular I_H is likely to be considerably lower than the -50 mV threshold reported for CA1 pyramidals (Maccaferri, Mangoni, et al., 1993; Magee, Hoffman, et al., 1998) because Cs^{2+} does not effect subicular subthreshold oscillations at -60 mV. Furthermore, Staff et al. (2000) found no change in resting potential (-66 mV) under caesium. The inferred activation range of about -65 to -90 mV suggests a Boltzmann equation with half-activation voltage of -76.0 and a slope factor of 5.0 mV.

$$m_{inf} = \frac{1}{1 + e^{\frac{V-(-76)}{5}}}$$

3.18.7.3 Activation kinetics

Since the depolarizing sag in subicular neurons appears to be overwhelmingly due to the Cs^{2+}-sensitive I_H current, the time and voltage dependence of the sag were used to constrain the possible kinetic models for the subicular I_H channel. In subicular neurons, the depolarizing sag appears in response to hyperpolarizing pulses that exceed about 50 ms in duration (Mattia, Kawasaki, et al., 1997). Application of caesium causes a near 50% increase in the voltage change for a given hyperpolarizing current (Staff, Jung, et al., 2000).

The magnitude of the sag following a hyperpolarizing step voltage is an indirect measure of the current's activation time constant. A slower activation time constant should lead to a larger sag ratio since more current is available to depolarize the membrane. The relatively small sag ratio of about 0.8 reported for subicular neurons (Staff, Jung, et al., 2000), suggests that the I_H current is significantly activated within the 30 to 40 ms taken to reach peak. Reproduction of this sag ratio was best achieved with an activation time constant of about 45 ms at -70 mV, which is somewhat smaller than the 50 and 60 ms (at -75 mV) found for CA1 somatic I_H (Magee, Hoffman, et al., 1998).

$$\tau_m = \frac{e^{\frac{V+125}{9.6}}}{1+e^{\frac{V+84}{8}}}$$

This time constant function reproduces the time course and amplitude of the depolarizing sag and (in conjunction with a model for the persistent sodium current) the rebound potential response characteristic of subicular pyramidals. The voltage dependence of the rebound potential was investigated by constructing an I-V curve, which was found to match literature findings.

3.18.7.4 Reversal potential

Estimates of the reversal potentials, E_H, for I_H range from -17 mV (Maccaferri, Mangoni, et al., 1993) to -49 mV (Halliwell and Grove 1989) to -55 mV (Halliwell and Adams 1982). We applied an E_H of -43 mV, which yielded the characteristic Cs^{2+}-sensitive 4-5 mV depolarizing deflection from at rest membrane potential (Staff, Jung, et al., 2000) and rebound potential.

3.18.7.5 Conductance range

The maximum conductance range of I_H in subicular pyramidals is estimated to be between about 5 and 36 nS. This estimate is derived below.

An I_H conductance appears to contribute strongly to the resting membrane potential in subicular pyramidal cells the since addition of extracellular Cs^{2+} causes membrane resistance to increase by between 50 and 110% across cell types (Staff, Jung, et al., 2000). As Staff and colleagues found no statistically significant differences between cell types (but see Menendez de la Prida, 2003) we will take their average membrane resistances (about 38 MOhm without Cs^{2+} and 65 MOhm with Cs^{2+}). An average resting membrane resistance of 38 MOhm corresponds to a resting conductance of about 26 nS (conductance is the inverse of resistance). The difference of 23 MOhm between the measured resistance with and without Cs^{2+} represents, to a first approximation, the I_H contribution. This crude analysis places an upper limit of about 9 nS on the resting I_H conductance in subicular pyramidals. A similar analysis of the paper by Magee (1998) yields an upper limit for resting I_H of 6 nS in CA1 pyramidals. Since Magee (1998) estimates that in CA1 neurons approximately 25% of somatic I_H channels are open at V_m this scales to an upper maximum I_H somatic conductance of about 24 nS. A parallel analysis for subicular neurons gives an upper bound for perisomatic g_{max} of about 36 nS.

The somatic conductance density for CA1 pyramidal neurons of 1-2 pS/um2 (Magee, Hoffman, et al., 1998) converts to a hippocampal somatic conductance of about 4 nS for an estimated perisomatic surface area of 2000 um2. This is likely to be an underestimate since the density of I_H increases rapidly with distance from the soma. Since subicular pyramidals exhibit a higher resting Cs^{2+}-sensitive conductance than CA1 pyramidals, the CA1 value places a plausible lower bound on the maximum perisomatic conductance of subicular I_H of about 5 nS. This value is identical to that reported for CA1 I_H (Maccaferri, Mangoni, et al., 1993; Halliwell and Adams 1982).

A perisomatic range for I_H g_{max} of 5 to 36 nS, approximately 25% of I_H active at V_{rest} and a resting conductance of about 26 nS suggests that I_H potentially accounts for between 5 and 34% of the somatic resting membrane conductance of subicular pyramidals.

Our final I_H gmax value is 7 nS. Our I_H model is nearly 20% activated at rest and depolarizes the passive membrane resting potential by about 1.5 mV. The success of this current model in reproducing the appropriate subthreshold characteristics of the subicular pyramidal cell is illustrated in Chapter IV Subicular Cell Models.

Table III-1 Subicular Hodgkin-Huxley channel model parameters

CHANNEL	FORMAT	ACTIVATION	ACTIVATION KINETICS	INACTIVATION	INACTIVATION KINETICS
I_{CaT}	mh	$m_{inf} = \frac{1}{1 + e^{\frac{V-(-45.1)}{-4}}}$	$\tau_m = -0.3(-1.1-e^{-0.03V})$	$h_{inf} = \frac{1}{1 + e^{\frac{V-(-80)}{6}}}$	$\tau_h = \frac{201.0}{1+e^{\frac{V-(-69.1)}{4.5}}} + 15.0$
I_{CaR}	Double activation kinetics	$m_{inf} = \frac{1}{1 + e^{\frac{V-(-14.5)}{-6.4}}}$	See section 1.7.11.5 for details	$h_{inf} = \frac{1}{1 + e^{\frac{V-(-65)}{5.5}}}$	$\tau_h = \frac{e^{\frac{V+370.6}{70.1}}}{1+e^{\frac{V+55.5}{41.5}}}$
I_{CaN}	m^2h	$m_{inf} = \frac{1}{1 + e^{\frac{V-(-24.8)}{-9.5}}}$	$\tau_m = \frac{e^{\frac{V-0.5}{120}}}{1+e^{\frac{V+50.6}{80.1}}}$	$h_{inf} = \frac{1}{1 + e^{\frac{V-(-48.6)}{8.2}}}$	$\tau_h = \frac{150}{1+e^{\frac{V-(-20)}{30}}}$
I_{NaP}*	m^2h	$m_{inf} = \frac{1}{1 + e^{\frac{V-(-55.3)}{-6.4}}}$	$\tau_m = \frac{e^{\frac{V+23.5}{24.1}}}{1+e^{\frac{V+35.2}{12.5}}}$	$h_{inf} = \frac{1}{1 + e^{\frac{V-(-57.4)}{5.6}}}$	$\tau_h = \frac{1}{0.003e^{\frac{V+103.1}{89.1}} + e^{\frac{V+190}{-29.5}}}$
I_{CaL}	m^2h	$m_{inf} = \frac{1}{1 + e^{\frac{V-(-14.5)}{-7.5}}}$	$\tau_m = \frac{e^{\frac{V+59.5}{55.5}}}{1+e^{\frac{V+20.6}{28.4}}}$	NA	NA

*The I_{NaP} model exhibits an additional stationary deactivation time constant as detailed in section 1.9.16.3

Table III-1 (continued) Subicular Hodgkin-Huxley channel model parameters

CHANNEL	FORMAT	ACTIVATION	ACTIVATION KINETICS	INACTIVATION	INACTIVATION KINETICS
$I_{CaP/Q}$	mh	$m_{inf} = \frac{1}{1 + e^{\frac{V-(-1)}{-7.1}}}$	$\tau_m = \frac{e^{\frac{V+119.5}{53}}}{1+e^{\frac{V+70.1}{42.9}}}$	NA	NA
I_A	mh	$m_{inf} = \frac{1}{1 + e^{\frac{V-(-20.1)}{-6.3}}}$	$\tau_m = \frac{e^{\frac{V-5}{55}}}{1+e^{\frac{V-10}{24.9}}}$	$h_{inf} = \frac{1}{1 + e^{\frac{V-(-59.5)}{5.8}}}$	$\tau_h = \frac{e^{\frac{V+420}{60}}}{1+e^{\frac{V+185.1}{45.9}}}$
I_{CT}	m	$m_{inf} = \frac{1+e^{\frac{V-(-30)}{-3.3}}}{1+e^{\frac{\log[Ca]_{fast}-(-6.5}{-0.1}}}$	$\tau_m = \frac{e^{\frac{V-10}{995.1}}}{1+e^{\frac{V-450}{134.9}}}$	$h_{inf} = \frac{1}{1 + e^{\frac{V-(-50)}{7.3}}}$	$\tau_h = \frac{e^{\frac{V-78.1}{9.5}}}{1+e^{\frac{V-47}{7.8}}}$
I_{DR}	m^4	$m_{inf} = \frac{1}{1 + e^{\frac{V-(-35.6)}{-10.2}}}$	$\tau_m = \frac{e^{\frac{V+256.1}{162.2}}}{1+e^{\frac{V+12.4}{38.9}}}$	NA	NA
I_M	m	$m_{inf} = \frac{1}{1 + e^{\frac{V-(-53.5)}{-2.9}}}$	$\tau_m = \frac{1}{0.004e^{\frac{V+126.5}{126.1}} + e^{\frac{V+170.4}{-20.9}}}$	NA	NA

Table III-1 (continued) Subicular Hodgkin-Huxley channel model parameters

CHANNEL	FORMAT	ACTIVATION	ACTIVATION KINETICS	INACTIVATION	INACTIVATION KINETICS
I_D	m	$m_{inf} = \frac{1}{1 + e^{\frac{V-(-52)}{-4}}}$	$\tau_m = \frac{e^{\frac{V+93.2}{105.2}}}{1+e^{\frac{V-7.5}{35.1}}}$	$h_{inf} = \frac{1}{1 + e^{\frac{V-(-82.1)}{5.5}}}$	$\tau_h = \frac{500}{1+e^{\frac{V-(-35)}{15.5}}}$
I_h	m	$m_{inf} = \frac{1}{1 + e^{\frac{V-(-76)}{-5}}}$	$\tau_m = \frac{e^{\frac{V+125}{9.6}}}{1+e^{\frac{V+84}{8}}}$	NA	NA

Chapter IV
SUBICULAR CELL MODELS

All models are wrong, but some are useful

W. Edwards Deming

4.1 Abstract

In this chapter we develop models of a range of electrophysiological features of subicular principal cells including rectification, frequency preference responses, the action potential, subicular bursting, plateau potentials, delayed firing, spike frequency adaptation, afterhyperpolarizations, and rebound firing. Subicular bursting, in particular, is analysed and simulated in considerable detail. Competing theories concerning the ionic composition of subicular bursting are assessed and a novel theory is proposed.

4.2 Modelling approach

Subicular pyramidals were modelled using an isopotential single compartment model. Despite the gross simplification of neuronal morphology this represents, single compartment simulations have a proven record of accurate and insightful reproduction of the salient aspects of current and voltage clamp behaviour of a broad range of neuronal cell types (McCormick and Huguenard 1992; LeMasson, Marder, et al., 1993; White, Klink, et al., 1998; Kopell, Ermentrout, et al., 2000; Schreiber, Erchova, et al., 2004; Wu, Enomoto, et al., 2005). Conceptually, single compartment simulations are broadly similar to acutely dissociated neuron studies - in both cases dendritic and axonal processes are shorn away eliminating the contribution of gated dendritic currents and ectopic axonal spikes to the somatic electrophysiological profile.

4.3 Limitations

An obvious limitation of the single compartment approach is the inability to accurately model processes that depend on the interactions of spatially separated ionic mechanisms. This limitation can manifest itself in one of two ways: a failure to model a particular process or the development of a conceptually inaccurate model of a process. These 'failure modes' are respectively illustrated in models developed to emulate the relationship between the excitatory peak of the PSTH and

the underlying EPSP in cat motoneurons (Jones and Bawa 1997), and the stepwise repolarization of calcium spikes in cortical dendrites (Reuveni, Friedman, et al., 1993). In both cases, the limitations of the single compartmental approach necessitated the use of multi-compartmental models.

The pitfalls associated with single compartment modelling can be largely avoided by a careful reading of the experimental literature, in order to determine whether the processes of interest are indeed spatially segregated. For example, there is good evidence that the most dramatic aspect of subicular pyramidal electrophysiology, the burst, is localised to the axosomatic region (Jung et al., 2001; Menendez de la Prida et al., 2003). Broader evidence for the active electrotonic isolation of dendrites and soma of central neurons generally has steadily accumulated (Hausser and Mel 2003). However, large-scale network simulations of the subiculum will eventually require multi-compartmental models.

Table IV-1 Passive membrane parameters of the subicular pyramidal models

RMP (mV)		-69
Input resistance (MOhm)		21, 41, 60
Surface area (μm^2)	Effective	1550 (33333)
	Perisomatic	
C_m (nF)		0.31
Time constant (ms)		6.5, 12.7, 18.6
Reversal potential (mV)	E_{Na}	+65
	E_K	-90
	E_H	-43
Temperature (° C)		33

4.4 Passive membrane properties

4.4.1 Resting membrane voltage

Average literature values for the resting membrane potential of subicular pyramidals range from -64 mV (Mason 1993) to -72 mV (Greene and Mason 1996). We set the resting membrane voltage at -70 mV, several millivolts below the average values reported for subicular neurons. This slightly hyperpolarized resting potential of the passive membrane was chosen to

compensate for the depolarization caused by the insertion of I_H, the mixed cation anomalous rectifier. The final membrane voltage was approximately -69 mV.

4.4.2 Leak conductance and input resistance

The leak conductance of a membrane is determined by combined contributions of passive Na^+ and K^+ and, to a lesser extent, Cl^- channels. Since the bilipid membrane itself is essentially impermeable to ions we can use the input resistance to derive a first order approximation of the leak conductance. Staff et al., 2000 determined the input resistances of bursters and regular firers under Cs^{2+}. Extracellular caesium eliminates the anomalous inward rectifier current, I_H, and substantially increases the membrane input resistance from an average of 38 MOhm to 60 MOhm. Since Staff et al., found no differences in R_m between subicular cell types the 60 MOhm value served as a convenient reference from which other literature values were emulated by the addition of appropriate shunt conductances. Two other resistances were commonly employed in the subicular models presented here: 41 (Mason et al., 1993), and 21 MOhm (Mattia et al., 1997a). As will be seen, the choice of input resistance value influenced the ease with which the various subicular electrophysiological features were modelled.

4.4.3 Surface area and capacitance

The absolute capacitance of a cell may be determined from the product of its specific membrane capacitance and surface area. The specific membrane capacity (capacitance per unit area), C_M, is quite consistent across nerve cell types and is generally about 1.0 $\mu F/cm^2$ (Hodgkin and Rushton 1946; Sah, Gibb, et al., 1988), comparable to the 0.8 $\mu F/cm^2$ for a pure lipid bilayer (Hille. 1992). The surface area of the perisomatic region of subicular pyramidal cells can be calculated in several ways:

4.4.3.1 Cell capacitance

Vreugdenhil and colleagues (2004) used cell capacitance as a proxy for membrane surface area of subicular pyramidals and implied an average capacitance of 17.2 pF/cell. This is within the range for dissociated CA1 cells (Sah et al., 1988). Assuming a CM of 1.0 $\mu F/cm^2$ for subicular cells yields an average perisomatic surface area of 1720 μm^2.

4.4.3.2 Visual estimation method

The average somatic cross-sectional profile surface area of large subicular pyramidal neurons is visually estimated to average 450 μm^2 (Menendez de la Prida, Suarez, et al., 2002). If the shape of the soma is approximated as a sphere with a diameter of 21 μm ($\sqrt{450}$) a surface area of about 1380 μm2 obtained - in reasonable agreement with the capacity-based measures. An intermediate value of 1550 μm2 was taken for the physical surface area.

4.4.3.3 RC circuit method

The isopotential passive cell membrane is typically modelled as an RC circuit with the membrane input resistance and capacitance in parallel. The time constant, τ, of such a circuit is given by the product of the resistance and capacitance (RC). Since the membrane time constant, τ_m and R_m are usually known, the effective electrotonic surface area, A', can be calculated if, as above, a standard value for C_M is assumed:

$$A' = C_m/C_M = (\tau_m/R_m)/C_M = 20\ ms/(60\ MOhm.1\ \mu F/cm^2) = 33333\ \mu m^2$$

This value, based on the τ_m and R_m derived from Staff et al. (2000) is over 20 times larger than that obtained by the other measures. Estimates of a similar magnitude are found using τ_m and R_m values from other studies e.g. 25000 μm^2 (10 ms, 40 MOhm) (Stewart and Wong 1993), 40000 μm^2 (12 ms, 30 MOhm) (Mason 1993) and 28000 μm^2 (8 ms, 25 MOhm) (Mattia, Kawasaki, et al., 1997).

Assuming that the RC model is plausible, the primary source of this discrepancy appears to be the contribution of the intact dendritic tree to the capacitance of the somatic region in slice preparations. Whilst the capacitance of the dissociated subicular pyramidal is about 17 pF (Vreugdenhil et al., 2004), the value for the intact cell is typically 20 times larger. Representative derived capacitance values (with the relevant τ_m and R_m in brackets) are 307 pF (20 ms/65 MOhm) (Staff, Jung, et al., 2000), 250 pF (10 ms/40 MOhm) (Stewart and Wong 1993), 400 pF (12 ms/30 MOhm) (Mason 1993) and 320 pF (8 ms/25 MOhm) (Mattia, Kawasaki, et al., 1997).

In the aforementioned slice studies, the measured time constants are mono-exponential which indicates that the cell is isopotential (Rall 1989) and that the high apparent surface area is, therefore, not a space clamp artefact. This conclusion is supported by the observation that subicular neurons are quite electrically compact due to a low electrotonic length and dendrite-to-soma conductance ratio (relative to CA1 neurons) (Taube 1993). Consequently, in

determinations of the cell capacitance of the cell model the large 'electrotonic' surface area of the intact cell was used rather than that of the acutely dissociated cell. Doing so more accurately reflects the passive responses to direct current injection of the perisomatic region of cells in slice preparations.

4.4.4 Time constant

The 60 MOhm resistance is associated with a membrane time constant close to the 20 ms reported by Staff et al. (2000). This value is unusual in that it is roughly two-fold higher than most reported literature values for subicular pyramidal neurons. There appear to be two primary reasons for this. Firstly, the Staff study used patch clamp electrodes instead of the more common 'sharp' electrode. Sharp electrodes introduce a non-selective shunt conductance when they pierce the cell membrane. This shunt contributes to artificially low time constant estimates. Secondly, Staff and colleagues measured the time constant under extracellular Cs^{2+}, which eliminates the contribution of the inward rectifier current, I_H, to the properties of the membrane potential. The loss of the I_H conductance raises the effective R_m and, consequently, the magnitude of the time constant. In simulations, the insertion of I_H and other complement of active conductances into the membrane bring the magnitude of the time constant into the range conventionally reported using sharp electrodes (data not shown). The time constants associated with the 41 and 21 MOhm input resistances are 12.5 and 6.5 ms, respectively.

4.4.5 Temperature

We adjusted the temperature-dependent rate constants of our model to reflect the conventional sub-physiological experimental slice recording temperature of approximately 33°C. This was done in order to facilitate replication of, and comparison with, the largest number of empirical studies.

4.4.6 Reversal potentials

Standard reversal potentials for sodium, potassium and the mixed cation currents of +65, -90, and -43 mV, respectively, were chosen.

4.5 Rectification

When the resistance of a conductor is not independent of the voltage across it, the conductor is said to show rectification. Current passes easier in one direction and the conductor exhibits a

non-linear resistance response. Subicular pyramidals exhibit rectification in both the hyperpolarizing and depolarizing directions.

4.5.1 Rectification in the hyperpolarizing direction

The voltage response of subicular pyramidals to long hyperpolarizing current pulses peaks within 20-40 ms and then 'sags' to a more depolarized potential (Taube, 1993; Behr et al., 1996; Stanford et al., 1998; Staff et al., 2000). This 'delayed inward rectification' is abolished by Cs^{2+}, but not by Ca^{2+} channel blockers or TTX, and is therefore most likely due to the mixed cation anomalous rectifier current, I_H (Mattia et al., 1997a; Staff et al., 2000).

The subthreshold responses of neurons are conveniently summarised using an I-V plot. The I-V responses of our model cell to hyperpolarizing current injections (Figure IV-1) replicate those seen experimentally. The convergence of the steady state (V_{ss}) and peak (V_{peak}) voltages and at very hyperpolarized potentials is caused by the saturation of I_H (see also Figure IV-2).

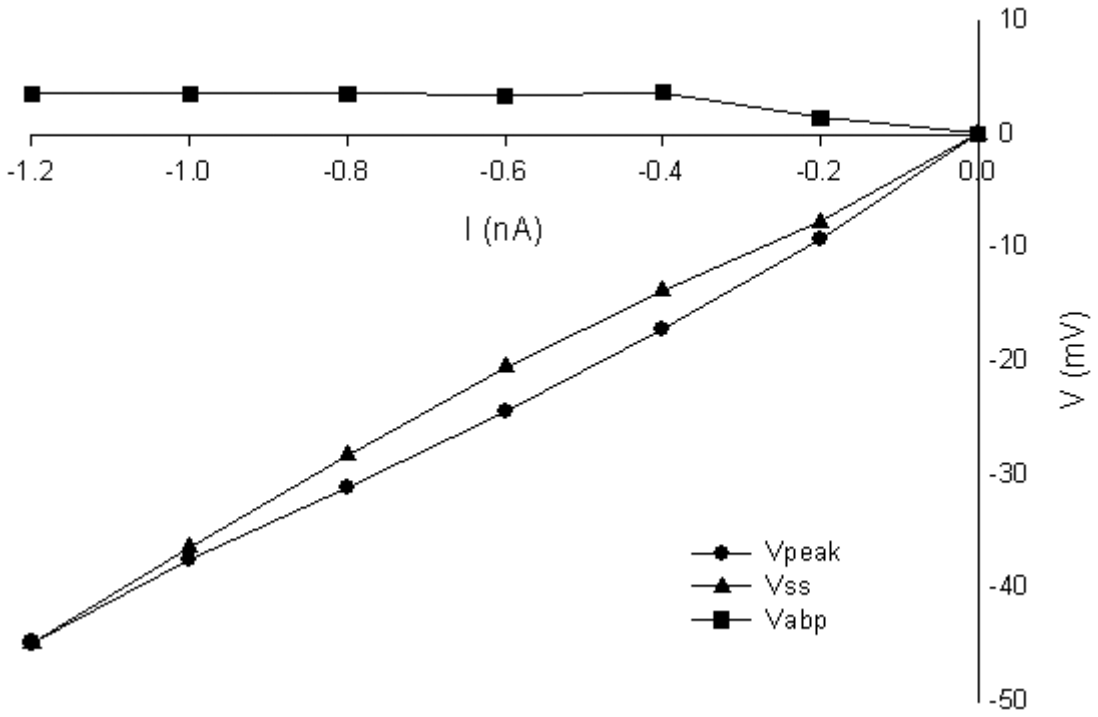

Figure IV-1. Hyperpolarized I-V responses for a subicular cell model. Four aspects of the hyperpolarization response are plotted: the peak voltage response, V_{peak} (circle), the steady state voltage response, V_{ss} (triangle), and the anodal break potential, ABP (square), following a 350 ms pulses.

Of note is the behaviour of the rebound depolarizing response (anodal break potential, ABP), seen at the end of a hyperpolarizing current, which is graded for lower currents but plateaus at higher currents. Behr et al. (1996) observed a similar response. In contrast, Stewart and Wong (1993) reported a linear ABP response in guinea pig subicular pyramidal cells. Whether the ABP plateaus or increase monotonically is dependent on the magnitude of the persistent sodium current, I_{NaP}. If sufficiently strong, I_{NaP} can amplify the I_H rebound to threshold. The model used to construct the I-V curve is incapable of rebound firing due to its relatively low I_{NaP} level of 7 nS. A model capable of rebound firing can be seen in Figure IV-26.

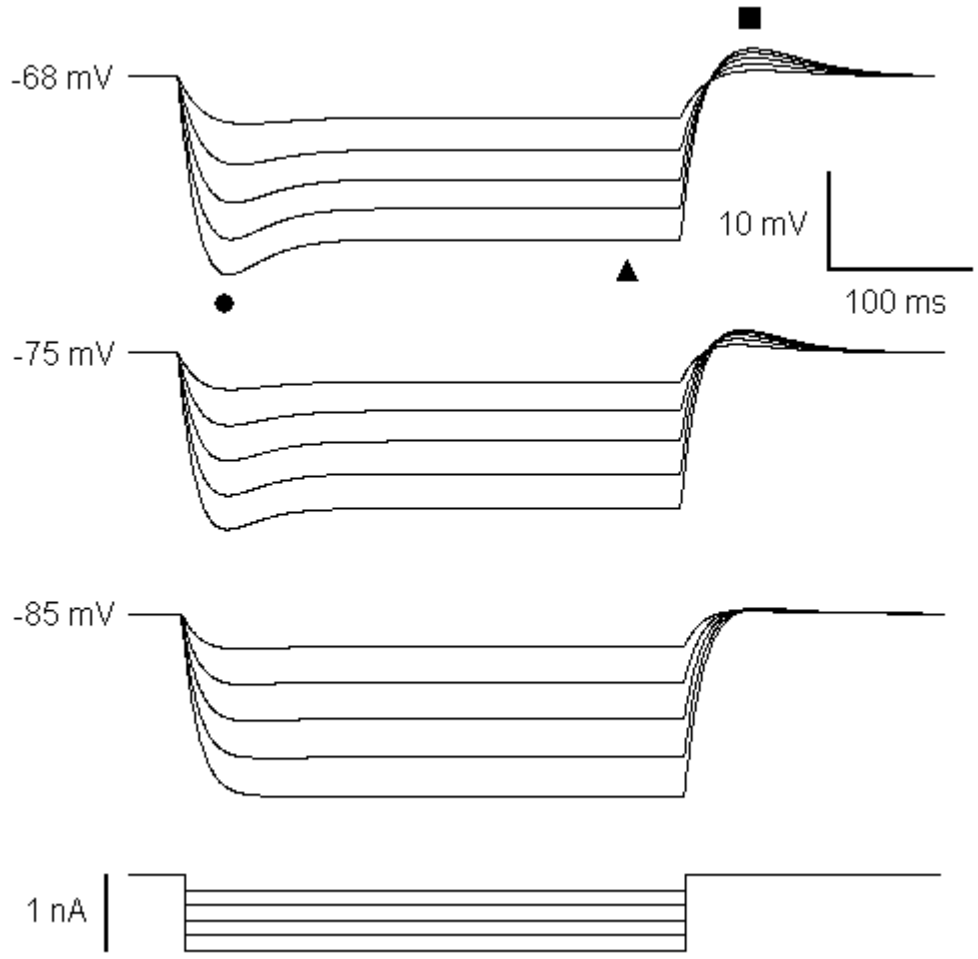

Figure IV-2. The magnitude of the sag response depends on the resting membrane potential. The sag response is suppressed by successively more hyperpolarized holding potentials. The pulse duration was 350 ms and the current amplitudes ranged from -0.2 to -1 in -0.2 nA steps. Symbol key as in Fig IV-1.

Behr et al. (1996) reported that the magnitude of the sag response is dependent on the resting membrane potential and disappears at hyperpolarized resting potentials. The model replicates

this voltage-dependent behaviour, which is caused by the saturation of I_H activation (Figure IV-2). This effect is also seen in the convergence of the model steady state and peak responses at very hyperpolarized voltages in Figure IV-1.

Although there are some reports suggesting that bursters and regular firers have similar hyperpolarizing responses (Behr et al., 1996; Staff et al., 2000), the general impression is that the depolarizing sag is more robust in bursters than in regular firers (Taube et al., 1993; Green and Totterdell, 1993; Stanford et al., 1998). Indeed, in some regular firers delayed inward rectification is almost absent (Stewart and Wong, 1996; Menendez de la Prida et al., 2003).

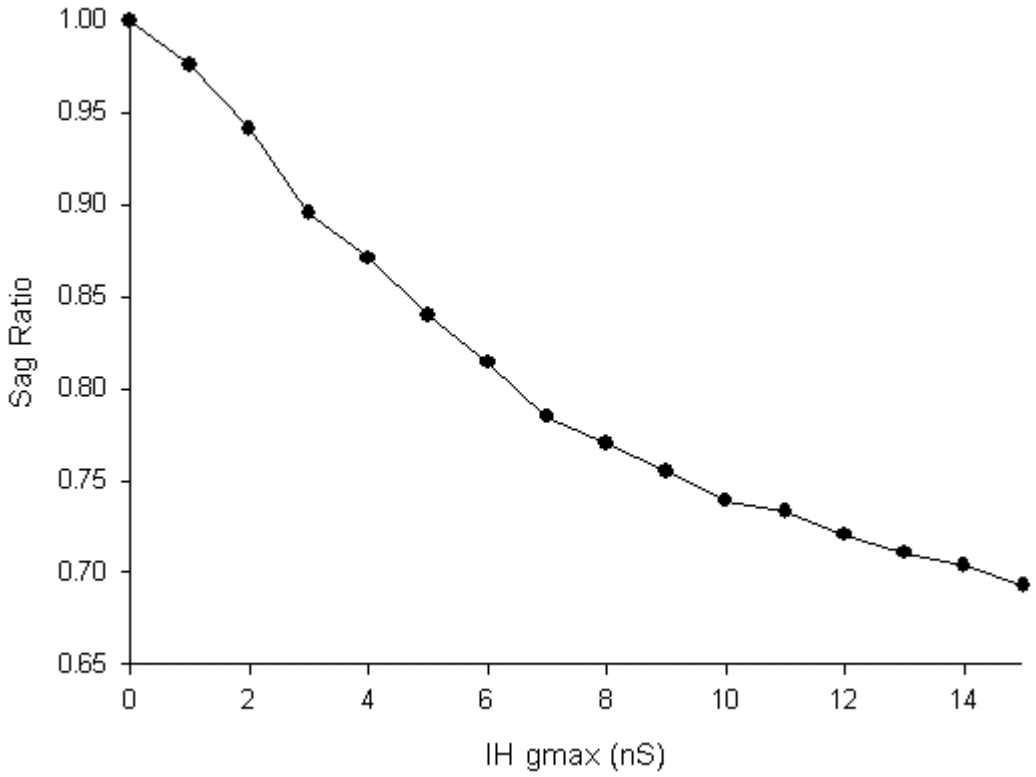

Figure IV-3. The sag ratio is a function of the maximum conductance of I_H. Responses were elicited using a hyperpolarizing current of –0.2 nA.

Significantly, the reported pattern of differences in the inward rectification response between regular and burst firers follows the trend for differences in input resistance for the two cell types. Papers that report no differences in the inward rectification properties of regular and burst firers also report no systematic differences in the input resistance (Taube, 1993; Behr et al., 1996; Staff et al., 2000) and *vice versa* (Stewart and Wong, 1993; Greene and Totterdell, 1993). On this basis, we conclude that, at least in the rat, the reported differences in depolarizing sag (commonly quantified as a 'sag ratio' - the ratio of the steady state to the peak voltage deflection)

between subicular pyramidal classes are due to variations in the level of expression of a common I_H isoform rather than the differential expression of I_H variants with different kinetics. In contrast, the anomalously non-linear I-V response of guinea pig subicular regular firers (Stewart and Wong, 1993) suggests the possible existence of different I_H isoforms.

Typical sag ratios for bursters vary from 0.77 (Green and Mason, 1996) to 0.8 (Staff et al., 2000) and for regular firers from 0.79 (Staff et al., 2000) to 0.93 (Green and Mason, 1996). Here we show how variations in the conductance levels of I_H can account for the reported variation in inward rectification properties of subicular bursters and regular firers. A plot of the sag ratio as a function of the maximum conductance of I_H shows a smooth transition from typical regular to burst firer sag ratios with increasing I_H maximum conductance (Figure IV-3).

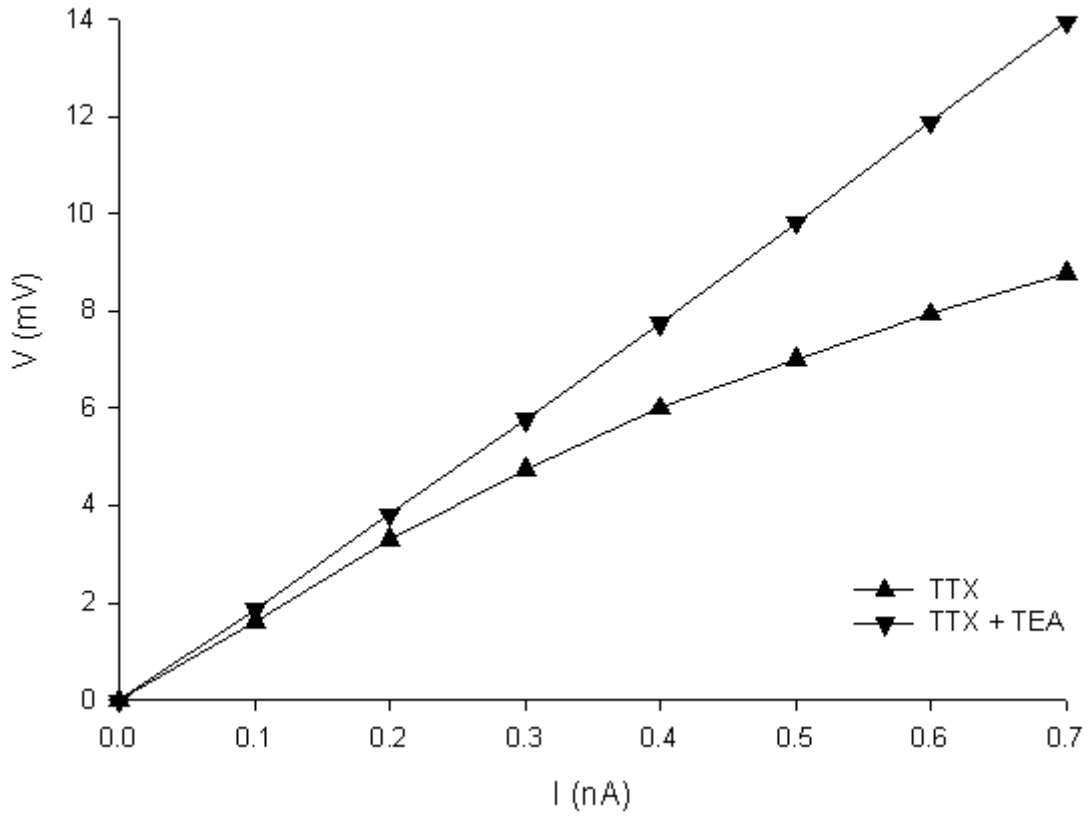

Figure IV-4. Subthreshold effects of TTX and TTX+TEA on the outward rectification in the depolarizing direction. Steady state voltage responses were taken after 100-150 ms. A high maximum conductance for I_M of 110 nS was used to amplify this effect.

4.5.2 Outward rectification

There is some conflict in the literature regarding the subthreshold I-V behaviour of subicular neurons in the depolarizing direction. Mattia et al. (1997a) and Stewart and Wong (1993) noted an amplifying trend in bursters, as did Staff et al. (2000) in regular firers and bursters. In contrast, Behr et al. (1997) reported an asymptotic trend.

Mattia et al. (1997a) reported that subicular bursters exhibit larger steady state subthreshold voltage responses to depolarizing than to hyperpolarizing stimuli. As the depolarizing current amplitude is increased the ratio of depolarizing to hyperpolarizing responses (V_d/V_h) is amplified. Such "inward rectification in the depolarizing direction" appears to be driven by I_{NaP} since it is abolished by TTX. Removal of I_{NaP} unmasks an outward rectification in the depolarizing direction that is driven by TEA-sensitive potassium currents. Under both TTX and TEA the outward rectification disappeared and V_d/V_h attained unity for all current levels (Mattia et al., 1997a).

Three classical voltage-gated potassium currents I_A, I_D and I_M are activated in the subthreshold domain (Storm, 1989), but only I_M is sensitive to TEA. The thresholds for I_A and I_D are also considerably more depolarized that that of I_M. For this reason, we model the outward rectification in the depolarizing direction using a combination of I_M and I_{NaP}. In Figure IV-4 we show the effects of TTX (sparing I_M) and the combination of TTX and TEA on the subthreshold responses of the cell. As is seen empirically, elimination of I_{NaP} results in a progressive diminution of the relative I-V response due to the action of I_M.

4.6 Resonance and subthreshold oscillations

The discovery that different behavioural and perceptual states of the brain are associated with different brain rhythms has sparked growing interest in the oscillatory behaviours of neurons (Buzsaki, 2002). A particularly important determinant of the ease with which a neuron can participate in population oscillations is resonance. Resonance is an easily measurable property that describes the ability of neurons to respond selectively to inputs at certain preferred frequencies. Recent research has uncovered a close association between population oscillations in the brain and resonance in individual neurons. Significantly, isolated CA1 pyramidal neurons exhibit resonance in the theta band (Leung and Yu 1998; Pike, Goddard, et al., 2000). Theta band frequencies (4-12 Hz) are a prominent feature of hippocampal population oscillations. In rats, theta oscillations dominate during exploration and movement behaviours and during REM

sleep (Bland 1986). The theta rhythm, therefore, appears to represent the brain's 'up-state' and is consequently associated with aspects of learning and memory (Buzsaki 2002). In particular, synaptic plasticity is linked to theta rhythm. Thus, LTP (LTD) is more easily induced at the peak (trough) of the theta oscillation (Pavlides, Greenstein, et al., 1988; Huerta and Lisman 1995). Furthermore, hippocampal place cell discharge is dependent on the presence of theta (Vinogradova 1995). Hippocampal theta rhythms can arise as a result of network properties, intrinsic neural properties, or both (Traub et al., 1989). In this section, we explore the intrinsic properties that underpin the frequency preferences of subicular pyramidals.

4.6.1 Resonance

A variety of ionic mechanisms support intrinsic resonance and oscillations (McCormick and Pape, 1990; Leung and Yim, 1991; White et al., 1998; Hu et al., 2002). Understanding the basic principles involved in the production of resonance is important because frequency preference captures the essential properties of neurons that serve as a substrate for coordinating network activity around a particular frequency in the brain.

There are three key manifestations of intrinsic frequency preference in neurons: resonance, amplified resonance and subthreshold oscillations (STOs). Hutcheon and Yarom (2000) provide a powerful conceptual framework for analysing the general intrinsic mechanisms that underpin these expressions of neuronal frequency preference. Briefly, a resonator is a 'notch' filter that responds strongly to inputs at its resonant frequency but weakly to frequencies above and below this frequency. In neurons, resonance arises from the overlapping band-pass ranges of the low band-pass passive membrane and a high band-pass slowly activating 'resonant' current that 'rectifies' or opposes changes in membrane voltage.

4.6.2 Passive membrane resonant response

The passive cell membrane responds strongly to low frequency inputs but poorly to high frequency inputs. As noted previously, we model the cell membrane as a simple RC circuit. The membrane time constant, τ_m, such a circuit is given by the product of the membrane resistance and capacitance (RC). Shifting from the time domain to the frequency domain, τ_m, expressed as a frequency, f_m, is given by $1/2\pi\tau_m$. Oscillating inputs below this frequency easily drive the membrane voltage to produce a strong voltage response. However, as the frequency rises beyond

f_m the ability of the membrane to follow the input falls and the voltage response is progressively diminished. Thus, the membrane acts as a low band-pass filter.

4.6.3 Resonant current

Two characteristics are required for a current to qualify as a resonant current: the ability to actively oppose changes in the membrane voltage and an activation time constant, τ_r that is significantly larger than the membrane time constant (Hutcheon and Yarom 2000). The second criteria can be explained more easily in frequency-domain terms. The slowly activating resonant current is only effective at frequencies below $1/2\pi\tau_r$. Beyond this frequency the current is too slow to respond to the input signal and the response is dominated by the frequency-domain characteristics of the cell membrane. The band-pass 'notch' frequencies are found between $1/2\pi\tau_r$ and $1/2\pi\tau_m$ whereby the rectifier current suppresses the membrane response at very low frequencies (below $1/2\pi\tau_r$) but passes higher frequencies. The converse holds for the cell membrane. Creation of an effective notch band-pass consequently requires a good separation of f_m and f_r, which in turn necessitates that τ_r is considerably slower than τ_m.

4.6.4 Unamplified resonance

Subicular pyramidals have significantly lower membrane resistance than CA1 pyramidals (Staff et al., 2000; although see Mason, 1993). A potentially important functional consequence of this is that the unamplified membrane responses of subicular neurons to sub-theta and theta band frequencies are considerably smaller than those of CA1 neurons.

4.6.5 Impedance analysis

The difference in the responses of subicular and CA1 neurons to theta frequency inputs can be quantified by comparing the theoretical impedance values of the subicular and CA1 passive membrane models. Impedance, Z, is the frequency domain equivalent of resistance in electrical circuits. At zero frequency the impedance of a circuit is equal to its resistance. The theoretical impedance magnitude, Z, of a RC passive membrane to an oscillating current input of frequency f is given by

$$Z = \frac{R_i}{\sqrt{(\tau_m^2(2\pi f)^2 + 1}}$$

where R_i is the input resistance and τ_m is the membrane time constant (Gutfreund, Yarom, et al., 1995).

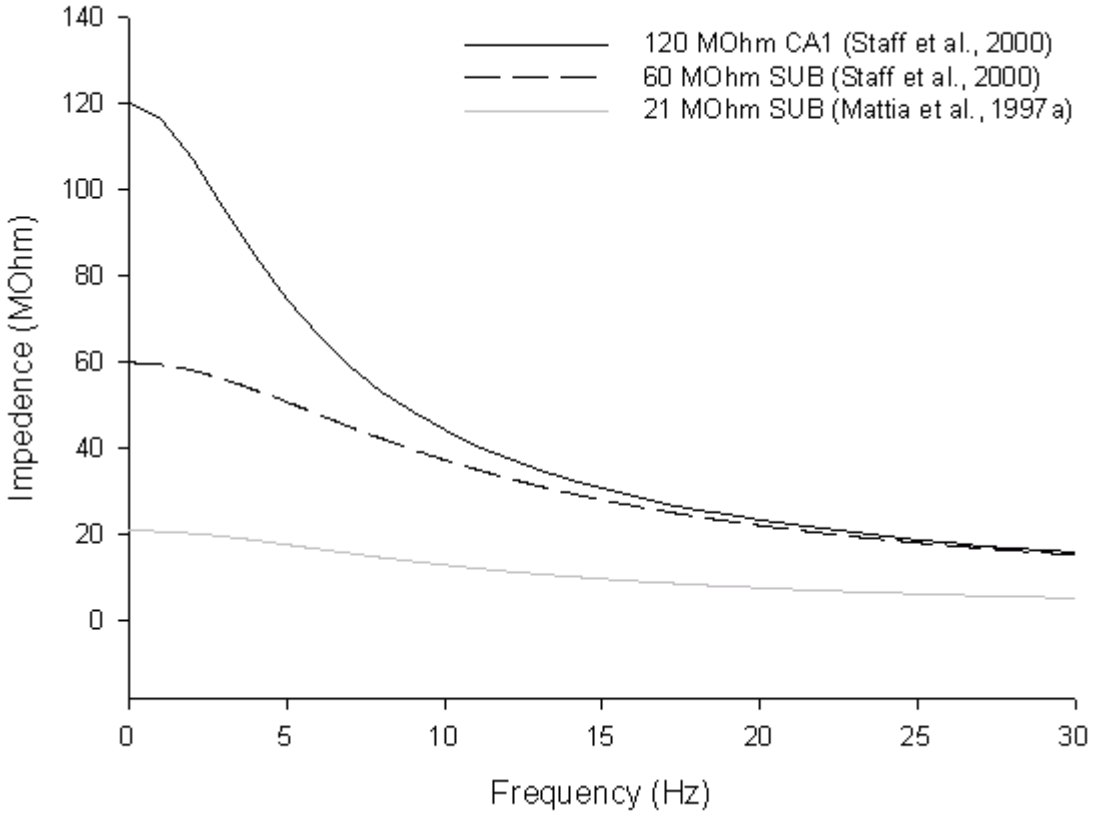

Figure IV-5. The effect of input resistance on the relationship between impedance magnitude and frequency for passive cell membranes with subicular (60 and 21 MOhm) and CA1 (120 MOhm) input resistances. The 60 MOhm subicular resistance is the average resistance of cells exposed to extracellular caesium and, along with the CA1 value, is taken from Staff et al. (2000). The 21 MOhm resistance is derived from Mattia et al. (1997a).

As can be seen in Figure IV-5, the higher membrane resistance of CA1 pyramidals results in higher impedance (and thus a stronger voltage response) in the theta band range (4-12 Hz) than subicular pyramidals. The effect of the lower membrane resistance is to attenuate the theta band resonant response of subicular neurons when an appropriate resonant current is inserted into the cell membrane. In the absence of amplification, subicular pyramidals are thus, on average, poorer theta pass-band filters than CA1 neurons, and are consequently less likely to be effectively entrained by theta band inputs. Since the maximum amplitude of the resonant response is determined by the passive membrane properties, this conclusion holds regardless of the efficiency of the resonant current. This insight is potentially significant, since Anderson and

O'Mara (2003) reported that subicular pyramidals are considerably less likely to be entrained by theta than other hippocampal areas. Only 32% of subicular cells are phase-locked to theta (Anderson and O'Mara 2003), compared to 65% in CA1 (Csicsvari, Hirase, et al., 1999).

The input signal most commonly used to probe the frequency response characteristics of a system is the ZAP (Impedance Amplitude Profile) signal. The ZAP signal is a constant amplitude swept sine wave stimulus with a frequency that increases linearly over time (See the bottom trace in Figure III-7B for an example). The voltage response of a passive membrane to a ZAP input is a trace that oscillates around an average voltage. The amplitude of these oscillations declines monotonically with time as the frequency increases and the ability of the membrane to respond to the input decreases (Figure III-7A). Resonance emerges as a peak or 'bulge' in the membrane voltage amplitude (Figure III-7B). This response peak is conventionally illustrated using an impedance-frequency plot. Empirical impedance is calculated as the ratio of Fourier transform of the membrane potential response to that of the input ZAP current (Hutcheon et al., 1995). A single number characterisation of the level of resonance is given by the Q value. The Q value is a function of the impedance magnitude of the cell at different frequencies and is calculated as the ratio of the impedance magnitude at the resonant frequency, Z_{res}, divided by that at 0.5 Hz, $Z_{0.5}$ (Hutcheon et al., 1995). A Q value of 1 indicates zero resonance. The specific case of theta resonance arises when a slowly activating rectifying current, such as I_M or I_H, suppresses the strong sub-theta frequency responses of the passive membrane.

4.6.6 Amplified resonance and subthreshold oscillations

The putative critical role of the theta rhythm in the temporal coding and decoding activities of neuronal assemblies (Buzsaki, 2002) along with the central role of the subiculum in gating hippocampal output is potentially at odds with the relatively weak theta-band impedance response of subicular pyramidal membranes. This functional incongruity is, at least partially, resolved by the presence of an amplifier current (Hutcheon and Yarom, 2000) in subicular pyramidals (Mattia et al., 1997b).

In direct contrast to a resonant current, an amplifier current acts as a weakly regenerative mechanism that actively potentiates membrane voltage fluctuations (Hutcheon and Yarom, 2000). To fulfil this function the amplifier current activation time constant must be fast relative to the membrane time constant. Currents that meet this criteria include the persistent sodium current, I_{NaP} (Hutcheon, Muira, et al., 1996), the dihydropyridine-sensitive, sustained, high-

threshold calcium current, I_{CaL} (Hutcheon and Yarom, 2000), and the transient, low-threshold calcium current, I_{CaT} (Puil et al., 1994). Whereas the membrane characteristics and the resonant current combine to act as a band-pass filter, the amplifier current serves as a band-pass amplifier and has marginal effect on the resonant frequency.

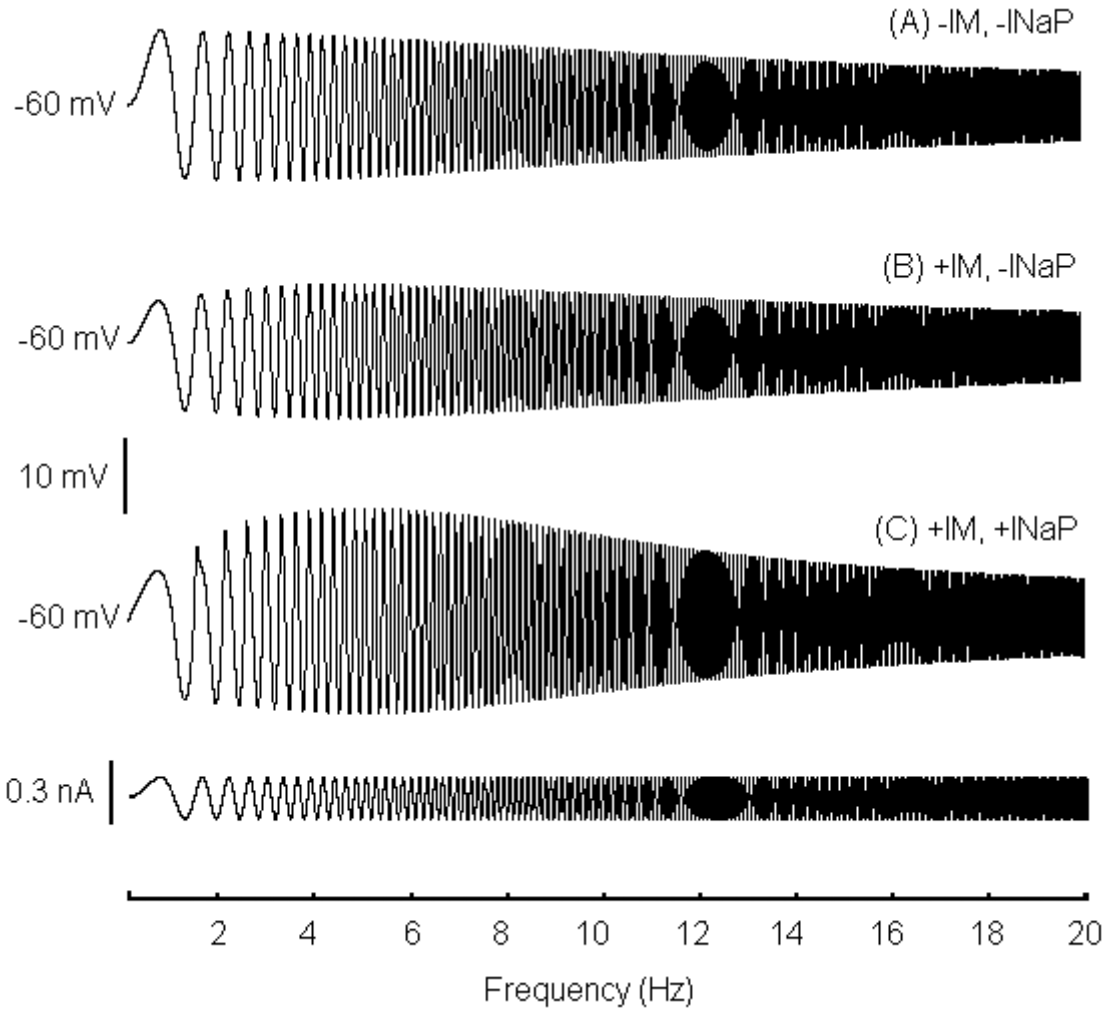

Figure IV-6. The effects of I_M and I_{NaP} on the response of subicular cell model at -60 mV to a ZAP stimulus. A: In the absence of I_M and I_{NaP} there is little resonant response. B: Addition of I_M (0.007 nS) causes a resonant peak near 5 Hz to appear. C: Further addition of I_{NaP} (0.007 nS) amplifies this resonance. In this simulation, the ZAP current was 0.2 nA. Constant holding currents of 0.17, 0.2, and 0.15 nA were also injected to maintain a -60 mV average voltage in conditions A, B, and C, respectively.

4.6.7 Subicular M- and H-resonance

The theta resonance of CA1 neurons exhibits a U-shaped dependence on voltage with strong responses at subthreshold depolarized (-60 mV) and hyperpolarized (-80 mV) potentials but

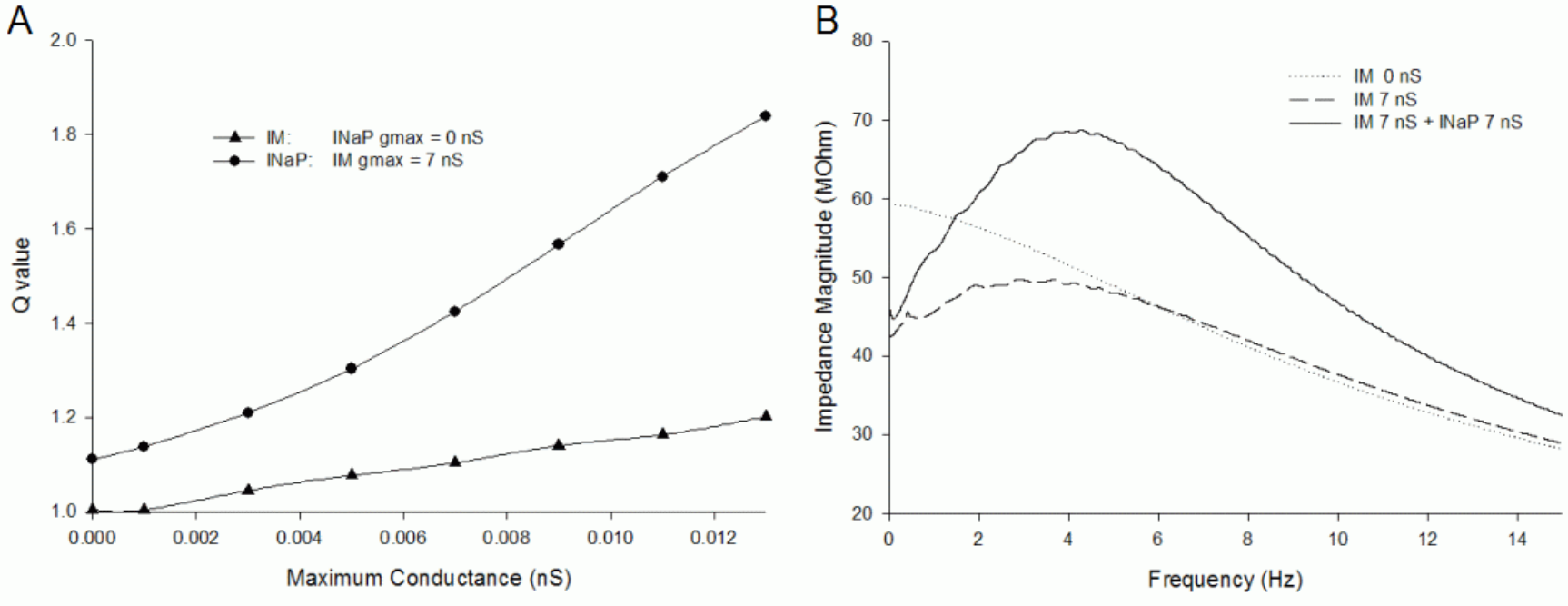

Figure IV-7 Quantitative characterisation of the effects of I_M and I_{NaP} on subicular response at -60 mV to a ZAP stimulus. A: The resonant response, as measured by the Q value, is a monotonic function of the maximum conductance of I_M and I_{NaP}. I_M (triangles) has a relatively small resonant effect in the absence of I_{NaP}. Addition of I_{NaP} (circles) to a cell containing I_M dramatically amplifies the response. B: Plot of the impedance profile for different combinations of I_M and I_{NaP}. The resonant frequency is the frequency associated with the maximum impedance value. Note the slight positive shift in the resonant frequency caused by the addition of I_{NaP}.

weaker responses near the resting potential (-72 mV) (Hu et al., 2002). The U-shaped response is due to the presence of two resonant currents, I_M and I_H, with distinct activation ranges. Depolarized resonance is mediated by I_M and is therefore termed 'M-resonance' whilst I_H is responsible for hyperpolarized H-resonance. In CA1 pyramidals, M-resonance is amplified by I_{NaP} and can manifest as subthreshold oscillations (Hu et al., 2002).

4.6.8 Simulation of M-resonance

The existence of several electrophysiological features associated with I_M, such as the medium AHP, and early spike frequency adaptation, along with subthreshold oscillations suggest that subicular neurons should also exhibit M-resonance. A role for I_{NaP} as an amplifier current in subicular neurons is suggested by the appearance of TTX-sensitive STOs at membrane voltages positive to about -70 mV (Mattia, Kawasaki, et al., 1997; Cooper, Moore, et al., 2003).

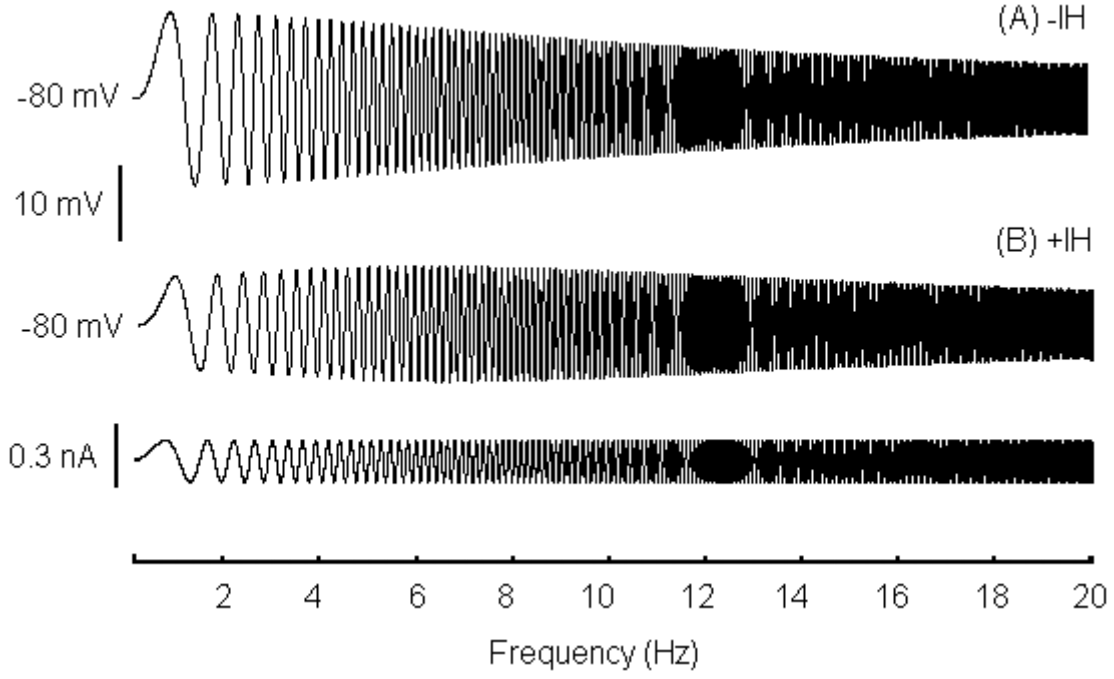

Figure IV-8. The effects of I_H on the response of subicular cell model at -80 mV to a ZAP stimulus. A: With the conductance for I_H set to zero there is little resonant behaviour. B: Addition of I_H (7 nS) suppresses the response to low frequencies and creates a resonant peak near 6 Hz. The ZAP current was 0.2 nA. Constant holding currents of -0.18, and -0.32 nA were also injected to maintain a -80 mV average voltage in each condition, respectively.

In Figure IV-6 and 7 the effects of I_M and I_{NaP} on the resonant response of a cell model depolarized to -60 mV are shown. The cell moves from displaying no resonance without I_M, to

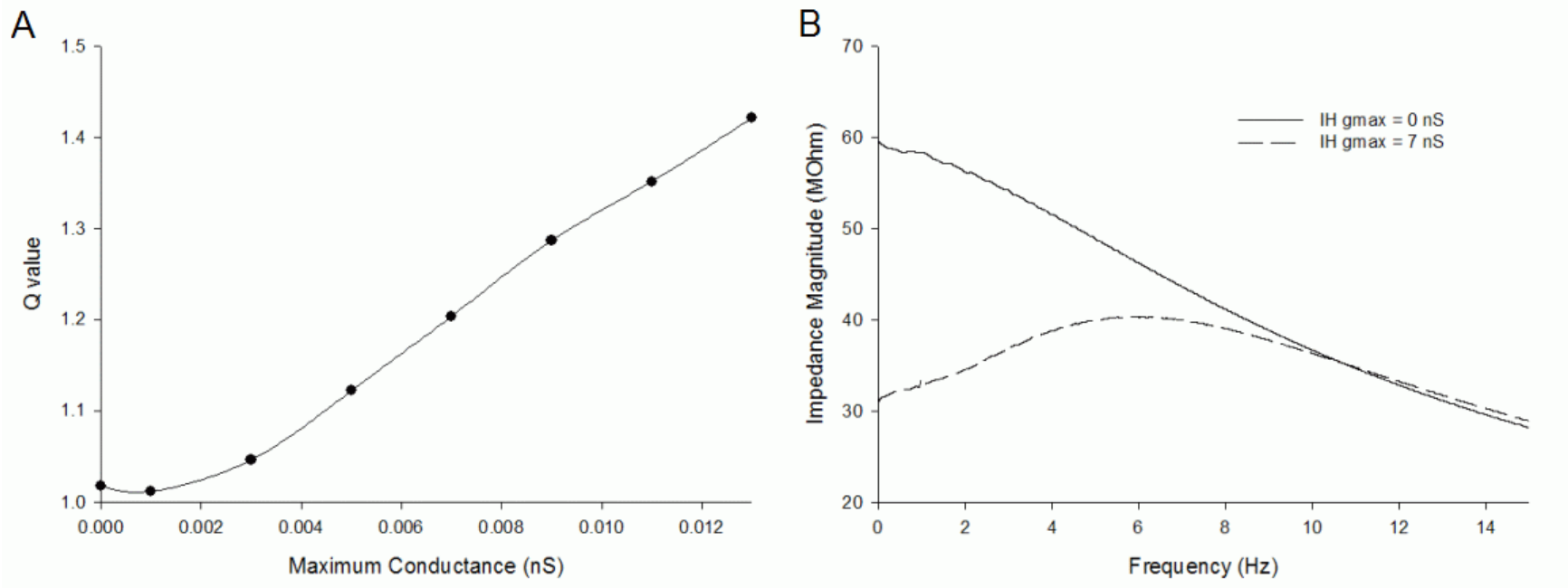

Figure IV-9 Quantitative characterisation of the effects of I_H on subicular response at -80 mV to a ZAP stimulus. A: The resonant response, as measured by the Q value, is a monotonic function of the maximum conductance of I_H. At this voltage I_H exerts a powerful effect on the resonant properties of the cell membrane. B: Plot of the impedance profile for different combinations of I_H. The resonant frequency is the frequency associated with the maximum impedance value. At a maximum conductance level of 7 nS I_H causes a resonant peak at 6 Hz.

modest resonance centred on 5 Hz with I_M, to amplified resonance with I_{NaP}. Addition of I_{NaP} causes a small positive shift in the resonant frequency. In all of these simulations, the fast sodium current is set to zero to prevent spikes. Note also that the ZAP current used in these simulations increases by 1 Hz every second. Thus, for clarity, the abscissa units are in Hz and not seconds.

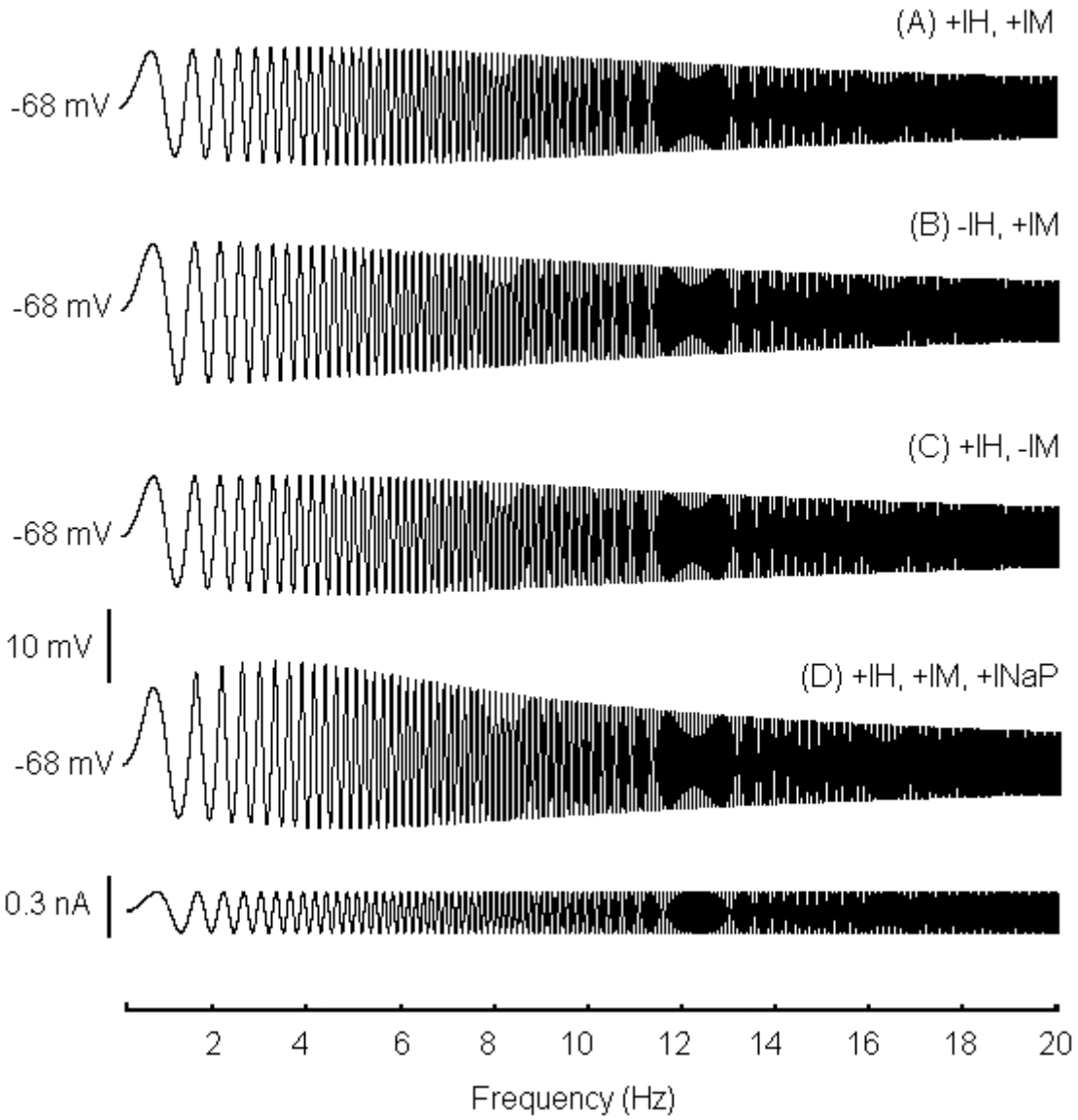

Figure IV-10. Subicular pyramidals exhibit H-resonance at resting potentials. A: Resonance centred at about 4.5 Hz is evident at resting potentials in the subicular cell model. B: Elimination of I_H abolishes this theta resonance. C: I_M contributes little to resonance at rest. D: Addition of I_{NaP} amplifies the resting resonance. The ZAP current was 0.15 nA. A constant holding current of +0.03 nA was also injected to maintain a resting potential of -68 mV when I_H was eliminated.

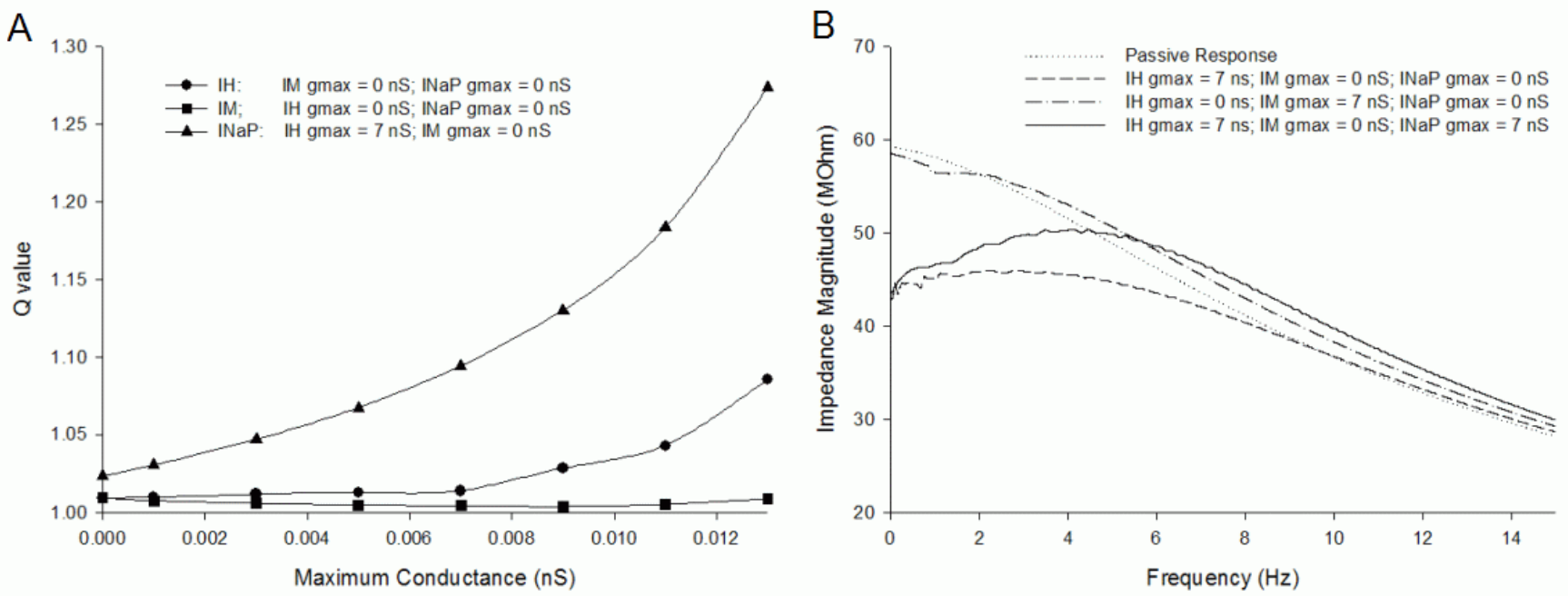

Figure IV-11 Quantitative characterisation of the effects of interactions between I_H, I_M and I_{NaP} on the subicular resonant response at -68 mV to a ZAP stimulus. A: The resonant response, as measured by the Q value, is a monotonic function of the maximum conductance of I_H (circles) and I_{NaP} (triangles). I_M (squares) has a negligible resonant effect at this voltage. Addition of I_{NaP} to a cell containing I_H dramatically amplifies the relatively weak resonant response. B: Plot of the impedance profile for different combinations of I_H, I_M and I_{NaP}. The resonant frequency is the frequency associated with the maximum impedance value. The response of a membrane containing I_M alone (dash-dots) is similar to the passive membrane response (dots). Note the slight positive shift in the resonant frequency caused by the addition of I_{NaP}.

4.6.9 Simulation of H-resonance

The presence of a current with I_H-like properties implicitly confers upon subicular neurons a form of H-resonance. Here we simulate the effect of I_H on the response of the subicular model to the ZAP stimulus centred at -80 mV. As can be seen in Figure IV-8 and 9 addition of I_H creates a resonant peak at approximately 6 Hz in the -80 mV range. As I_{NaP} only activates beyond about -70 mV, addition of the current to the model had no effect on the degree of H-resonance (data not shown).

Hu et al. (2002) found that CA1 pyramidals display little resonance at voltages near rest. However, the significant contribution of I_H to the resting input resistance of subicular pyramidals (Staff et al., 2000), and the hyperpolarized activation threshold of subicular I_{NaP} (Cooper et al., 2003) suggests that subicular cells should exhibit H-resonance at resting potentials. This prediction is supported by the subicular cell model, which exhibits pronounced resonance at resting membrane potentials. Elimination of I_H, but not I_M, eliminates resting resonance (Figure IV-10 and 11). As expected, I_{NaP} also amplifies the resting resonance.

The unamplified H-resonance peak of 5 Hz at -68 mV is smaller than the 6 Hz seen at -80 mV. The small drop in the activation time constants can explain this effect for I_H across these voltages. The respective frequencies associated with the activation time constants of I_H at -68 and -80 mV are 3.5 and 3.9 Hz. The frequency corresponding to the membrane time constant is about 8 Hz. Since the resonant frequency is located between the membrane and current frequencies, an increase in the current frequency also forces an increase in the resonant frequency.

The addition of I_{NaP} caused an unexpected distortion of the ZAP envelope on the depolarized side that shifted the peak towards 3.5 Hz (Figure IV-10D and 11B). The hyperpolarized peak remained near 5 Hz. This effect was found to be caused by the combination of a slight reduction in I_{NaP} due to slow inactivation at lower frequencies (<10 Hz) and lower I_{NaP} activation at higher frequencies due to the smaller depolarizations involved (data not shown).

4.6.10 Subicular subthreshold oscillations

Intrinsic subthreshold membrane oscillations (STOs) appear to be a widespread phenomena and has been reported in the cells of many areas including CA1 (Chapman and Lacaille 1999), CA3 (MacVicar and Dudek 1981; Psarropoulou and Avoli 1995), entorhinal cortex (Alonso and Llinas 1989; Klink and Alonso 1993), and subiculum (Mattia et al., 1997b; Cooper et al., 2003;

Menendez de la Prida et al., 2003). Subthreshold oscillations enable neurons to actively filter their response to oscillating input. The theta-range frequency of STOs suggests a role in theta amplification and entrainment.

Subicular bursters and regular firers generate persistent subthreshold oscillations of the membrane potential during steady-state depolarization positive to about -60 mV (Mattia et al., 1997b; Cooper et al., 2003). Application of TTX completely abolishes the STOs, implicating I_{NaP} as the primary amplifier current (Mattia et al., 1997b; Cooper et al., 2003). STO amplitude is unaffected by antagonists of calcium currents, excitatory amino acid and $GABA_A$ receptors, or the anomalous rectifier inhibitor, Cs^{2+} (Mattia et al., 1997b). Interestingly, carbachol, a cholinergic agonist and known inhibitor of I_{NaP} (MittmanN and Alzheimer 1998), also significantly reduces the amplitude, but not the frequency, of subicular STOs (D'Antuono, Kawasaki, et al., 2001).

The amplitude of STOs in subicular pyramidals is dependent on the membrane potential. Progressive increases in the Vm beyond about -60 mV evoked first occasional action potentials riding on the positive-going STO wave, then clustered spikes separated by regions of STOs, and finally tonic firing (Mattia et al., 1997b; Cooper et al., 2003).

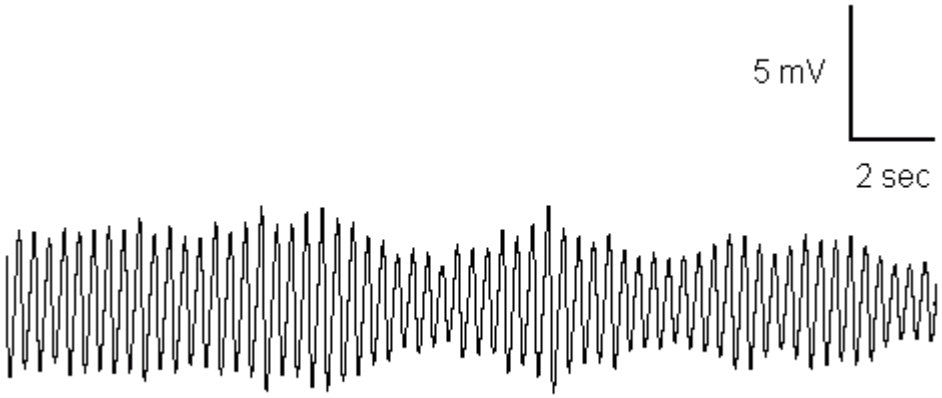

Figure IV-12. Stable theta-range oscillations in a subthreshold model of a subicular pyramidal., Oscillations were initiated with the onset of a sustained current that depolarized the membrane to approximately -60 mV and maintained a frequency of roughly 3.5 Hz. The non-standard parameter values for I_{NaP}, I_M, I_{DR}, and I_A were 8.5, 15.5, 400 and 100 nS, respectively. All other currents were set to zero. The uniform random noise term varied from 0 to 2 (potentially doubling the maximum conductance of I_{NaP}). Membrane resistance was 60 MOhm.

STOs have been shown to amplify weak near-threshold EPSPs through stochastic resonance (White, Klink, et al., 1998). A similar mechanism appears to operate in subicular pyramidals since Cooper et al. (2003) found that simulated EPSPs are amplified by STOs in a voltage-dependent and TTX-sensitive manner. Interestingly, there is no difference in amplification between regular and burst firers. The implied presence of I_{NaP} in subicular regular firers seems to bolster the argument that regular firers are bursters in suppressed form.

Table IV-2. Ionic conductances/permeabilities for the cell models

Currents	g_{max} (μS) or p_{max} (cm/s)
I_{NaF}	2.0
I_{CaT}	0
I_{CaN}	0
Persistent inward currents	
I_{NaP}	0.007
I_{CaL}	0 - 1.0
$I_{CaP/Q}$	0 - 4.0
Transient outward currents	
I_A	0.15
I_{CT}	0 - 0.12
Persistent outward currents	
I_{DR}	0.3
I_M	0.005
I_{AHP}	0 - 0.0023
I_D	0 - 0.04
Anomalous currents	
I_H	0.007

4.6.11 Simulation of subthreshold oscillations

Within the theoretical framework of Hutcheon and Yarom (2000) self-sustaining subthreshold oscillations emerge as a result of increasing the strength of an amplifier current. In entorhinal cortex, STOs arise from the stochastic flicker of voltage-gated sodium channels (White, Klink, et al., 1998). We emulated this idea by adding a normally distributed noise component to the persistent sodium current model. Using this model, no realistic STOs were observed at any

membrane potential. However, both stable and damped theta oscillations were found for certain sharply defined configurations of currents in a system that included an I_{NaP} model containing a uniformly distributed random error term (Figure IV-12). The random noise component was essential to the phenomenon since no oscillations were seen in an otherwise equivalent system that lacked the noise term. The high sensitivity of these oscillations to changes in parameters precluded a systematic investigation of their dependence on I_M and I_{NaP} kinetics.

4.7 Calcium dynamics

The calcium dynamics that determine the level of intracellular calcium involve a complex network of biophysical processes including; calcium entry through gated calcium channels, intracellular release and uptake via membrane-bound calcium pumps, diffusion of calcium through the intracellular space, and the action of cytosolic calcium binding proteins (buffers) (Yamada, Koch, et al., 1998).

4.7.1 Proportional model

In the present model, the primary function of changes in internal calcium concentration is to activate the calcium-dependent potassium channels; the fast transient calcium-dependent potassium current, I_{CT}, and slow calcium-dependent potassium current, I_{AHP}. To that end, we use a simple exponentially decaying Ca^{2+} pool model that phenomenologically describes the influx and efflux of calcium using aggregated flow processes (Traub and Llinas 1979; Traub, Wong, et al., 1991; McCormick and Huguenard 1992; De Schutter and Bower 1994).

For a single compartment, the change in intracellular calcium is given by:

$$\frac{d[Ca^{2+}]_i}{dt} = -\frac{I_{Ca}}{2Fv} - \beta([Ca^{2+}]_i - [Ca^{2+}]_{min})$$

where the first term describes the net inflow of calcium from calcium channels into a compartment of volume, v. F is the Faraday constant (96487 coulombs/mole) and z is the valence of calcium (i.e. 2). The second term accounts for the exponential relaxation of intracellular calcium levels to the baseline concentration, $[Ca^{2+}]_{min}$. This value is generally taken to be 50 nM (Borg-Graham 1998). The time constant of this decay is given by $1/\beta$.

β, the 'inverse time constant' (Traub, Wong, et al., 1991), 'diffusion rate constant' (McCormick and Huguenard 1992) or 'calcium buffering constant' (LeMasson, Marder, et al., 1993), represents the loss of intracellular calcium due to several mechanisms. Large values of β increase

this rate of loss and force $[Ca^{2+}]_i$ to closely mirror changes in I_{Ca}, thereby resulting in smaller and faster cytoplasmic calcium transients. Representative literature values for this constant range from 0.002 ms^{-1} (Traub and Llinas 1979) to 10 ms^{-1} (De Schutter and Bower 1994).

4.7.2 Ca^{2+}-dependent currents and calcium pools

A complicating factor in the determination of an appropriate value for β is introduced by the respective fast and slow kinetics of the Ca^{2+}-dependent K^+ currents, I_{CT} and I_{AHP}. The rapid deactivation required for I_{CT} to repolarize the spike and produce the fAHP (Storm 1987) implies a fast decaying $[Ca^{2+}]_i$, and hence, a large β value. In contrast, I_{AHP}, responsible for the slow AHP, must activate cumulatively during repetitive firing in response to a calcium pool that rises with successive action potentials and decays gradually (Lancaster and Adams 1986).

Following Borg-Graham (1989) and Warman et al. (1994), we resolved these conflicting demands by implementing two different calcium pools; a fast sub-membrane pool 'seen' by I_{CT} and a slowly decaying 'bulk' intracellular pool effecting I_{AHP}. Our fast sub-membrane pool has a β value of 0.5 ms^{-1} and a depth of 1 μm whilst the slow cytoplasmic pool has a β value of 0.004 ms^{-1} and a depth of 5 μm. The maximum calcium concentration attained by the fast submembrane pool is, due to its highly localised nature, assumed to be about an order of magnitude higher than that attained by the bulk intracellular pool. This difference is accordingly reflected in the relative calcium concentration sensitivities of the associated calcium-dependent potassium channels: I_{CT}, coupled to the fast pool, has an activation range of 200-800 nM whilst the activation range of I_{AHP}, linked to the slow pool, is 50-120 nM.

This '2-pool' approach may be justified on the basis of an observed selective coupling of calcium-dependent potassium channels with specific calcium channels. For example, activation of the fast transient potassium current, I_{CT} is specifically linked to calcium flux through N- and L-type calcium channels in mouse neocortical neurons (Sun, Gu, et al., 2003). Whilst in rat CA3 pyramidals mobilisation of intracellular calcium-activated calcium stores via L-type channels are implicated in the activation of I_{AHP} (Tanabe, Gahwiler, et al., 1998).

For reasons of simplicity, we have made no attempt to replicate the linkages of specific calcium channel types with particular calcium pools. In the model, both calcium pools are subserved by the same aggregate calcium current but with different dynamics determined by the associated β value. Notwithstanding, to maintain a semblance of charge conservation, the calcium current is split between the fast and slow pools in the ratio 1:10, respectively.

4.8 The action potential

4.8.1 Function of the action potential

The action potential (AP) is often regarded as the fundamental unit of information in the brain. Ironically, although the spike is usually considered as a discrete digital signal, its shape is an important determinant of its neuronal signalling properties. For example, the charge transfer through R-type calcium channels is very sensitive to action potential shape (Sochivko et al., 2003) hence, the level of intracellular calcium is likewise dependent on spike morphology. Whilst the rising phase of the spike is relatively invariant, the shape, amplitude, and duration of the repolarization phase are subject to modulation by voltage- and calcium-gated potassium channels (Magee 1998).

4.8.2 Spike properties

The literature is divided as to whether subicular regular firing and burst firing pyramidal cells possess similar action potential characteristics. Staff et al. (2000) report that the spike threshold, duration, amplitude, half-width, and maximum rate of rise characteristics of the first spike in a burst and the first spike from a regular firing cell are similar. Other studies that report no difference in some or all of these properties include Taube (1993), Mason (1993), Behr et al. (1996), Stewart (1997), and Stanford et al. (1998). These studies also tend to report no, or few, significant differences in passive membrane properties between the two firing types. An exception to this trend is Wellmer et al. (2002). This group reported no differences in the spike thresholds of control (-50 mV) and experimental cells subjected to status epilepticus (-49.9 mV) but did find significant differences in the spike amplitudes, the passive input resistance, and membrane time constants of the two cell groups. Regular firers constituted 51 and 18% respectively of these groups.

4.8.3 Spike threshold

The value of the spike threshold is dependent on the particular definition and measurement technique used. Most literature estimates of the spike threshold appear to be determined 'by eye' although more quantitative approaches have been applied and include; the voltage at which the second derivative is at a maximum (Mainen, Joerges, et al., 1995) and the voltage at which the slope of the voltage trace exceeds a predetermined value (Andersen, Storm, et al., 1986). In the subiculum literature, Mason (1993) and Menendez de la Prida (2003) measured spike threshold

as the voltage difference between rest and the foot of the fast upstroke of the spike, whilst Behr et al. (1996), Staff et al. (2000), and Wellmer et al. (2004) gave the absolute voltage of the foot of the spike.

Of those studies that report spike thresholds for regular and burst firing cells most found no difference (Behr et al., 1996; Stanford et al., 1998; Staff et al., 2000; Wellmer et al., 2002). The Wellmer et al. (2002) study reported thresholds of cells from control and SE-experienced rats rather than specific cell types.

The picture of relatively homogenous spike properties across subicular cell types is complicated by a smaller number of studies that have found significant differences in the spike thresholds of regular and both weak and strong bursting cells (Menendez de la 2003; Menendez de la and Gal 2004).

An obvious reason for this discrepancy is difficult to determine. Conspicuous potential sources of variation, such as the number of animals or the standard error (or deviation), provide no substantial clues. One potentially significant factor that may reconcile these discrepant results is the age of the animals used in the experiments. The Menendez de la Prida (2003) study utilised young rats that were between 17 and 20 days old. The Staff et al. (2003) study included older rats (ranging from 14-63 days old), as did the Taube (1993) study (60 to 90 days old), which also reported no differences in basic parameters between the cell types.

The age of the animals is potentially significant, since both the complement of ion channels carried by the neurons and the morphology of the neurons neurites are known to change over the course of development. For example, the membrane density of active sodium channels increases significantly from the embryonic stage to maturity. In rat neocortical neurons, there is a 6- to 10-fold increase in Na^+ current density during the first 14 days postnatal alone (Huguenard, Hamill, et al., 1988). The time course of the sodium current also changes such that the sodium current decay in immature neurons is mono-exponential, whilst mature neurons exhibit a second, slowly decaying, component with a time course 5 to 10 times slower than the fast element (Huguenard et al., 1988).

In a comparable manner, the dendritic length and spine density of rat pyramidal neurons only reach adult levels after about the twentieth postnatal day (Minkwitz 1976; Pokorny and Yamamoto 1981). This is significant because theoretical studies suggest that neural morphology can influence the electrotonic 'compactness' and firing mode of a neuron (Mainen and Sejnowski

1996; Duijnhouwer, Remme, et al., 2001). Unfortunately, this 'age hypothesis' is somewhat confounded by the Menendez de la Prida and Gal (2004) study which used a mix of juvenile (17-20 days old) and adult (about 60 days old) rats.

Mendendez de la Prida (2003) reported significant differences in the spike thresholds for regular firers (20.1 mV), weak bursters (16.9 mV) and strong bursters (13.7 mV), with a trend for progressively larger depolarization requirements from strong bursters to regular firers. That the firing probability of subicular pyramidals is correlated more strongly with the firing threshold than with other intrinsic properties, such as resting membrane potential or input resistance (Mendendez de la Prida, 2003), indicates the potential functional importance of this measure. Significantly, Menendez de la Prida and Gal (2004) found that firing threshold was one of several predictors of the propensity of a cell to lead population activity.

While all action potential properties, such as threshold, amplitude and duration are ultimately determined by the relative strength and kinetics of inward and outward currents, the spike threshold is most directly related to the activation kinetics of the fast sodium current, I_{NaF}.

The spike threshold for the first spike in the model is determined by the voltage-dependence of the transition from the C3 closed state to the open state in the Markov I_{NaF} model. The threshold for this transition is about -55 mV, which corresponds to the roughly -55 mV firing threshold for the subicular model. The maximum repolarization rate, obtained by taking the first derivative of the voltage spike rise, is about 180 mV/ms. This value is approximately 1.6 times lower than that reported by Staff et al. (2000). The peak spike repolarization rate of about -40 mV/ms is over two times slower than the corresponding literature value, although it is within the range reported for hippocampal pyramidals (Borg-Graham, 1998).

The slow rate of rise of the action potentials of this model is primarily due to the Markov model of I_{NaF}. Interestingly, it was relatively easy to modify the kinetics of I_{NaF} to replicate empirical depolarization rates. This could be done by simultaneously increasing the conductance levels and the transition rate from the open to the inactive state. However, the large conductance values for I_{NaF}, and the concomitant increases in the repolarizing currents, swamped the effects of I_{NaP}. Due to the subthreshold activation range of I_{NaP}, attempts to increase the level of this current are constrained by the need to avoid spontaneous firing of the cell. Realistic depolarization rates were achieved with I_{NaF} levels of around 25 μS. However, since the maximum level of I_{NaP} is restricted to about 20 nS, I_{NaP} ends up being only 0.008% of the size of

I_{NaF}. In contrast, values on the order of 5% are found empirically (Vreugdenhil et al., 2004). As preliminary simulations had demonstrated that evoking spike doublet was relatively straightforward it was decided to retain the slowly depolarizing spikes and defer the task of redesigning the fast sodium current.

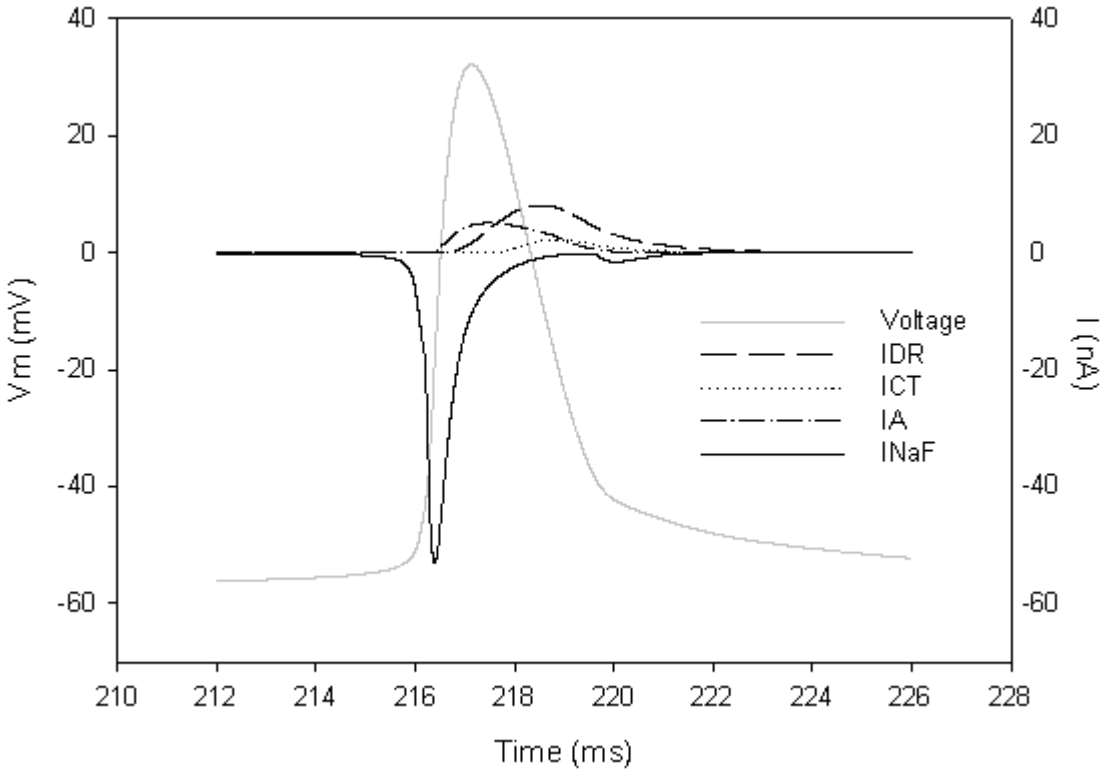

Figure IV-13. Plot of the relative contributions of I_{NaF}, I_{DR}, I_{CT}, and I_A to the action potential.

In the model, repolarization was driven primarily by I_{DR} (Figure IV-13.). As expected from the kinetics of the I_{DR} model, I_{DR} contributes to all phases of repolarization. I_A and I_{CT} contributed also but to a much smaller extent. The rapid activation of I_A enables it to participate in the early phase of spike repolarization. Furthermore, the comparatively slow activation I_{CT} ensure that it plays a role in the late phase of repolarization, as is found in the hippocampal pyramidals.

4.9 Subicular bursting

A burst is simply defined as several high frequency (~200 Hz) spikes riding upon a depolarizing envelope and terminated by a hyperpolarization tens of milliseconds in duration.

4.9.1 An adaptive two-component model of subicular bursting

There appears to be a division within the subicular literature as to whether the minimum number of spikes required for a burst is two (Stewart and Wong, 1993; Mason, 1993; Staff et al., 2000; Menendez de la Prida, 2003; Cooper et al., 2005) or three (Greene and Totterdell, 1997; Wellmer et al., 2002).

This seemingly trivial difference in spike number masks an important, although largely overlooked, mechanistic distinction, identified by Stewart and Wong (1993), between the early and late components of a subicular burst. As we will see, this two-component model of subicular bursting has implications for the depolarization-sensitivity of bursting, the subdivision of bursters according to burst propensity, the debate over the ionic mechanisms underpinning the burst, and the population frequency-following abilities of subicular bursters.

4.9.2 Strong and weak bursters

Staff et al. (2000) observed novel repetitive theta frequency burst firing in response to direct somatic stimulation in a subset of subicular bursters. On this basis, these workers introduced a new subdivision of subicular bursters into strong bursters, which respond to long suprathreshold stimuli with multiple bursts, and weak bursters, which produce a single burst, followed by a spike train. Strong bursters are rarely, if ever, seen when using sharp electrodes but are readily observed with patch clamp electrode configurations. It should be emphasised that the repetitive bursts reported for strong bursters are, almost invariably, spike doublets (Staff et al., 2000; Jung et al., 2001; Menendez de la Prida, 2005; Cooper et al., 2005), and thus most likely constitute the early component of the burst as opposed to fully fledged burst events. This inference assumes, of course, that rat calcium current kinetics are similar to those of guinea pig.

4.9.3 High and low threshold bursters

A related subdivision of bursters into low- and high-threshold bursters has been made using sharp electrodes (Wellmer, Su, et al., 2002). Low-threshold bursters (LTBs) respond to just-threshold stimulation with a burst, whilst high-threshold bursters (HTBs) require strongly depolarizing stimuli to burst. As with other sharp electrode studies, neither cell type bursts repetitively. The strong/weak and the high-threshold/low-threshold dichotomies appear to be mechanistically equivalent since, in both classification systems, burst propensity is found to be proportional to the area of the largely Ca^{2+}-dependent afterdepolarization (ADP) (Jung et al.,

2001; Wellmer et al., 2002). This evident mechanistic similarity highlights the discrepancy between the electrophysiological behaviours seen in sharp and patch clamp electrode studies.

4.9.4 Burst mechanism theories

Of central importance to understanding bursting is the mechanism that drives the burst's depolarizing envelope. This potential, which follows the fast AHP of a single spike, is known as the afterdepolarizing potential (ADP). The ADP can exhibit a "passive" decay to rest or an "active" depolarization (Borg-Graham, 1998). In the case of bursting cells, the active ADP constitutes the depolarizing envelope that carries burst spikes. The size of the ADP is usually defined as the integral of the voltage waveform between the fast AHP and rest (Jensen et al., 1996; Wellmer et al., 2002). Generally speaking, the larger the single spike ADP, the stronger the burst. In both CA1 (Jensen, Azouz, et al., 1996) and subiculum (Jung et al., 2001; Wellmer et al., 2002; Menendez de la Prida et al., 2003), larger ADPs are associated with more robust bursting.

Several competing theories have been proposed as possible mechanisms for the ionic basis of subicular bursting. We introduce each of these below:

4.9.4.1 Dendritic reflux currents

The subicular burst is almost certainly localised to the perisomatic region and does not appear to require a substantive contribution from the dendrites (Jung et al., 2001; Menendez de la Prida et al., 2003). However, although, whilst not seriously suggested to dominate subicular bursting, the possibility of a contributory role in ADP formation for a putative dendritic reflux current has been considered (Jung et al., 2001). In defence of this idea, a number of modelling studies have concluded that the burst ADP of hippocampal pyramidals is amplified by passive the capacitive recharging of the soma by the dendrites (Traub 1982; Borg-Graham 1998; Warman EN 1994). At the end of the action potential the dendrites are at a higher potential compared to the soma, passive equalisation of this gradient results in a depolarizing current into the soma. However, given that the dendrites possess a broad repertoire of active conductances it seems unlikely that unregulated passive reflux accounts for either the somatic single spike or burst ADPs *in vivo*. This notion is indirectly supported by the presence of I_H in subicular regular and burster firers (Staff, Jung, et al., 2000). In CA1 pyramidals, dendritic I_H suppresses subthreshold excitability (Magee, Hoffman, et al., 1998) and acts to electrotonically disconnect somatic and distal spike initiation zones (Berger, Senn, et al., 2003). Dendritic potassium conductances are also likely to

contribute to the suppression of reflux transients (Hoffman, Magee, et al., 1997; Aradi and Holmes 1999). On this basis, we concluded that the ADP is primarily due to the activation of excitatory channels, such as in CA1 and dentate gyrus pyramidals, where the burst and single spike ADPs are driven by sodium (Azouz, Jensen, et al., 1996; Su, Alroy, et al., 2001) and/or calcium conductances (Wong and Prince 1981; Zhang, Valiante, et al., 1993).

4.9.4.2 Sodium electrogenesis

Mattia et al. (1997a) argued for a sodium burst electrogenesis on the basis of three key observations:

1. The depolarizing burst envelope is abolished by TTX
2. Calcium channel blockers fails to prevent the burst
3. The calcium substitute, barium, increases burst duration and amplitude.

Although Mattia et al., observed a TTX-resistant hump, these events (which had activation thresholds some 30 mV positive to rest) were only seen in the presence of TEA. The humps were blocked by Ca^{2+}-channel inhibitors and were therefore classified as high-threshold calcium events. The finding of Cooper et al. (2005) that a low level (~10%) of sodium inactivation is sufficient to convert strong bursters into regular firing mode provides a further indication of the importance of the contribution of sodium currents to the burst ADP. The reduction in sodium drive causes a drop in the initial slope of the ADP and an attendant failure of the burst. Menendez de la Prida et al. (2003) also reported that a small reduction in INa causes bursting to fail in both weak and strong bursters.

It seems probable (see below for more details) that the magnitude of the persistent sodium current determines the sodium contribution to the ADP, especially given its low activation threshold. Under some circumstances, this contribution can be substantial. In TLE patients, for example, the persistent sodium current can constitute over 50% of the total sodium current in subicular pyramidals (Vreugdenhil et al., 2004).

4.9.4.3 Calcium electrogenesis

Taube (1993) observed TTX-resistant potentials in 90% of bursting and 50% of regular firing subicular pyramidals. These potentials were evoked at a similar rheobase for both cell types

(which were significantly lower than that for CA1 cells). On this basis, Taube (1993) suggested that subicular bursting is driven by calcium conductances.

Jung et al. (2001) conducted a more detailed analysis of subicular burst electrogenesis using a patch clamp electrode set-up. Voltage clamp analysis of the response of subicular bursters to a 1 ms -70 to 0 mV step revealed two distinct inward current components. The first component is TTX-sensitive. The second, which emerged at the offset of the voltage step, is eliminated by 1 mM Ni^{2+}, and also by a zero Ca^{2+} medium, but not by TTX. The size of this 'calcium tail current', I_{CaTail}, determines the magnitude of the burst ADP and is correlated with burst propensity. Tail currents (and burst ADPs) of subicular pyramidals are largest in strong bursters, smaller in weak bursters, and smaller still in regular firers. Jung et al. (2001) also showed that bursting, in response to a short (10 ms) just-threshold stimulus, is blocked either by zero calcium or by a low concentration of TTX (15 nM). However, only the zero calcium condition abolishes the ADP of both bursts and single spikes. A similar situation prevails in CA1 pyramidals (Metz, Jarsky, et al., 2005). Jung et al. (2001) therefore concluded that a calcium-dependent ADP driven by a high voltage activated (HVA) currents causes subicular bursting. Since initiation of this calcium tail current requires the depolarization caused by an action potential, the subicular burst is, therefore, only indirectly reliant on sodium conductances.

This conclusion is also compatible with the aforementioned finding by Mattia et al. (1997a) that TTX abolished or markedly reduced all burst components including afterdepolarizations and the slow spike. No calcium ADP was seen because, without a Na^{+}-driven action potential, the threshold for the calcium tail current was not reached (the maximum imposed depolarization reported by Mattia et al. (1997a) was less than 10 mV).

Since the size of the tail current is distributed in a rather graded manner, Jung et al. (2001) further suggested that the burst propensity of subicular pyramidals might more properly be considered to lie along a continuum.

Unfortunately, the compelling calcium tail current hypothesis is not without its shortcomings. Anomalously, Jung et al. (2001) also found that bursting was potentiated by the non-selective calcium channel suppressors Cd^{2+} and zero-Ca^{2+} medium, and was resistant to low concentrations of nickel sufficient to inhibit the T-type calcium current. The bursting that persists under divalent metal cations was explained as an abnormal form arising from the indirect inhibition of the spike repolarization function of the fast Ca^{2+}-dependent potassium current, I_{CT},

and a putative shift in the voltage-dependence of I_{NaF} under zero calcium (Frankenhaeuser and Hodgkin 1957).

Spike broadening and progressively elevated firing threshold for secondary spikes are certainly accordant with the loss of I_{CT}. However, the zero-Ca^{2+} bursts are similar in appearance to the 1 mM Cd^{2+} bursts presented in Jung et al. (2001), the charybdotoxin (an I_{CT} inhibitor) bursts presented in Staff et al. (2000), and the Co^{2+} and Cd^{2+} burst presented in Mattia et al. (1997a). Furthermore, the fast sodium spike under voltage clamp appears the same in control and zero-Ca^{2+} (Jung et al., 2001). These similarities indirectly suggest that zero calcium does not significantly alter subicular I_{NaF} kinetics.

Further, the calcium tail hypothesis is both constrained and complemented by the Wellmer et al. (2002) findings that, whilst the calcium-dependent low threshold bursters exhibit ADPs that are substantially larger than either high threshold bursters or regular firers, there is no statistical difference between the ADP size (and presumably the calcium tail current) of sodium-dependent HTBs and regular firers. Furthermore, LTBs are converted into HTBs by inhibition of calcium channels (Wellmer et al., 2002). ADP size thus appears to be a measure of the strength of calcium-dependent, but not necessarily, sodium-dependent bursting. In this regard it is also significant that, whilst a 10% drop in the sodium current cleanly eliminates bursting (Cooper et al., 2005), bursting is not suppressed by a selective reduction of the calcium tail current of 31% by omega-conotoxin MVIIC (Jung et al., 2001).

It should also be noted that the TTX-sensitive subthreshold oscillations (Mattia et al., 1997b), subthreshold plateau potentials (Mason, 1993; Menendez de la Prida et al., 2003), and anodal break potentials (see below) that occur at the termination of a hyperpolarizing current pulse (Stewart and Wong, 1993; Behr et al., 1996; Mattia et al., 1997a) suggest the existence of a functionally significant low threshold sodium current that is at odds with the high threshold ADP postulated by the calcium-tail theory of subicular bursting (Jung et al., 2001).

4.9.4.4 Na^{+}/Ca^{2+}-electrogenesis and the adaptive two-component model of bursting

Evidently, whilst the size of the ADP is primarily determined by calcium conductances there is a variable, but vital, contribution from sodium currents. Several authors argue that composite sodium and calcium currents drive the subicular burst (Stewart and Wong, 1993; Wellmer et al., 2002; Menendez de la Prida et al., 2003). In this section we review some of the evidence for this notion. However, we also amplify this idea by suggesting that the subicular burst is composed of

two distinct and dissociable sodium- and calcium-dependent components that have different characteristics and functions within the subiculum. We feel that the idea of an adaptive two-component subicular burst model provides a powerful explanatory framework that reconciles much of the discrepant data on subicular single cell electrophysiology in the literature. In the discussion we will expand on the idea that these components have different frequency preferences and are up- and downregulated differentially in order to modulate the computational properties of subicular bursting cells.

The key study underpinning the two-component subicular burst hypothesis is that of Stewart and Wong (1993). These authors employed a variable interval double pulse experiment that dissected the guinea pig subicular burst response into early and late burst components (EBC and LBC, respectively). They found that progressive reduction of the interval between paired suprathreshold depolarizing pulses cause the LBC to fail with a refractory period of about 300-350 ms, leaving a residual early burst component. This EBC is typically a spike doublet (but can also present as a single spike) with a refractory period below 50 ms (the smallest interval reported).

Stewart and Wong (1993) also investigated the pharmacology of the early and late burst components. The EBC was found to be TTX-sensitive and thus sodium dependent. Under TTX, the late component could be evoked by using stronger depolarizing (>15 mV) stimuli and was inhibited by cadmium (1 mM). Conversely, application of calcium channel inhibitors eliminated the late and spared the early burst component.

Complementary results were found by Wellmer et al. (2005) who found that zero calcium, or Ni^{2+} (1 mM), reversibly convert low threshold bursters (LTB) into high threshold bursters (HTB). Conversely, the response of high threshold bursters is largely unaffected by calcium channel inhibitors (Wellmer et al., 2002).

Menendez de la Prida et al. (2003) also probed the ionic mechanisms underlying weak and strong brusting and found that a reduction of external calcium from 2 to 1 mM does not appreciably effect weak bursters, but does reduce the duration of bursts in strong bursters. This is suggestive of a selective suppression of the late burst component. Significantly, low concentrations of TTX block both bursting and the ADP evoked by subthreshold depolarizing current pulses in both weak and strong bursters.

The matched time courses, in weak and strong bursters, of ADP elimination by TTX hints that the contribution of the persistent sodium current to the burst ADP is similar in both cell types (Menendez de la Prida, Suarez, et al., 2003). This notion receives indirect support from the apparent conservation of total sodium current (transient plus persistent) in subicular cells derived from TLE patients despite a wide range of levels of I_{NaP} (Vreugdenhil et al., 2004). There is no significant difference in the rate of spike depolarization between weak and strong bursters (Staff et al., 2000). Since the spike repolarization rate is determined by the size of the fast transient sodium current, similar rates of spike repolarization suggest similar I_{NaF} contributions, which imply similar I_{NaP} levels by the conservation assumption. If the early sodium component is similar in weak and strong bursters then the idea that the strong bursting is simply weak bursting with an enhanced late component is strengthened.

Collectively, these results provide compelling support for the idea that subicular bursting involves dissociable early sodium and late calcium components. The two-component model can also reconcile the contradictions faced by theories that postulate burst mechanisms based primarily on sodium or calcium alone. In the following sections we develop models of these components and explore how these models can explain firing mode switching, depolarization-sensitivity of bursting. We also examine the evidence that these components are differentially regulated.

For clarification it should probably be noted that, despite the use of the terms 'sodium-dependent' and 'calcium-dependent', 'early' and 'late' refer primarily to the duration or strength of the burst. Bursts with a stronger calcium contribution tend to be longer than those without and thus exhibit a late component. The fast kinetics of the calcium channels ensures that there is an appreciable calcium current contribution to bursts of all sizes. Doublet firing is commonly seen in untreated subicular pyramidals both *in vivo* and *in vitro*.

4.9.5 Model of the early burst component

In this section, we develop a computational model of the sodium-dependent, early burst component. The sodium-dependent early component constitutes the minimal burst, since a small reduction in I_{Na} causes bursting to fail in both weak and strong bursters (Menendez de la Prida, Suarez, et al., 2003; Cooper, Chung, et al., 2005). Stewart and Wong (1993) reported that the isolated early burst component was insensitive to calcium channel inhibitors. Furthermore, Jung et al. (2001) observed that selective inhibition of calcium currents did not cause bursting to fail.

Consequently, to facilitate model development we took as our starting point an idealised version of zero calcium bursting.

In the absence of extracellular calcium, or in the presence of calcium channel blockers, subicular bursters exhibit an abnormal form of Na^+-dependent bursting (Jung et al., 2001). The spikes seen during this form of bursting are broader and shorter than conventional burst spikes. Zero Ca^{2+} bursting is electrophysiologically simple in that there is nominally no contribution from calcium currents or Ca^{2+}-dependent potassium currents.

Within the two-component burst framework, zero calcium bursting is explained as an early burst component artificially amplified by the absence of repolarization driven by the calcium-dependent potassium current, I_{CT}. This current plays a significant role in spike repolarization and its loss leads to a pronounced spike broadening (Jung et al., 2001). There is also likely to be a smaller contribution (ignored in this idealised model) from the effects of zero calcium and divalent cation calcium channel inhibitors on non-calcium ion channels (Gorman and Hermann 1979; Armstrong and Cota 1999).

The zero calcium model of the early burst component builds upon the previous passive model by adding the fast sodium current, I_{NaF}, the persistent Na^+ current, I_{NaP}, the delayed rectifier K^+ current, I_{DR}, and the fast transient potassium current, I_A. Using these channels we were able to construct a model that responded to just-threshold stimuli with a spike doublet or triplet (Table IV-2, see also Figure IV-14). The stability of the sodium-dependent doublet depended critically on the level of I_{NaP}. The implications of this sensitivity for subicular electrophysiology are explored in the sections on firing mode switching and the depolarization-sensitivity of bursters.

4.9.6 HH OR Markov

As mentioned previously, a critical factor in determining whether we could model a spike doublet was the nature of the sodium channel model. Although standard action potentials were easily modelled, realistic doublet firing was not. Despite numerous simulations and adjustments, the HH I_{NaF} model proved unsuitable. Interestingly, once the 5 State Markov model of I_{NaF} was designed and implemented, doublet firing and bursting were readily attained.

4.9.7 Calcium component

In this section, we develop a model of the calcium-dependent late component.

4.9.7.1 Kinetics of the late component

Jung et al. (2001) examined the kinetics of the late component in some detail. Although, Jung et al. (2001) reported that the compound HVA calcium current had an activation threshold close to -40 mV the supplied Boltzmann activation parameters (V_{half} of -13 mV, k of 12 mV) suggest a threshold closer to -50 mV. A -50 mV threshold is also more consonant with the calcium 'hump' thresholds of about -47 and -53 mV implied by Taube (1993) and Stewart and Wong (1993), respectively.

Whilst the early burst component is demonstrably subject to slow inactivation, the evidence for frequency-dependent inactivation of the late component is equivocal. Notably, the kinetic profile of the guinea pig late subicular burst component differs from that found in the rat. Guinea pig late component appears to be dominated by an inactivating composite calcium current that exhibits slow recovery from inactivation (100s of ms). In contrast, the calcium current does not appear to undergo cumulative slow inactivation in response to 10 Hz stimulation in the rat (Cooper et al., 2005).

Part of the reason for the lack of inactivation seen in the Cooper study may be due to the short stimulus used i.e. brief (~10 ms) repetitive simulated excitatory postsynaptic currents (EPSCs). Jung et al. (2001) observed that the calcium tail current is significantly inactivated (~60%) in response to 50-100 ms depolarizations (Stewart and Wong used paired 50 ms depolarizations). This suggests that even a brief burst-inducing stimulus should elicit a measurable degree of inactivation. For this reason, the lack of slow inactivation seen by Cooper et al., implies that the recovery from inactivation of the rat calcium tail current is rapid (<100 ms). Significantly, this sub-100 ms recovery period inferred in the rat is considerably shorter than the ~250 ms refractory period for the late component reported in guinea pig by Stewart and Wong (1993). In direct contrast to the guinea pig, the rat calcium component appears capable of maintaining higher firing frequencies than the sodium component.

4.9.7.2 Model development strategy

The conceptual scheme used to construct the late calcium-dependent component was to successively add appropriate calcium currents to the early component model. I_{CT} was then adjusted to preserve the burst and prevent hyper-excitability.

Our primary reference for the composition of the late burst component is the study by Jung et al. (2001) on the pharmacology of the calcium tail current. However, the problem of the

determining the relative contribution of particular calcium currents to the composition of the calcium tail current is highly unconstrained. The blockers employed in the Jung study; I_{CaP}, I_{Q}, I_{CaN}, I_{CaL}, I_{CaR} and I_{CaT} potentially inhibit at least six calcium currents. In order to determine the most prominent currents and constrain the problem, we assess the probable contribution of each current to the tail.

Omega-conotoxin MVIIC, which suppresses the tail current by 31%, is a N-/P/Q-type blocker. However, as noted above, the contribution of I_{CaN} to subicular calcium tail current is unlikely to be large given the lack of evidence for a role for the current in hippocampal somatic events (Rascol et al., 1991). We therefore assume that approximately one third of the tail current is accounted for by the hybrid P/Q-type current. Nimodipine blocks 12% of the tail current and is an inhibitor of the T- and L-type channels (Randall and Tsien, 1995). About 20% of the tail is also suppressed by low concentrations of Ni^{2+}, an inhibitor of T-and R-type channels. Since there is scant evidence for I_{CaT} in subicular pyramidals, we conclude that approximately 12% of the tail current is accounted for by I_{CaL} and a further 20% by I_{CaR}. The model tail current is therefore composed of $I_{CaP/Q}$, I_{CaL}, and I_{CaR}. Although these currents only appear to account for just over 60% of the total tail current, for convenience, we further assume that uniform partial inhibition of these currents by the blockers explains the deficit. As a result, to a first approximation, the relative contributions to the tail current by $I_{CaP/Q}$, I_{CaL}, and I_{CaR} are 49, 19 and 32%, respectively.

It should be noted that this is an estimate of the relative contributions to the calcium current in response to a 1 ms depolarizing pulse and does not necessarily reflect the contributions of these currents to longer depolarizations. Evidence that longer depolarizations do indeed alter the composition comes from the observation that approximately 60% of the peak calcium current inactivates during 50-100 ms steps from -70 to 0 mV (Jung et al., 2001). We attribute this fraction to I_{CaR}, since I_{CaL} and $I_{CaP/Q}$ are generally non-inactivating. The mono-exponential inactivation time constant of this decay is 10 ms which is somewhat faster than the 41 ms at 0 mV used in our inactivation time constant function for I_{CaR}.

Using the aforementioned development strategy, a full subicular burst model was constructed, subject to the constraint that the sodium doublet was spared when the calcium currents were eliminated (Figure IV-14). The final calcium contributions were quite different from our initial estimates. The respective contributions for $I_{CaP/Q}$, I_{CaL}, and I_{CaR} are 11, 3 and 86% (Table IV-2). The overwhelming contribution from I_{CaR} certainly indicates that the 60% estimate was nearer

the mark than the 32% value. Nonetheless, the parameter set presented here is almost certainly not unique and more realistic sets may exist.

The effects of calcium channel inhibition were investigated by selectively reducing the effective conductance of each channel type. Since I_{CaR} is only partially suppressed by the Ni^{2+} (50-100 μM) used in the Jung et al. (2001) study (Randall and Tsien 1995), we suppressed I_{CaR} by 66%. As reported by Jung et al., large decreases in I_{CaR} did not eliminate bursting. However, complete elimination of I_{CaR} lead to damped oscillations that terminated in a plateau potential at about -35 mV. Large reductions (50-100%) in I_{CaL} did not eliminate the burst but did shorten burst duration. Similar effects were seen in response to small reductions (25%) in $I_{CaP/Q}$. Anomalously, larger reductions (50-100%) in $I_{CaP/Q}$ abolished the burst. The effects of complete elimination of calcium on the burst can be seen in Figure IV-14.

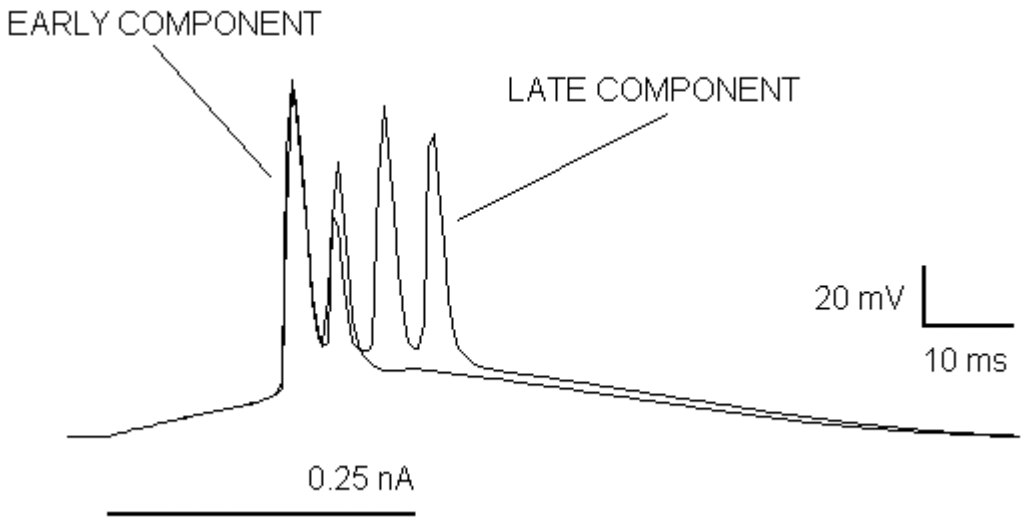

Figure IV-14. This 2-component subicular burst is reduced to a residual sodium-dependent (early component) doublet following elimination of the calcium currents. In this model, the I_{NaP} and I_{DR} conductances are 8 and 320 nS, respectively. The cell membrane resistance is 60 MOhm.

The presence of calcium currents in our models did not reliably increase the duration of the burst, as is found experimentally. Whether the doublet was augmented depended, in a non-obvious manner, on a number of factors including the membrane resistance, the stimulus strength and the level of I_{NaP}.

4.9.8 TTX-resistant events

The late burst component can be elicited as a high threshold calcium event under conditions in which sodium channels are abolished. Stewart and Wong (1993) found that the TTX-resistant event required a depolarization of about 16 mV in order to activate the high voltage activated (HVA) calcium current (compared to a 6 mV depolarization required to activate the early burst component) (Stewart and Wong, 1993). High threshold TTX-resistant calcium responses were also observed by Taube (1993) who evoked 'hump-like' calcium potentials in 90% of bursting neurons and 50% regular firers by depolarizations of up to 30 mV in magnitude. In rare cases, increasing the stimulus strength transforms the calcium hump into a calcium spike, similar to those elicited from CA1 pyramidals. However, these spikes are difficult to obtain and in the majority of cases increasing the current injection does not change the qualitative nature of the neuronal response (Taube, 1993).

As is seen experimentally (Taube, 1993), TTX-resistant potentials were observed in the model following the elimination of sodium currents (data not shown). These 'calcium humps' are only elicited using stimuli strong enough to depolarize the membrane by >20 mV.

4.9.9 Firing mode switching

Burst firing, *in vivo*, is correlated with a number of behaviors, including goal identification and approach, and the sleep-wake cycle (Ranck, 1973; Otto et al., 1991; Weyand et al., 2001). Dysregulation of this association is also associated with certain disease states. For example, Parkinsonism in rat and primates is characterised by a shift in the firing mode of subthalamic nucleus neurons from regular to burst firing (Beurrier, Congar, et al., 1999). In the subiculum, *in vivo*, bursting cells oscillate between a bursting and regular firing mode (Sharp and Green 1994; Cooper, Chung, et al., 2005). During the sleep-wake cycle, for instance, the level of subicular bursting is increased during slow wave sleep (SWS) compared to the awake state and REM sleep (Staba, Wilson, et al., 2002). Spontaneous firing mode switching has also been observed in vitro (Harris and Stewart 2001; Cooper, Chung, et al., 2005).

4.9.10 Which sodium current mediates burst termination?

Commensurate with their central role in the early burst component, sodium currents appear to control the transition from bursting to regular spiking in the subiculum. Cooper et al. (2005) determined that cumulative slow inactivation of the sodium current causes a drop in the initial

slope of the spike ADP and a consequent failure of the second spike. This observation raises the question as to which sodium current, I_{NaF} or I_{NaP}, controls subicular mode transitions. We investigated this question by examining the effects of reducing the maximum conductance (simulating slow inactivation) of I_{NaF} and I_{NaP} on the spike doublet. To simplify analysis for subsequent simulations we use a reduced bursting model cell comprised of the early burst (i.e. doublet) component in which the calcium conductances of the late burst component are set to zero.

Reductions of the maximum conductance of I_{NaF} below about 65% of initial values cause the burst to fail (Figure IV-15). Interestingly, in other simulations with higher membrane resistances, a progressive reduction of the maximum conductance of I_{NaF} from 100 to 25% simply caused a progressive degeneration of the spikes to damped low amplitude oscillations (data not shown). In this situation, no realistic mode switching was observed.

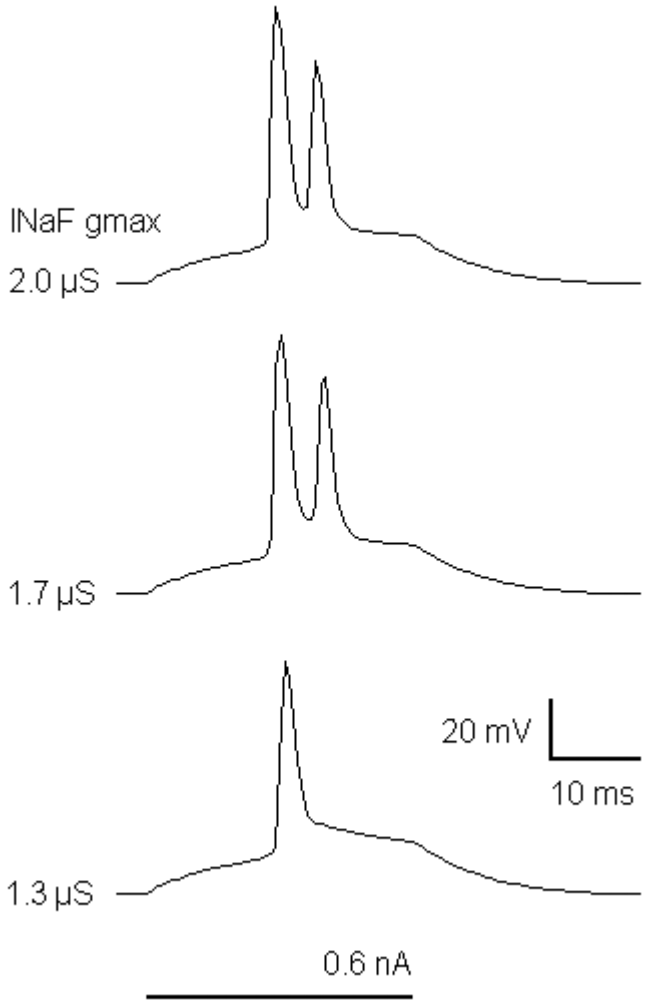

Figure IV-15. The burst mode fails when levels of I_{NaF} fall by 35%. The stimulus duration in this simulation was 30 ms.

Small graded reductions in the maximum conductance of I_{NaP} had two effects (Figure IV-16). Firstly, it caused a slight increase (~3 ms) in the interval between the doublet spikes. Secondly, and more importantly, the second spike cleanly failed when I_{NaP} was reduced by 28%. Resistance of the burst to I_{NaP} reduction was slightly increased with increased I_{NaP} time constants of deactivation (data not shown).

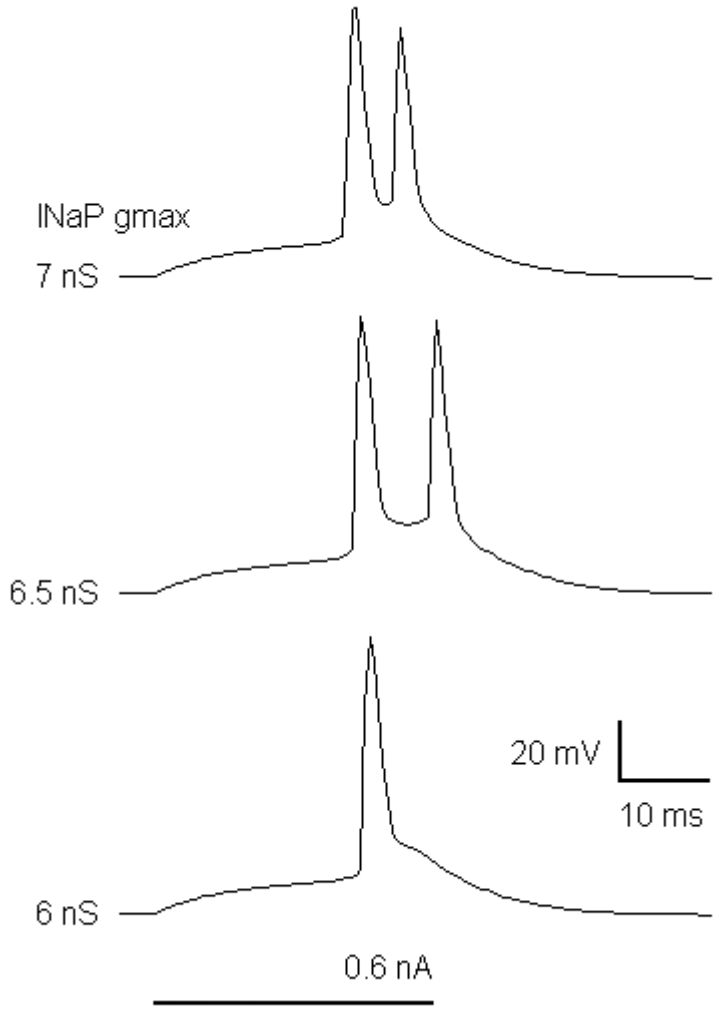

Figure IV-16. Burst firing in subicular bursters is highly sensitive to I_{NaP} inactivation. In this simulation, a 28% decrease in the maximum conductance of I_{NaP} causes the burst to fail. The stimulus duration in this simulation was 30 ms.

4.9.11 Frequency dependence of bursting

Cooper et al. (2005) also reported that subicular bursting fails at frequencies of greater than 10 Hz due to cumulative inactivation of the sodium current. Our model replicates this behaviour, exhibiting mode switching in response to an 11 Hz supra-threshold stimulus (Figure IV-17.). An 11 Hz stimulus gives a burst refractory period of about 91 ms, in good agreement with the Cooper et al. (2005) results. Mode switching was due to the slow inactivation of the persistent sodium current and occurred, in the simulation shown, when the I_{NaP} inactivation gate failed to recover to a value above about 0.8. Unsurprisingly, increasing the maximum conductance of I_{NaP}

or the stimulus strength also influenced the frequency dependence by making the burst more resistant to failure.

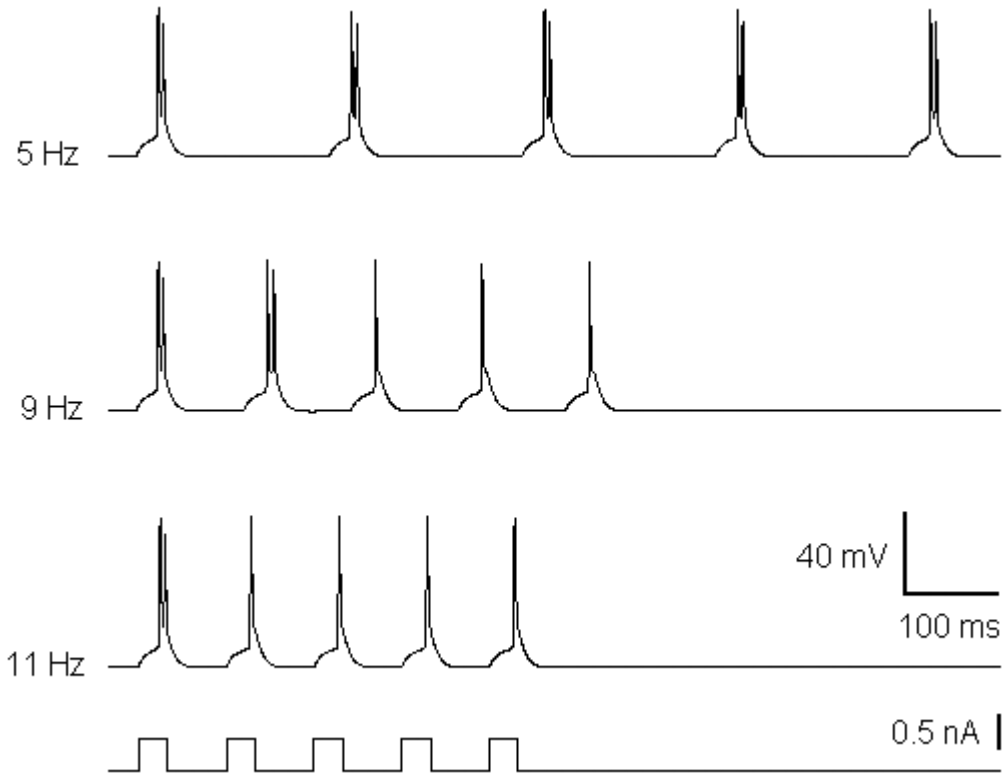

Figure IV-17. Subicular firing mode transitions are frequency dependent. Increasing the inter-stimulus frequency from 5 to 11 Hz causes a progressive decrease in the duration of repetitive bursting. The repetitive stimulus current is 30 ms in duration and 0.5 nA in strength. The stimulus protocol is shown for the 11 Hz condition.

These results suggest that slow inactivation of the persistent sodium current play an important role in firing mode switching in subicular bursters. Generally speaking, we found subicular burst firing to be more robust to decreases in I_{NaF} than to drops in I_{NaP} levels across a range of conditions. The sensitivity of bursting to the level of I_{NaP} inactivation is illustrated in Figure IV-16. However, it should be noted that the firing mode switching is associated with a significant decrease in the total sodium current (Cooper et al., 2005). Since I_{NaP} usually only constitutes a small fraction of the total sodium current it is likely that I_{NaF} inactivation is significant *in vivo*. Slow inactivation was not incorporated into the I_{NaF} model used in this study. Interestingly, inconsistencies regarding the relative contributions of these sodium currents can be reconciling if it is assumed that both the fast and persistent sodium currents are different modes of the same channel (Taddese and Bean, 2002). This conclusion receives some support from the observation

that the total subicular sodium currents reported by Vreugdenhil et al. (2002) are conserved i.e. high and low I_{NaP} cell populations carry equal total sodium currents. Nonetheless, in our simulations, subicular I_{NaF} is incapable of driving bursting in the absence of the low threshold I_{NaP}. I_{NaF} is thus necessary but not sufficient for subicular bursting. On this basis we attribute primary control of subicular bursting to I_{NaP}.

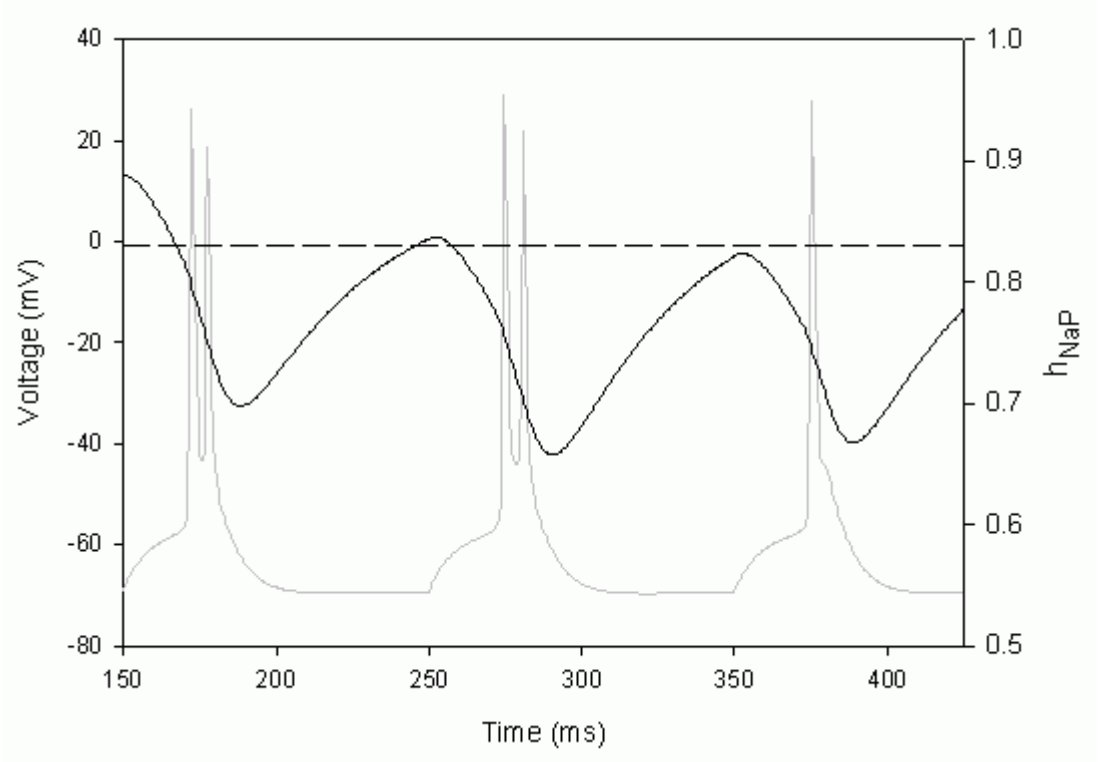

Figure IV-18. Subicular burst firing is very sensitive to I_{NaP} inactivation. In this plot the magnitude of the I_{NaP} inactivation variable, h_{NaP}, (black line) is plotted over the voltage response (grey line) of a subicular burster to three 30 ms stimuli of at 10 Hz. Bursting fails on the third stimuli because the maximum pre-stimulus recovery value of h_{NaP} falls below a critical value. The reference line (dashed) is set at 0.83.

As mentioned above, the precise frequency dependence is also influenced by the intensity of the stimulus: large stimuli could force repetitive doublet firing at higher frequencies. This finding appears to be mechanistically analogous to the finding by Mattia et al. (1997a) that depolarized bursters could be induced to burst by increasing the stimulus intensity. Significantly, with sufficiently high levels of stimulus current input, gamma frequency (40 Hz) doublet firing was exhibited (Figure IV-19). Subicular bursters *in vivo* exhibit similar behaviour during gamma population activity (Stanford et al., 1998). There was also a small increase in the stable frequency when the deactivation time constant of I_{NaP} was increased (data not shown).

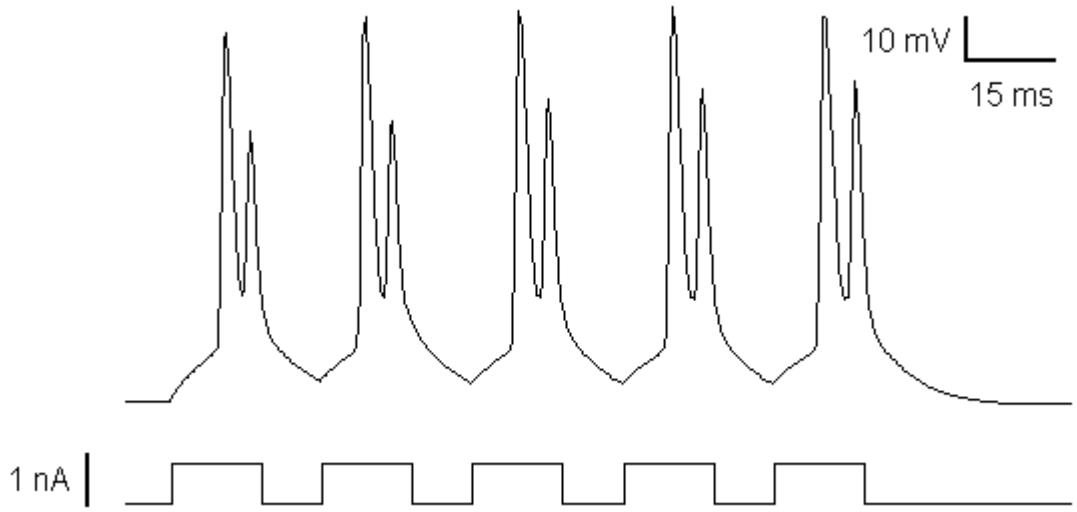

Figure IV-19. The subicular cell model can respond with gamma frequency doublet firing in response to five 20 ms stimuli of 0.8 nA at 40 Hz.

4.9.12 4-AP burst electrogenesis

Staff et al. (2000) were able to induce bursting in regular firers by applying the potassium channel toxin 4-aminopyridine (4-AP) in concentrations designed to selectively inhibit the potassium delay current, I_D. One interpretation of this finding is that most subicular regular firers are repressed bursters. We explored this idea by performing the reverse experiment i.e. adding I_D to the early bursting component model and noting the effects (Figure IV-20). Increasing levels of I_D g_{max} first induced a slight widening (~4 ms) of the doublet spike interval followed by the abrupt failure of the second spike. The collapse of the early burst component converts the cell to regular firing mode. These results suggest that regulation of I_D may constitute a mechanism for controlling the ratio of bursters to regular firers. In addition to I_D, I_{DR} and I_A were both capable of converting bursters into regular firing cells. Evidently, almost any potassium current with activation kinetics sufficiently rapid to participate in spike repolarization is capable of mediating subicular firing mode switching if increased to a high enough level. The relative importance of the various potassium currents in regulating firing *in vivo* will obviously depend on the maximum permissible expression levels found physiologically. Interestingly, whilst Yue and Yaari (2004) found that CA1 pyramidal cell burst transitions were heavily reliant on I_M, in our simulations this current did not play an important role in determining burst mode. The reason for this was that levels of I_M sufficient to suppress bursting caused unrealistically deep afterhyperpolarizations.

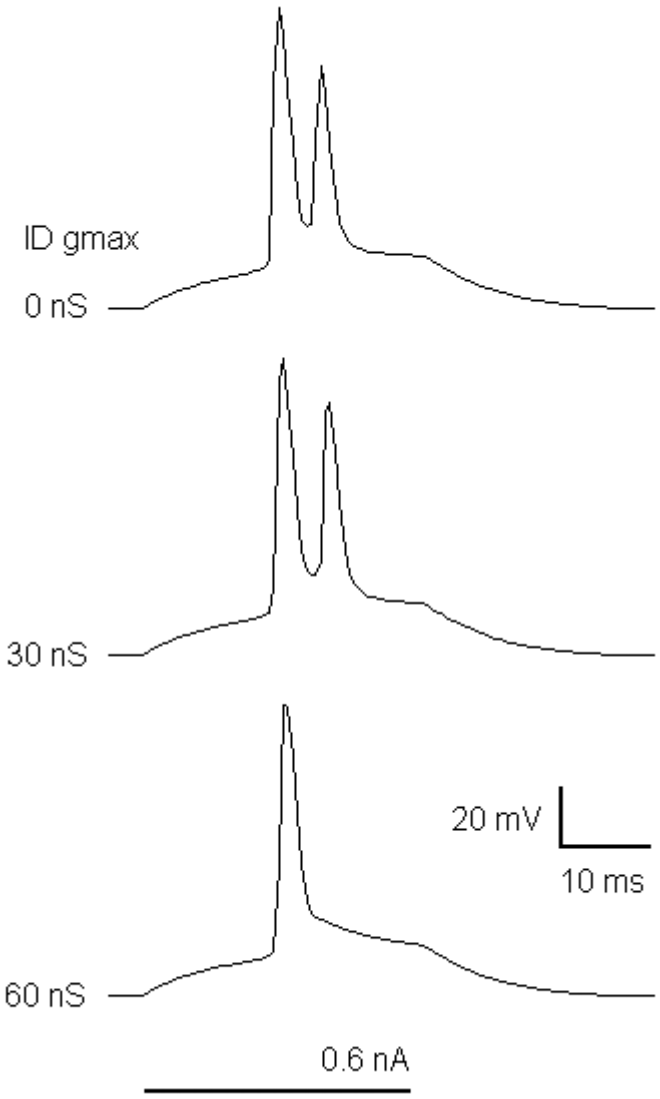

Figure IV-20. Subicular bursting cells can be converted into regular firers by I_D mediated suppression of excitability. Progressive addition of I_D to a model of the burst causes the second spike of the doublet to fail, thereby converting the burster into a regular firing cell.

Within the context of the two-component burst model the question arises of whether 4-AP bursting by regular firers is primarily due to a sodium- or a calcium-based mechanism. We suggest that 4-AP bursting is due primarily to a sodium-based mechanism, since the absolute magnitude of the peak and integral of the calcium tail current of regular firers (obtained with Na^+ and K^+ currents blocked) is small - less than half that of either burst type (Jung et al., 2001).

4.9.13 Voltage dependency of bursting

Stewart and Wong (1993) noted that direct depolarization of the membrane potential to subthreshold voltages caused the late burst component to fail leaving a single spike or spike

doublet. A number of groups have also found that subicular burst firing is abolished by sustained depolarizations to potentials close to threshold (Stewart and Wong, 1993; Mason, 1993; Mattia et al., 1997b; Stewart, 1997; Menendez de la Prida et al., 2003). This consensus has been challenged recently in papers reporting robust bursting in both strong and weak bursters, despite a resting potential depolarized to near firing threshold (Staff, Jung, et al., 2000; Cooper, Moore, et al., 2003).

Within the context of the two-component model, the relative sensitivity of subicular bursters to depolarization is due to the sensitivity to inactivation of the early component, which in turn, is due to the sensitivity to inactivation of I_{NaP}. Consequently, firing-mode switching due to an imposed depolarized holding potential is mechanistically equivalent to that mode switching induced by repetitive firing. Differences in the sensitivity of subicular bursters to depolarization- or frequency-dependent firing-mode switching must therefore be explained in terms of differences in the inactivation rates of subicular I_{NaP}. This notion is supported by the existence of at least two populations of I_{NaP} in subicular pyramidals; a slowly inactivating form with a time constant of about 150 ms and a very slowly inactivating component that eventually disappears over about 10 seconds (Vreugdenhil et al., 2004). Cells that carry the slowly inactivating isoform will readily exhibit firing-mode switching at depolarized potentials. Similarly, cells carrying the very slowly inactivating isoform will also exhibit depolarization-sensitive suppression of bursting. A caveat is that these cells may exhibit 'pseudo' depolarization insensitivity if they are held at a depolarized conditioning potential for significantly less than 10 seconds. The effect of depolarization-induced inactivation of I_{NaP} on bursting can be seen in Figure IV-18.

Differential expression of I_{NaP} isoforms with varied inactivation kinetics constitutes a coherent explanation for the apparently contradictory literature findings. An obvious implication of this hypothesis is that depolarization-sensitivity and frequency-dependent firing-mode transitions should co-vary. In other words, cells that exhibit one should exhibit the other. Although, if this is true then it is difficult to reconcile the observation by Staff et al. (2000) that subicular bursting is resistant to depolarization with the finding by Cooper et al. (2005) that bursting is frequency-dependent.

4.9.14 Why strong bursters are not seen in sharp electrode studies

Repetitive bursting in response to sustained depolarization (strong bursting) has only been reported in patch clamp configurations (Staff et al., 2000; Jung et al., 2001; Cooper et al., 2003;

Menendez de la Prida et al., 2003; Cooper et al., 2005). Sharp electrodes introduce a non-selective shunt conductance when they pierce the membrane and it is conceivable that the sequelae of this event weaken the burst mechanism. We propose that the lack of strong bursting in sharp preparations can be explained by the hypothesis that the non-selective shunt conductance amplifies the effect of the I_{NaP} inactivation burst termination mechanism in subicular neurons.

One potential mechanism is as follows: bursting causes a fractional loss of available active channels due to inactivation (Cooper et al., 2005). It is plausible to assume that a similar fractional channel loss occurs under both sharp and patch electrodes. However, by Ohm's law, the higher membrane input resistance found in the patch clamp configuration means that same proportional loss has less effect on the ability of the remaining channels to drive voltage change than in the sharp configuration. As a result, bursting is more robust under patch clamp than under sharp electrodes.

A potential problem with this explanation is that the input resistances reported in the sharp electrode study by the Wellmer et al. (2002) were higher than those of many patch clamp studies. However, this anomaly may be explained coherently if it is assumed that the cost of compensating for a shunt, of whatever size, lowers the energy status of the cell rendering it unable to replenish its transmembrane ionic gradients fast enough to support repetitive bursting. Such an effect could conceivably be achieved if the shunt reduced the reserve capacity of Na^+/K^+ ion-exchange pumps. Empirically, this mechanism might be expressed as a drop in the reversal potential for sodium.

The net effect of each of these mechanisms is that the efficacy of I_{NaP} is reduced. Consequently, it is likely that such processes also contribute to the mechanism of depolarization sensitivity of subicular bursting proposed above. Thus, it is probable that a burster that exhibits depolarization-insensitive bursting under patch clamp would exhibit depolarization-sensitive bursting if assessed using sharp electrodes. This hypothesis receives indirect support from the observation that simply increasing the stimulus strength can induce depolarized bursting under sharp electrodes (Mattia et al., 1997b).

We found that, in some models, addition of a non-selective shunt could convert strong bursters into weak bursters (Figure IV-21). Increasing the deactivation time constant of I_{NaP} could reinstate strong bursting (data not shown).

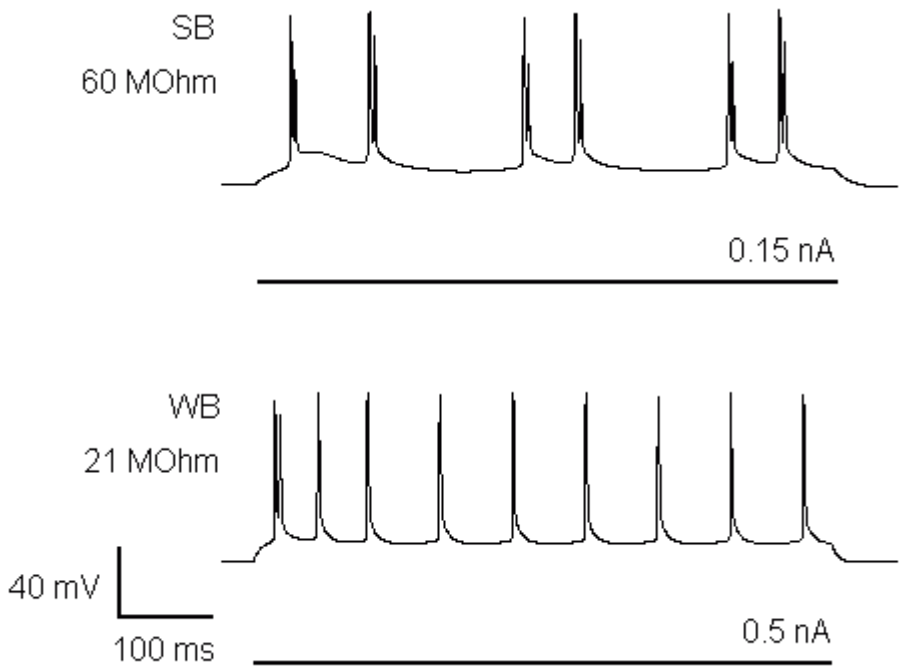

Figure IV-21. The level of membrane input resistance modulates the strength of subicular bursting. Reducing input resistance from 60 to 41 MOhm converts a strong burster into a weak burster. A weak burster, in this context, is a cell model that cannot be made to burst repetitively simply by manipulating the stimulus intensity.

4.9.15 Input resistance as a mechanism for controlling bursting

One implication of this hypothesis is that, *in vivo*, a graded regulation of strong bursting (as expressed by burst train length) can be effected by manipulating the passive leak channels responsible for the resting input resistance. Increasing neuronal input resistance could serve to increase the stability of repetitive bursting and thus raise overall levels of excitability, and *vice versa*. This notion is bolstered by reports that neurotransmitters can modulate leak conductances. Dopamine, for example, can induce a reduction of input resistance in subicular neurons (Behr, Gloveli, et al., 2000). In the hippocampus, acetylcholine, noradrenaline (Madison and Nicoll 1986) and serotonin (Andrade and Nicoll 1987) can exert similar effects.

4.9.16 Weak bursting

Generally speaking it proved very difficult to devise a robust model that switched smoothly from bursting to regular firing. Prospective models exhibited repetitive doublet firing, stopped firing altogether after the burst, or displayed other forms of irregular behaviour. Although we did eventually determine parameters that produced a burst followed by non-adapting spiking (Figure

IV-23) this behaviour was relatively unstable. This instability precluded the construction of a frequency-input plot for the bursting cell tonic phase.

4.10 Plateau potential and delayed spiking

Mason (1993) reported that most subicular neurons (~77%) responded to short (10 ms) just-threshold depolarizing pulses with a spike or doublet that continues or begins after the end of the pulse. These spikes ride on a variable length plateau potential (PP) that persists beyond the end of the stimulating pulse for tens of milliseconds. In the absence of spikes, about 50% of the (putative bursting) cells exhibit a variable length plateau potential (Mason 1993), the length of the plateau appears to be too long to be explained in terms of a passive charging current from the dendrites and is suggestive of the involvement of active conductances. The plateau potential behaviour of subicular bursters is in contrast to that of CA1 neurons, which display an apparently exponential decay following pulse termination (Mason, 1993). Some subicular regular firers exhibit a similar decay profile (Wellmer et al., 2002).

A more pronounced depolarizing plateau potential is evoked in subicular bursters by carbachol, a muscarinic receptor agonist (Kawasaki and Avoli 1996). The mechanism of this PP, which outlasts the depolarizing pulse by between 140 and 2800 ms, is unlikely to be the same as that reported by Mason (1993).

4.10.1 Mechanism

Mason (1993) observed that there were never more than two spikes in response to a just-threshold 10 ms stimulus. This invites comparisons with the ionic mechanisms of the spike doublets of the early burst component identified by Stewart and Wong (1993). The lack of evidence for a low-threshold calcium current in subicular pyramidals leaves the persistent sodium current as the only plausible candidate for the production of the plateau potential. Mason (1993) also noted a high level of variation in the shape of the plateau potential for a given current injection. A related 'latency jitter' was observed in the onset of the early and late burst components by Stewart and Wong (1993). The exact nature of this variation is unknown but is possibly due to random perturbations arising from stochastic ionic and cellular processes, and the electronic noise introduced by the equipment used. One potentially significant source of noise is the persistent sodium channel itself. In entorhinal cortex, I_{NaP} channel noise contributes to the production of subthreshold oscillations (White, Klink, et al., 1998).

4.10.2 Model of plateau potential

We were able to replicate the plateau potential and delayed firing shown by Mason (1993). In the model, burst firing began a variable time after the offset of a 20 ms current pulse (Figure IV-22A). The firing latency was very sensitive to the magnitude of the stimulus current. Unsurprisingly, the slowly deactivating INaP due to the sodium current carried the plateau potential. The slow deactivation proved integral to our ability to model plateau potentials (Figure IV-22B). By decreasing the rate of deactivation we increased the duration of the PP. Attempts to replicate this behaviour using an I_{NaP} model with conventionally symmetrical rapid activation and deactivation were unsuccessful (the activation rate of the I_{NaP} model is similar to that of the fast sodium channel). The plateau potential thus appears to represent the slow decay of an unsuccessful ADP regenerative event. Increasing the deactivation time constant of I_{NaP} slows down the decay of this thwarted ADP.

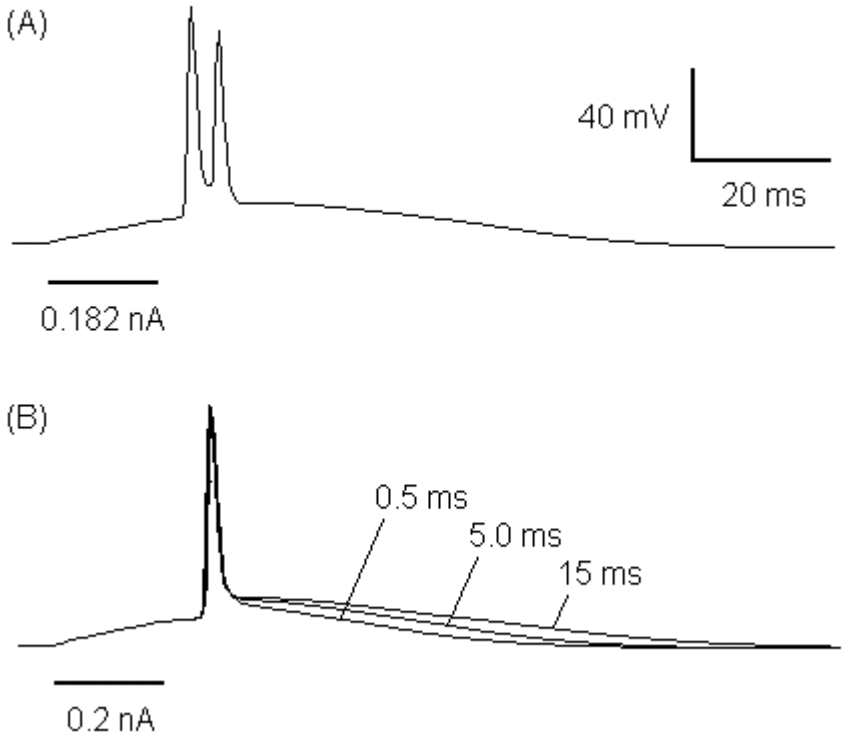

Figure IV-22. I_{NaP} controls subicular delayed firing and plateau potential duration. A: Doublet firing in this model occurs 6 ms after the termination of the current pulse. The I_{NaP} deactivation time constant in this condition is 5 ms. B: Three superimposed voltage traces from models with I_{NaP} deactivation time constants of 0.5, 5, and 15 ms illustrate how the rate of I_{NaP} deactivation controls the duration of the PP. The I_{NaP} conductances in conditions A and B were 10 and 8 nS, respectively.

4.11 Spike frequency adaptation

Spike frequency adaptation (SFA) is defined as a progressive increase in the interspike interval (ISI) during a train of action potentials. In the subiculum, the tonic phase of subicular bursters is generally non-adapting (Behr et al., 1996; Mattia et al., 1997b; Staff et al., 2000; Wozny et al., 2005), whereas regular firing cells commonly exhibit SFA in response to sustained suprathreshold stimulation (Behr et al., 1996, Wozny et al., 2005) (although see Staff et al., 2000). However, the level of adaptation reported is inconsistent. Whereas Mason (1993) observed that most subicular regular firing cells (66%) exhibited pronounced SFA, Greene and Mason (1996) commented on the variability of the degree of spike frequency adaptation in these cells. Insight into the nature of this variability was provided by Menendez de la Prida et al. (2003) who found that the frequency distribution of SFA for subicular regular firers naturally resolves into two populations of adapting and tonically firing cells with overlapping gaussian distributions. Tonically firing regular firers (RST) have an average adaptation index[*] of 0.72, whereas that of adapting regular firers (RSA) is 0.27.

Interestingly, the input resistance of RST cells is significantly lower than that of RSA cells. The opposite case would be expected if the difference between the two subtypes were solely due to increased levels of I_{AHP} in RSA cells. Since the average input resistance reported for RST cells is not significantly different to that for bursting cells (Menendez de la Prida et al., 2003), a possible explanation for this paradox is that the RST cells are suppressed bursters. One potential mechanism for this suppression via I_D has already been examined in the 4-AP burst electrogenesis section whereby failure of the burst due to I_D-damping leaves a non-adapting regular spike train (Figure IV-20). We were also able to emulate spike frequency adaptation in RSA cells by adding I_{AHP} to the 4-AP suppressed burster model (Figure IV-23B). Elimination of I_{AHP} in the model converted RSA back into RST cells, and removal of I_D converted the cell back into a weak burster. Of potential functional significance, removal of I_D suppression in an RSA cell unmasked a weak burster with an adapting regular spike train. Weak bursters with adapting spike trains have not been reported in the literature.

[*] Subicular SFA has been quantified in at least two ways: the adaptation index (Menendez de la Prida et al., 2003), defined as the ratio of the first to the last ISI; and its inverse, the accommodation index (Wozny et al., 2005), defined as the ratio of the last to the first interspike interval.

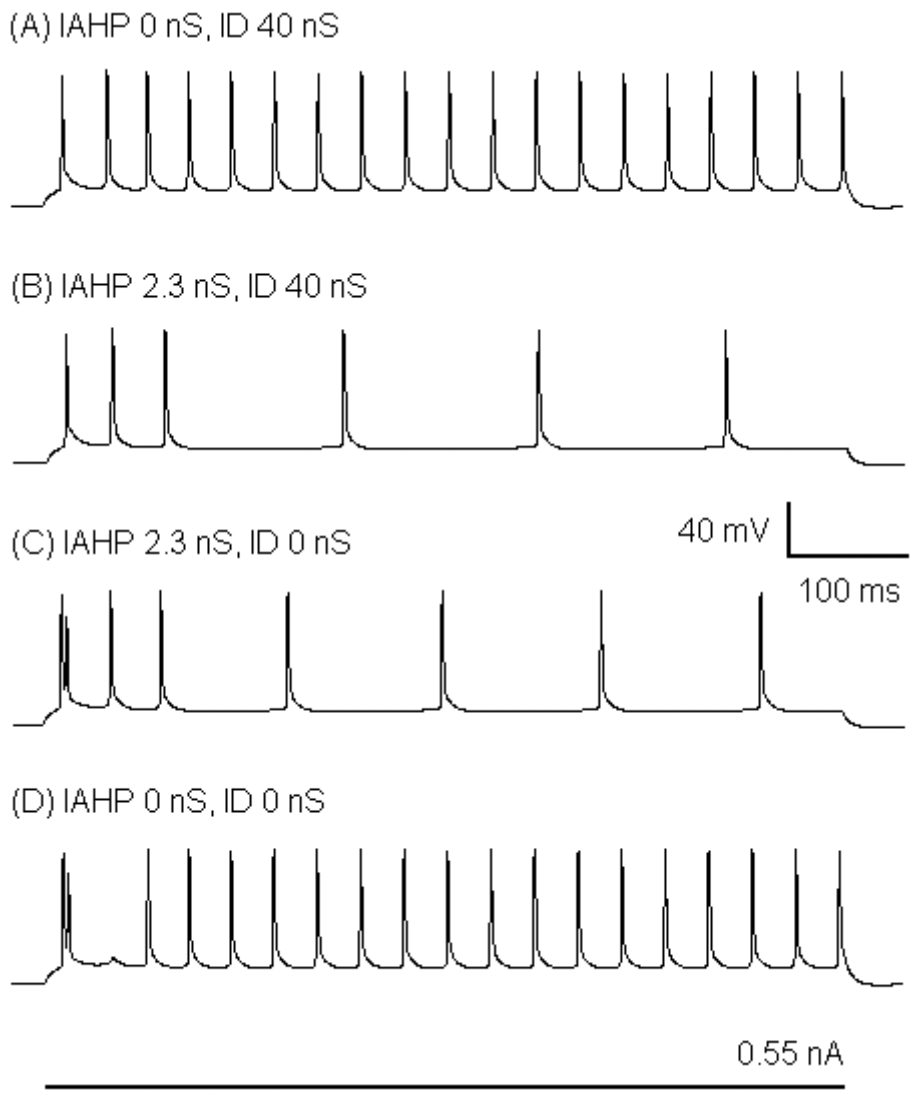

Figure IV-23. Subicular cell types can be inter-converted along SFA and burst propensity dimensions. The addition of I_{AHP} converts non-adapting regular firers (A) and bursters (D) into adapting regular (B) and burst firers (C). Note how suppression of I_D in adapting regular firers (B) converts them into adapting bursters (C).

In the human subiculum, Wozny et al. (2005) found that a pattern of adapting regular firers and non-adapting bursters persists across the division of spontaneously active and 'silent' cells (no attempt was made in this study to assess the distribution of SFA within regular firers). The level of spontaneously active cells is dramatically higher in tissue from temporal lobe epilepsy (TLE) patients exhibiting Ammon's horn sclerosis (AHS), the cell loss and gliosis that characterises TLE, than in non-AHS control tissue (Wozny et al., 2005). Nonetheless, Wozny et al. (2005) found no differences in the distribution of SFA across bursters and regular firers between these tissue types.

4.12 Afterhyperpolarizations

In hippocampal pyramidal cells, spikes are typically followed by three after-hyperpolarizations (AHPs): a fast AHP (fAHP) lasting 2-5 ms, a medium AHP (mAHP) lasting up to 100 ms, and a slow AHP (sAHP) lasting several hundred milliseconds (Storm 1989). A burst AHP is also exhibited following a burst elicited in response to a brief stimulus. Subicular pyramidals can exhibit all of these hippocampal AHPs.

4.12.1 Fast afterhyperpolarization

The fast afterhyperpolarization (fAHP) is defined as the lowest voltage between the fast spike and the afterdepolarization (ADP) within the first couple of milliseconds of the spike (Storm, 1987). In subicular burst cells, the fast AHP is abolished by application of the Ca^{2+} channel blockers Co^{2+} and Cd^{2+} whilst at the same time the spike width is increased by 10% (Mattia et al., 1997). This suggests that the fast transient Ca^{2+}-dependent potassium current, I_{CT}, mediates the fAHP of subicular neurons.

Our simulations are notable for the absence of the fAHP. This is primarily due to the limitations of the I_{CT} model employed in this study. Although a wide range of I_{CT} levels, calcium-dependencies, and fast calcium pool kinetics were tried, attainment of accurate fAHPs proved elusive. Future models of I_{CT} will remedy this deficit. Of note, is the observation that the lack of a fAHP in our model is comparable to the effects of applying extracellular cobalt and cadmium to subicular pyramidals (Mattia et al., 1997b).

4.12.2 Medium afterhyperpolarization

Hippocampal cells typically exhibit a medium afterhyperpolarization (mAHP) that follows a spike or spike train that lasts up to about 100 ms (Storm, 1989). The mAHP has a large calcium-dependent component (Storm 1989; Williamson and Alger 1990) that is blocked by TEA and charybdotoxin, which suggests the agency of I_{CT}. The remaining component is blocked by carbachol indicating a role for the muscarinic-sensitive potassium current, I_M (Williamson and Alger, 1990).

Both regular and burst firing subicular pyramidals exhibit a noticeable mAHP following the termination of a sustained suprathreshold stimulus (Behr et al., 1996; Wozny et al., 2005).[*]

[*] Note that Behr et al. (1996) and Wozny et al. (2005) refer to the mAHP as the fAHP.

Mattia et al. (1997b) reported that Co^{2+} and Cd^{2+} reduced the amplitude of the mAHP was by 45%. This group also found that the amplitude of the mAHP increases as a function of stimulus intensity.

Wozny et al. (2005) examined the mAHP of subicular regular firers from patients with Ammon's horn sclerosis (AHS). These workers found no significant differences in the mAHP of cells from AHS and non-AHS tissue. Similarly, Behr et al. (1996) found no statistical difference between the amplitude and peak time of the mAHP of regular firing (24 ms, -3.0 mV) and burst firing cells (22.5 ms, -3.0 mV), which suggests that the ionic machinery underlying the phenomenon is similar in both cell types.

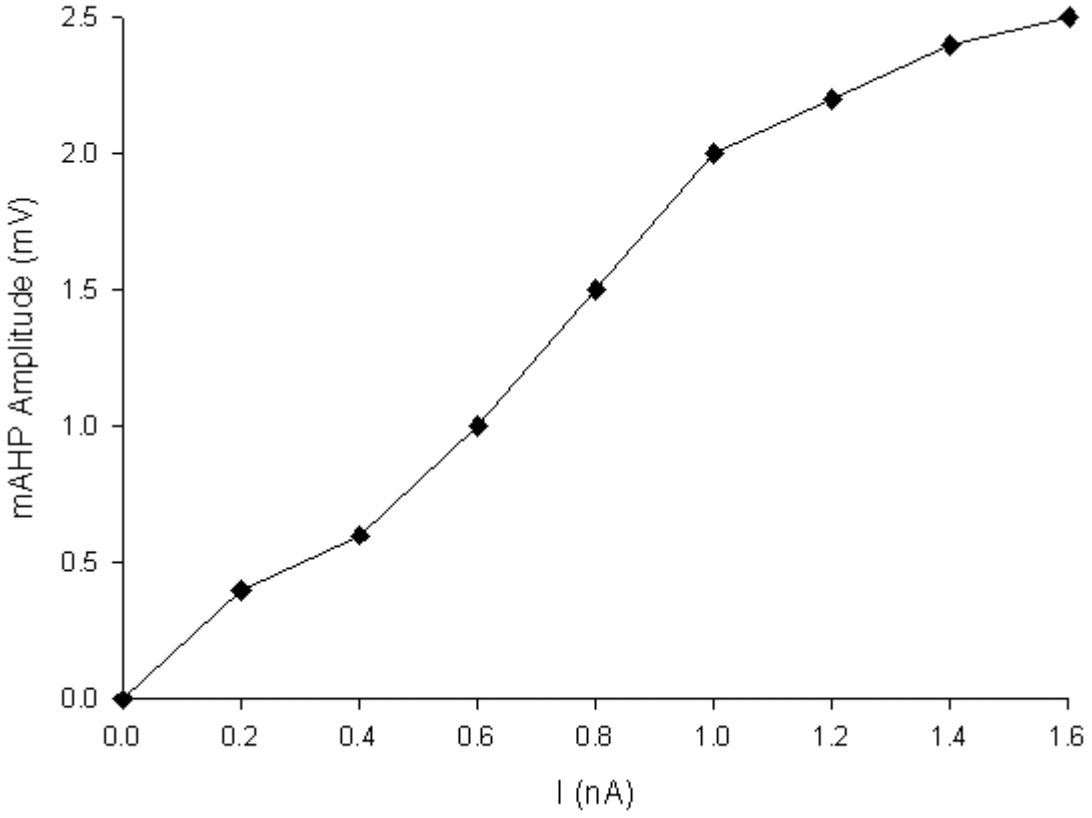

Figure IV-24. Plot of mAHP peak amplitude against stimulus intensity. The maximum conductance of I_M in this model is 7 nS. Note that I_{NaF} was eliminated in order to maintain a stable response profile.

Related to the mAHP is the burst AHP (bAHP) that follows bursts elicited by short depolarizing stimuli. In subicular pyramidals, Behr et al. (1996) reported that the bAHP peaked with an average amplitude of -6.5 mV after 29.3 ms. Mattia et al. (1997b) observed bAHPs that lasted for 113 ms, on average, and exhibited a smaller peak amplitude of -2.7 mV.

Application of calcium channel inhibitors reduced bAHP amplitude by 76% although the large standard deviation (24%) suggests that the effect is highly variable (Mattia et al., 1997). Assuming that the inhibitors were uniformly effective, this suggests that in some neurons the burst AHP is almost entirely due to calcium-dependent potassium channels, whilst in others the contribution of these channels to the bAHP is well below 50%. Stewart and Wong (1993) found that the burst AHP were unaffected by hyperpolarization although single spikes were eliminated.

In the model, the mAHP and bAHP are carried by I_M. As with the fAHP, the I_{CT} model employed did not contribute substantially to the medium and burst AHPs. The depth of the I_M-mediated mAHP varied with the level of I_M, the membrane input resistance and the stimulus intensity (Figure IV-24).

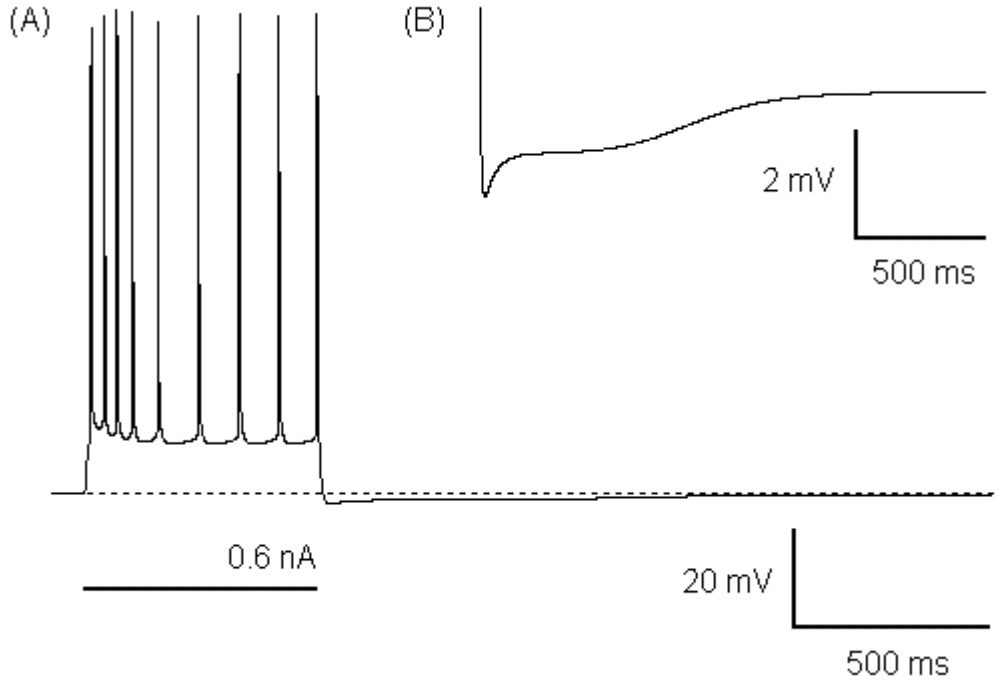

Figure IV-25. The slow AHP in a model of a subicular regular firer. A: The medium and slow AHPs are visible following the termination of the 600 ms pulse. B: An expanded view of these AHPs reveals more clearly the medium and slow components. The maximum conductance of I_{AHP} is 3.4 nS.

4.12.3 Slow afterhyperpolarization

In hippocampal pyramidals, the slow voltage-insensitive Ca^{2+}-activated potassium current, I_{AHP}, generates the slow afterhyperpolarization (sAHP) (Madison and Nicoll 1984). Blockage of the sAHP in subicular pyramidals by zero calcium (Wellmer et al., 2004) suggests a similar

mechanism operates in the subiculum, although subicular bursters do not generally exhibit a sAHP (Behr, Empson, et al., 1996; Wozny, Knopp, et al., 2005). For example, over 85% of bursting cells examined by Behr et al. (1996) lacked a sAHP. Similarly, Mattia et al. (1997) found no clear sAHP component in subicular bursting cells. Since the same current mediates both the sAHP and SFA, it is unsurprising that such a division exists between regular and burst firers. Furthermore, it is likely that the non-adapting regular firers described by Menendez de la Prida et al. (2003) also lack a sAHP, as is seen in our simulations. The empirically plausible sAHP exhibited in Figure IV-25 last for about 1500 ms and has a maximum depth of 1 mV.

Depression of the sAHP is associated with the transition of inter-ictal discharges to the ictal mode (Matsumoto and Ajmone-Marsan 1964). This inverse correlation of the sAHP with excitability is reflected in human subicular cells where the amplitude of the sAHP is significantly decreased in spontaneously active cells as compared to 'silent' cells (Wozny et al., 2005). Since the proportion of spontaneously active subicular regular firing cells is dramatically increased in patients with temporal lobe epilepsy, it appears that the sAHP plays an active role in regulating the firing propensity of subicular regular cells. A related point is that the presence of the sAHP in regular firers (and potentially some bursters as well) is likely to limit their ability to respond to gamma frequency population oscillations. Stanford et al. (1998) report that the response of subicular regular firers to gamma frequency afferent inputs from CA1 is weak compared to that of bursters. Control of I_{AHP} expression is therefore a potentially useful mechanism for controlling the level of entrainment by high frequency afferents.

4.13 Rebound firing

Subicular pyramidals respond to the release of a hyperpolarizing conditioning potential with a depolarizing rebound potential (anodal break potential or post inhibitory response) (Stewart and Wong, 1993; Behr et al., 1996; Mattia et al., 1997). Subicular regular and burster firers tend to differ in the magnitude of their anodal break potential (ABP). Bursters exhibit larger ADPs that are more likely to reach firing threshold than regular firers (Stewart and Wong, 1993; Behr et al., 1996; Greene and Totterdell, 1997; Stanford et al., 1998).

The subicular ABP is strongly attenuated by either caesium or TTX (Stewart and Wong, 1993). The TTX-sensitive component is almost certainly due to I_{NaP} and serves to amplify the I_H (Cs-sensitive) contribution. The magnitude of the anodal break potential (ABP) can be large enough to trigger spikes or bursts (Stewart and Wong, 1993; Mattia et al., 1997a), which implies

that I_{NaP} is significantly de-inactivated by the hyperpolarization. For example, figure 1A of the Stewart and Wong (1993) paper illustrates a rebound burst triggered by an ABP over 15 mV in amplitude for a neuron with a resting potential of -75 mV.

We found that the I_{NaP} levels used for the previous models were insufficient to drive rebound bursting. However, by increasing I_{NaP} conductance levels the model successfully reproduced both the anodal break potential and rebound spiking and bursting (Figure IV-26). As expected, I_H and I_{NaP} were responsible for the model's anodal break potential and rebound firing (data not shown).

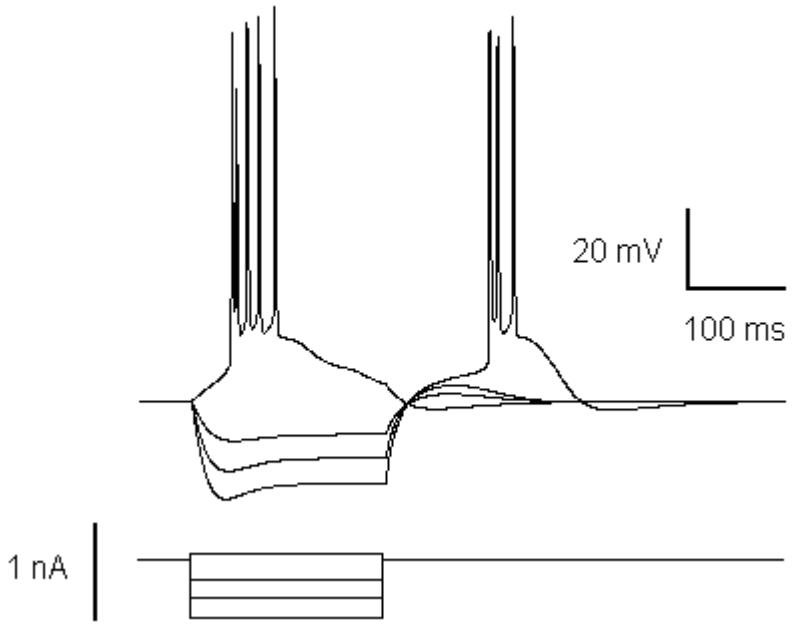

Figure IV-26. Subicular anodal break potential and rebound bursting. Stimulus currents used are +0.08, -0.2, -0.4, and -0.6 nA. I_{NaP} and I_{DR} had maximum conductance values of 16 and 400 nS, respectively. The cell input resistance was 60 MOhm.

The amplitude of the ABP is both time- and stimulus-dependent in an asymptotic fashion (Mattia et al., 1997a). Our model exhibits both of these features (data not shown, but see Figure IV-2 for an example of the stimulus dependence of the ABP). Some slight further de-inactivation of I_{NaP} occurs during hyperpolarization and appears to exert some influence on the time-dependence of the ABP. The exact level of de-inactivation is determined by the duration of the stimulus and the time constant of the I_{NaP} inactivation gate. Whether a rebound burst or spike occurred was found to be quite sensitive to the maximum conductance level of I_{NaP}. The level of I_{NaP} required to achieve rebound bursting was over twice that used in the previous experiments. However, the levels used (~1% of the I_{NaF} density) are still within the average level seen in the rat (5%).

Although there are some reports suggesting that bursters and regular firers have similar hyperpolarizing responses (Behr et al., 1996; Staff et al., 2000), the general impression is that the depolarizing sag is more robust in bursters than in regular firers (Taube et al., 1993; Green and Totterdell, 1993; Stanford et al., 1998; Menendez de la Prida et al., 2003). Indeed, in some regular firers delayed inward rectification is almost absent (Stewart and Wong, 1996). Since the mixed cation anomalous rectifier current, I_H, mediates this response, it may be concluded that I_H expression is generally greater in bursters than regular firers. Higher I_H levels also contribute to the larger ABP and higher rebound-firing propensity of bursting cells.

4.13.1 I_D and the anodal break potential

In our model, the addition of the potassium delay current, I_D, caused a damping of the anodal break potential, in addition to converting bursters into regular firers. The level of suppression was broadly proportional to the maximum conductance level of I_D (data not shown). Since regular firers tend to exhibit lower ABPs, this finding lends further support to the hypothesis that I_D plays a role in regulating subicular bursting.

Although there are some reports suggesting that bursters and regular firers have similar hyperpolarizing responses (Behr et al., 1996; Staff et al., 2000), the general impression is that the depolarizing sag is more robust in bursters than in regular firers (Taube et al., 1993; Green and Totterdell, 1993; Stanford et al., 1998; Menendez de la Prida et al., 2003). Indeed, in some regular firers delayed inward rectification is almost absent (Stewart and Wong, 1996).

Chapter V
DISCUSSION

A wise man proportions his belief to the evidence.

David Hume (1711-1776)

5.1 Overview

In this section we discuss some of the implications of our findings regarding subicular resonance. We also review evidence that suggests that the early and late burst components are differentially regulated and go on to consider why the subicular burst is so complicated. We then address some of the stronger objections to the adaptive two-component burst theory, before discussing the role and regulation of SFA in the subiculum. Finally, we consider a modest proposal for revolutionising the analysis of intracellular electrophysiological data.

5.2 Entrainment and resonant communication

A neuron will respond most strongly to input with a frequency that matches its resonant frequency. One theoretical consequence of this fact is a form of adaptive functional connectivity known as selective resonant communication (Izhikevich 2002). Thus, for example, a neuron that synapses onto two other neurons with different resonant frequencies, can selectively communicate with one of the two neurons simply by tuning its output frequency to match the resonant frequency of the target neuron. Conversely, it is possible that modulation of the resonant frequency of a downstream neuron could alter its ability to be entrained by population oscillations. Resonance, especially when amplified into subthreshold oscillations, thereby provides a means of implementing dynamic functional connectivity in an otherwise static network.

Within the subiculum, we have shown that depolarized resonance appears to be handled by I_M. The 25% drop in STO frequency caused by divalent metal cations (Mattia et al., 1997b) suggests that I_M tuning, and thus subicular resonant communication, is a possibility *in vivo*. Furthermore, a role for the subiculum in modulating theta entrainment in downstream areas is suggested by the ability of ibotenic acid lesions of the ventral subiculum to reduce the power of entorhinal cortical

theta during REM (Laxmi, Meti, et al., 2000). One immediate consequence of reduced theta entrainment is a drop in the efficacy with which afferent bursts induce synaptic modifications. A single burst can induce LTP (LTD) at peak (trough) of the wave theta (Huerta and Lisman, 1995). By impairing theta phase locking the efficacy of bursts in inducing synaptic modifications is reduced. Consequently, regulation of entrainment can potentially impact on learning and memory functions. Of potential relevance, in this regard, is the observation that single subicular neurons receive convergent inputs from CA1 and entorhinal cortex (Gigg, Finch, et al., 2000) and that tetanic stimulation of the same region of CA1 induces LTP in ventral subiculum, but LTD in dorsal subiculum (Methot, Tancredi, et al., 1997).

An interesting corollary to these ideas concerns two novel cell types identified using intra- and extracellular techniques. Menendez de la Prida et al. (2003) reported the existence of a subgroup of regular-like cells that, in response to depolarizing stimuli, fired spikes interspersed with theta-range subthreshold membrane oscillations. Given the possibility that the level of theta entrainment exhibited by a cell is a function of its STO amplitude, it is plausible to predict that MPO cells are strongly entrained by theta. It is, therefore, tempting to identify MPO cells with the theta-modulated cells identified in freely moving animals by Anderson and O'Mara (2003). Theta-modulated cells are a novel type of regular firers whose firing rate is strongly modulated by the theta population oscillation.

Whilst the Menendez de la Prida study examined ventral subicular electrophysiology (interestingly MPO cells were localized at the extreme distal aspect of the ventral subiculum) the Anderson and O'Mara study looked at the dorsal subiculum. Validation of the hypothesis that MPO and theta-modulated cell types are identical will obviously require extracellular and intracellular characterisation of identified cells in the same region of the subiculum.

We also suggested how the lower input resistance of subicular pyramidals, compared to CA1 cells, could contribute to the lower theta entrainment of the subiculum relative to CA1. The lower intrinsic resonant properties of subicular cells can be compensated for by the presence of I_{NaP}. I_{NaP} can amplify the resonant response into subthreshold oscillations. Accordingly, the channels governing input resistance and I_{NaP} constitute targets for regulating subicular entrainment with theta and, potentially, resonant communication with other structures. Moreover, since I_{NaP} controls the amplitude of subicular subthreshold oscillations, the ability of a neuron to participate in resonant communication may also be influenced by brain state-dependent

regulation of I_{NaP}. For example, dopamine hyperpolarizes the activation threshold of I_{NaP} (Gorelova and Yang 2000).

5.3 The function of the burst

A number of converging lines of evidence suggest that a high B/R ratio is the brain's "learning mode". Rats subjected to learning paradigms display increased levels of bursting (Otto, Eichenbaum, et al., 1991). Long-term synaptic plasticity is greatly enhanced by postsynaptic bursting (Thomas, Watabe, et al., 1998; Pike, Meredith, et al., 1999). Furthermore, the performance of cognitively impaired rodents in several tests of learning and memory is improved by the novel "cognition enhancers" linopirdine and XE991 (Fontana, Inouye, et al., 1994). These compounds are selective blockers of I_M (Aiken, Lampe, et al., 1995; Schnee and Brown 1998; Wang, Pan, et al., 1998), which has recently been shown to be capable of mediating the transition between regular and burst firing modes in CA1 pyramidal neurons (Yue and Yaari 2004).

Lisman (1997) suggests that bursts are the functional units of information in the brain based on the fact that synapses reliably transmit bursts, but not single spikes. Bursts significantly increase the reliability (release probability) of synapses through the mechanism of paired-pulse facilitation (Zucker 1989). Consequently, bursts carry more information. For example, place maps constructed from the activity of hippocampal place cell have sharper contours if constructed using bursts instead of spikes (O'Mara, Commins, et al., 2001).

Bursting input increases the likelihood of firing of subicular bursting pyramidals. Thus, a repetitive (x5) stimulus, with a burst-like ISI of 5 ms, reliably triggers bursting (Stewart 1997). Regular firing cells responded to the same repetitive stimuli with either a large EPSP or a single spike. Significantly, whereas bursting cells still fired bursts when the ISI was increased to 10 ms, regular cells failed to produce spikes.

5.4 Differential regulation of the early and late burst components

The adaptive two-component burst model of the subicular burst lends itself to nuanced control of different functional aspects of the burst. The sodium component drives the early doublet and controls firing mode switching, whilst the calcium currents can act to extend the duration of the burst.

There is considerable inferential evidence that the early and late components of the subicular burst are subject to differential modulation and that, consequently, electrophysiological phenotypes in the subiculum are not particularly stable. Wellmer et al. (2002) reported that a pilocarpine-induced 40-minute episode of status epilepticus (SE) caused a dramatic alteration in the relative proportions of regular firers (decreased from 61 to 18%), low threshold bursters (increased from 4 to 29%) and high threshold bursters (increased from 35% to 53%). Since calcium-dependent LTBs can be downgraded to sodium-dependent HTBs by inhibition, it is plausible to assume that the only permissible cell type transitions, under SE, are regular firing to HTB, and HTB to LTB. In other words, a regular firer can ultimately end up as either type of burster, whereas a HTB can only become a LTB. If this constraint is correct, then 43% of cells were converted from regular to HTB mode, whereas only 25% were converted from HTB to LTB mode, under the same conditions. Thus, the early burst component appears to be about 1.7 times more easily upregulated than the late component by a brief episode of status epilepticus.

Obviously, this conclusion does not necessarily mean that the total conductance of sodium or calcium channels must be increased to enhance bursting. As mentioned previously, a viable alternative is the constitutive suppression of potassium currents, such as I_D. As has been shown empirically (Staff et al., 2000), and computationally in this work (Figure IV-20), alterations in the magnitude of I_D exert powerful effects upon subicular firing mode. In fact, there is indirect evidence that I_D suppression may be one of the more important mechanisms by which epileptic episodes induce bursting in the subiculum. Stewart and Wong (1993) found that, under picrotoxin-induced suppression of interneuron activity, sustained tetanic afferent barrage from CA1 could convert regular firing subicular cells into bursters. Hippocampus-subiculum projections are glutamatergic (Taube, 1993), and it is also known that I_D is suppressed by metabotropic glutamate receptor activation in hippocampal pyramidal neurons (Wu and Barish, 1999). This constitutes a plausible mechanism whereby the level of I_D activation is strongly downregulated by intense excitatory network activity. I_D is not the only candidate for such regulation, since the activation of metabotropic glutamate receptors also inhibits the calcium-dependent potassium channel, I_{CT} (Gebremedhin, Yamaura, et al., 2003). Moreover, since I_{CT} is linked to calcium currents it provides a potential control point through which the late burst component, and thus burst duration, can be selectively modulated.

Nonetheless, increases in inward currents are undoubtedly a significant locus for the pathological upregulation of burst propensity. In human patients with TLE, for example,

subicular pyramidals exhibit significant increases in the I_{NaP} fraction of the total sodium current (Vreugdenhil et al., 2004). I_{NaP} is an obvious target for downregulation of bursting, since a small reduction in this current abolishes bursting in both weak and strong bursters, as demonstrated here and experimentally (Menendez de la Prida et al., 2003; Cooper et al., 2005).

Interestingly, the R-type calcium current, a significant element of the late burst component, is reportedly also inhibited by metabotropic glutamate and $GABA_B$ receptor activation (Wu, Borst, et al., 1998).

5.5 Why is the subicular burst so complex?

The key phenomenological feature of the mechanisms of the adaptive two-component model of subicular bursting is that it facilitates the systematic variation of the duration of the burst. We propose that one of the primary determinants of subicular burst duration is the prevailing population oscillation. In brief, during low-frequency oscillations (e.g. theta) the full burst is favoured, whereas during high frequency rhythms (e.g. gamma) the brief early component is favoured.

5.5.1 Long bursts

The theta oscillation is the on-line or "open loop" state of the hippocampus and is thought to be critical for temporal coding and the modification of synaptic weights (Buzsaki 2002). During theta a burst can induce homosynaptic LTP (LTD) when applied at the peak (trough) of theta oscillations (Huerta and Lisman 1995). Crucially, the degree of synaptic modification is strongly dependent on the duration of the burst. Whereas doublets produce little alteration, and triplets produce some, bursts with four spikes induce near-maximal synaptic modification. Beyond synaptic modification, burst duration can also form the basis of a code that can signal the slope of theta range sinusoidal inputs (Kepecs, Xiao-Jing Wang, et al., 2002).

5.5.2 Short bursts

Gamma firing bursters play an important role in subicular activity. Subicular gamma oscillations (30-100 Hz) are differentiated from those of CA1 by the presence of population doublets correlated with single cell burst firing. This suggests that subicular bursting neurons amplify the hippocampal gamma activity and transmit it to other areas of the brain (Colling, Stanford, et al., 1998).

The ability of subicular bursters to participate in gamma oscillations places a constraint on the duration of the burst since, at 40 Hz, there is only a 25 ms interval during which time the burst mechanism must activate, terminate, and de-inactivate. Perhaps unsurprisingly, subicular bursters do not appear to be able to support 40 Hz subicular pyramidal bursting in response to tonic stimulation (Stanford, Traub, et al., 1998). However, in their model of a subicular burster, Stanford et al. (1998) were able to elicit gamma bursting when the cell was subjected to 40 Hz alternating depolarizing and hyperpolarizing stimuli. On this basis, these workers suggested that subicular gamma bursting is dependent on similarly patterned input and is, in essence, a network phenomenon. Our model exhibited 40 Hz bursting using 40 Hz depolarizing stimuli, without the unrealistic requirement for hyperpolarizing steps (Figure IV-19). This suggests a complementary conclusion, namely, that subicular bursters possess an intrinsic somatic gamma (or near-gamma) frequency firing capacity.

As mentioned above, the R-type calcium current, a driver of the late burst component, is inhibited by activation of the metabotropic glutamate and $GABA_B$ receptors (Wu, Borst, et al., 1998). Since failure of the late burst component can reduce the duration of the burst, one may speculate that the sensitivity of I_{CaR} to glutamatergic afferents is one reason why nominally early component spike doublets dominate heavy network activity, such as gamma oscillations (Stanford et al., 1998). In this regard, it is also noteworthy that subicular population activity is distinguished by the inability of bicuculline, a $GABA_A$ receptor antagonist, to induce stable epileptiform activity, as it does in CA1 and other cortical regions (Colling, Stanford, et al., 1998). The reason for this appears to be the presence of a strong $GABA_B$ inhibitory network (Colling, Stanford, et al., 1998). Since I_{CaR} is inhibited by $GABA_B$ receptor activation, an important function of this network may be to suppress the late burst component and allow controlled, high frequency, early component bursting during gamma activity. A further influence on the late component arises because high levels of network activity are also likely to cause a reduction in the level of external calcium. In subiculum, a reduction of extracellular calcium from 2 to 1 mM reduces the duration of bursts in strong bursters (Menendez de la Prida et al., 2003).

5.6 Objections to the adaptive two-component burst theory

There are several lines of evidence that suggest that bursting and regular firers are not interconvertible and represent a dichotomy. In this section we address some of the more powerful arguments against the dynamic interconversion model.

5.6.1 Different cell types, different projections

We have shown how electrophysiological features such as bursting and spike frequency adaptation can be smoothly varied to interconvert bursters and regular firers. However, an objection to this view is that if the expression of subicular cells types is dynamic then why do the cell types have different distribution patterns across the subiculum? It is well established that, *in vitro,* subicular cell types are differentially distributed across the proximodistal and deep-superficial axes (Greene and Mason, 1996; Greene and Totterdell, 1997; Staff et al., 2000; Menendez de la Prida et al., 2003). It is also well established that discrete subregions of the subiculum have different projection targets. An obvious conclusion suggested from these findings is that stable regular firing and burst firing projection cells have different output targets. This indeed appears to be the case. Stewart (1997) found that some bursting cells, but no regular firing cells, were antidromically activated by stimulation of presubiculum. Conversely, some regular cells, but not bursting cells, were activated by stimulation of the deep entorhinal cortex. On the basis of the implied differential projection targets of the two cell types, Stewart concluded that the burst-regular cell division is a robust dichotomy. Although it may be argued that the small numbers of cells tested in this study undermines this conclusion, similar findings were found for population activity. From the same recording location, population bursts were evoked when presubiculum was stimulated, whereas a population spike was seen under EC stimulation (Stewart, 1997).

However, slice preparation represents an artificially stable brain state, with none of the fluctuations in neuromodulators, and consequent variations in EPF expression, found *in vivo*. The B/R ratio is essentially fixed in the brain slice, whereas the electrophysiological profile of the subiculum is highly dynamic under both normal (Staba et al., 2002) and pathological conditions (Behr et al., 2000; Wellmer et al., 2002). As a result, the findings of Stewart (1997) supports the conclusion that individual subicular cells project to different regions, but not necessarily the inference that cell types are invariant in the living brain.

Indeed, the observation that no subicular cell type preference is shown by brain structures that project to the subiculum, such as presubiculum, entorhinal cortex (Stewart, 1997) and CA1 (Taube, 1993), provides indirect support for the idea that cell types are not invariant categories since a lack of specificity makes sense from a computational perspective. Dynamic regulation of cell types, along with effectively random afferent connections to circumscribed areas, allows for a high level of control and flexibility in how the subiculum processes particular inputs. Apropos, the intrinsic properties of subicular neurons, and not the amplitude of synaptic currents, determine their responsiveness to local stimulation (Menendez de la 2003). In combination with the topographical organisation of subicular efferent projections (Witter and Amaral 1991), such a mechanism would allow for target-specific modulation of the gain of subicular input and output.

One implication of this idea is that the functional properties of subicular cells should vary by location, but not apparent cell type. Consonant with this prediction, Sharp and Green (1994) observed that the average pattern of cell firing rate, spatial coherence, and place field size between the proximal and distal regions of the dorsal subiculum is mirrored by regular firing and bursting cells (Sharp and Green, 1994).

5.6.2 Different cell types, different morphologies and electrophysiologies

Strong bursters overwhelmingly have pyramidal somata whereas regular firers and weak bursters were equally likely to have ovoid somata (Menendez de la Prida et al., 2003). Furthermore, there appears to be a functional separation of strong bursters from weak bursters and regular firers in terms of their response to synaptic stimuli. Strong bursters typically respond with spike bursts whereas over 50% of weak bursters, and practically all regular firers are silent (Menendez de la Prida et al., 2003). These salient morphological and electrophysiological differences suggest that, of all the subicular pyramidal cell types, strong bursters are most likely to represent a distinct and stable phenotype. However, this inference is belied by the relative ease with which low threshold bursters (the sharp electrode equivalent of strong bursters) are formed. Approximately 26% of all non-LTB cells are converted into low threshold bursters by a single episode of status epilepticus (Wellmer et al., 2002).

There is some indirect evidence for the stable conversion of bursters to regular firers. We have already suggested that non-adapting regular firing cells exhibit the expected characteristics of suppressed bursters. Additionally, a recent pilocarpine study found that an episode of status epilepticus caused a precipitous decline in the fraction of bursters from 59 to 18% (Knopp, Kivi,

et al., 2005). The 30% cell loss observed in this study is insufficient to account for the drop in the burst fraction, and suggests that a sizable fraction of bursters were converted to regular firers following the seizure. It is probably significant that the duration of the seizure in this study (80 min) was twice that of the Wellmer et al. (2002) study, which showed an increase in the burst fraction.

There is otherwise little direct evidence for stable burster to regular firer conversions. Thus, since there have been no studies, to date, investigating the effects of reduced subicular network activity on the B/R ratio, it is difficult to estimate the rate at which strong bursters are converted to weak bursters or regular firers. It would be interesting to determine the effect of deafferentiation, for example, on the process of burster to regular firer conversion. In any case, it would appear highly unlikely that the strong burster phenotype is immune to the functional adaptation that characterises the operation of the brain.

Furthermore, the notable activity-dependent redistribution of the delayed rectifier in subicular pyramidals following an episode of status epilepticus is suggestive (Misonou, Mohapatra, et al., 2004). Since both ion channel distribution and somatic morphology are stabilised by the cell's cytoskeleton, it would also be interesting to investigate whether changes in the electrophysiological phenotype of subicular cells are accompanied by concomitant alterations in somatic morphology.

As a final point, there is suggestive evidence that the cell type of subicular cells is primarily determined by the input that they receive. A recent report suggests that while synapses formed by CA1 afferents on subicular bursters express a large pre-synaptically initiated LTP, those on subicular regular firers exhibit a smaller post-synaptically initiated potentiation (Behr 2006). Given the evident capacity of strong input to convert regular firing cells into bursters firing, the pre-synaptic locus of the stronger LTP seen by bursters hints that the process of transformation of subicular pyramidals is normally initiated (and possibly maintained) by extrinsic signals. A requirement for synapses of extra-subicular origin is possibly suggested by the finding that there are no differences between cell types in the amplitudes of the excitatory postsynaptic currents (EPSCs) induced by local synapses (Menendez de la Prida 2003).

5.7 Function and regulation of spike frequency adaptation

Experimental and computational studies have suggested a number of roles for spike frequency adaptation (SFA) including stabilisation of cortical synchrony (Crook, Ermentrout, et al., 1998),

novelty detection via decorrelation (Barlow and Foldiak 1989), dynamic coding in the visual cortex (Schwabe, Adorjan, et al., 2001) and firing-mode switching in pattern generating networks (Katz and Frost 1997). Sleep deprivation studies have also linked SFA to both the sleep-wake cycle and hippocampal-dependent learning. Sleep deprived rats display significant deficits in hippocampus-dependent spatial learning tasks but not in amygdala-dependent learning tasks (McDermott, LaHoste, et al., 2003). Significantly, in CA1 pyramidal neurons derived from rats deprived of REM sleep for 72 hours, spike frequency adaptation is twice as strong than in control rats (McDermott et al., 2003). Given the importance of spike phase precession in the hippocampal complex, the increased levels of SFA could have significant ramifications for temporal encoding of spatial and nonspatial information.

Spike frequency adaptation can also transform the neuronal transfer (input-output) function from linear to logarithmic (Engel, Schultens, et al., 1999). Engel et al. (1999) showed how SFA increases the input response range of model neurons by over 2-fold. This change from a linear (proportional) to logarithmic a response means that a unit change in output requires ten-fold increase in stimulus intensity.

The neurotransmitter acetylcholine (ACh) features prominently in a number of major theories of hippocampal population oscillations (Traub, Miles, et al., 1992), learning and memory (Buzsaki 2002; Hasselmo 1999), and the sleep-wake cycle (Graves, Pack, et al., 2001). Acetylcholine is linked to SFA in hippocampal pyramidal neurons via its ability to inhibit the muscarinic potassium current, I_M, (Brown and Adams 1980; Halliwell and Adams 1982) and the slow calcium-activated potassium afterhyperpolarizing current, I_{AHP}, (Cole and Nicoll 1984). Significantly, in subicular cells, Behr et al. (2000) found that the medium and slow AHPs are transiently (<48 h) downregulated by kindling (the phenomenon whereby repeated seizures lower the seizure threshold). Since these AHPs are largely mediated by I_M and I_{AHP} it appears that kindling utilises a mechanism that downregulates the influence of potassium currents on the cells firing rate. Both I_M and I_{AHP} are inhibited by ACh (Halliwell and Adams 1982; MadisonD. V., Lancaster, et al., 1987)

This rapid disinhibition of the discharge rate in regular firers may constitute a requisite stage in the conversion of regular firers into bursters, and may explain why adapting bursters have not been reported in the literature despite the ease with which they are modelled (Figure IV-23C).

The normal inverse correlation between peak magnitude of the slow AHP and the discharge rate of the cell disappears after kindling (Behr, Gloveli, et al., 2000). On this basis, Behr et al.

(2000) concluded that the currents underlying the sAHP and the slowing of the discharge rate are different. However, in our simulations we found that below a certain level of I_{AHP}, the ability of the current to influence the discharge rate declined significantly (data not shown). Since the data of Behr et al., suggests that kindling causes a systematic and substantial drop in the size of the sAHP (their Figure 2C), it seems more likely that the lack of correlation simply reflects a low level of I_{AHP}, rather than the activity of other currents.

5.8 Conclusions

The importance of the subiculum, a pivotal mediator of hippocampal interactions with cortical and subcortical regions (Naber et al., 2000), has only recently begun to be reflected in the amount of attention paid to it by the hippocampal research community. This thesis constitutes a concerted attempt to understand the single cell electrophysiology that subserves the central role of the subiculum. We have explored ionic mechanisms for a wide range of the electrophysiological features exhibited by subicular pyramidal cells that support the functional role of the subiculum as an integrator, comparator, and distributor.

Naber et al. (2000) argued that the subiculum occupies a central position within the hippocampal learning and memory system. The subiculum is therefore noteworthy with regard to the high level of convergent inputs and divergent outputs that it handles. We argue that the evidence indicates that the expression of EPFs in subicular pyramidal cells reflect the demands this places upon the subiculum. Specifically, the organising hypothesis for this thesis has been the claim that within the subiculum there is only a single electrophysiological class of subicular pyramidal cell and that the particular properties of any given subicular pyramidal are largely brain state-dependent. In other words, the level of cellular plasticity within the subiculum is such that any particular SPC subtype can, in principle, be dynamically converted to any other SPC. Since pyramidal cell subtypes are defined by the level of expression of various EPFs, the claim for a universal SPC is equivalent to the claim that EPF expression in subicular cells is adaptive.

We have examined, in some detail, the mechanisms by which subicular cellular plasticity might be expressed but have paid attention to three EPFs in particular, frequency preference, bursting, and spike frequency adaptation.

5.8.1 Frequency preferences and selective communication

Our analysis of subicular frequency preferences suggests that SPCs, unlike CA1 pyramidals, exhibit resonance at hyperpolarized, rest and depolarized potentials. Since, resonance levels influence the level of entrainment of a cell with population oscillations, subicular pyramidals appear to be well suited to participating in population oscillations, particularly theta, at a variety of depolarization states. Furthermore, the kinetics of I_M, the current responsible for putative subicular M-resonance, are subject to modulation by a range of factors that reflect network activity including the level of internal calcium (Tokimasa, Shirasaki, et al., 1996) and metabotropic glutamate receptor activation (Ikeda, Lovinger, et al., 1995). The level of expression of M-resonance in subicular pyramidals, and therefore the level of subicular entrainment, would appear to be subject to adaptive regulation.

Selective resonant communication constitutes a potential mechanism through which membrane resonance can be used by the subiculum to differentially coordinate its inputs and outputs. The suggested ability of subicular bursters to tailor the burst type to the prevailing population oscillation is relevant in this regard.

5.8.2 Adaptive two-component burst model and population oscillations

The adaptive two-component burst model provides a framework for understanding the regulation of burst expression within the subiculum. We have furnished models of, and gathered empirical support for, the existence of functional variations in burst length, and the amplification and suppression of bursting. As implemented in this thesis, the theory provides insight into a wide of aspects of subicular electrophysiology including the high level of variation in the B/R ratio reported in the literature, the prevalence of spike doublets during gamma, the behaviour of SPCs during different population oscillations, and the frequency-dependence of firing mode.

One significant way in which bursting is linked to frequency preference is through the influence of theta phase on the magnitude and sign of synaptic plasticity induced by bursts both within the subiculum and in its downstream targets. This linkage highlights a feature of adaptive EPFs that is likely to be important in understanding brain operation - their interrelatedness. The claim that EPF expression in subicular cells is adaptive opens up the possibility of integrated regulation of EPF expression at a variety of levels of control.

5.8.3 Spike frequency adaptation

The ability of SFA to regulate the discharge rate of the cell enables this EPF to act as a governor of overall levels of excitability within the subiculum. By forcing a neuron to progressively adapt to strong stimulation, SFA can potentially forestall the feed-forward cascade of cellular plasticity that leads to the expression of constitutive bursting. Alternatively stated, we hypothesise that SFA acts to control the size of the population of non-bursters that are available for recruitment as bursters. The fact that regular firers can be partitioned into adapting and non-adapting populations, the high level of variation in the expression of SFA across studies, and the apparent lack of adapting bursters (suggesting that downregulation of SFA appears to be an early step in the pathological transition from regular firers to bursters) lends credence to this view.

Obviously, although the detailed arguments presented in this thesis are specific to the subiculum, many of these arguments have a more general significance regarding the operation of other brain regions. In any case, we believe that there is sufficient evidence to view the subiculum as a potentially highly adaptive structure. What is lacking, however, is an understanding of the timescales over which these changes take place, and the nested control systems that modulate these changes. With the notable exception of the sleep-wake cycle, most of the evidence presented here is a reflection of the impact of extreme conditions, such as status epilepticus. Furthermore, little is known about how adaptive EPF expression interacts with synaptic plasticity, synaptogenesis, neurogenesis and a range of other manifestations of brain plasticity. What is also lacking is an appropriate empirical framework within which these issues can be effectively addressed. The feature-based analysis, outlined in the next section, is presented as a pragmatic conceptual framework designed to redress this deficit.

5.9 A modest proposal: feature-based electrophysiological analysis

The immense structural and dynamical complexity of the brain dictates that the ultimate goal of neuroscience must be a computational model of the human brain and nervous system (Mel 2000). The construction of computational models forces into the open the assumptions that underpin the mental models that embody our understanding of the brain. Computational models allow us to explicitly test the implications of our assumptions and theories. The operation and structure of the brain are characterised by interrelationships of staggering complexity at all levels of brain organisation. Consequently, attempts to gather electrophysiological facts should ideally be governed by principles that maximise the discovery of relationships between those facts.

These revealed relationships and principles form the substrate upon which progressively more coherent models, both mental and computational, are constructed.

The quality of neuroscientific models, both mental and computational, is constrained by the quality of the available data. This data, in turn, is constrained by the conceptual frameworks that govern its collection. In reviewing the nature of the available subicular electrophysiological data in terms of its suitability for constructing neuronal models, we have come to a surprising conclusion. Namely, that the conventional approach to gathering and organising intracellular electrophysiological data around cell types is fundamentally flawed.

In this section, we argue that deeper insights into the function and behaviour of brain areas, such as the subiculum, are more likely to come from explicitly unveiling the evolving correlations between the electrical and physiological features of neurons than from the assiduous collation of cell types. In other words, we suggest that questions such as 'what are the functions of bursting cells?' potentially forestall many productive lines of inquiry and may actually retard progress in developing a functional understanding of the brain. A key question, in this context, is whether the act of defining canonical cell types, such as bursters and regular firers, serves to aid or hinder conceptual understanding of the operation and function of the subiculum, in particular, and the brain, in general.

Central to answering this question is the prosaic recognition that the functional properties of a cell are determined by its level of expression of various electrophysiological features (EPFs), such as bursting and SFA. A 'cell type' is thus convenient shorthand for referring to a particular co-varying cluster of EPFs. Thus, a subicular bursting cell, for example, is not only expected to exhibit bursting, but is also generally expected to exhibit other features, such as a non-adapting regular spike train, a negligible slow afterhyperpolarization, and rebound firing.

However, without detailed prior knowledge of the functional interactions of EPFs, cell types only represent a rather uninformed 'best guess' as to the most important functional correlations between a limited set of EPFs. Therefore, although the cell-type approach tacitly acknowledges the importance of EPFs and their correlations, it treats them in a haphazard and unsystematic manner. Cell types represent, in effect, the outcome of a crude intuitive principal components analysis of EPFs.

These arguments obviously apply equally to the dynamic physiological features of neurons, such as soma morphology, soma size, and dendritic arborisation. Consequently, the idea that cell

types are not necessarily the most useful, or reliable, categories is given credence by the finding that estimates of the percentage of bursting cells in the subiculum are strongly dependent on the morphological sampling techniques employed (Menendez de la Prida et al., 2002; Greene and Totterdell, 1997).

An important fact, that has a direct bearing on the utility of cell types, is that the expression of EPFs in a particular cell, and therefore across a region, can vary substantially as a function of brain state. For instance, the level of subicular bursting alters dramatically during the sleep-wake cycle (Staba, Wilson, et al., 2002). Stated otherwise, EPFs are not a fixed property of the cell. The cell type approach, with its static categories, is a poor conceptual system for handling such dynamic variation.

Another obvious characteristic of the brain, intimately related to the aforementioned dynamic variation, is the sheer range of variability in the levels of expression of electrophysiological features in brain structures. Conventionally, this variation is expressed in relation to particular cell types. Hence, for example, principal cells within the subiculum are classified into bursting and regular firing cell types and the magnitude of the slow afterhyperpolarization is then reported for each class of cells as an average along with the associated standard deviation (or error).

The conspicuous feature of this approach is the low information content of the final analysis. A large amount of potentially insightful information concerning how EPFs correlate within, and between, cells is lost. By treating bursting propensity, for example, as a cell type category, rather than as a variable, the opportunity to explore the nature of its relationships with other EPFs is squandered. Furthermore, since a cell type effectively represents a poorly defined cluster of EPFs, several other dimensions are similarly constrained. As a result, the innate electrophysiological heterogeneity of the brain is belied by the 'representative' averages and voltage traces typically presented in published papers. This outcome is hardly surprising since, from the cell type-based perspective, such biological variation is essentially viewed as a source of noise that confounds the identification of canonical cell types. However, it seems probable that these maligned patterns of variation are likely to be more revealing of the principles of brain function than the ad hoc cell types that are routinely imposed on electrophysiological data. Indeed, within the feature-based perspective, the quantification and characterisation of this variation is considered key to developing a deep understanding of brain function.

Further evidence that cell type analysis is an inefficient framework for analysing and representing electrophysiological data is the routine disposal of so called 'unclassified' cells - that

significant fraction of cells that do not fit preconceived categories. With the exception of experimental artefacts, unclassifiable cells are, by definition, neurons that exhibit clusters of EPF values that have not been labelled as a cell type. Unsurprisingly, these 'ostracised' cells are readily accommodated by the feature-based approach, since it is only the patterns of EPF expression levels and their correlations that are of principal interest.

The pantheon of subicular cell types has undergone progressive subdivisions. The original subicular cell categories of regular and burst firers (Mason, 1993; Stewart and Wong, 1993) have since been separated into weak and strong bursters (Staff et al., 2000), and tonic and adapting regular firers (Menendez de la Prida et al., 2003). A subtype of regular firers, MPOs, exhibiting pronounced membrane potential subthreshold oscillations has also been identified (Menendez de la Prida et al., 2003). The rate of cell type proliferation is likely to increase substantially with the advent of functional genomics approaches to neuronal cell typing (Sugino, Hempel, et al., 2006).

The alternative feature-based approach is a systematic conceptual framework for analysing and representing electrophysiological data that emphasises the instantaneous and dynamical correlations between EPFs, on both the single cell and population levels. Briefly, whereas the cell type approach examines the correlations of EPFs with particular cell types, the feature-based approach entails quantifying the levels of EPF expression (such that each EPF can be then be treated as a cell variable or dimension) and then analysing the static and dynamic correlations between the EPFs themselves.

Each EPF, when quantified using an index, represents a dimension upon which any neuron can be placed. The 'full' set of EPFs constitutes a hyperdimensional EPF state space, within which each particular neuron represents a point. Since the expression of many EPFs change with changing brain state, a particular cell will follow a defined trajectory through this state space as it is modulated. Some of these EPFs, such as burst strength and anodal break potential amplitude, co-vary to some extent (Menendez de la Prida et al., 2003). Other, such as spike frequency adaptation and spontaneous firing propensity, apparently do not (Wozny et al., 2005). As a result, the nature of the correlations between EPFs will constrain the possible trajectories a particular cell can take. It is also likely that, as brain state changes, certain EPF correlations will vary in magnitude and direction.

An extensive armoury of well-established techniques is available for implementing the feature-based approach. Potential methods include EPF scatter plots and waterfall graphs, single cell EPF histograms, EPF probability distributions, correlation matrices, and principal components

analysis. Many of these approaches, of course, have already been applied to the analysis of intracellular data (Staff et al., 2000; Jung et al., 2001; Staba et al., 2002; Menendez de la Prida et al., 2002, 2003; Cooper et al., 2005), but usually in a manner constrained by the cell type approach. In addition, there is ample scope for the development of novel graphical and mathematical techniques for exploring the nature of EPF relationships.

The claim for the superior utility of feature-based analysis rests on the assumption that the quantification and correlation of EPFs is central to understanding brain function. Stated otherwise, fundamental information about brain operation is contained in the magnitude, direction, and evolution of EPF correlations. As noted above, this view is uncontentious since it is implied, although not coherently implemented, by the conventional cell type-based approach. In contrast, the feature-based approach provides a convenient conceptual framework for cogently accommodating the remarkable level of static and dynamical electrophysiological variation present in the subiculum and other brain structures. Although this variation is present on both single cell and population levels, similar feature-based techniques can be applied to both levels.

Feature-based analysis also offers the possibility of linking different vertical levels of brain organisation in a functionally meaningful manner. Going up, a straightforward example is the linking of population doublets with the firing of subicular bursting cells (Stanford et al., 1998). A related instance is the correlation of single neuron bursts/min with stage of the sleep wake cycle by Staba et al. (2002). At a deeper level, shared ion channels link the mechanisms of many electrophysiological features. For instance, the slow afterhyperpolarization and spike frequency adaptation are both dependent on the slow calcium-dependent potassium current, I_{AHP}. As a result, identifying EPF correlations may shed light on hitherto unsuspected integrated ionic mechanisms and control systems. The ability of feature-based analysis to uncover correlations within, and between, levels of brain organisation open up novel prospects for understanding brain function. More subtle and extensive correlations of brain states, population activity parameters, single-cell EPFs, and channel activity await discovery.

There is a welcome trend in the literature towards greater quantification of EPFs using indexes (Staff et al., 2000; Jung et al., 2001; Wozny et al., 2002; Menendez de la Prida, 2002; Menendez de la Prida et al., 2003; Cooper et al., 2005). Even burst propensity is submitting to more refined graduations. For example, Su et al. (2001) defined four levels of bursting in CA1; high threshold bursting and three grades of low threshold bursting (although perhaps a less subjective measure, such as the size of the afterdepolarization, is more suitable for the purposes of feature-based

analysis). Unfortunately, the sustained focus on the characterisation of cell types continues to impede the systematic application of powerful graphical and formal correlation analysis techniques to neuronal electrophysiology.

Within the feature-based framework, the notion of a cell type largely disappears and is replaced by evolving patterns of contingent correlations between electrophysiological features. With correlational analysis, we can begin to delineate the volumes of state space, or orbits, permissible to cells during normal and pathological brain states. Further advances in experimental techniques will confer the ability to follow changes in EPF expression in the freely behaving animal. Gradually, the rules governing the dynamical deformation of these volumes, as a function of brain state, will begin to be revealed. Ultimately, we suggest, the feature-based approach will facilitate the discovery of deep principles of brain organisation and function that are simply beyond the power of the cell type-based approach to uncover.

Chapter VI
FUTURE RESEARCH

Our theories determine what we measure.

Albert Einstein (1879-1955)

The present models constitute the opening phase of the development of a large-scale biophysically realistic model of the mammalian subiculum. Naturally, there are a number of model refinements and extensions that are planned on the channel, cellular and network levels.

6.1 I_{CT} model

The inability of the model to adequately replicate the contribution of I_{CT} to the fast and medium AHPs is due to the limitations of the present model for I_{CT}. In addition, the relatively slow repolarization time is also partially attributable to the I_{CT} model. Future research will address this problem.

6.2 I_{NaF} and I_{NaP} models

During a subicular burst there is usually a progressive increase in the spike threshold of successive spikes. However, the bursts generated by our model did not accurately reflect this trend and usually displayed a decreasing threshold following the second spike. This phenomenon can partially be traced to the I_{NaF} Markov model employed in this study. The design of this current model is such that, within a burst, the second spike threshold is likely to be the highest. This occurs because the high threshold closed state is preferentially entered from the open state, prior to lower threshold closed states. The effects of graded thresholds on future models will be assessed in more detail.

Based on the model responses, we concluded that the persistent sodium current primarily drives the early burst component. However, as reviewed previously, there is indirect evidence that the subicular fast and persistent sodium currents are due to different conduction modes of the same channel. The nature of the biophysical basis for the fast and persistent sodium currents of the hippocampal complex has implications for understanding sodium current regulation in normal and pathological conditions. In order to investigate this issue further, we will develop a

Markov model of the sodium channel that exhibits both transient and persistent modes. The slow peak rate of rise of action potentials, compared to empirical values, produced by the present Markov fast sodium model will also be addressed.

6.3 Calcium current dependencies

In our model the relative contribution of the various calcium currents to the late burst component is comparatively arbitrary. Plausible assumptions were made regarding the contributions of different calcium channel classes and a constrained and trial error process lead to the final non-unique configuration. A more coherent approach awaits more detailed analysis and future experimental research.

6.4 Muscarinic-activated non-specific cation current, I_{NCM}

Application of acetylcholine agonists to subicular pyramidals evokes large plateau potentials apparently mediated by a latent cation current. In order to investigate the effects of cholinergic afferents on the subiculum, future simulations will include a model of I_{NCM}.

6.5 Burst ADP behaviour

Bursts longer than three spikes did not exhibit the characteristic rising firing threshold found *in vivo*. It may be that the dendritic reflux current is required to amplify the ADP. This issue will be investigated in the spatially extended model. Further, although there was a realistic decrement in spike amplitude, there was not a significant decrease in spike width. This deficiency is related to the I_{CT} model.

6.6 Subthreshold oscillations

Although, we managed to simulate theta-range subthreshold oscillations the instability of the oscillations was unrealistic. A more extensive modelling investigation of this phenomenon is warranted - especially in the context of possible resonant communication in the subiculum.

6.7 Spatially distributed electrophysiological events

The present work used a single compartment to model the morphology of subicular neurons and therefore necessarily focused on spatially discrete processes. However, many important neuronal information-processing events, such as those involving learning, require interactions between spatially segregated ionic mechanisms. One specific example is the mechanism by which

dendrites facilitate sustained gamma frequency doublets in response to 40 Hz EPSPs (Stanford et al., 1998). Future modelling efforts will be directed towards investigating and developing subicular and hippocampal cell models with more realistic neuronal morphologies. It should also be noted that depolarization-inactivated bursters are still capable of responding to orthodromic stimuli with a burst (Stewart, 1997). This behaviour suggests the presence of a dendritic burst mechanism similar to the 'burst firing dendrites' identified by Greene and Totterdell (1997).

6.8 Brain state dependent regulation of neuronal activity

As explored in the discussion, neuronal ion channels are subject to a wide range of modulatory controls. Neurotransmitters and modulators such as dopamine, serotonin, noradrenaline and somatostatin alter the response characteristics of subicular ion channels. The next step in the development of biophysically plausible ion channel models is the incorporation quantitative neuroeffector sensor functions. Incorporation of such functions into the activation and inactivation rate functions of our ion channel models would allow more realistic simulation of the effect of multiple types of afferent stimulation on subicular single cell and network activity.

6.9 Adaptive conductances and phenomenological templates

Electrophysiological behaviours arise as a consequence of particular patterns of channel distributions. Finding appropriate patterns is generally the most tedious and time-consuming aspect of biophysical neuronal modelling. One of the reasons that the currents chapter is so long is that we felt that a careful reading of the literature would provide a set of modelling constraints sufficient to dramatically reduce the level of trial and error needed to converge on a robust working model. Whilst this approach was generally very successful, it operates at a relatively low level of abstraction, that of individual currents. Empirical and modelling work on adaptive conductances suggests that the expression levels of a neuron's complement of ion channels vary in an integrated manner in response to ongoing neuronal activity (LeMasson, Marder, et al., 1993; Golowasch, Abbott, et al., 1999). For example, there appears to be a systematic relationship between the levels of subicular I_{AHP} and I_D since they appear to co-vary across regular and bursting cells. This level of coordination implies the existence of higher-order control mechanisms that operate on 'cassettes' of currents. An interesting future research project would be to explicate the abstract functional heuristics and conservation rules that underpin the high-order genetic and biochemical control mechanisms used by the neuron to regulate the

activity of whole sets of currents. This is an aspect of the aforementioned 'feature-based' approach to intracellular electrophysiology.

6.10 Large-scale network simulations

There is a growing body of high-quality research elucidating the properties and behaviour of the pyramidal and interneuron networks of the subiculum. Unfortunately, time constraints prevented the extension of this work to include the simulation of large networks of subicular neurons. Future work will remedy this deficit.

6.11 Learning and adaptive synapses

A natural corollary to the previous point is the development of synapse models in order to investigate learning and memory in simulated subicular networks.

6.12 Cellular automata

The ability of subicular pyramidal neurons to switch firing modes (Cooper et al., 2005), in conjunction with the observation that subicular microcircuits are dynamically composed (Menendez de la Prida and Gal, 2004), is suggestive of the behaviour of von Neumann's cellular automata (Marchal 1998) as emulated in Conway's 'Game of Life (Gardiner 1970). The Game of Life consists of a fixed grid of cells, each of which can exist in one of two states, commonly designated 'alive' or 'dead'. The state of each cell is determined by the state of the surrounding cells according to a very small set of simple rules e.g. a cell with two or three neighbouring cells survives for the next generation but dies if surrounded by four or more. With every time step the states of all the cells are updated according to such rules.

The remarkable feature of the Game of Life is that complex self-sustaining patterns can emerge from the application of these simple transformation rules to a starting configuration of cell states. One common pattern (or 'reaction') known as the glider, flows across the grid maintaining its form, even though the identity of its constituent cells changes as it moves.

The firing modes of subicular pyramidals are comparable to the cell states of the Game of Life. It would be fascinating to investigate the possibility that high-order, self-organised microcircuit patterns, analogous to the reactions found in the Game of Life, emerge and propagate in the subiculum.

Appendix A

Simulation code for the universal cell model

```
# UNIVERSAL SUBICULAR CELL FRAME

# Written by David Delany 2005/6
# PhD SUBICULAR PRINCIPAL CELL MODEL

# CHANNELS: INaF,INaP,IDR,IA,ID,IM,IAHP
# CHANNELS: ICT,ICaT,ICaR,ICaL,ICaP/Q,ICaN,IH

# UNITS: millivolts, milliseconds, nanofarads, nanoamps
# UNITS: microns, microsiemens, molar

# CELL MODEL

# Effective Surface Area=33333 um2
# Actual Surface Area=1550 um2
par Cap=.31,ENa=65,EK=-90

V'=(I-Ileak-Imodel+istep)/Cap
2V=(I-Ileak-Imodel+istep)/Cap

# CURRENT CLAMP

par I=0,imp=0.35,t_on=150,t_dur=45,freq=1
interval=1000/freq
t_onii=t_on+interval
t_oniii=t_onii+interval
t_oniv=t_oniii+interval
t_onv=t_oniv+interval

istepi(t)=imp*heav(t-t_on)*heav(t_on+t_dur-t)
istepii(t)=imp*heav(t-t_onii)*heav(t_onii+t_dur-t)
istepiii(t)=imp*heav(t-t_oniii)*heav(t_oniii+t_dur-t)
istepiv(t)=imp*heav(t-t_oniv)*heav(t_oniv+t_dur-t)
istepv(t)=imp*heav(t-t_onv)*heav(t_onv+t_dur-t)

istep=istepi(t)+istepii(t)+istepiii(t)+istepiv(t)+istepv(t)
aux i=I+istep

# PASSIVE LEAK CURRENT

par gleak=0.0167,shunt=0,Eleak=-70
Ileak=(gleak+shunt)*(V-Eleak)
aux i_leak=ileak
#Shunt 60 MOhm -> 41 MOhm (Behr): add 0.0077 uS
```

```
#Shunt 60 MOhm -> 21 MOhm (Mattia): add 0.03095 uS

# SODIUM CURRENTS

# FAST SODIUM CURRENT, NaF 5-STATE MARKOV MODEL

INaF=NaF_GMAX*Open*(V-ENa)

Open'=Ciii_O*Close_iii+Cii_O*Close_ii+Ci_O*Close_i-Open*(O_Ciii+O_Cii+O_Ci+O_I)
Close_iii'=Cii_Ciii*Close_ii+O_Ciii*Open-Ciii_O*Close_iii
Close_ii'=Ci_Cii*Close_i+O_Cii*Open-Close_ii*(Cii_Ciii+Cii_O)
Close_i'=I_Ci*(1-Close_iii-Close_ii-Close_i-Open)+O_Ci*Open-Close_i*(Ci_Cii+Ci_O)

# State transition rate functions
Ciii_O=3/(1+exp((V-(Ciii_O_Vh))/(-1)))
Cii_O=3/(1+exp((V-(Cii_O_Vh))/(-1)))
Ci_O=3/(1+exp((V-(Ci_O_Vh))/(-1)))
O_I=O_I_rate
O_Ci=3/(1+exp((V-(O_Ci_Vh))/2))
O_Cii=3/(1+exp((V-(O_Cii_Vh))/2))
O_Ciii=3/(1+exp((V-(O_Ciii_Vh))/2))
I_Ci=1/(1+exp((V-(I_Ci_Vh))/1))
Ci_Cii=1/(1+exp((V-(Ci_Cii_Vh))/1))
Cii_Ciii=1/(1+exp((V-(CiiCiiiVh))/1))

par O_I_rate=3,O_Ciii_Vh=-57,O_Cii_Vh=-51,O_Ci_Vh=-49
par I_Ci_Vh=-40,Ci_O_Vh=-39,Cii_O_Vh=-42,Ciii_O_Vh=-51
par Ci_Cii_Vh=-55,CiiCiiiVh=-60

par NaF_GMAX=2
aux NaF_g=NaF_GMAX*Open
aux I_NaF=INaF
aux Inactiv=1-Close_iii-Close_ii-Close_i-Open

#PERSISTENT SODIUM CURRENT, INaP

INaP=NaP_GMAX*NaP_m^NaP_expo*NaP_h*(V-ENa)

NaP_m'=(NaP_m_inf-NaP_m)/NaP_m_tau
NaP_m_inf=1/(1+exp((V-NaP_Vhalf)/NaP_Slope))

NaP_F_tau=(exp((V+23.5)/24.1))/(1+exp((V+35.2)/12.5))
NaP_S_tau=NaP_Slow
NaP_m_tau=if(heav(2V))then(NaP_F_tau)else(NaP_S_tau)

NaP_h'=(NaP_h_inf-NaP_h)/NaP_h_tau
NaP_h_inf=1/(1+exp((V-(-57.4))/5.6))
NaP_h_tau=1/((0.003*exp((V+103.1)/89.1))+exp((V+190)/(-29.5)))
```

```
par NaP_Slow=0.5
par NaP_GMAX=0.019
par NaP_Vhalf=-55.3,NaP_Slope=-6.4,NaP_expo=2
aux i_NaP=INaP
aux g_NaP=NaP_GMAX*NaP_m^NaP_expo*NaP_h
aux NaP_tau=NaP_m_tau
init NaP_h=0.852

# SUMMED SODIUM CURRENTS
INa=INaF+INaP
aux I_Na=INa

# POTASSIUM CURRENTS

# IDR - DELAYED RECTIFIER CURRENT
IDR=IDR_GMAX*IDR_m^4*(V-EK)
IDR_m'=(IDR_m_inf-IDR_m)/IDR_tau
IDR_m_inf=1/(1+exp((V-Vhalf_IDR)/Slope_IDR))

IDR_tau=(exp((V+256.1)/162.2))/(1+exp((V+12.4)/38.9))

par IDR_GMAX=0.4,Vhalf_IDR=-35.6,Slope_IDR=-10.2
aux i_DR=IDR
aux g_DR=IDR_GMAX*IDR_m^4
init IDR_m=0.038

# FAST TRANSIENT K CURRENT, IA

IA=GMAX_IA*IA_m^IA_expo*IA_h*(V-EK)

IA_m'=(IA_m_inf-IA_m)/IA_m_tau
IA_m_inf=1/(1+ exp((V-(IA_Vhalf))/(IA_Slope)))
IA_m_tau=IA_activ*(exp((V-5)/54))/(1+exp((V-10)/24.9))

IA_h'=(IA_h_inf-IA_h)/IA_h_tau
IA_h_inf=1/(1+exp((V-(-59.5))/5.8))
IA_h_tau=(exp((V+420.0)/60.0))/(1+exp((V+185.1)/45.9))

par GMAX_IA=0.1,IA_expo=1
par IA_VHalf=-20.1,IA_Slope=-6.3,IA_activ=1
i_A=IA
aux g_A=GMAX_IA*IA_m^IA_expo*IA_h
init IA_h=0.82

# IM - MUSCARINIC K CURRENT

IM=IM_GMAX*IM_m*(V-Ek)
IM_m'=(IM_m_inf-IM_m)/IM_tau
IM_m_inf=1/(1+exp((V-IM_Vhalf)/IM_Slope))
```

```
IM_tau=1/((0.004*exp((V+126.5)/126.1))+exp((V+170.4)/(-20.9)))

par IM_GMAX=0.07,IM_Vhalf=-53.5,IM_Slope=-2.9
aux i_M=IM
aux g_M=IM_GMAX*IM_m

# FAST DELAY CURRENT, ID

ID=ID_GMAX*ID_m^ID_expo*ID_h*(V-Ek)

ID_m'=(ID_m_inf-ID_m)/ID_m_tau
ID_m_inf=1/(1+exp((V-(ID_Vhalf))/(ID_Slope)))
ID_m_tau=(exp((V+93.2)/105.2))/(1+exp((V-7.5)/35.1))

ID_h'=(ID_h_inf-ID_h)/ID_h_tau
ID_h_inf=1/(1+exp((V-(-82.1))/5.5))
ID_h_tau=ID_tau/(1+exp((V-(-35))/15.5))

par ID_tau=500
par ID_GMAX=0
aux i_D=ID
aux g_D=ID_GMAX*ID_m^ID_expo*ID_h
par ID_Vhalf=-52,ID_Slope=-4,ID_expo=1
init ID_h=0.07

# TRANSIENT CALCIUM-DEPENDENT K CURRENT, ICT

ICT=CT_GMAX*CT_m*CT_h*(V-EK)

#200-800 nM [Ca,1] activation range
CT_m'=(CT_m_inf-CT_m)/CT_m_tau
CT_m_inf=(1/(1+exp((log10(Cai)-(-6.5))/(-0.1))))/(1+exp((V-(CT_Vhalf))/(CT_Slope)))
CT_m_tau=(exp((V-10.0)/995.1))/(1+exp((V-450.0)/134.9))

CT_h'=(CT_h_inf-CT_h)/CT_h_tau
CT_h_inf=1/(1+exp((V-(-50.0))/7.3))
CT_h_tau=(exp((V+78.1)/9.5))/(1+exp((V+47.0)/7.8))

par CT_GMAX=0,CT_Vhalf=-30,CT_Slope=-3.3
aux I_CT=ICT
init CT_h=0.92

# SLOWLY ACTIVATING Ca-DEPENDENT POTASSIUM CURRENT, IAHP

IAHP=AHP_GMAX*AHP_m*(V-EK)

# 55-120 nM [Ca,1] activation range
AHP_m'=(AHP_m_inf-AHP_m)/AHP_m_tau
AHP_m_inf=1/(1+exp((log10(Caii)-(AHP_Vhalf))/(AHP_Slope)))
```

```
par AHP_Vhalf=-5.9,AHP_Slope=-0.05
par AHP_GMAX=0,AHP_m_tau=100
aux I_AHP=IAHP
aux AHP_g=AHP_GMAX*AHP_m

# SUMMED POTASSIUM CURRENTS

IK=IDR+ID+IA+IM+IAHP+ICT
aux I_K=IK

# CALCIUM CURRENTS

# FAST TRANSIENT CA CURRENT, ICaT

ICaT=CaT_PMAX*CaT_m^expo*CaT_h*GHKi

CaT_m'=(CaT_m_inf-CaT_m)/CaT_m_tau
CaT_m_inf=1/(1+exp((V-(CaT_Vhalf))/(CaT_Slope)))
CaT_m_tau=-0.3*(-1.1-exp(-0.03*V))

CaT_h'=(CaT_h_inf-CaT_h)/CaT_h_tau
CaT_h_inf=1/(1+exp((V-(CaT_Vh))/6.0))
CaT_h_tau=(201.0/(1+exp((V-(-69.1))/4.5)))+15.0

par CaT_Vh=-80
par CaT_PMAX=0
par CaT_Vhalf=-45.1,CaT_Slope=-4,expo=1
aux I_CaT=ICaT
init CaT_h=0.12

# FAST TRANSIENT CA CURRENT, ICaN

ICaN=CaN_PMAX*CaN_m^CaN_expo*CaN_h*GHKi

CaN_m'=(CaN_m_inf-CaN_m)/CaN_m_tau
CaN_m_inf=1/(1+exp((V-(CaN_Vhalf))/(CaN_Slope)))
CaN_m_tau=(exp((V-0.5)/120.0))/(1+exp((V+50.6)/80.1))

CaN_h'=(CaN_h_inf-CaN_h)/CaN_h_tau
CaN_h_inf=1/(1+exp((V-(CaN_Vh))/6.0))
CaN_h_tau=150/(1+ exp((V-(-20))/30))

par CaN_Vh=-48.6
par CaN_PMAX=0
par CaN_Vhalf=-24.8,CaN_Slope=-9.5,CaN_expo=2
aux I_CaN=ICaN

init CaN_h=0.96
```

```
# HIGH THRESHOLD, SLOWLY INACTIVATING CALCIUM CURRENT, ICaP/Q

ICaP=CaP_PMAX*CaP_m*GHKi
CaP_m'=(CaP_m_inf-CaP_m)/CaP_m_tau
CaP_m_inf=1/(1+ exp((V-(CaP_Vhalf))/(CaP_Slope)))
CaP_m_tau=(exp((V+119.5)/53))/(1+exp((V+70.1)/42.9))

par CaP_PMAX=0
par CaP_Vhalf=-1.0,CaP_Slope=-7.1

# HIGH THRESHOLD NONINACTIVATING CALCIUM CURRENT,IL

ICaL = CaL_PMAX*CaL_m^2*GHKi

CaL_m'=(CaL_m_inf-CaL_m)/CaL_m_tau
CaL_m_inf=1/(1+ exp((V-(CaL_Vhalf))/(CaL_Slope)))
CaL_m_tau=(exp((V+59.5)/55.5))/(1+exp((V+20.6)/28.4))

par CaL_PMAX=0
par CaL_Vhalf=-14.5,CaL_Slope=-7.5
aux I_CaL=ICaL

# RESIDUAL CALCIUM CURRENT, ICaR

ICaR=CaR_PMAX*CaR_f*CaR_s*Car_h*GHKi

CaR_f'=(CaR_m_inf-CaR_f)/CaR_f_tau
CaR_f_tau=(exp((V-224.0)/110.2))/(1+exp((V-94.3)/18.9))

CaR_s'=(CaR_m_inf-CaR_s)/CaR_s_tau
CaR_s_tau=3.0*exp(-0.03*V)

CaR_m_inf=1/(1+ exp((V-(-14.5))/(-6.4)))

Car_h'=(CaR_h_inf-CaR_h)/CaR_h_tau
CaR_h_inf=1/(1+ exp((V-(-65))/5.5))
CaR_h_tau=(exp((V+370.6)/70.1))/(1+exp((V+55.5)/41.5))

par CaR_PMAX=0
aux I_CaR=ICaR

# GOLDMAN HODGKIN KATZ EQUATION

# Faraday constant, F, coulombs/mole; Valency, z - unitless; Volume, Vol, um^3
number Faraday=96485,GasR=8.3147,TempAbs=273.14,z=2
par Ca_out=2e-3,Ca_min=50e-9,Temp=33,Area=1550

GHKi=0.001*z*Faraday*GHK_frag*(Cai-Ca_out*exp(-GHK_frag))/(1-exp(-GHK_frag))
```

```
GHKii=0.001*z*Faraday*GHK_frag*(Caii-Ca_out*exp(-GHK_frag))/(1-exp(-GHK_frag))
GHK_frag=0.001*z*V*Faraday/(GasR*(TempAbs+Temp))
aux GHKi=GHKi
aux GHKii=GHKii

# CALCIUM POOLS

# Ca1, Fast submembrane pool
par beta1=0.5,Depth1=1
Cai'=(-0.00518*0.1*ICa/(Area*Depth1))-(beta1*(Cai-Ca_min))
init Cai=50e-9

# Ca2, Slow cytoplasmic pool
par beta2=0.004,Depth2=5
Caii'=(-0.00518*0.9*ICa/(Area*Depth2))-(beta2*(Caii-Ca_min))
init Caii=50e-9

# SUMMED CALCIUM CURRENTS

ICa=ICaT+ICaP+ICaL+ICaN+ICaR
aux I_Ca=ICa

# HYPERPOLARISATION-ACTIVATED INWARD RECTIFIER, IH

IH=IH_GMAX*IH_m*(V-EH)
IH_m'=(IH_m_inf-IH_m)/IH_tau
IH_m_inf=1/(1+exp((V-(-76))/5))
#IH_tau=60.0/(1+exp((V+70.0)/8.0))
IH_tau=(exp((V+125)/9.6))/(1+exp((V+84)/8))

par IH_GMAX=0.007,EH=-43
aux i_H=IH
aux g_H=IH_GMAX*IH_m
init IH_m=0.17

# SUMMED ACTIVE CURRENTS

Imodel=INa+IK+ICa+IH

# INTEGRATOR SETTINGS

@ total=200,dt=.5,meth=qualrk,atoler=1e-4,toler=1e-5,bound=1e10
@ xlo=140,xhi=200,ylo=-100,yhi=50
@ MAXSTOR=1000000
init V=-67.4
done
```

References

1. Abel HJ, Lee JC, Callaway JC, Foehring RC (2004) Relationships between intracellular calcium and afterhyperpolarizations in neocortical pyramidal neurons. J.Neurophysiol. 91:324-335.

2. Aggleton JP, Keith AB, Rawlins JN, Hunt PR, Sahgal A (1992) Removal of the hippocampus and transection of the fornix produce comparable deficits on delayed non-matching to position by rats. Behav.Brain Res. 52:61-71.

3. Agrawal N, Alonso A, Ragsdale DS (2003) Increased persistent sodium currents in rat entorhinal cortex layer V neurons in a post-status epilepticus model of temporal lobe epilepsy. Epilepsia 44:1601-1604.

4. Ahern GP, Hsu SF, Klyachko VA, Jackson MB (2000) Induction of persistent sodium current by exogenous and endogenous nitric oxide. J Biol Chem 275:28810-5.

5. Aiken SP, Lampe BJ, Murphy PA, Brown BS (1995) Reduction of spike frequency adaptation and blockade of M-current in rat CA1 pyramidal neurones by linopirdine (DuP 996), a neurotransmitter release enhancer. Br. J. Pharmacol. 11:1163-1168.

6. Akopian A, Johnson J, Gabriel R, Brecha N, Witkovsky P (2000) Somatostatin modulates voltage-gated K(+) and Ca(2+) currents in rod and cone photoreceptors of the salamander retina. J.Neurosci. 20:929-936.

7. Alkadhi KA, Tian LM (1996) Veratridine-enhanced persistent sodium current induces bursting in CA1 pyramidal neurons. Neuroscience 71:625-32.

8. Alonso A, Klink R (1993) Differential electroresponsiveness of stellate and pyramidal-like cells of medial entorhinal cortex layer II. J Neurophysiol 70:128-43.

9. Alonso A, Llinas RR (1989) Subthreshold Na+-dependent theta-like rhythmicity in stellate cells of entorhinal cortex layer II. Nature 342:175-7.

10. Alroy G, Su H, Yaari Y (1999) Protein kinase C mediates muscarinic block of intrinsic bursting in rat hippocampal neurons. J.Physiol 518 (Pt 1):71-79.

11. Alzheimer C, Schwindt PC, Crill WE (1993) Modal gating of Na+ channels as a mechanism of persistent Na+ current in pyramidal neurons from rat and cat sensorimotor cortex. J.Neurosci. 13:660-673.

12. Amaral DG, Dolorfo C, varez-Royo P (1991) Organization of CA1 projections to the subiculum: a PHA-L analysis in the rat. Hippocampus 1:415-435.

13. Andersen P, Storm J, Wheal HV (1986) Thresholds of action potentials evoked by synapses on the dendrites of pyramidal cells in the rat hippocampus in vitro. J. Physiol. 383:509-526.

14. Anderson MI, O'Mara SM (2003) Analysis of recordings of single-unit firing and population activity in the dorsal subiculum of unrestrained, freely moving rats. J.Neurophysiol. 90:655-665.

15. Andrade R, Nicoll RA (1987) Pharmacologically distinct actions of serotonin on single pyramidal neurones of the rat hippocampus recorded in vivo. J. Physio. (Lond.) 394:99-124.

16. Aradi I, Holmes WR (1999) Role of multiple calcium and calcium-dependent conductances in regulation of hippocampal dentate granule cell excitability. J.Comput.Neurosci. 6:215-235.

17. Armstrong CM , Cota G (1999) Calcium block of Na channels and its effect on closing rate. Proc. Natl. Acad. Sci. USA 96:4154-4157.

18. Ashwood TJ, Lancaster B, Wheal HV (1986) Intracellular electrophysiology of CA1 pyramidal neurones in slices of the kainic acid lesioned hippocampus of the rat. Exp.Brain Res. 62:189-198.

19. Assandri R, Egger M, Gassmann M, Niggli E, Bauer C, Forster I, Gorlach A (1999) Erythropoietin modulates intracellular calcium in a human neuroblastoma cell line. J. Physiol. 516:343-352.

20. Avery RB, Johnston D (1996) Multiple channel types contribute to the low-voltage-activated calcium current in hippocampal CA3 pyramidal neurons. J.Neurosci. 16:5567-5582.

21. Aylward RL, Totterdell S (1993) Neurons in the ventral subiculum, amygdala and entorhinal cortex which project to the nucleus accumbens: their input from somatostatin-immunoreactive boutons. J. Chem. Neuroanat. 6:31-42.

22. Azouz R, Jensen MS, Yaari Y (1996) Ionic basis of spike after-depolarization and burst generation in adult rat hippocampal CA1 pyramidal cells. J Physiol (Lond) 492 (Pt 1):211-23.

23. Bains JS, Follwell MJ, Latchford KJ, Anderson JW, Ferguson AV (2001) Slowly inactivating potassium conductance (I(D)): a potential target for stroke therapy. Stroke 32:2624-2634.

24. Bal T, McCormick DA (1997) Synchronized oscillations in the inferior olive are controlled by the hyperpolarization-activated cation current I(h). J Neurophysiol 77:3145-56.

25. Baldelli P, Magnelli V, Carbone E (1999) Selective up-regulation of P- and R-type Ca2+ channels in rat embryo motoneurons by BDNF. Eur.J.Neurosci. 11:1127-1133.

26. Bargas J, Galarraga E (1995) Ion channels: Keys to neuronal specialization. In: Handbook of Brain Theory and Neural Networks. (Arbib MA, ed), pp 496-501. Cambridge MA: MIT Press.

27. Barlow HB, Foldiak P (1989) Adaptation and decorrelation in the cortex. In: The Computing Neuron (Durbin R, Miall C, Mitchison G, eds), pp 454-472. NewYork: Addison-Wesley.

28. Barman SA, Zhu S, White RE (2004) PKC activates BKCa channels in rat pulmonary arterial smooth muscle via cGMP-dependent protein kinase. Am.J.Physiol Lung Cell Mol.Physiol 286:L1275-L1281.

29. Bayliss DA, Li YW, Talley EM (1997) Effects of serotonin on caudal raphe neurons: inhibition of N- and P/Q-type calcium channels and the afterhyperpolarization. J.Neurophysiol. 77:1362-1374.

30. Bean BP (1989) Multiple types of calcium channels in heart muscle and neurons. Modulation by drugs and neurotransmitters. Ann.N.Y.Acad.Sci. 560:334-345.

31. Beck H, Steffens R, Heinemann U, Elger CE (1999) Ca(2+)-dependent inactivation of high-threshold Ca(2+) currents in hippocampal granule cells of patients with chronic temporal lobe epilepsy. J.Neurophysiol. 82:946-954.

32. Behr, J. ESF Exploratory Workshop on the subiculum in normal and pathological brain function. Oxford, September 21st-23rd 2005. 2006.

33. Behr J, Empson RM, Schmitz D, Gloveli T, Heinemann U (1996) Electrophysiological properties of rat subicular neurons in vitro. Neurosci.Lett. 220:41-44.

34. Behr J, Empson RM, Schmitz D, Gloveli T, Heinemann U (1997) Effects of serotonin on synaptic and intrinsic properties of rat subicular neurons in vitro. Brain Res. 773:217-222.

35. Behr J, Gloveli T, Heinemann U (2000a) Kindling induces a transient suppression of afterhyperpolarization in rat subicular neurons. Brain Res 867:259-64.

36. Behr J, Gloveli T, Schmitz D, Heinemann U (2000b) Dopamine depresses excitatory synaptic transmission onto rat subicular neurons via presynaptic D1-like dopamine receptors. J Neurophysiol 84:112-9.

37. Benardo LS, Masukawa LM, Prince DA (1982) Electrophysiology of isolated hippocampal pyramidal dendrites. J Neurosci 2:1614-22.

38. Berger AJ, Takahashi T (1990) Serotonin enhances a low-voltage-activated calcium current in rat spinal motoneurons. J.Neurosci. 10:1922-1928.

39. Berger T, Senn W, Luscher HR (2003) Hyperpolarization-activated current Ih disconnects somatic and dendritic spike initiation zones in layer V pyramidal neurons. J.Neurophysiol. 90:2428-2437.

40. Bernstein GM, Mendonc A, Wadia J, Macintyre Burnham W, Jones OT (1999) Kindling induces a long-term enhancement in the density of n-type calcium channels in the rat hippocampus. Neuroscience 94:1083-1095.

41. Beurrier C, Congar P, Bioulac B, Hammond C (1999) Subthalamic nucleus neurons switch from single-spike activity to burst- firing mode. J. Neurosci. 19:599-609.

42. Bland BH (1986) The physiology and pharmacology of hippocampal formation theta rhythms. Progress in Neurobiology 26:1-54.

43. Bonci A, Grillner P, Mercuri NB, Bernardi G (1998) L-Type calcium channels mediate a slow excitatory synaptic transmission in rat midbrain dopaminergic neurons. J.Neurosci. 18:6693-6703.

44. Bond CT, Herson PS, Strassmaier T, Hammond R, Stackman R, Maylie J, Adelman JP (2004) Small conductance Ca2+-activated K+ channel knock-out mice reveal the identity of calcium-dependent afterhyperpolarization currents. J.Neurosci. 24:5301-5306.

45. Borg-Graham, L. Modelling the somatic electrical behaviour of hippocampal pyramidal neurons. 87. Massachusetts Institute of Technology.

46. Borg-Graham LJ (1998) Interpretations of data and mechanisms for hippocamapal pyramidal cell models. In: Cerebral Cortex, Volume 13: Cortical Models (Ulinski PS, Jones EG, Peters A, eds), New York: Plenum Press.

47. Bourinet E, Soong TW, Sutton K, Slaymaker S, Mathews E, Monteil A, Zamponi GW, Nargeot J, Snutch TP (1999) Splicing of alpha 1A subunit gene generates phenotypic variants of P- and Q-type calcium channels. Nat.Neurosci. 2:407-415.

48. Bourinet E, Zamponi GW, Stea A, Soong TW, Lewis BA, Jones LP, Yue DT, Snutch TP (1996) The alpha 1E calcium channel exhibits permeation properties similar to low-voltage-activated calcium channels. J.Neurosci. 16:4983-4993.

49. Bowden SE, Fletcher S, Loane DJ, Marrion NV (2001) Somatic colocalization of rat SK1 and D class (Ca(v)1.2) L-type calcium channels in rat CA1 hippocampal pyramidal neurons. J.Neurosci. 21:RC175.

50. Brand S, Seeger T, Alzheimer C (2000) Enhancement of persistent Na+ current by sea anemone toxin (ATX II) exerts dual action on hippocampal excitability. Eur J Neurosci 12:2387-96.

51. Brett RS, Lancaster B (1985) Activation of potassium channels by rapid application of calcium to inside-out patches of cultured hippocampal neurons. Soc. Neurosci. Abstr. 10:241.

52. Brown AM, Schwindt PC, Crill WE (1994) Different voltage dependence of transient and persistent Na+ currents is compatible with modal-gating hypothesis for sodium channels. J. Neurophysio. 71:256-264.

53. Brown CD, Dudley AJ (1996) Chloride channel blockers decrease intracellular pH in cultured renal epithelial LLC-PK1 cells. Br J Pharmacol 118:443-4.

54. Brown DA, Adams PR (1980) Muscarinic suppression of a novel voltage-sensitive K+ current in a vertebrate neurone. Nature 283:673-676.

55. Brown DA, Constanti A (1980) Intracellular observations on the effects of muscarinic agonists on rat sympathetic neurones. Br J Pharmacol 70:593-608.

56. Brown DA, Gahwiler BH, Griffith WH, Halliwell JV (1990) Membrane currents in hippocampal neurons. Prog.Brain Res. 83:141-160.

57. Brown DA, Griffith WH (1983a) Calcium-activated outward current in voltage-clamped hippocampal neurones of the guinea-pig. J.Physiol 337:287-301.

58. Brown DA, Griffith WH (1983b) Persistent slow inward calcium current in voltage-clamped hippocampal neurones of the guinea-pig. J.Physiol 337:303-320.

59. Brown HF, DiFrancesco D, Noble SJ (1979) How does adrenaline accelerate the heart? Nature 280:235-236.

60. Brown SD, Wolf EA, Twyman RE, White HS (1993) The novel anticonvulsant topiramate enhances GABA-mediated chloride flux. Epilepsia 34:123-124.

61. Brown SP, Safo PK, Regehr WG (2004) Endocannabinoids inhibit transmission at granule cell to Purkinje cell synapses by modulating three types of presynaptic calcium channels. J.Neurosci. 24:5623-5631.

62. Budde T, Munsch T, Pape HC (1998) Distribution of L-type calcium channels in rat thalamic neurones. Eur.J.Neurosci. 10:586-597.

63. Butler A, Tsunoda S, McCobb DP, Wei A, Salkoff L (1993) mSlo, a complex mouse gene encoding "maxi" calcium-activated potassium channels. Science 261:221-224.

64. Buzsaki G (2002) Theta oscillations in the hippocampus. Neuron 33:325-340.

65. Canteras NS, Swanson LW (1992) Projections of the ventral subiculum to the amygdala, septum, and hypothalamus: a PHAL anterograde tract-tracing study in the rat. J Comp Neurol 324:180-94.

66. Cantrell AR, Catterall WA (2001) Neuromodulation of Na+ channels: an unexpected form of cellular plasticity. Nat.Rev.Neurosci. 2:397-407.

67. Cantrell AR, Ma JY, Scheuer T, Catterall WA (1996) Muscarinic modulation of sodium current by activation of protein kinase C in rat hippocampal neurons. Neuron 16:1019-1026.

68. Cantrell AR, Scheuer T, Catterall WA (1999) Voltage-dependent neuromodulation of Na+ channels by D1-like dopamine receptors in rat hippocampal neurons. J.Neurosci. 19:5301-5310.

69. Catterall WA (2000) Structure and regulation of voltage-gated Ca2+ channels. Annu. Rev. Cell Dev. Biol. 16:521-555.

70. Catterall WA , Goldin AL, Waxman SG (2003) International Union of Pharmacology. XXXIX. Compendium of voltage-gated ion channels: sodium channels. Pharmacol.Rev. 55:575-578.

71. Caulfield MP , Robbins J, Higashida H, Brown DA (1993) Postsynaptic actions of acetylcholine: the coupling of muscarinic receptor subtypes to neuronal ion channels. Prog.Brain Res. 98:293-301.

72. Chapman CA, Lacaille JC (1999) Intrinsic theta-frequency membrane potential oscillations in hippocampal CA1 interneurons of stratum lacunosum-moleculare. J Neurophysiol 81:1296-307.

73. Chavis P, Ango F, Michel JM, Bockaert J, Fagni L (1998) Modulation of big K+ channel activity by ryanodine receptors and L-type Ca2+ channels in neurons. Eur.J.Neurosci. 10:2322-2327.

74. Chay TR (1991) The Hodgkin-Huxley Na+ channel model versus the five-state Markovian model. Biopolymers 31:1483-502.

75. Chen C, Zhang J, Vincent JD, Israel JM (1990) Two types of voltage-dependent calcium current in rat somatotrophs are reduced by somatostatin. J. Physiol. 425:29-42.

76. Chen ZF, Kamiryo T, Henson SL, Yamamoto H, Bertram EH, Schottler F, Patel F, Steiner L, Prasad D , Kassell NF, Shareghis S, Lee KS (2001) Anticonvulsant effects of gamma surgery in a model of chronic spontaneous limbic epilepsy in rats. J.Neurosurg. 94:270-280.

77. Chi XX, Xu ZC (2000) Differential changes of potassium currents in CA1 pyramidal neurons after transient forebrain ischemia. J.Neurophysiol. 84:2834-2843.

78. Chikwendu A, McBain CJ (1996) Two temporally overlapping "delayed-rectifiers" determine the voltage-dependent potassium current phenotype in cultured hippocampal interneurons. J.Neurophysiol. 76:1477-1490.

79. Cho YH, Jaffard R (1995) Spatial location learning in mice with ibotenate lesions of entorhinal cortex or subiculum. Neurobiol.Learn.Mem. 64:285-290.

80. Christie BR, Eliot LS, Ito K, Miyakawa H, Johnston D (1995) Different Ca2+ channels in soma and dendrites of hippocampal pyramidal neurons mediate spike-induced Ca2+ influx. J Neurophysiol. 73:2553-7.

81. Colbert CM, Johnston D (1998) Protein kinase C activation decreases activity-dependent attenuation of dendritic Na+ current in hippocampal CA1 pyramidal neurons. J.Neurophysiol. 79:491-495.

82. Cole AE, Nicoll RA (1984) Characterization of a slow cholinergic post-synaptic potential recorded ``in vitro'' from rat hippocampal pyramidal cells. J. Physiol. Lond. 352:173-188.

83. Colino A, Halliwell JV (1987) Differential modulation of three separate K-conductances in hippocampal CA1 neurons by serotonin. Nature 328:73-7.

84. Colino A, Halliwell JV (1993) Carbachol potentiates Q current and activates a calcium-dependent non-specific conductance in rat hippocampus in vitro. Eur J Neurosci 5:1198-209.

85. Colling SB, Stanford IM, Traub RD, Jefferys JG (1998) Limbic gamma rhythms. I. Phase-locked oscillations in hippocampal CA1 and subiculum. J Neurophysiol 80:155-61.

86. Colling SB, Wheal HV (1994) Fast sodium action potentials are generated in the distal apical dendrites of rat hippocampal CA1 pyramidal cells. Neurosci.Lett. 172:73-96.

87. Connor JA, Stevens CF (1971) Prediction of repetitive firing behaviour from voltage clamp data on an isolated neurone soma. J Physiol (Lond) 213:31-53.

88. Constanti A, Galvan M (1983) Fast inward-rectifying current accounts for anomalous rectification in olfactory cortex neurones. J Physiol 335:153-78.

89. Cooper DC, Chung S, Spruston N (2005) Output-mode transitions are controlled by prolonged inactivation of sodium channels in pyramidal neurons of subiculum. PLoS.Biol. 3:e175.

90. Cooper DC, Moore SJ, Staff NP, Spruston N (2003) Psychostimulant-induced plasticity of intrinsic neuronal excitability in ventral subiculum. J.Neurosci. 23:9937-9946.

91. Coulter DA, Huguenard JR, Prince DA (1989) Calcium currents in rat thalamocortical relay neurones: kinetic properties of the transient, low-threshold current. J Physiol (Lond) 414:587-604.

92. Coulter DA, Sombati S, DeLorenzo RJ (1993) Selective effects of topiramate on sustained repetitive firing and spontaneous bursting in cultured hippocampal neurons. Epilepsia 34:123.

93. Cox DH, Dunlap K (1992) Pharmacological discrimination of N-type from L-type calcium current and its selective modulation by transmitters. J.Neurosci. 12:906-914.

94. Cox DH, Dunlap K (1994) Inactivation of N-type calcium current in chick sensory neurons: calcium and

voltage dependence. J.Gen.Physiol 104:311-336.

95. Cribbs LL, Lee JH, Yang J, Satin J, Zhang Y, Daud A, Barclay J, Williamson MP, Fox M, Rees M, Perez-Reyes E (1998) Cloning and characterization of alpha1H from human heart, a member of the T-type Ca2+ channel gene family. Circ.Res. 83:103-109.

96. Crill WE (1999) Functional implications of dendritic voltage-dependent conductances. J Physiol Paris 93:17-21.

97. Crook SM, Ermentrout GB, Bower JM (1998) Spike frequency adaptation affects the synchronization properties of networks of cortical oscillators. Neural Computation 10:837-854.

98. Csicsvari J, Hirase H, Czurko A, Mamiya A, Buzsaki G (1999) Oscillatory coupling of hippocampal pyramidal cells and interneurons in the behaving rat. J. Neurosci. 19:274-287.

99. Currie KP, Fox AP (2002) Differential facilitation of N- and P/Q-type calcium channels during trains of action potential-like waveforms. J.Physiol 539:419-431.

100. D'Angelo E, Nieus T, Maffei A, Armano S, Rossi P, Taglietti V, Fontana A, Naldi G (2001) Theta-frequency bursting and resonance in cerebellar granule cells: experimental evidence and modeling of a slow k+-dependent mechanism. J.Neurosci. 21:759-770.

101. D'Antuono M , Kawasaki H, Palmieri C, Avoli M (2001) Network and intrinsic contributions to carbachol-induced oscillations in the rat subiculum. J Neurophysiol 86:1164-78.

102. De Schutter E, Bower JM (1994) An active membrane model of the cerebellar Purkinje cell. I. Simulation of current clamps in slice. J Neurophysiol 71:375-400.

103. de WJr, Fosset M, Mourre C, Schmid-Antomarchi H, Bernardi H, Lazdunski M (1989) Pharmacology and regulation of ATP-sensitive K+ channels. Pflugers Arch. 414 Suppl 1:S80-S87.

104. Deisseroth K, Heist EK, Tsien RW (1998) Translocation of calmodulin to the nucleus supports CREB phosphorylation in hippocampal neurons. Nature 392:198-202.

105. DeLorenzo RJ, Sombati S, Coulter DA (2000) Effects of topiramate on sustained repetitive firing and spontaneous recurrent seizure discharges in cultured hippocampal neurons. Epilepsia 41 Suppl 1:S40-S44.

106. Destexhe A, Babloyantz A (1993) A model of the inward current Ih and its possible role in thalamocortical oscillations. Neuroreport 4:223-226.

107. Destexhe A, Mainen ZF, Sejnowski TJ (1994) Synthesis of models for excitable membranes, synaptic transmission and neuromodulation using a common kinetic formalism. Journal of Computational Neuroscience 1:195-231.

108. Destexhe A, Neubig M, Ulrich D, Huguenard J (1998) Dendritic low-threshold calcium currents in thalamic relay cells. J.Neurosci. 18:3574-3588.

109. Dietrich D, Kirschstein T, Kukley M, Pereverzev A, von der BC, Schneider T, Beck H (2003) Functional specialization of presynaptic Cav2.3 Ca2+ channels. Neuron 39:483-496.

110. Dinan TG, Crunelli V, Kelly JS (1987) Neuroleptics decrease calcium-activated potassium conductance in hippocampal pyramidal cells. Brain Res. 407:159-162.

111. Ding JP, Lingle CJ (2002) Steady-state and closed-state inactivation properties of inactivating BK channels. Biophys.J. 82:2448-2465.

112. Doerner D, Pitler TA, Alger BE (1988) Protein kinase C activators block specific calcium and potassium current components in isolated hippocampal neurons. J.Neurosci. 8:4069-4078.

113. Dreier JP, Heinemann U (1991) Regional and time dependent variations of low Mg2+ induced epileptiform activity in rat temporal cortex slices. Exp.Brain Res. 87:581-596.

114. Du W, Aloyo VJ, Harvey JA (1997) Harmaline competitively inhibits [3H]MK-801 binding to the NMDA receptor in rabbit brain. Brain Res. 770:26-29.

115. Duijnhouwer J, Remme MWH, van Ooyen A (2001) Influence of dendritic topology on firing patterns in model neurons. Neurocomputing 38-40:183-189.

116. Dunlap K. LJITTJ (1995) Exocytotic Ca21 channels in mammalian central neurons. Trends Neurosci. 18:89-98.

117. Dworetzky SI, Trojnacki JT, Gribkoff VK (1994) Cloning and expression of a human large-conductance calcium-activated potassium channel. Brain Res.Mol.Brain Res. 27:189-193.

118. Elliott EM, Malouf AT, Catterall WA (1995) Role of calcium channel subtypes in calcium transients in hippocampal CA3 neurons. J Neurosci 15:6433-44.

119. Engel J, Schultens HA, Schild D (1999) Small conductance potassium channels cause an activity-dependent spike frequency adaptation and make the transfer function of neurons logarithmic. Biophysical Journal 76:1310-1319.

120. Erickson KR, Ronnekleiv OK, Kelly MJ (1993) Role of a T-type calcium current in supporting a depolarizing potential, damped oscillations, and phasic firing in vasopressinergic guinea pig supraoptic neurons. Neuroendocrinology 57:789-800.

121. Ermentrout GB (1998) XPP.

122. Ertel SI, Ertel EA (1997) Low-voltage-activated T-type Ca2 + channels. TIPS 18:37-42.

123. Faber ES, Sah P (2003) Ca2+-activated K+ (BK) channel inactivation contributes to spike broadening during repetitive firing in the rat lateral amygdala. J.Physiol 552:483-497.

124. Fibiger HC, Phillips AC (1988) Mesocorticolimbic systems and reward. In: Annals of the New York Academy of Science - The mesocorticolimbic system (Kalivas DW, Nemeroff CB, eds), pp 206-2 15. New York: NY Academy of Science.

125. Finch DM, Tan AM, Isokawa-Akesson M (1988) Feedforward inhibition of the rat entorhinal cortex and subicular complex. J.Neurosci. 8:2213-2226.

126. Fisher PR, Noegel AA, Fechheimer M, Rivero F, Prassler J, Gerisch G (1997) Photosensory and thermosensory responses in Dictyostelium slugs are specifically impaired by absence of the F-actin cross-linking gelation factor (ABP-120). Curr.Biol. 7:889-892.

127. Fisher R, Johnston D (1990) Differential modulation of single voltage-gated calcium channels by cholinergic and adrenergic agonists in adult hippocampal neurons. J.Neurophysiol. 64:1291-1302.

128. Fisher RE, Gray R, Johnston D (1990) Properties and distribution of single voltage-gated calcium channels in adult hippocampal neurons. J.Neurophysiol. 64:91-104.

129. Fishman MC, Spector I (1981) Potassium current suppression by quinidine reveals additional calcium currents in neuroblastoma cells. Proc Natl Acad Sci USA 78:5245-5249.

130. Fleidervish IA, Friedman A, Gutnick MJ (1996) Slow inactivation of Na+ current and slow cumulative spike adaptation in mouse and guinea-pig neocortical neurones in slices. J Physiol 493 (Pt 1):83-97.

131. Foehring RC , Mermelstein PG, Song WJ, Ulrich S, Surmeier DJ (2000) Unique properties of R-type calcium currents in neocortical and neostriatal neurons. J.Neurophysiol. 84:2225-2236.

132. Fontana DJ, Inouye GT, Johnson RM (1994) Linopirdine (DuP 996) improves performance in several tests of learning and memory by modulation of cholinergic neurotransmission. Pharmacol. Biochem. Behav. 49:1075-1082.

133. Forsythe ID , Tsujimoto T, Barnes-Davies M, Cuttle MF, Takahashi T (1998) Inactivation of presynaptic calcium current contributes to synaptic depression at a fast central synapse. Neuron 20:797-807.

134. Forti L, Pietrobon D (1993) Functional diversity of L-type calcium channels in rat cerebellar neurons. Neuron 10:437-450.

135. Fox AP, Nowycky MC, Tsien RW (1987a) Kinetic and pharmacological properties distinguishing three types of calcium currents in chick sensory neurones. J.Physiol 394:149-172.

136. Fox AP, Nowycky MC, Tsien RW (1987b) Single-channel recordings of three types of calcium channels in chick sensory neurones. J.Physiol 394:173-200.

137. Fozzard HA, Hanck DA (1996) Structure and function of voltage-dependent sodium channels: comparison of brain II and cardiac isoforms. Physiol Rev. 76:887-926.

138. Franciolini F (1988) Calcium and voltage dependence of single Ca2+-activated K+ channels from cultured hippocampal neurons of rat. Biochim. Biophys. Acta 93:419-427.

139. Franciolini F, Petris A (1988) Single chloride channels in cultured rat neurones. Arch Biochem Biophys 261:97-102.

140. Frankenhaeuser B, Hodgkin AL (1957) The action of calcium of the electrical properties of squid axons. J. Physiol. (Lond.) 137:218-244.

141. French CR, Gage PW (1985) A threshold sodium current in pyramidal cells in rat hippocampus. Neurosci.Lett. 56:289-293.

142. French CR, Sah P, Buckett KJ, Gage PW (1990) A voltage-dependent persistent sodium current in mammalian hippocampal neurons. J Gen Physiol 95:1139-57.

143. French SJ, Ritson GP, Hidaka S, Totterdell S (2005) Nucleus accumbens nitric oxide immunoreactive interneurons receive nitric oxide and ventral subicular afferents in rats. Neuroscience 135:121-131.

144. Froehner SC (1988) New insights into the molecular structure of the dihydropyridine-sensitive calcium channel. Trends Neurosci. 11:90-92.

145. Funahashi M , Harris E, Stewart M (1999) Re-entrant activity in a presubiculum-subiculum circuit generates epileptiform activity in vitro. Brain Res 849:139-46.

146. Gabrieli JDE, Brewer JB, Desmond JE, Glover GH (1997) Separate neural bases of two fundamental memory processes in the human medial temporal lobe. Science 276:264-266.

147. Gahwiler BH , Llano I (1989) Sodium and potassium conductances in somatic membranes of rat Purkinje cells from organotypic cerebellar cultures. J.Physiol 417:105-122.

148. Galani R, Jarrard LE, Will BE, Kelche C (1997) Effects of postoperative housing conditions on functional recovery in rats with lesions of the hippocampus, subiculum, or entorhinal cortex. Neurobiol.Learn.Mem. 67:43-56.

149. Gardiner M (1970) The fantastic combinations of John Conway's new solitaire game "life". Scientific American120-123.

150. Gasparini S , Kasyanov AM, Pietrobon D, Voronin LL, Cherubini E (2001) Presynaptic R-type calcium channels contribute to fast excitatory synaptic transmission in the rat hippocampus. J.Neurosci. 21:8715-

8721.

151. Gebremedhin D, Yamaura K, Zhang C, Bylund J, Koehler RC, Harder DR (2003) Metabotropic glutamate receptor activation enhances the activities of two types of Ca2+-activated k+ channels in rat hippocampal astrocytes. J.Neurosci. 23:1678-1687.

152. Giese KP, Storm JF, Reuter D, Fedorov NB, Shao LR, Leicher T, Pongs O, Silva AJ (1998) Reduced K+ channel inactivation, spike broadening, and after-hyperpolarization in Kvbeta1.1-deficient mice with impaired learning. Learn.Mem. 5:257-273.

153. Gigg J, Finch DM, O'Mara SM (2000) Responses of rat subicular neurons to convergent stimulation of lateral entorhinal cortex and CA1 in vivo. Brain Res. 884:35-50.

154. Goldberg JA , Wilson CJ (2005) Control of spontaneous firing patterns by the selective coupling of calcium currents to calcium-activated potassium currents in striatal cholinergic interneurons. J.Neurosci. 25:10230-10238.

155. Goldin AL (2001) Resurgence of sodium channel research. Annu.Rev.Physiol 63:871-894.

156. Golding NL, Jung HY, Mickus T, Spruston N (1999) Dendritic calcium spike initiation and repolarization are controlled by distinct potassium channel subtypes in CA1 pyramidal neurons. J.Neurosci. 19:8789-8798.

157. Goldman DF (1943) Potential, impedance, and rectification in membranes. J. Gen. Physiology 27:37-60.

158. Golowasch J , Abbott LF, Marder E (1999) Activity-dependent regulation of potassium currents in an identified neuron of the stomatogastric ganglion of the crab Cancer borealis. J Neurosci 19:RC33.

159. Gong L, Gao TM, Li X, Huang H, Tong Z (2000) Enhancement in activities of large conductance calcium-activated potassium channels in CA1 pyramidal neurons of rat hippocampus after transient forebrain ischemia. Brain Res. 884:147-154.

160. Gong LW, Gao TM, Huang H, Tong Z (2001) Properties of large conductance calcium-activated potassium channels in pyramidal neurons from the hippocampal CA1 region of adult rats. Jpn.J.Physiol 51:725-731.

161. Gong LW, Gao TM, Huang H, Zhou KX, Tong Z (2002) ATP modulation of large conductance Ca(2+)-activated K(+) channels via a functionally associated protein kinase A in CA1 pyramidal neurons from rat hippocampus. Brain Res. 951:130-134.

162. Gonzalez-Burgos G, Barrionuevo G (2001) Voltage-gated sodium channels shape subthreshold EPSPs in layer 5 pyramidal neurons from rat prefrontal cortex. J.Neurophysiol. 86:1671-1684.

163. Gorelova NA , Yang CR (2000) Dopamine D1/D5 receptor activation modulates a persistent sodium current in rat prefrontal cortical neurons in vitro. J Neurophysiol 84:75-87.

164. Gorman AL, Hermann A (1979) Internal effects of divalent cations on potassium permeability in molluscan neurones. J Physiol 296:393-410.

165. Govindaiah, Rao BS, Raju TR, Meti BL (1997) Loss of hippocampal CA1 neurons and learning impairment in subicular lesioned rats. Brain Res 745:121-6.

166. Graves L, Pack A, Abel T (2001) Sleep and memory: a molecular perspective. Trends Neurosci 24:237-43.

167. Greene JR, Mason A (1996) Neuronal diversity in the subiculum: correlations with the effects of somatostatin on intrinsic properties and on GABA-mediated IPSPs in vitro. J Neurophysiol 76:1657-66.

168. Greene JR, Totterdell S (1997) Morphology and distribution of electrophysiologically defined classes of pyramidal and nonpyramidal neurons in rat ventral subiculum in vitro. J.Comp Neurol. 380:395-408.

169. Grissmer S, Nguyen AN, Aiyar J, Hanson DC, Mather RJ, Gutman GA, Karmilowicz MJ, Auperin DD, Chandy KG (1994) Pharmacological characterization of five cloned voltage-gated K+ channels, types Kv1.1, 1.2, 1.3, 1.5, and 3.1, stably expressed in mammalian cell lines. Mol. Pharmacol. 45:1227-1234.

170. Gu N, Vervaeke K, Hu H, Storm JF (2005) Kv7/KCNQ/M and HCN/h, but not KCa2/SK channels, contribute to the somatic medium after-hyperpolarization and excitability control in CA1 hippocampal pyramidal cells. J.Physiol 566:689-715.

171. Gustafsson B, Galvan M, Grafe P, Wigstrom H (1982) A transient outward current in a mammalian central neurone blocked by 4-aminopyridine. Nature 299:252-254.

172. Gutfreund Y , Yarom Y, Segev I (1995) Subthreshold oscillations and resonant frequency in guinea-pig cortical neurons: physiology and modelling. J Physiol 483 (Pt 3):621-40.

173. Gutman GA (2003) International Union of Pharmacology. XLI. Compendium of Voltage-Gated Ion Channels: Potassium Channels. Pharmacol. Rev. 55:583–586.

174. Habermann CJ, O'Brien BJ, Wassle H, Protti DA (2003) AII amacrine cells express L-type calcium channels at their output synapses. J.Neurosci. 23:6904-6913.

175. Halliwell JV (1983) Calcium-loading reveals two distinct Ca-currents in voltage-clamped hippocampal neurones in vitro. J. Physio. (Lond.) 341:100.

176. Halliwell JV, Adams PR (1982) Voltage-clamp analysis of muscarinic excitation in hippocampal neurons. Brain Res 250:71-92.

177. Halliwell JV, Grove EA (1989) 9-Amino-1,2,3,4-tetrahydroacridine (THA) blocks agonist-induced potassium conductance in rat hippocampal neurones. Eur.J.Pharmacol. 163:369-372.

178. Halliwell JV, Othman IB, Pelchen-Matthews A, Dolly JO (1986) Central action of dendrotoxin: selective reduction of a transient K conductance in hippocampus and binding to localized acceptors. Proc.Natl.Acad.Sci.U.S.A 83:493-497.

179. Hammarstrom AK, Gage PW (1998) Inhibition of oxidative metabolism increases persistent sodium current in rat CA1 hippocampal neurons. J Physiol 510 (Pt 3):735-41.

180. Hampson RE, Deadwyler SA (2003) Temporal firing characteristics and the strategic role of subicular neurons in short-term memory. Hippocampus 13:529-541.

181. Hans M, Urrutia A, Deal C, Brust PF, Stauderman K, Ellis SB, Harpold MM, Johnson EC, Williams ME (1999) Structural elements in domain IV that influence biophysical and pharmacological properties of human a1A-containing high-voltage activated calcium channels. Biophys. J. 76:1384-1400.

182. Harris E, Stewart M (2001) Intrinsic connectivity of the rat subiculum: II. Properties of synchronous spontaneous activity and a demonstration of multiple generator regions. J.Comp Neurol. 435:506-518.

183. Harris E, Witter MP, Weinstein G, Stewart M (2001) Intrinsic connectivity of the rat subiculum: I. Dendritic morphology and patterns of axonal arborization by pyramidal neurons . J.Comp Neurol. 435:490-505.

184. Harris-Warrick RM, Sparks DL (1995) Neural control. Curr.Opin.Neurobiol. 5:721-726.

185. Hasselmo ME (1999) Neuromodulation: Acetylcholine and memory consolidation. Trends Cog. Sci. 3:351-359.

186. Hausser M (2000) The Hodgkin-Huxley theory of the action potential. Nat.Neurosci. 3 Suppl:1165.

187. Hausser M, Mel B (2003) Dendrites: bug or feature? Current Opinion in Neurobiology 13:372-383.

188. Hayashi T, Poronnik P, Young JA, Cook DI (1996) The ACh-evoked, Ca2+-activated whole-cell K+ current in mouse mandibular secretory cells. Whole-cell and fluorescence studies. J.Membr.Biol. 152:253-259.

189. Hell JW, Westenbroek RE, Warner C, Ahlijanian MK, Prystay W, Gilbert MM, Snutch TP, Catterall WA (1993) Identification and differential subcellular localization of the neuronal class C and class D L-type calcium channel a1 subunits. J Cell Biol 123:949-962.

190. Herman JP, Cullinan WE, Morano MI, Akil H, Watson SJ (1995) Contribution of the ventral subiculum to inhibitory regulation of the hypothalamo-pituitary-adrenocortical axis. J Neuroendocrinol 7:475-82.

191. Herman JP, Dolgas CM, Carlson SL (1998) Ventral subiculum regulates hypothalamo-pituitary-adrenocortical and behavioural responses to cognitive stressors. Neuroscience 86:449-459.

192. Hertzer K (2005) Graphmatica. kSoft Inc. Version 2.0e.

193. Hicks GA, Marrion NV (1998) Ca2+-dependent inactivation of large conductance Ca2+-activated K+ (BK) channels in rat hippocampal neurones produced by pore block from an associated particle. J.Physiol 508 (Pt 3):721-734.

194. Higashima M, Kinoshita H, Koshino Y (1998) Contribution of T-type calcium channels to afterdischarge generation in rat hippocampal slices. Brain Res. 781:127-134.

195. Hilaire C, Diochot S, Desmadryl G, Baldy-Moulinier M, Richard S, Valmier J (1996) Opposite developmental regulation of P- and Q-type calcium currents during ontogenesis of large diameter mouse sensory neurons. Neuroscience 75:1219-1229.

196. Hilborn MD, Vaillancourt RR, Rane SG (1998) Growth factor receptor tyrosine kinases acutely regulate neuronal sodium channels through the src signaling pathway. J.Neurosci. 18:590-600.

197. Hille. B (1992) Ionic channels of excitable membranes. Sunderland, MA: Sinauer Associates.

198. Hillman H (1991) A new hypothesis for electrical transmission in the mammalian central nervous system. Med.Hypotheses 34:220-224.

199. Hodgkin AL, Huxley AF (1952) A quantitative description of membrane current and its application to conduction and excitation in nerve. J. Physiol. Lond. 117:500-544.

200. Hodgkin AL, Katz B (1949) The effect of sodium ions on the electrical activity of the giant axon of the squid. J. Physiology 108:37-77.

201. Hodgkin AL, Rushton WAH (1946) The electrical constants of a crustacean nerve fibre. Proceedings of the Royal Society B-133:444-79.

202. Hoffman DA, Magee JC, Colbert CM, Johnston D (1997) K+ channel regulation of signal propagation in dendrites of hippocampal pyramidal neurons. Nature 387:869-75.

203. Hoffmann EK, Dunham PB (1995) Membrane mechanisms and intracellular signalling in cell volume regulation. Int Rev Cytol 161:173-262.

204. Horn R, Vandenberg CA (1984) Statistical properties of single sodium channels. J Gen Physiol 84:505-34.

205. Horning MS, Trombley PQ (2001) Zinc and copper influence excitability of rat olfactory bulb neurons by multiple mechanisms. J.Neurophysiol. 86:1652-1660.

206. Hotson JR, Prince DA (1980) A calcium-activated hyperpolarization follows repetitive firing in hippocampal neurons. J Neurophysiol 43:409-19.

207. Hou SW, Zheng P, Sun FY (2004) Melatonin inhibits outward delayed rectifier potassium currents in hippocampal CA1 pyramidal neuron via intracellular indole-related domains. J.Pineal Res. 36:242-249.

208. Hsiao CF, Del Negro CA, Trueblood PR, Chandler SH (1998) Ionic basis for serotonin-induced bistable membrane properties in guinea pig trigeminal motoneurons. J.Neurophysiol. 79:2847-2856.

209. Hu H, Vervaeke K, Storm JF (2002) Two forms of electrical resonance at theta frequencies, generated by M-current, h-current and persistent Na+ current in rat hippocampal pyramidal cells. J.Physiol 545:783-805.

210. Hu S, Labuda MZ, Pandolfo M, Goss GG, McDermid HE, Ali DW (2003) Variants of the KCNMB3 regulatory subunit of maxi BK channels affect channel inactivation. Physiol Genomics 15:191-198.

211. Huerta PT, Lisman JE (1995) Bidirectional synaptic plasticity induced by a single burst during cholinergic theta oscillation in CA1 in vitro. Neuron 15:1053-63.

212. Huguenard JR, Gutnick MJ, Prince DA (1993) Transient Ca2+ currents in neurons isolated from rat lateral habenula. J.Neurophysiol. 70:158-166.

213. Huguenard JR, Hamill OP, Prince DA (1988) Developmental changes in Na+ conductances in rat neocortical neurons: appearance of a slowly inactivating component. J Neurophysiol 59:778-95.

214. Huguenard JR, McCormick DA (1992) Simulation of the currents involved in rhythmic oscillations in thalamic relay neurons. J Neurophysiol 68:1373-83.

215. Huguenard JR, Prince DA (1992) A novel T-type current underlies prolonged Ca(2+)-dependent burst firing in GABAergic neurons of rat thalamic reticular nucleus. J Neurosci 12:3804-17.

216. Hutcheon B, Muira RM, Puil E (1996) Subthreshold membrane resonance in neocortical neurons. J. Neurophysiol. 76:683-697.

217. Hutcheon B, Yarom Y (2000) Resonance, oscillation and the intrinsic frequency preferences of neurons. Trends Neurosci 23:216-22.

218. Hyams D (2001) CurveExpert. Version 1.3.

219. Ikeda SR, Lovinger DM, McCool BA, Lewis DL (1995) Heterologous expression of metabotropic glutamate receptors in adult rat sympathetic neurons: subtype-specific coupling to ion channels. Neuron 14:1029-1038.

220. Ikemoto Y, Ono K, Yoshida A, Akaike N (1989) Delayed activation of large-conductance Ca2+-activated K channels in hippocampal neurons of the rat. Biophys J 56:207-12.

221. Inchauspe CG, Martini FJ, Forsythe ID, Uchitel OD (2004) Functional compensation of P/Q by N-type channels blocks short-term plasticity at the calyx of held presynaptic terminal., J.Neurosci. 24:10379-10383.

222. Ingram SL, Williams JT (1996) Modulation of the hyperpolarization-activated current (Ih) by cyclic nucleotides in guinea-pig primary afferent neurons. J.Physiol 492 (Pt 1):97-106.

223. Ino M, Yoshinaga T, Wakamori M, Miyamoto N, Takahashi E, Sonoda J, Kagaya T, Oki T, Nagasu T, Nishizawa Y, Tanaka I, Imoto K, Aizawa S, Koch S, Schwartz A, Niidome T, Sawada K, Mori Y (2001) Functional disorders of the sympathetic nervous system in mice lacking the 1B subunit (Cav 2.2) of N-type calcium channels. Proc. Natl. Acad. Sci. USA 98:5323-5328.

224. Isbrandt D, Leicher T, Waldschutz R, Zhu X, Luhmann U, Michel U, Sauter K, Pongs O (2000) Gene structures and expression profiles of three human KCND (Kv4) potassium channels mediating A-type currents I(TO) and I(SA). Genomics 64:144-154.

225. Ishizuka N (2001) Laminar organization of the pyramidal cell layer of the subiculum in the rat. J.Comp Neurol. 435:89-110.

226. Isomura Y, Fujiwara-Tsukamoto Y, Imanishi M, Nambu A, Takada M (2002) Distance-dependent Ni(2+)-sensitivity of synaptic plasticity in apical dendrites of hippocampal CA1 pyramidal cells. J.Neurophysiol. 87:1169-1174.

227. Izhikevich EM (2002) Resonance and selective communication via bursts in neurons having subthreshold oscillations. Biosystems 67:95-102.

228. Jaffe DB, Johnston D, Lasser-Ross N, Lisman JE, Miyakawa H, Ross WN (1992) The spread of Na+ spikes determines the pattern of dendritic Ca2+ entry into hippocampal neurons. Nature 357:244-246.

229. Jaffe DB, Ross WN, Lisman JE, Lasser-Ross N, Miyakawa H, Johnston D (1994) A model for dendritic Ca2+ accumulation in hippocampal pyramidal neurons based on fluorescence imaging measurements. J Neurophysiol 71:1065-77.

230. Jensen MS, Azouz R, Yaari Y (1996) Spike after-depolarization and burst generation in adult rat hippocampal CA1 pyramidal cells. J Physiol (Lond) 492 (Pt 1):199-210.

231. Jentsch TJ (2000) Neuronal KCNQ potassium channels: physiology and role in disease. Nat. Rev. Neurosci. 1:21-30.

232. Jentsch TJ, Gunther W (1997) Chloride channels: an emerging molecular picture. Bioessays 19:117-26.

233. Jones KE, Bawa P (1997) Computer simulation of the responses of human motoneurons to composite 1A EPSPS: effects of background firing rate. J Neurophysiol 77:405-20.

234. Jones LP, DeMaria CD, Yue DT (1999) N-type calcium channel inactivation probed by gating-current analysis. Biophys.J. 76:2530-2552.

235. Jones OT, Bernstein GM, Jones EJ, Jugloff DG, Law M, Wong W, Mills LR (1997) N-Type calcium channels in the developing rat hippocampus: subunit, complex, and regional expression. J.Neurosci. 17:6152-6164.

236. Jones RS, Heinemann U (1988) Verapamil blocks the afterhyperpolarization but not the spike frequency accommodation of rat CA1 pyramidal cells in vitro. Brain Res 462:367-71.

237. Jones SW (1985) Muscarinic and peptidergic excitation of bull-frog sympathetic neurons. J. Physiol. 366:63-87.

238. Jun K, Piedras-Renteria ES, Smith SM, Wheeler DB, Lee SB, Lee TG, Chin H, Adams ME, Scheller RH, Tsien RW, Shin HS (1999) Ablation of P/Q-type Ca(2+) channel currents, altered synaptic transmission, and progressive ataxia in mice lacking the alpha(1A)-subunit. Proc.Natl.Acad.Sci.U.S.A 96:15245-15250.

239. Jung HY, Staff NP, Spruston N (2001) Action potential bursting in subicular pyramidal neurons is driven by a calcium tail current. J Neurosci 21:3312-21.

240. Kametani H, Kawamura H (1990) Alterations in acetylcholine release in the rat hippocampus during sleep-wakefulness detected by intracerebral dialysis. Life Sci. 47:421-426.

241. Kaneda M, Oomura Y, Ishibashi O, Akaike N (1988) Permeability to various cations of the voltage-dependent sodium channel of isolated rat hippocampal pyramidal neurons. Neurosci.Lett. 88:253-256.

242. Kang J, Huguenard JR, Prince DA (2000) Voltage-gated potassium channels activated during action potentials in layer V neocortical pyramidal neurons. J.Neurophysiol. 83:70-80.

243. Kasai H, Takagi H, Ninomiya Y, Kishimoto T, Ito K, Yoshida A, Yoshioka T, Miyashita Y (1996) Two

components of exocytosis and endocytosis in phaeochromocytoma cells studied using caged Ca2+ compounds. J.Physiol 494 (Pt 1):53-65.

244. Katz PS, Frost WN (1997) Removal of spike frequency adaptation via neuromodulation intrinsic to the tritonia escape swim central pattern generator. J. Neuroscience 17:7703-7713.

245. Kawasaki H, Avoli M (1996) Excitatory effects induced by carbachol on bursting neurons of the rat subiculum. Neurosci.Lett. 219:1-4.

246. Kawasaki H, Tancredi V, D'Arcangelo G, Avoli M (1998) Multiple actions of the novel anticonvulsant drug topiramate in the rat subiculum in vitro. Brain Res. 807:125-134.

247. Kay AR, Sugimori M, Llinas R (1998) Kinetic and stochastic properties of a persistent sodium current in mature guinea pig cerebellar Purkinje cells. J Neurophysiol 80:1167-79.

248. Kay AR, Wong RK (1987) Calcium current activation kinetics in isolated pyramidal neurones of the Ca1 region of the mature guinea-pig hippocampus. J.Physiol 392:603-616.

249. Kepecs A, Xiao-Jing Wang X-J, Lisman J (2002) Bursting neurons signal input slope. J. Neurosci. 22:9053-9062.

250. Keros S, McBain CJ (1997) Arachidonic acid inhibits transient potassium currents and broadens action potentials during electrographic seizures in hippocampal pyramidal and inhibitory interneurons. J.Neurosci. 17:3476-3487.

251. Khawaled R, Bruening-Wright A, Adelman JP, Maylie J (1999) Bicuculline block of small-conductance calcium-activated potassium channels. Pflugers Arch. 438:314-321.

252. King Jr. JD, Meriney SD (2005) Proportion of N-Type Calcium Current Activated by Action Potential Stimuli. J. Neurophysiol**.** 94:3762-3770.

253. Klee R, Ficker E, Heinemann U (1995) Comparison of voltage-dependent potassium currents in rat pyramidal neurons acutely isolated from hippocampal regions CA1 and CA3. J Neurophysiol 74:1982-95.

254. Klink R, Alonso A (1993) Ionic mechanisms for the subthreshold oscillations and differential electroresponsiveness of medial entorhinal cortex layer II neurons. J Neurophysiol 70:144-57.

255. Klöckner U, Lee JH, Cribbs LL, Daud A, Hescheler J, Pereverzev A, Perez-Reyes E, Schneider T (1999) Comparison of the Ca2+ currents induced by expression of three cloned alpha1 subunits, alpha1G, alpha1H and alpha1I of low-voltage-activated T-type Ca2+ channels. Eur. J. Neurosci. 11:4171-4178.

256. Kloosterman F, Witter MP, Van HT (2003) Topographical and laminar organization of subicular projections to the parahippocampal region of the rat. J.Comp Neurol. 455:156-171.

257. Knopfel T, Rietschin L, Gahwiler BH (1989) Organotypic Co-Cultures of Rat Locus Coeruleus and Hippocampus. Eur.J.Neurosci. 1:678-689.

258. Knopfel T, Vranesic I, Gahwiler BH, Brown DA (1990) Muscarinic and b-adrenergic depression of the slow Ca2+ activated potassium conductance in hippocampal CA3 pyramidal cells is not mediated by a reduction of the depolarization-induced cytosolic Ca2+ transients. Proc. Natl. Acad. Sci. USA 87:4083-4087.

259. Knopp A, Kivi A, Wozny C, Heinemann U, Behr J (2005) Cellular and network properties of the subiculum in the pilocarpine model of temporal lobe epilepsy. J.Comp Neurol. 483:476-488.

260. Koizumi A, Watanabe SI, Kaneko A (2001) Persistent Na+ current and Ca2+ current boost graded depolarization of rat retinal amacrine cells in culture. J.Neurophysiol. 86:1006-1016.

261. Kopell N, Ermentrout GB, Whittington MA, Traub RD (2000) Gamma rhythms and beta rhythms have different synchronization properties. Proc Natl Acad Sci U S A 97:1867-72.

262. Koschak A, Reimer D, Huber I, Grabner M, Glossmann H, Engel J, Striessnig J (2001) alpha 1D (Cav1.3) subunits can form l-type Ca2+ channels activating at negative voltages. J.Biol.Chem. 276:22100-22106.

263. Kosel KC, Van Hoesen GW, Rosene DL (1983) A direct projection from the perirhinal cortex (area 35) to the subiculum in the rat. Brain Res. 269:347-351.

264. Kubie JL MR (1991) Multiple representations in the hippocampus. Hippocampus 1:240-2.

265. Kuzmiski JB , Barr W, Zamponi GW, MacVicar BA (2005) Topiramate inhibits the initiation of plateau potentials in CA1 neurons by depressing R-type calcium channels. Epilepsia 46:481-489.

266. Kuzmiski JB , MacVicar BA (2001) Cyclic nucleotide-gated channels contribute to the cholinergic plateau potential in hippocampal CA1 pyramidal neurons. J.Neurosci. 21:8707-8714.

267. Lacinova L (2004) Pharmacology of recombinant low-voltage activated calcium channels. Curr.Drug Targets.CNS.Neurol.Disord. 3:105-111.

268. Lambert RC, Maulet Y, Mouton J, Beattie R, Volsen S, De WM, Feltz A (1997) T-type Ca2+ current properties are not modified by Ca2+ channel beta subunit depletion in nodosus ganglion neurons. J.Neurosci. 17:6621-6628.

269. Lancaster B , Adams PR (1986) Calcium-dependent current generating the afterhyperpolarization of hippocampal neurons. J Neurophysiol 55:1268-82.

270. Lancaster B, Nicoll RA (1987) Properties of two calcium-activated hyperpolarizations in rat hippocampal neurones. J.Physiol 389:187-203.

271. Lancaster B, Nicoll RA, Perkel DJ (1991) Calcium activates two types of potassiumchannels in rat hippocampal neurons in culture. J. Neurosci. 11:23-30.

272. Lancaster B , Zucker RS (1994) Photolytic manipulation of Ca2+ and the time course of slow, Ca(2+)-activated K+ current in rat hippocampal neurones. J Physiol 475:229-39.

273. Lang R, Lee G, Liu W, Tian S, Rafi H, Orias M, Segal AS, Desir GV (2000) KCNA10: a novel ion channel functionally related to both voltage-gated potassium and CNG cation channels. Am. J. Physiol. 278:F1013–1021.

274. Laxmi TR, Meti BL, Bindu PN (2000) Ventral subicular lesion alters rhythmical slow wave activity (theta) of CA1 area of hippocampus and entorhinal cortex. Brain Res 869:236-40.

275. Lee J-H, Daud A, Cribbs LL, Lacerda AE, Klockner U, Pereverzev A, Schneider T, Perez-Reyes E (1999a) Cloning an expression of a novel member of the low voltage-activated T-type calcium channel family. J. Neurosci. 19:1912-1921.

276. Lee JH, Daud AN, Cribbs LL, Lacerda AE, Pereverzev A, Klockner U, Schneider T, Perez-Reyes E (1999b) Cloning and expression of a novel member of the low voltage-activated T-type calcium channel family. J. Neurosci. 19:1912-1921.

277. LeMasson G, Marder E, Abbott LF (1993) Activity-dependent regulation of conductances in model neurons. Science 259:1915-7.

278. Leresche N, Parri HR, Erdemli G, Guyon A, Turner JP, Williams SR, Asprodini E, Crunelli V (1998) On the action of the anti-absence drug ethosuximide in the rat and cat thalamus. J.Neurosci. 18:4842-4853.

279. Lesage F, Guillemare E, Fink M, Duprat F, Lazdunski M, Romey G, Barhanin J (1996) TWIK-1, a

ubiquitous human weakly inward rectifying K+ channel with a novel structure. EMBO J. 15:1004-1011.

280. Leung LS, Yu HW (1998) Theta-frequency resonance in hippocampal CA1 neurons in vitro demonstrated by sinusoidal current injection. J Neurophysiol 79:1592-6.

281. Li X-Y, McArdle JJ (1997) Novel transient outward K+ current of mature murine hippocampal neurones. Eur. J. Physiol. 434:195-202.

282. Li Y, Bennett DJ (2003) Persistent sodium and calcium currents cause plateau potentials in motoneurons of chronic spinal rats. J.Neurophysiol. 90:857-869.

283. Lien CC, Jonas P (2003) Kv3 potassium conductance is necessary and kinetically optimized for high-frequency action potential generation in hippocampal interneurons. J. Neurosci. 23:2058–2068.

284. Lingle CJ, Zeng XH, Ding JP, Xia XM (2001) Inactivation of BK channels mediated by the NH(2) terminus of the beta3b auxiliary subunit involves a two-step mechanism: possible separation of binding and blockade. J.Gen.Physiol 117:583-606.

285. Llinas R, Sugimori M, Cherksey BD, Smith RG, Delbono O, Stefani E, Appel S (1993) IgG from amyotrophic lateral sclerosis patients increases current through P-type calcium channels in mammalian cerebellar Purkinje cells and in isolated channel protein in lipid bilayer. Proc.Natl.Acad.Sci.U.S.A 90:11743-11747.

286. Llinás R, Sugimori M, Hillman DE, Cherksey B (1992) Distribution and functional significance of the P-type, voltage-dependent Ca2+ channels in the mammalian central nervous system. Trends. Neurosci. 15:351-355.

287. Llinas RR, Sugimori M (1980) Electrophysiological properties of in vitro Purkinje cell somata in mammalian cerebellar slices. J. Physiol. 305:171-195.

288. Llinas RR, Sugimori M, Cherksey B (1989) Voltage-dependent calcium conductances in mammalian neurons. The P channel. Ann.N.Y.Acad.Sci. 560:103-111.

289. Locke RE, Nerbonne JM (1997) Role of voltage-gated K+ currents in mediating the regular-spiking phenotype of callosal-projecting rat visual cortical neurons. J.Neurophysiol. 78:2321-2335.

290. Ludwig A, Zong X, Jeglitsch M, Hofmann F, Biel M (1998) A family of hyperpolarization-activated mammalian cation channels. Nature 393:587-591.

291. Luthi A, McCormick DA (1998) H-current: properties of a neuronal and network pacemaker. Neuron 21:9-12.

292. Ma JY, Catterall WA, Scheuer T (1997) Persistent sodium currents through brain sodium channels induced by G protein betagamma subunits. Neuron 19:443-452.

293. Maccaferri G, Mangoni M, Lazzari A, DiFrancesco D (1993) Properties of the hyperpolarization-activated current in rat hippocampal CA1 pyramidal cells. J Neurophysiol 69:2129-36.

294. MacVicar BA, Dudek FE (1981) Electrotonic coupling between pyramidal cells: a direct demonstration in rathippocampal slices. Science 213:782-785.

295. Madison DV, Nicoll RA (1984) Control of the repetitive discharge of rat CA 1 pyramidal neurones in vitro. J.Physiol 354:319-331.

296. Madison DV, Nicoll RA (1986) Actions of noradrenaline recorded intracellularly in rat hippocampal CA1 pyramidal neurones, in vitro. J.Physiol 372:221-244.

297. MadisonD. V., Lancaster B, Nicoll RA (1987) Voltage clamp analysis of cholinergic action in the

hippocampus. J. Neurosci. 7:733-741.

298. Magee J, Hoffman D, Colbert C, Johnston D (1998) Electrical and calcium signaling in dendrites of hippocampal pyramidal neurons. Annu Rev Physiol 60:327-46.

299. Magee JC (1998) Dendritic hyperpolarization-activated currents modify the integrative properties of hippocampal CA1 pyramidal neurons . J Neurosci 18:7613-24.

300. Magee JC (2001) Dendritic mechanisms of phase precession in hippocampal CA1 pyramidal neurons. J Neurophysiol 86:528-32.

301. Magee JC, Carruth M (1999) Dendritic voltage-gated ion channels regulate the action potential firing mode of hippocampal CA1 pyramidal neurons. J.Neurophysiol. 82:1895-1901.

302. Magee JC, Johnston D (1995) Characterization of single voltage-gated Na+ and Ca2+ channels in apical dendrites of rat CA1 pyramidal neurons. J.Physiol 487 (Pt 1):67-90.

303. Mainen ZF, Joerges J, Huguenard JR, Sejnowski TJ (1995) A model of spike initiation in neocortical pyramidal neurons. Neuron 15:1427-39.

304. Mainen ZF, Sejnowski TJ (1996) Influence of dendritic structure on firing pattern in model neocortical neurons. Nature 382:363-6.

305. Maletic-Savatic M, Lenn NJ, Trimmer JS (1995) Differential spatiotemporal expression of K1 channel polypeptides in rat hippocampal neurons developing in situ and in vitro. J. Neurosci. 15:3840-3851.

306. Mantegazza M, Franceschetti S, Avanzini G (1998) Anemone toxin (ATX II)-induced increase in persistent sodium current: effects on the firing properties of rat neocortical pyramidal neurones. J Physiol 507 (Pt 1):105-16.

307. Marchal P (1998) John von Neumann: The founding father of artificial life. Artificial Life 4:229-235.

308. Marchetti C , Carbone E, Lux HD (1986) Effects of dopamine and noradrenaline on Ca channels of cultured sensory and sympathetic neurons of chick. Pflugers Arch. 406:104-111.

309. Maren S (1999) Neurotoxic or electrolytic lesions of the ventral subiculum produce deficits in the acquisition and expression of Pavlovian fear conditioning in rats. Behav.Neurosci. 113:283-290.

310. Markram H, Sakmann B (1994) Calcium transients in dendrites of neocortical neurons evoked by single subthreshold excitatory postsynaptic potentials via low-voltage-activated calcium channels. Proc. Natl. Acad. Sci. USA 91:5207-5211.

311. Marrion NV, Tavalin SJ (1998) Selective activation of Ca2+-activated K+ channels by co-localized Ca2+ channels in hippocampal neurons. Nature 395:900-905.

312. Marrion NV, Zucker RS, Marsh SJ, Adams PR (1991) Modulation of M-current by intracellular Ca2+. Neuron 6:533-545.

313. Martinez-Pinna J, McLachlan EM, Gallego R (2000) Distinct mechanisms for activation of Cl- and K+ currents by Ca2+ from different sources in mouse sympathetic neurones. J.Physiol 527 Pt 2:249-264.

314. Mason A (1993) Electrophysiology and burst-firing of rat subicular pyramidal neurons in vitro: a comparison with area CA1. Brain Res. 600:174-178.

315. Mathworks (2002) MATLAB. Version 6.5.

316. Matsumoto H, Ajmone-Marsan C (1964) Cortical cellular phenomena in experimental epilepsy: ictal manifestations. Exp. Neurol. 9:305-326.

317. Mattia D, Hwa GG, Avoli M (1993) Membrane properties of rat subicular neurons in vitro. J. Neurophysiol. 70:1244-8.

318. Mattia D, Kawasaki H, Avoli M (1997a) In vitro electrophysiology of rat subicular bursting neurons. Hippocampus 7:48-57.

319. Mattia D, Kawasaki H, Avoli M (1997b) Repetitive firing and oscillatory activity of pyramidal-like bursting neurons in the rat subiculum . Exp Brain Res 114:507-17.

320. McCormick DA, Bal T (1997) Sleep and arousal: thalamocortical mechanisms. Annu Rev Neurosci 20:185-215.

321. McCormick DA, Huguenard JR (1992) A model of the electrophysiological properties of thalamocortical relay neurons. J Neurophysiol 68:1384-400.

322. McCormick DA, Pape HC (1990) Properties of a hyperpolarization-activated cation current and its role in rhythmic oscillation in thalamic relay neurones. Journal of Physiology 431:291-318.

323. McDermott CM, LaHoste GJ, Chen C, Musto A, Bazan NG, Magee JC (2003) Sleep deprivation causes behavioral, synaptic, and membrane excitability alterations in hippocampal neurons. J. Neurosci. 23:9687-9695.

324. McDonald TF, Trautwein W, Pelzer DJ (1994) Regulation and modulation of calcium channels in cardiac, skeletal and smooth musle cells. Physiol. Rev. 74:365-507.

325. McNaughton BL, Barnes CA, Gerrard JL, Gothard K, Jung MW, Knierim JJ, Kudrimoti H, Qin Y, Skaggs WE, Suster M, Weaver KL (1996) Deciphering the hippocampal polyglot: the hippocampus as a path integration system. J Exp Biol 199:173-85.

326. Mel BW (2000) In the brain, the model is the goal., Nature Neuroscience Supplement 3:1183.

327. Menendez de la PL (2003) Control of bursting by local inhibition in the rat subiculum in vitro. J.Physiol 549:219-230.

328. Menendez de la PL, Gal B (2004) Synaptic contributions to focal and widespread spatiotemporal dynamics in the isolated rat subiculum in vitro. J.Neurosci. 24:5525-5536.

329. Menendez de la PL, Suarez F, Pozo MA (2002) The effect of different morphological sampling criteria on the fraction of bursting cells recorded in the rat subiculum in vitro. Neurosci.Lett. 322:49-52.

330. Menendez de la PL, Suarez F, Pozo MA (2003) Electrophysiological and morphological diversity of neurons from the rat subicular complex in vitro. Hippocampus 13:728-744.

331. Mermelstein PG, Bito H, Deisseroth K, Tsien RW (2000) Critical dependence of cAMP response element-binding protein phosphorylation on L-type calcium channels supports a selective response to EPSPs in preference to action potentials. J.Neurosci. 20:266-273.

332. Mermelstein PG, Foehring RC, Tkatch T, Song WJ, Baranauskas G, Surmeier DJ (1999) Properties of Q-type calcium channels in neostriatal and cortical neurons are correlated with beta subunit expression. J.Neurosci. 19:7268-7277.

333. Methot M, Tancredi V, Avoli M (1997) Long-term potentiation and long-term depression in the rat subiculum in vitro. Soc. Neurosci. (Abstr.) 47:20.

334. Metz AE, Jarsky T, Martina M, Spruston N (2005) R-Type Calcium Channels Contribute to Afterdepolarization and Bursting in Hippocampal CA1 Pyramidal Neurons. J. Neurosci. 25:5763-5773.

335. Mickus T, Jung HY, Spruston N (1999) Slow sodium channel inactivation in CA1 pyramidal cells. Ann N

Y Acad Sci 868:97-101.

336. Microsoft (2001) Microsoft Paint. Version 5.1.

337. Mikami A, Imoto K, Tanabe T, Niidome T, Mori Y, Takeshima H, Narumiya S, Numa S (1989) Primary structure and functional expression of the cardiac dihydropyridine-sensitive calcium channel. Nature 340:230-33.

338. Mills LR, Niesen CE, So AP, Carlen PL, Spigelman I, Jones OT (1994) N-type Ca2+ channels are located on somata, dendrites, and a subpopulation of dendritic spines on live hippocampal pyramidal neurons. J.Neurosci. 14:6815-6824.

339. Minkwitz HG (1976) [Development of neuronal structure in the hippocampus during pre- and post-natal ontogenesis in the albino rat. III. Morphometric determination of ontogenetic changes in dendrite structure and spine distribution on pyramidal neurons (CA1) of the hippocampus]. J Hirnforsch 17:255-75.

340. Mintz IM, Adams ME, Bean BP (1992) P-type calcium channels in rat central and peripheral neurons. Neuron 9:85-95.

341. Misonou H, Mohapatra DP, Park EW, Leung V, Zhen D, Misonou K, Anderson AE, Trimmer JS (2004) Regulation of ion channel localization and phosphorylation by neuronal activity. Nat.Neurosci. 7:711-718.

342. Mittman S, Guo J, Agnew WS (1999) Structure and alternative splicing of the gene encoding alpha1G, a human brain T calcium channel alpha1 subunit. Neurosci.Lett. 274:143-146.

343. MittmanN T, Alzheimer C (1998) Muscarinic inhibition of persistent Na+ in rat neocortical pyramidal neurons. J. Neurophysiol. 79:1579-1582.

344. Moczydlowski E, Latorre R (1983) Gating kinetics of Ca2+-activated K+ channels fromrat muscle incorporated into planar lipid bilayers. Evidence for two voltage-dependent Ca2+ binding reactions. J. Gen. Physiol. 82:511-542.

345. Mogul DJ, Adams ME, Fox AP (1993) Differential activation of adenosine receptors decreases N-type but potentiates P-type Ca2+ current in hippocampal CA3 neurons. Neuron 10:327-334.

346. Moore SD, Madamba SG, Joels M, Siggins GR (1988) Somatostatin augments the M-current in hippocampal neurons. Science 239:278-80.

347. Moosmang S, Biel M, Hofmann F, Ludwig A (1999) Differential distribution of four hyperpolarization-activated cation channels in mouse brain. Biol.Chem. 380:975-980.

348. Moosmang S, Stieber J, Zong X, Biel M, Hofmann F, Ludwig A (2001) Cellular expression and functional characterization of four hyperpolarization-activated pacemaker channels in cardiac and neuronal tissues. Eur. J. Biochem. 268:1646-1652.

349. Mortimer JA , Gosche KM, Riley KP, Markesbery WR, Snowdon DA (2004) Delayed recall, hippocampal volume and Alzheimer neuropathology: findings from the Nun Study. Neurology 62:428-432.

350. Mourre C, Cervera P, Lazdunski M (1987) Autoradiographic analysis in rat brain of the postnatal ontogeny of voltage-dependent Na+ channels, Ca2+-dependent K+ channels and slow Ca2+ channels identified as receptors for tetrodotoxin, apamin and (-)-desmethoxyverapamil. Brain Res. 417:21-32.

351. Murakoshi H , Trimmer JS (1999) Identification of the Kv2.1 K+ channel as a major component of the delayed rectifier K+ current in rat hippocampal neurons. J.Neurosci. 19:1728-1735.

352. Naber PA, Witter MP, Lopes Silva FH (2000) Networks of the hippocampal memory system of the rat. The pivotal role of the subiculum. Ann N Y Acad Sci 911:392-403.

353. Nahm SS, Jung KY, Enger MK, Griffith WH, Abbott LC (2005) Differential expression of T-type calcium channels in P/Q-type calcium channel mutant mice with ataxia and absence epilepsy. J.Neurobiol. 62:352-360.

354. Nakajima Y, Nakajima S, Leonard RJ, Yamaguchi K (1986) Acetylcholine raises excitability by inhibiting the fast transient potassium current in cultured hippocampal neurons. Proc.Natl.Acad.Sci.U.S.A 83:3022-3026.

355. Nakashima YM, Todorovic SM, Pereverzev A, Hescheler J, Schneider T, Lingle CJ (1998) Properties of Ba2+ currents arising from human alpha1E and alpha1Ebeta3 constructs expressed in HEK293 cells: physiology, pharmacology and comparison to native T-type Ba2+ currents. Neuropharmacology 37:957-972.

356. Neuhoff H, Neu A, Liss B, Roeper J (2002) I(h) channels contribute to the different functional properties of identified dopaminergic subpopulations in the midbrain. J.Neurosci. 22:1290-1302.

357. Nilius B (1998) Signal transduction in vascular endothelium: the role of intracellular calcium and ion channels. Verh.K.Acad.Geneeskd.Belg. 60:215-250.

358. Noma A, Irisawa H (1976) Membrane currents in the rabbit sinoatrial node cell as studied by the double microelectrode method. Pflugers Arch. 364:45-52.

359. Normann C, Peckys D, Schulze CH, Walden J, Jonas P, Bischofberger J (2000) Associative long-term depression in the hippocampus is dependent on postsynaptic N-type Ca2+ channels. J.Neurosci. 20:8290-8297.

360. Nowycky MC, Fox AP, Tsien RW (1985) Three types of neuronal calcium channel with different calcium agonist sensitivity. Nature 316:440-443.

361. Numann RE, Wadman WJ, Wong RK (1987) Outward currents of single hippocampal cells obtained from the adult guinea-pig. J Physiol 393:331-53.

362. Nutan KS, Meti BL (2000) Deficits in operant behavior and alteration of CA1, CA3 hippocampal dendritic arborization due to subicular lesions. J.Neurosci.Res. 59:806-812.

363. O'Donnell P, Grace AA (1995) Synaptic interactions among excitatory afferents to nucleus accumbens neurons: hippocampal gating of prefrontal cortical input. J. Neurosci. 15:3622-3639.

364. O'Mara S (2005) The subiculum: what it does, what it might do, and what neuroanatomy has yet to tell us. J.Anat. 207:271-282.

365. O'Mara SM, Commins S, Anderson M, Gigg J (2001) The subiculum: a review of form, physiology and function. Prog Neurobiol 64:129-55.

366. Obermair GJ , Szabo Z, Bourinet E, Flucher BE (2004) Differential targeting of the L-type Ca2+ channel alpha 1C (CaV1.2) to synaptic and extrasynaptic compartments in hippocampal neurons. Eur.J.Neurosci. 19:2109-2122.

367. Oliver D, Lien C-C, Soom M, Baukrowitz T, Jonas P, Fakler B (2004) Functional Conversion Between A-Type and Delayed Rectifier K+ Channels by Membrane Lipids. Science 304:265-270.

368. Olsen OH, Nadim F, Calabrese RL (1995) Modeling the leech heartbeat elemental oscillator. II. Exploring the parameter space. J.Comput.Neurosci. 2:237-257.

369. Otto T, Eichenbaum H, Wiener SI, Wible CG (1991) Learning-related patterns of CA1 spike trains parallel stimulation parameters optimal for inducing hippocampal long-term potentiation. Hippocampus 1:181-192.

370. O'Keefe J (1979) A review of the hippocampal place cells. Prog. Neurobiol. 13:419–439.

371. Palmieri C, Kawasaki H, Avoli M (2000) Topiramate depresses carbachol-induced plateau potentials in subicular bursting cells. Neuroreport 11:75-8.

372. Pape HC (1996) Queer current and pacemaker: the hyperpolarization-activated cation current in neurons. Annu Rev Physiol 58:299-327.

373. Parent L, Schneider T, Moore CP, Talwar D (1997) Subunit regulation of the human brain alpha1E calcium channel. J. Membr. Bio. 160:127-140.

374. Patil PG, Brody DL, Yue DT (1998) Preferential closed-state inactivation of neuronal calcium channels. Neuron 20:1027-1038.

375. Patlak J (1991) Molecular kinetics of voltage-dependent Na+ channels. Physiological Reviews 71.

376. Pavlides C, Greenstein YJ, Grudman M, Winson J (1988) Long-term potentiation in the dentate gyrus is induced preferentially on the positive phase of theta-rhythm. Brain Res 439:383-7.

377. Pedarzani P , Storm JF (1993) PKA mediates the effects of monoamine transmitters on the K+ current underlying the slow spike frequency adaptation in hippocampal neurons. Neuron 11:1023-1035.

378. Pennefather P, Lancaster B, Adams PR, Nicoll RA (1985) Two distinct Ca-dependent K currents in bullfrog sympathetic ganglion cells. Proc Natl Acad Sci U S A 82:3040-4.

379. Perez-Reyes E (2003) Molecular physiology of low-voltage-activated t-type calcium channels. Physiol Rev. 83:117-161.

380. Perez-Reyes E, Cribbs LL, Daud A, Lacerda AE, Barclay J, Williamson MP, Fox M, Rees M, Lee JH (1998) Molecular characterization of a neuronal low-voltage-activated T-type calcium channel. Nature 391:896-900.

381. Perkins KL, Wong RK (1995) Intracellular QX-314 blocks the hyperpolarization-activated inward current Iq in hippocampal CA1 pyramidal cells. J.Neurophysiol. 73:911-915.

382. Peters HC, Hu H, Pongs O, Storm JF, Isbrandt D (2005) Conditional transgenic suppression of M channels in mouse brain reveals functions in neuronal excitability, resonance and behavior. Nat.Neurosci. 8:51-60.

383. Phillips PE , Stamford JA (2000) Differential recruitment of N-, P- and Q-type voltage-operated calcium channels in striatal dopamine release evoked by 'regular' and 'burst' firing. Brain Res. 884:139-146.

384. Piedras-Renteria ES, Tsien RW (1998) Antisense oligonucleotides against alpha1E reduce R-type calcium currents in cerebellar granule cells. Proc.Natl.Acad.Sci.U.S.A 95:7760-7765.

385. Pierson P, Tribollet E, Raggenbass M (2001) Effect of vasopressin on the input-output properties of rat facial motoneurons. Eur.J.Neurosci. 14:957-967.

386. Pike FG, Goddard RS, Suckling JM, Ganter P, Kasthuri N, Paulsen O (2000) Distinct frequency preferences of different types of rat hippocampal neurones in response to oscillatory input currents. J. Physiol. 529 (Pt. 1):205-213.

387. Pike FG, Meredith RM, Olding AW, Paulsen O (1999) Rapid report: postsynaptic bursting is essential for “Hebbian” induction of associative long-term potentiation at excitatory synapses in rat hippocampus. J. Physiol. (Lond.) 518:571-576.

388. Pineda JC, Waters RS, Foehring RC (1998) Specificity in the interaction of HVA Ca2+ channel types with Ca2+-dependent AHPs and firing behavior in neocortical pyramidal neurons. J.Neurophysiol. 79:2522-2534.

389. Plummer MR, Hess P (1991) Reversible uncoupling of inactivation in N-type calcium channels. Nature

351:657-659.

390. Pokorny J, Yamamoto T (1981) Postnatal ontogenesis of hippocampal CA1 area in rats. I. Development of dendritic arborisation in pyramidal neurons. Brain Res Bull 7:113-20.

391. Pongs O, Leicher T, Berger M, Roeper J, Bahring R, Wray D, Giese KP, Silva AJ, Storm JF (1999) Functional and molecular aspects of voltage-gated K+ channel beta subunits. Ann.N.Y.Acad.Sci. 868:344-355.

392. Poolos NP, Johnston D (1999) Calcium-activated potassium conductances contribute to action potential repolarization at the soma but not the dendrites of hippocampal CA1 pyramidal neurons. J.Neurosci. 19:5205-5212.

393. Porter NM, Thibault O, Thibault V, Chen KC, Landfield PW (1997) Calcium channel density and hippocampal cell death with age in long-term culture. J.Neurosci. 17:5629-5639.

394. Pouille F, Cavelier P, Desplantez T, Beekenkamp H, Craig PJ, Beattie RE, Volsen SG, Bossu JL (2000) Dendro-somatic distribution of calcium-mediated electrogenesis in purkinje cells from rat cerebellar slice cultures. J.Physiol 527 Pt 2:265-282.

395. Pravettoni E, Bacci A, Coco S, Forbicini P, Matteoli M, Verderio C (2000) Different localizations and functions of L-type and N-type calcium channels during development of hippocampal neurons. Dev.Biol. 227:581-594.

396. Psarropoulou C, Avoli M (1995) Subthreshold membrane-potential oscillations in immature rat CA3 hippocampal neurones. Neuroreport 6:2561-4.

397. Puil E, Meiri H, Yarom Y (1994) Resonant behavior and frequency preferences of thalamic neurons. J Neurophysiol 71:575-82.

398. Qi JS, Qiao JT (2001) Suppression of large conductance Ca2+-activated K+ channels by amyloid beta-protein fragment 31-35 in membrane patches excised from hippocampal neurons. Sheng Li Xue.Bao. 53:198-204.

399. Qu Y, Curtis R, Lawson D, Gilbride K, Ge P, DiStefano PS, Silos-Santiago I, Catterall WA, Scheuer T (2001) Differential modulation of sodium channel gating and persistent sodium currents by the beta1, beta2, and beta3 subunits. Mol.Cell Neurosci. 18:570-580.

400. Rall W (1989) Cable theory for dendritic neurons. In: Methods in Neuronal Modelling: From Synapses to Networks (Koch C, Segev I, eds), pp 9-62. Cambridge, MA: MIT Press.

401. Ramakers GM, Storm JF (2002) A postsynaptic transient K(+) current modulated by arachidonic acid regulates synaptic integration and threshold for LTP induction in hippocampal pyramidal cells. Proc.Natl.Acad.Sci.U.S.A 99:10144-10149.

402. Raman IM, Sprunger LK, Meisler MH, Bean BP (1997) Altered subthreshold sodium currents and disrupted firing patterns in Purkinje neurons of Scn8a mutant mice. Neuron 19:881-891.

403. Randall A, Tsien RW (1995) Pharmacological dissection of multiple types of Ca2+ channel currents in rat cerebellar granule neurons. J.Neurosci. 15:2995-3012.

404. Randall A, Tsien RW (1998) Distinctive Biophysical and Pharmacological Features of T-Type Calcium Channels. In: In Low-Voltage-Activated T-Type Calcium Channels (Tsien RW, Clozel J. P., Nargeot J, eds), pp 29-43. Basel, Switzerland: Adis International.

405. Randall AD, Tsien RW (1997) Contrasting Biophysical and Pharmacological Properties of T-type and R-type Calcium Channels. Neuropharmcology 36:879-893.

406. Rascol O, Potier B, Lamour Y, Dutar P (1991) Effects of calcium channel agonist and antagonists on calcium-dependent events in CA1 hippocampal neurons. Fundam.Clin.Pharmacol. 5:299-317.

407. Rawlins JN, Feldon J, Tonkiss J, Coffey PJ (1989) The role of subicular outputs in the development of the partial reinforcement extinction effect. Exp.Brain Res. 77:153-160.

408. Raynor K, Reisine T (1992) Somatostatin receptors. Crit Rev.Neurobiol. 6:273-289.

409. Reckziegel G, Beck H, Schramm J, Elger CE, Urban BW (1998) Electrophysiological characterization of Na+ currents in acutely isolated human hippocampal dentate granule cells. J.Physiol 509 (Pt 1):139-150.

410. Regan LJ (1991) Voltage-dependent calcium currents in Purkinje cells from rat cerebellar vermis. J.Neurosci. 11:2259-2269.

411. Reuveni I, Friedman A, Amitai Y, Gutnick MJ (1993) Stepwise repolarization from Ca2+ plateaus in neocortical pyramidal cells: evidence for nonhomogeneous distribution of HVA Ca2+ channels in dendrites. J.Neurosci. 13:4609-4621.

412. Riegert C, Galani R, Heilig S, Lazarus C, Cosquer B, Cassel JC (2004) Electrolytic lesions of the ventral subiculum weakly alter spatial memory but potentiate amphetamine-induced locomotion. Behav.Brain Res. 152:23-34.

413. Robinson RB, Siegelbaum SA (2003) Hyperpolarization-activated cation currents: from molecules to physiological function. Ann. Rev. Physiol. 65:453-480.

414. Rudy B, Chow A, Lau D, Amarillo Y, Ozaita A, Saganich M, Moreno H, Nadal MS, Hernandez-Pineda R, Hernandez-Cruz A, Erisir A, Leonard C, Vega-Saenz de ME (1999) Contributions of Kv3 channels to neuronal excitability. Ann.N.Y.Acad.Sci. 868:304-343.

415. Runden-Pran E, Haug FM, Storm JF, Ottersen OP (2002) BK channel activity determines the extent of cell degeneration after oxygen and glucose deprivation: a study in organotypical hippocampal slice cultures. Neuroscience 112:277-288.

416. Sah DW, Bean BP (1994) Inhibition of P-type and N-type calcium channels by dopamine receptor antagonists. Mol.Pharmacol. 45:84-92.

417. Sah P (1995) Properties of channels mediating the apamin-insensitive afterhyperpolarization in vagal motoneurons. J.Neurophysiol. 74:1772-1776.

418. Sah P, Bekkers JM (1996) Apical dendritic location of slow afterhyperpolarization current in hippocampal pyramidal neurons: Implications for the integration of long-term potentiation. J. Neurosci. 16:4537.

419. Sah P, French CR, Gage PW (1985) Effects of noradrenaline on some potassium currents in CA1 neurones in rat hippocampal slices. Neurosci.Lett. 60:295-300.

420. Sah P, Gibb AJ, Gage PW (1988) The sodium current underlying action potentials in guinea pig hippocampal CA1 neurons. J Gen Physiol 3:373-98.

421. Sah P, Isaacson JS (1995) Channels underlying the slow afterhyperpolarization in hippocampal pyramidal neurons: neurotransmitters modulate the open probability. Neuron 15:435-441.

422. Santoro B, Chen S, Luthi A, Pavlidis P, Shumyatsky GP, Tibbs GR, Siegelbaum SA (2000) Molecular and functional heterogeneity of hyperpolarization-activated pacemaker channels in the mouse CNS. J.Neurosci. 20:5264-5275.

423. Santoro B, Liu DT, Yao H, Bartsch D, Kandel ER, Siegelbaum SA, Tibbs GR (1998) Identification of a gene encoding a hyperpolarizationactivated pacemaker channel of brain. Cell 93:717-729.

424. Sather WA, Tanabe T, Zhang J-F, Mori Y, Adams ME, Tsien RW (1993) Distinctive biophysical and pharmacological properties of class A (BI) calcium channel a1 subunits. Neuron 1:291-303.

425. Schaller KL , Krzemien DM, Yarowsky PJ, Krueger BK, Caldwell JH (1995) A novel, abundant sodium channel expressed in neurons and glia. Journal of Neuroscience 15:3231-3242.

426. Schenk F, Morris RG (1985) Dissociation between components of spatial memory in rats after recovery from the effects of retrohippocampal lesions. Exp. Brain. Res. 58:11-28.

427. Schnee ME, Brown BS (1998) Selectivity of linopirdine (DuP 996), a neurotransmitter release enhancer, in blocking voltage-dependent and calcium-activated potassium currents in hippocampal neurons. J.Pharmacol.Exp.Ther. 286:709-717.

428. Schreiber S, Erchova I, Heinemann U, Herz AVM (2004) Subthreshold Resonance Explains the Frequency-Dependent Integration of Periodic as Well as Random Stimuli in the Entorhinal Cortex. J. Neurophysiol. 92:408-415.

429. Schroter KH , Ruppersberg J, Wunder F, Rettig J, Stocker M, Pongs O (1991) Cloning and functional expression of a TEA-sensitive A-type potassium channel from rat brain. FEBS Lett. 278:211-216.

430. Schwabe L, Adorjan P, Obermayer K (2001) Spike-frequency adaptation as a mechanism for dynamic coding in V1. Neurocomputing 38-40:351-358.

431. Schwarz JR (1986) The effect of temperature on Na currents in rat myelinated nerve fibres. Pflugers Arch. 406:397-404.

432. Schwarz JR (1988) [Membrane currents and action potentials of myelinated nerve fibers and their modification by diphenylhydantoin and tocainide]. EEG.EMG.Z.Elektroenzephalogr.Elektromyogr.Verwandte.Geb. 19:115-122.

433. Schweitzer P, Madamba SG, Siggins GR (1998) Somatostatin increases a voltage-insensitive K+ conductance in rat CA1 hippocampal neurons. J Neurophysiol 79:1230-8.

434. Schwindt PC , Crill WE (1995) Amplification of synaptic current by persistent sodium conductance in apical dendrite of neocortical neurons. J Neurophysiol 74:2220-4.

435. Schwindt PC , Spain WJ, Crill WE (1992) Effects of intracellular calcium chelation on voltage-dependent and calcium-dependent currents in cat neocortical neurons. Neuroscience 47:571-578.

436. Segal M (1972) Hippocampal unit responses to perforant path simulation. Exp. Neurol. 35:541-546.

437. Segal M, Barker JL (1984) Rat hippocampal neurons in culture: potassium conductances. J. Neurophysiol. 51:1409-1433.

438. Segal M, Barker JL, Owen DG (1987) Chloride conductances in central neurons. Isr J Med Sci 23:95-100.

439. Segal MM, Douglas AF (1997) Late sodium channel openings underlying epileptiform activity are preferentially diminished by the anticonvulsant phenytoin. J.Neurophysiol. 77:3021-3034.

440. Segev I, Burke RE (1998) Compartmental models of complex neurons. In: Methods in Neuronal Modelling: From Synapses to Networks (Koch C, Segev I, eds), pp 93-136. Cambridge, MA: MIT Press.

441. Seutin V, Massotte L, Renette MF, Dresse A (2001) Evidence for a modulatory role of Ih on the firing of a subgroup of midbrain dopamine neurons. Neuroreport 12:255-258.

442. Shah M, Haylett DG (2000) Ca(2+) channels involved in the generation of the slow afterhyperpolarization in cultured rat hippocampal pyramidal neurons. J Neurophysiol 83:2554-61.

443. Shah MM, Mistry M, Marsh SJ, Brown DA, Delmas P (2002) Molecular correlates of the M-current in cultured rat hippocampal neurons. J.Physiol 544:29-37.

444. Shao LR, Halvorsrud R, Borg-Graham L, Storm JF (1999) The role of BK-type Ca2+-dependent K+ channels in spike broadening during repetitive firing in rat hippocampal pyramidal cells. J.Physiol 521 Pt 1:135-146.

445. Shapiro MS, DeCoursey TE (1991) Permeant ion effects on gating kinetics of the type l potassium channel in mouse lymphocytes. J. Gen. Physiol. 97:1251-1278.

446. Sharp PE (1999) Complimentary roles for hippocampal versus subicular/entorhinal place cells in coding place, context, and events. Hippocampus 9:432-443.

447. Sharp PE (1999b) Comparison of the timing of hippocampal and subicular spatial signals: implications for path integration. Hippocampus 9:158-172.

448. Sharp PE, Green C (1994) Spatial correlates of firing patterns of single cells in the subiculum of the freely moving rat. J.Neurosci. 14:2339-2356.

449. Shen KZ, Surprenant A (1991) Noradrenaline, somatostatin and opioids inhibit activity of single HVA/N-type calcium channels in excised neuronal membranes. Pflugers Arch. 418:614-616.

450. Sheng M, Liao YJ, Jan YN, Jan LY (1993) Presynaptic A-current based on heteromultimeric K+ channels detected in vivo. Nature 365:72-75.

451. Shepard PD, Stump D (1999) Nifedipine blocks apamin-induced bursting activity in nigral dopamine-containing neurons. Brain Res. 817:104-109.

452. Sims SM, Kelly ME, Dixon SJ (1991) K+ and Cl- currents in freshly isolated rat osteoclasts. Pflugers Arch. 419:358-370.

453. Smart TG (1987) Single calcium-activated potassiumchannels recorded fromcultured rat sympathetic neurones. J. Physiol. (London) 389:337-360.

454. Smith MR, Smith RD, Plummer NW, Meisler MH, Goldin AL (1998) Functional analysis of the mouse Scn8a sodium channel. J.Neurosci. 18:6093-6102.

455. Smith RD, Goldin AL (1998) Functional analysis of the rat I sodium channel in xenopus oocytes. J.Neurosci. 18:811-820.

456. Sochivko D, Chen J, Becker A, Beck H (2003) Blocker-resistant Ca2+ currents in rat CA1 hippocampal pyramidal neurons. Neuroscience 116:629-638.

457. Sochivko D, Pereverzev A, Smyth N, Gissel C, Schneider T, Beck H (2002) The Ca(V)2.3 Ca(2+) channel subunit contributes to R-type Ca(2+) currents in murine hippocampal and neocortical neurones. J.Physiol 542:699-710.

458. Softky W (1994) Sub-millisecond coincidence detection in active dendritic trees. Neuroscience 58:13-41.

459. Song D, Wang Z, Berger TW (2002) Contribution of T-type VDCC to TEA-induced long-term synaptic modification in hippocampal CA1 and dentate gyrus. Hippocampus 12:689-697.

460. Soong TW, Stea A, Hodson CD, Dubel SJ, Vincent SR, Snutch TP (1993) Structure and functional expression of a member of the low voltage activated calcium channel family. Science 260:1133-1136.

461. Soriano E, Martinez A, Farinas I, Frotscher M (1993) Chandelier cells in the hippocampal formation of the rat: the entorhinal area and subicular complex. J.Comp Neurol. 337:151-167.

462. Spadoni F, Hainsworth AH, Mercuri NB, Caputi L, Martella G, Lavaroni F, Bernardi G, Stefani A (2002) Lamotrigine derivatives and riluzole inhibit INa,P in cortical neurons. Neuroreport 13:1167-1170.

463. Spruston N, Schiller Y, Stuart G, Sakmann B (1995) Activity-dependent action potential invasion and calcium influx into hippocampal CA1 dendrites. Science 268:297-300.

464. Staba RJ, Wilson CL, Bragin A, Fried I, Engel Jr. J (2002) Sleep states differentiate single neuron activity recorded from human epileptic hippocampus, entorhinal cortex, and subiculum. J.Neurosci. 22:5694-5704.

465. Staff NP, Jung HY, Thiagarajan T, Yao M, Spruston N (2000) Resting and active properties of pyramidal neurons in subiculum and CA1 of rat hippocampus. J Neurophysiol 84:2398-408.

466. Stafstrom CE, Schwindt PC, Chubb MC, Crill WE (1985) Properties of persistent sodium conductance and calcium conductance of layer V neurons from cat sensorimotor cortex in vitro. J. Neurophysiol. 53:153-170.

467. Stanford IM , Traub RD, Jefferys JG (1998) Limbic gamma rhythms. II. Synaptic and intrinsic mechanisms underlying spike doublets in oscillating subicular neurons. J Neurophysiol 80:162-71.

468. Stanley EF, Atrakchi AH (1990) Calcium currents recorded from a vertebrate presynaptic nerve terminal are resistant to the dihydropyridine nifedipine. Proc.Natl.Acad.Sci.U.S.A 87:9683-9687.

469. Stea A, Dubel SJ, Snutch TP (1999) alpha 1B N-type calcium channel isoforms with distinct biophysical properties. Ann. NY Acad. Sci. 868:118-130.

470. Stewart M (1997) Antidromic and orthodromic responses by subicular neurons in rat brain slices. Brain Res 769:71-85.

471. Stewart M, Wong RK (1993) Intrinsic properties and evoked responses of guinea pig subicular neurons in vitro. J Neurophysiol 70:232-45.

472. Stocker M (2004) Ca(2+)-activated K+ channels: molecular determinants and function of the SK family. Nat.Rev.Neurosci. 5:758-770.

473. Stocker M, Krause M, Pedarzani P (1999) An apamin-sensitive Ca2+-activated K+ current in hippocampal pyramidal neurons. Proc.Natl.Acad.Sci.U.S.A 96:4662-4667.

474. Storm JF (1987a) Action potential repolarization and a fast after-hyperpolarization in rat hippocampal pyramidal cells. J.Physiol 385:733-759.

475. Storm JF (1987b) Intracellular injection of a Ca2+ chelator inhibits spike repolarization in hippocampal neurons. Brain Res 435:387-92.

476. Storm JF (1987c) Phorbol esters broaden the action potential in CA1 hippocampal pyramidal cells. Neurosci.Lett. 75:71-74.

477. Storm JF (1988) Temporal integration by a slowly inactivating K+ current in hippocampal neurons. Nature 336:379-381.

478. Storm JF (1989) An after-hyperpolarization of medium duration in rat hippocampal pyramidal cells. J.Physiol 409:171-190.

479. Storm JF (1990) Potassium currents in hippocampal pyramidal cells. Prog. Brain Res. 83:161-187.

480. Stuart G, Sakmann B (1995) Amplification of EPSPs by axosomatic sodium channels in neocortical pyramidal neurons. Neuron 15:1065-1076.

481. Stuart GJ, Sakmann B (1994) Active propagation of somatic action potentials into neocortical pyramidal

cell dendrites. Nature 367:69-72.

482. Su H, Alroy G, Kirson ED, Yaari Y (2001) Extracellular calcium modulates persistent sodium current-dependent burst-firing in hippocampal pyramidal neurons. J Neurosci 21:4173-82.

483. Sugino K, Hempel CM, Miller MN, Hattox AM, Shaprio P, Wu C, Huang ZJ, Nelson SB (2006) Molecular taxonomy of major neuronal classes in the adult mouse brain. Nat. Neurosci. 9:99-107.

484. Sullivan JM (1999) Mechanisms of cannabinoid-receptor-mediated inhibition of synaptic transmission in cultured hippocampal pyramidal neurons. J.Neurophysiol. 82:1286-1294.

485. Sun X, Gu XQ, Haddad GG (2003) Calcium influx via L- and N-type calcium channels activates a transient large-conductance Ca2+-activated K+ current in mouse neocortical pyramidal neurons. J.Neurosci. 23:3639-3648.

486. Suzuki WA, Zola-Morgan S, Squire LR, Amaral DG (1993) Lesions of the perirhinal and parahippocampal cortices in the monkey produce long-lasting memory impairment in the visual and tactual modalities. J. Neurosci. 13:2430-2451.

487. Swanson LW (1982) Normal hippocampal circuitry. Neuroscience Research Progress Bulletin 20:624-637.

488. Swartz KJ, Bean BP (1992) Inhibition of calcium channels in rat CA3 pyramidal neurons by a metabotropic glutamate receptor. J.Neurosci. 12:4358-4371.

489. Systat Software (2004) Sigmaplot. Version 9.0.

490. Taddese A, Bean BP (2002) Subthreshold sodium current from rapidly inactivating sodium channels drives spontaneous firing of tuberomammillary neurons. Neuron 33:587-600.

491. Takahashi K , Akaike N (1991) Calcium antagonist effects on low-threshold (T-type) calcium current in rat isolated hippocampal CA1 pyramidal neurons. J Pharmacol Exp Ther 256:169-75.

492. Takahashi K , Ueno S, Akaike N (1991) Kinetic properties of T-type Ca2+ currents in isolated rat hippocampal CA1 pyramidal neurons. J.Neurophysiol. 65:148-155.

493. Takahashi K , Wakamori M, Akaike N (1989) Hippocampal CA1 pyramidal cells of rats have four voltage-dependent calcium conductances. Neurosci Lett 104:229-34.

494. Talley EM, Cribbs LL, Lee JH, Daud A, Perez-Reyes E, Bayliss DA (1999) Differential distribution of three members of a gene family encoding low voltage-activated (T-type) calcium channels. J. Neurosci. 19:1895-1911.

495. Talukder G, Harrison NL (1995) On the mechanism of modulation of transient outward current in cultured rat hippocampal neurons by di- and trivalent cations. J.Neurophysiol. 73:73-79.

496. Tan HL, Kupershmidt S, Zhang R, Stepanovic S, Roden DM, Wilde AA, Anderson ME, Balser JR (2002) A calcium sensor in the sodium channel modulates cardiac excitability. Nature 415:442-447.

497. Tanabe M, Gahwiler BH, Gerber U (1998) L-Type Ca2+ channels mediate the slow Ca2+-dependent afterhyperpolarization current in rat CA3 pyramidal cells in vitro. J.Neurophysiol. 80:2268-2273.

498. Taube JS (1993) Electrophysiological properties of neurons in the rat subiculum in vitro. Exp Brain Res 96:304-18.

499. Taube JS, Kesslak JP, Cotman CW (1992) Lesions of the rat postsubiculum impair performance on spatial tasks. Behav. Neural Biol. 57:131-143.

500. Tavalin SJ, Shepherd D, Cloues RK, Bowden SE, Marrion NV (2004) Modulation of single channels

underlying hippocampal L-type current enhancement by agonists depends on the permeant ion. J.Neurophysiol. 92:824-837.

501. Taverna S, Sancini G, Mantegazza M, Franceschetti S, Avanzini G (1999) Inhibition of Transient and Persistent Na+ Current Fractions by the New Anticonvulsant Topiramate. J Pharmacol Exp Ther 288:960-968.

502. Thibault O, Landfield PW (1996) Increase in single L-type calcium channels in hippocampal neurons during aging. Science 272:1017-20.

503. Thomas MJ, Watabe AM, Moody TD, Makhinson M, O'Dell TJ (1998) Postsynaptic complex spike bursting enables the induction of LTP by theta frequency synaptic stimulation. J Neurosci 18:7118-26.

504. Thompson SM , Masukawa LM, Prince DA (1985) Temperature dependence of intrinsic membrane properties and synaptic potentials in hippocampal CA1 neurons in vitro. J Neurosci 5:817-24.

505. Timmermann DB, Westenbroek RE, Schousboe A, Catterall WA (2002) Distribution of high-voltage-activated calcium channels in cultured gamma-aminobutyric acidergic neurons from mouse cerebral cortex. J.Neurosci.Res. 67:48-61.

506. Timmons SD, Geisert E, Stewart AE, Lorenzon NM, Foehring RC (2004) alpha2-Adrenergic receptor-mediated modulation of calcium current in neocortical pyramidal neurons. Brain Res. 1014:184-196.

507. Tokimasa T (1985) Spontaneous muscarinic suppression of the Ca-activated K-current in bullfrog sympathetic neurons. Brain Res. 344:134-141.

508. Tokimasa T, Akasu T (1990) Extracellular calcium ions are required for muscarine-sensitive potassium current in bullfrog sympathetic neurons. J. Auton. Nerv. Syst. 29:163-174.

509. Tokimasa T, Shirasaki T, Yoshida M, Ito M, Tanaka E, Mitsumoto T, Akasu T, Tanaka M, Higashi H, Nakano T (1996) Calcium-dependent potentiation of M-current in bullfrog sympathetic neurons. Neurosci.Lett. 214:79-82.

510. Tombaugh GC , Somjen GG (1996) Effects of extracellular pH on voltage-gated Na+, K+ and Ca2+ currents in isolated rat CA1 neurons. J Physiol 493 (Pt 3):719-32.

511. Tottene A, Moretti A, Pietrobon D (1996) Functional diversity of P-type and R-type calcium channels in rat cerebellar neurons. J.Neurosci. 16:6353-6363.

512. Traub RD (1982) Simulation of intrinsic bursting in CA3 hippocampal neurons. Neuroscience 7:1233-42.

513. Traub RD, Llinas R (1979) Hippocampal pyramidal cells: significance of dendritic ionic conductances for neuronal function and epileptogenesis. J Neurophysiol 42:476-96.

514. Traub RD, Miles R, Buzsaki G (1992) Computer simulation of carbachol-driven rhythmic population oscillations in the CA3 region of the in vitro rat hippocampus. J Physiol 451:653-72.

515. Traub RD, Wong RK, Miles R, Michelson H (1991) A model of a CA3 hippocampal pyramidal neuron incorporating voltage- clamp data on intrinsic conductances. J Neurophysiol 66:635-50.

516. Tseng GN, Boyden PA (1989) Multiple types of Ca2+ currents in single canine Purkinje cells. Circ.Res. 65:1735-1750.

517. Tu H, Deng L, Sun Q, Yao L, Han JS, Wan Y (2004) Hyperpolarization-activated, cyclic nucleotide-gated cation channels: roles in the differential electrophysiological properties of rat primary afferent neurons. J.Neurosci.Res. 76:713-722.

518. Turner RW, Maler L, Deerinck T, Levinson SR, Ellisman MH (1994) TTX-sensitive dendritic sodium

channels underlie oscillatory discharge in a vertebrate sensory neuron. J.Neurosci. 14:6453-6471.

519. Ueda K, Shinohara S, Yagami T, Asakura K, Kawasaki K (1997) Amyloid beta protein potentiates Ca2+ influx through L-type voltage-sensitive Ca2+ channels: a possible involvement of free radicals. J.Neurochem. 68:265-271.

520. Ulrich D (2002) Dendritic resonance in rat neocortical pyramidal cells. J. Neurophysiol. 87:2753-2759.

521. Valentino K , Newcomb R, Gadbois T, Singh T, Bowersox S, Bitner S, Justice A, Yamashiro D, Hoffman BB, Ciaranello R (1993) A selective N-type calcium channel antagonist protects against neuronal loss after global cerebral ischemia. Proc.Natl.Acad.Sci.U.S.A 90:7894-7897.

522. Valiante TA , bdul-Ghani MA, Carlen PL, Pennefather P (1997) Analysis of current fluctuations during after-hyperpolarization current in dentate granule neurones of the rat hippocampus. J.Physiol 499 (Pt 1):121-134.

523. Vega-Saenz de Miera E, Moreno H, Fruhling D, Kentros C, Rudy B (1992) Cloning of ShIII (Shawlike) cDNAs encoding a novel high-voltage-activating, TEA-sensitive, type-A K+ channel. Proc. R. Soc. Lond. B. Biol. Sci. 248:9-18.

524. Vega-Saenz De Miera E, Rudy B, Sugimori M, Llinas R (1997) Molecular characterization of the sodium channel subunits expressed in mammalian cerebellar Purkinje cells. Proc. Natl. Acad. Sci. USA 94:7059-7064.

525. Vergara C, Latorre R, Marrion NV, Adelman JP (1998) Calcium-activated potassium channels. Curr.Opin.Neurobiol. 8:321-329.

526. Viana F, Hille B (1996) Modulation of high voltage-activated calcium channels by somatostatin in acutely isolated rat amygdaloid neurons. J.Neurosci. 16:6000-6011.

527. Vilchis C, Bargas J, Ayala GX, Galvan E, Galarraga E (2000) Ca2+ channels that activate Ca2+-dependent K+ currents in neostriatal neurons. Neuroscience 95:745-752.

528. Vinogradova OS (1995) Expression, control, and probable functional significance of the neuronal theta-rhythm. Progress in Neurobiology 45:523-583.

529. Vogalis F, Storm JF, Lancaster B (2003) SK channels and the varieties of slow after-hyperpolarizations in neurons. Eur.J.Neurosci. 18:3155-3166.

530. Vreugdenhil M, Hoogland G, van Veelen CW, Wadman WJ (2004) Persistent sodium current in subicular neurons isolated from patients with temporal lobe epilepsy. Eur.J.Neurosci. 19:2769-2778.

531. Vreugdenhil M, van Veelen CW, van Rijen PC, Lopes da Silva FH, Wadman WJ (1998b) Effect of valproic acid on sodium currents in cortical neurons from patients with pharmaco-resistant temporal lobe epilepsy. Epilepsy Res. 32:309-320.

532. Vreugdenhil M, van Veelen CWM, van Rijen PC, Lopes da Silva FH, Wadman WJ (1998a) Sodium currents in isolated rat CA1 neurons after kindling epileptogenesis. Neuroscience 86:99-107.

533. Wang HS, Pan Z, Shi W, Brown BS, Wymore RS, Cohen IS, Dixon JE, McKinnon D (1998) KCNQ2 and KCNQ3 potassium channel subunits: molecular correlates of the M-channel. Science 282:1890-1893.

534. Warman EN, Durand DM, Yuen GL (1994) Reconstruction of hippocampal CA1 pyramidal cell electrophysiology by computer simulation. J. Neurophysiol. 71:2033-45.

535. Watson TW, Pittman QJ (1988) Pharmacological evidence that somatostatin activates the m-current in hippocampal pyramidal neurons. Neurosci Lett 91:172-6.

536. Weisskopf MG, Bauer EP, LeDoux JE (1999) L-Type Voltage-Gated Calcium Channels Mediate NMDAIndependent Associative Long-Term Potentiation at Thalamic Input Synapses to the Amygdala. Journal of Neuroscience 19:10512-10519.

537. Wellmer J, Su H, Beck H, Yaari Y (2002) Long-lasting modification of intrinsic discharge properties in subicular neurons following status epilepticus. Eur.J.Neurosci. 16:259-266.

538. Westenbroek RE, Bausch SB, Lin RC, Franck JE, Noebels JL, Catterall WA (1998) Upregulation of L-type Ca2+ channels in reactive astrocytes after brain injury, hypomyelination, and ischemia. J.Neurosci. 18:2321-2334.

539. Wheeler DB, Randall A, Tsien RW (1994) Roles of N-type and Q-type Ca21 channels in supporting hippocampal synaptic transmission. Science 264:107-111.

540. White JA, Klink R, Alonso A, Kay AR (1998) Noise from voltage-gated ion channels may influence neuronal dynamics in the entorhinal cortex. J. Neurophysiol. 80:262-9.

541. White TD, Tan AM, Finch DM (1991) Functional connections of the rat medial cortex and basal forebrain: an in vivo intracellular study. Neuroscience 44:571-583.

542. Williams ME, Feldman DH, McCue AF, Brenner R, Veliçelebi G, Ellis SB, Harpold MM (1992) Structure and functional expression of a1, a2, and ß subunits of a novel human neuronal calcium channel subtype. Neuron 8:71-84.

543. Williams ME , Marubio LM, Deal CR, Hans M, Brust PF, Philipson LH, Miller RJ, Johnson EC, Harpold MM, Ellis SB (1994) Structure and functional characterization of neuronal alpha 1E calcium channel subtypes. J.Biol.Chem. 269:22347-22357.

544. Williamson A, Alger BE (1990) Characterization of an early afterhyperpolarization after a brief train of action potentials in rat hippocampal neurons in vitro. J Neurophysiol 63:72-81.

545. Witter MP, Amaral DG (1991) Entorhinal cortex of the monkey: V. Projections to the dentate gyrus, hippocampus, and subicular complex. J.Comp Neurol. 307:437-459.

546. Witter MP, Groenewegen HJ (1990) The subiculum: cytoarchitectonically a simple structure, but hodologically complex. Prog.Brain Res. 83:47-58.

547. Witter MP, Groenewegen HJ, Lopes da Silva FH, Lohman AHM (1989) Functional organisation of the extrinsic and intrinsic circuitry of the parahippocampal region. Prog. Neurobiol. 33 :161-253.

548. Witter MP, Ostendorf RH, Groenewegen HJ (1990) Heterogeneity in the Dorsal Subiculum of the Rat. Distinct Neuronal Zones Project to Different Cortical and Subcortical Targets. Eur.J.Neurosci. 2:718-725.

549. Witter MP, Wouterlood FG, Naber PA, Van Haeften T (2000) Anatomical organization of the parahippocampal-hippocampal network. Ann N Y Acad Sci 911:1-24.

550. Wolfart J, Roeper J (2002) Selective coupling of T-type calcium channels to SK potassium channels prevents intrinsic bursting in dopaminergic midbrain neurons. J.Neurosci. 22:3404-3413.

551. Womack MD, Chevez C, Khodakhah K (2004) Calcium-activated potassium channels are selectively coupled to P/Q-type calcium channels in cerebellar Purkinje neurons. J.Neurosci. 24:8818-8822.

552. Wong RK, Prince DA (1981) Afterpotential generation in hippocampal pyramidal cells. J Neurophysiol 45:86-97.

553. Wozny C, Knopp A, Lehmann TN, Heinemann U, Behr J (2005) The subiculum: a potential site of ictogenesis in human temporal lobe epilepsy. Epilepsia 46 Suppl 5:17-21.

554. Wu LG, Borst JG, Sakmann B (1998) R-type Ca2+ currents evoke transmitter release at a rat central synapse. Proc.Natl.Acad.Sci.U.S.A 95:4720-4725.

555. Wu N, Enomoto A, Tanaka S, Hsiao C-F, Nykamp DQ, Izhikevich E, Chandler SH (2005) Persistent Sodium Currents in Mesencephalic V Neurons Participate in Burst Generation and Control of Membrane Excitability. J. Neurophysiol. 93:2710–2722.

556. Wu RL, Barish ME (1999) Modulation of a slowly inactivating potassium current, I(D), by metabotropic glutamate receptor activation in cultured hippocampal pyramidal neurons. J Neurosci 19:6825-37.

557. Yaari Y, Hamon B, Lux HD (1987) Development of two types of calcium channels in cultured mammalian hippocampal neurons. Science 235:680-682.

558. Yagami T, Ueda K, Sakaeda T, Itoh N, Sakaguchi G, Okamura N, Hori Y, Fujimoto M (2004) Protective effects of a selective L-type voltage-sensitive calcium channel blocker, S-312-d, on neuronal cell death. Biochem.Pharmacol. 67:1153-1165.

559. Yamada WM, Koch C, Adams PR (1998) Multiple channels and calcium dynamics. In: Methods in Neuronal Modelling: From Synapses to Networks (Koch C, Segev I, eds), pp 97-134. Cambridge, MA: MIT Press.

560. Yamakage M, Namiki A (2002) Calcium channels - basic aspects of their structure, function and gene encoding; anesthetic action on the channels - a review. Canadian Journal of Anesthesia 49:151-164.

561. Yasuda R, Sabatini BL, Svoboda K (2003) Plasticity of calcium channels in dendritic spines. Nature Neuroscience 6:948-955.

562. Yim CY, Mogenson GJ (1988) Neuromodulatory action of dopamine in the nucleus accumbens: an in viva intracellular study. Neuroscience 26:403-415.

563. Yue C, Yaari Y (2004) KCNQ/M channels control spike afterdepolarization and burst generation in hippocampal neurons. J.Neurosci. 24:4614-4624.

564. Zamponi GW, Bourinet E, Snutch TP (1996) Nickel block of a family of neuronal calcium channels: subtype- and subunit-dependent action at multiple sites. J.Membr.Biol. 151:77-90.

565. Zbicz KL, Weight FF (1985) Transient voltage and calcium-dependent outward currents in hippocampal CA3 pyramidal neurons. J. Neurophysiol. 53:1038-1058.

566. Zenisek D, Henry D, Studholme K, Yazulla S, Matthews G (2001) Voltage-dependent sodium channels are expressed in nonspiking retinal bipolar neurons. J.Neurosci. 21:4543-4550.

567. Zhang A, Fan SH, Cheng TP, Altura BT, Wong RK, Altura BM (1996) Extracellular Mg2+ modulates intracellular Ca2+ in acutely isolated hippocampal CA1 pyramidal cells of the guinea-pig. Brain Res. 728:204-208.

568. Zhang L, Valiante TA, Carlen PL (1993) Contribution of the lowthreshold T-type calcium current in generating the postspike depolarizing after-potential in dentate granule neurons of immature rats. J. Neurophysiol. 70:223-231.

569. Zhang X, Velumian AA, Jones OT, Carlen PL (2000) Modulation of high-voltage-activated calcium channels in dentate granule cells by topiramate. Epilepsia 41 Suppl 1:S52-S60.

570. Zhong CB, Pan YP, Tong XY, Xu XH, Wang XL (2005) Delayed rectifier potassium currents and Kv2.1 mRNA increase in hippocampal neurons of scopolamine-induced memory-deficient rats. Neurosci.Lett. 373:99-104.

571. Zhou FM, Hablitz JJ (1996) Layer I neurons of the rat neocortex. II. Voltage-dependent outward currents.

J.Neurophysiol. 76:668-682.

572. Zucker RS (1989) Short-term synaptic plasticity. Neuroscience 12:13-31.